National Aeronautics and
Space Administration

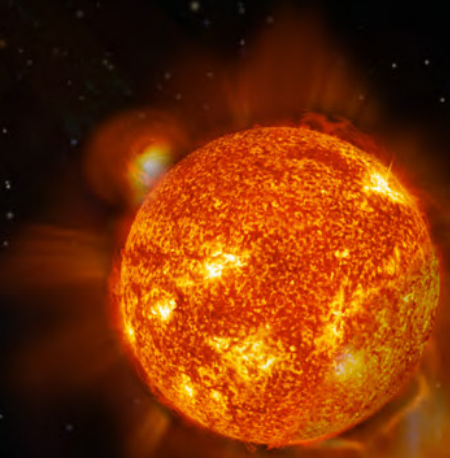

NASA Science and Technology Definition Team for the **Geospace Dynamics Constellation**

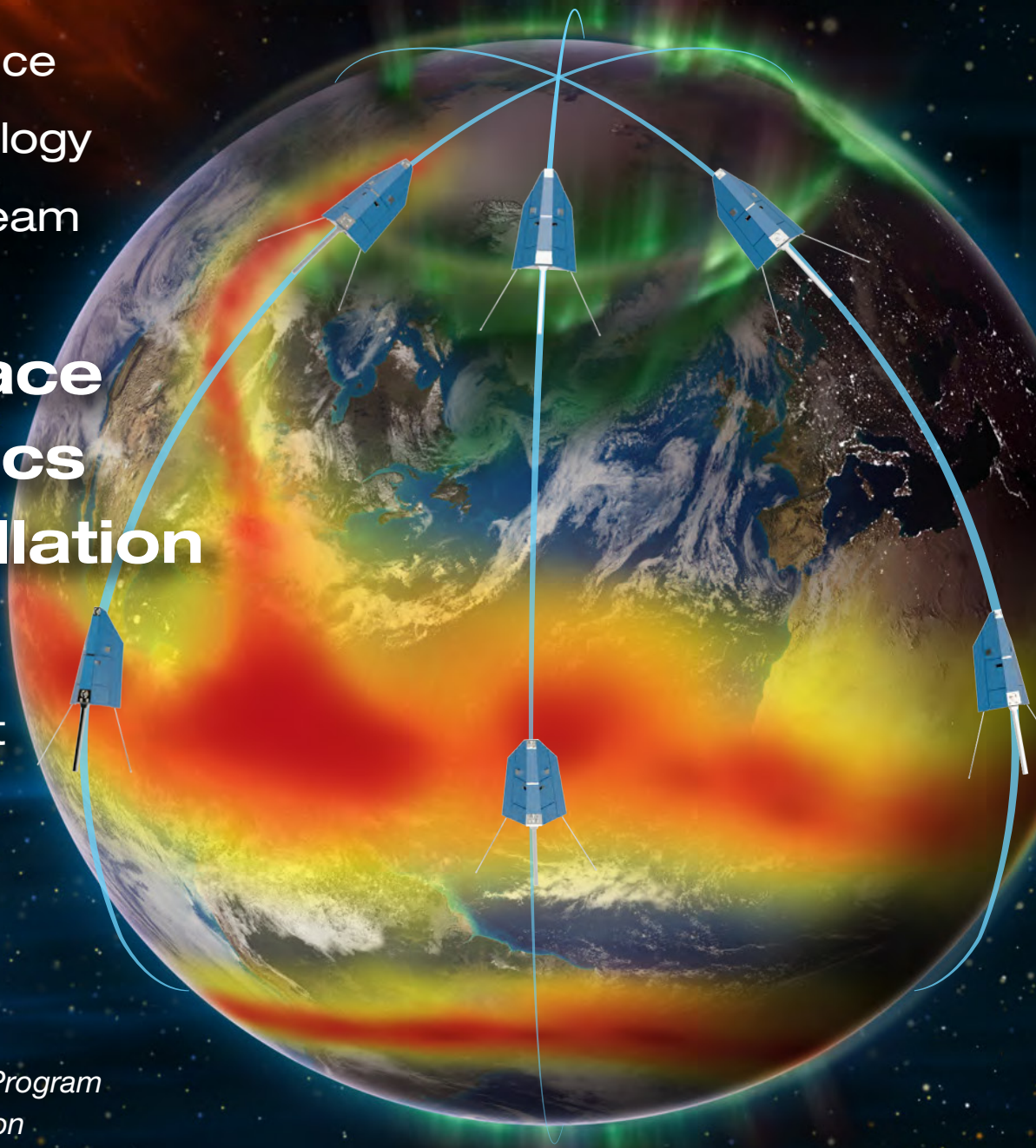

Final Report

Living With a Star Program
Heliophysics Division

www.nasa.gov

Geospace Dynamics Constellation
Science and Technology Definition Team

Jaynes, Allison
Co-Chair
Department of Physics and Astronomy
University of Iowa
Iowa City, IA 52242

Bishop, Rebecca
Sub-group Lead
Space Science Department
The Aerospace Corporation
El Segundo, CA 90245

Zesta, Eftyhia
Sub-group Lead
Geospace Physics Laboratory
NASA Goddard Space Flight Center
Greenbelt, MD 20771

Bale, Stuart
Space Science Laboratory
University of California, Berkeley
Berkeley, CA 94720

Clemmons, James
Department of Physics
University of New Hampshire
Durham, NH 03824

Gelinas, Lynette
Space Science Department
The Aerospace Corporation
El Segundo, CA 90245

Lu, Gang
High Altitude Observatory
National Center for Atmospheric Research
Boulder, CO 80301

Mlynczak, Martin
Climate Science Branch
NASA Langley Research Center
Hampton, VA 23681

Randall, Cora
Laboratory for Atmospheric and Space Physics
University of Colorado
Boulder, CO 80303

Ridley, Aaron
Co-Chair
Department of Climate
and Space Science and Engineering
University of Michigan
Ann Arbor, MI 48109

Heelis, Rod
Sub-group Lead
Department of Physics
University of Texas at Dallas
Richardson, TX 75083

Anderson, Brian
Applied Physics Laboratory
The Johns Hopkins University
Laurel, MD 20723

Cattell, Cynthia
School of Physics and Astronomy
University of Minnesota
Minneapolis, MN 55455

Connor, Hyunju
Geophysical Institute
University of Alaska
Fairbanks, Alaska 99775

Goncharenko, Larisa
Haystack Observatory
Massachusetts Institute of Technology
Westford, MA 01886

Matsuo, Tomoko
Department of Aerospace Engineering Sciences
University of Colorado
Boulder, CO 80309

Pfaff, Robert
ITM Physics Laboratory
NASA Goddard Space Flight Center
Greenbelt, MD 20771

The Team thanks Odile de la Beaujardiere, Kenneth Dymond, and Jeng-hwa (Sam) Yee for their contributions to the GDC STDT.

The Team thanks Jasper Gjerloev, Davide Masutti, I. Jonathan Rae, Rumi Nakamura, and Matt Taylor for their presentations to the STDT, and the Heliophysics community for the responses submitted to the GDC STDT Request for Information.

Headquarters and Support Staff

Leisner, Jared
Executive Secretary
NASA Headquarters
Washington, D.C. 20546

Mesarch, Michael
Flight Dynamics Support
NASA Goddard Space Flight Center
Greenbelt, Maryland 20771

Fung, Shing
Publication Support Management
ITM Physics Laboratory
NASA Goddard Space Flight Center
Greenbelt, Maryland 20771

Hrybyk-Keith, Mary Pat
Art Support
TRAX International Corporation
NASA Goddard Space Flight Center
Greenbelt, Maryland 20771

Power, Ronald
Art Support
Booz Allen Hamilton
McLean, VA 22102
On contract to NASA Headquarters

Garcia-Sage, Katherine
Modeling Support
Community Coordinate Modeling Center
NASA Goddard Space Flight Center
Greenbelt, Maryland 20771

Gallagher, Dennis
STDT Management
NASA Marshall Space Flight Center
Huntsville, Alabama 35824
On detail to NASA Headquarters

Bull, Ryan
Flight Dynamics Support
Applied Physics Laboratory
The Johns Hopkins University
Laurel, Maryland 20723

Ames, J. Michael
Publicatiom Support
ADNET Systems Inc.
NASA Goddard Space Flight Center
Greenbelt, Maryland 20771

Milano, Jennifer
Publication Support
Booz Allen Hamilton
Washington, DC 20005
On contract to NASA Headquarters

Kuznetsova, Maria
Modeling Support Management
Community Coordinate Modeling Center
NASA Goddard Space Flight Center
Greenbelt, Maryland 20771

Robinson, Robert
Modeling Support
Catholic University of America
Community Coordinate Modeling Center
NASA Goddard Space Flight Center
Greenbelt, Maryland 20771

Table of Contents

GDC Goal 1

Understand how the high latitude ionosphere-thermosphere system responds to variable solar wind/magnetosphere forcing.

GDC Goal 2

Understand how internal processes in the global ionosphere-thermosphere system redistribute mass, momentum, and energy.

IONOSPHERE

The ionosphere is a layer of plasma formed by the ionization of the neutral atmosphere by solar ultraviolet and x-ray irradiance, and high-latitude auroral precipitation. The ionosphere extends from below the mesopause up to the magnetosphere. This layer is most dense on the dayside and falls off at night and has significant structure due to the aurora and dynamics of the atmosphere.

THERMOSPHERE

The thermosphere is the hottest part of the atmosphere, reaching temperatures of 600K-1500K, depending on solar conditions. It is not well mixed, so atomic oxygen is the dominant species above 200 km altitude. Winds in the thermosphere are upwards of 200 m/s, with heating events spreading across the globe in less than 6 hours. The thermosphere is most dense and hottest in the late afternoon near the subsolar point, and coldest before dawn. Significant structuring in density, temperature, and composition, can occur at high latitudes due to the aurora, heating, and dynamics.

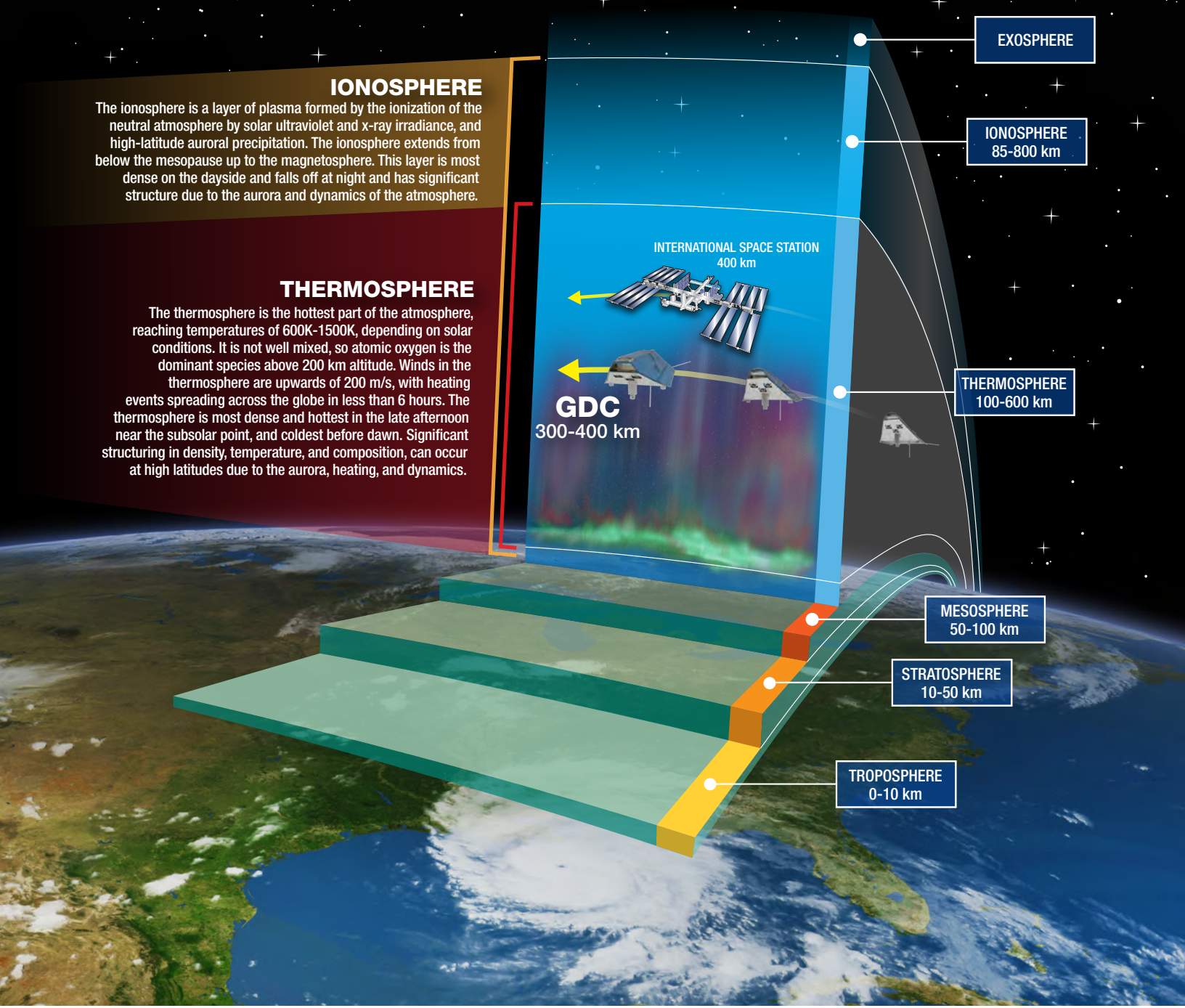

EXECUTIVE SUMMARY

The boundary between the Earth's atmosphere and space is a pivotal region that is truly the anchor of geospace– it is here, in the ionosphere-thermosphere (IT), where every physical process in geospace starts, is modified, or ends. It is also here, in this data-starved region, where low-Earth-orbit satellites reside. Despite its importance, this region of the Earth's space environment is the least understood as a global system. Furthermore, this key region of space is the seat of numerous critical space weather processes that affect our human society. Fully exploring the global IT system is vital to understanding the many ways in which near-Earth geospace affects daily life on Earth.

The ionosphere-thermosphere (IT) region is critically undersampled and we still don't understand how it is driven to extremes by the atmosphere from below and the magnetospheric/solar inputs from above. The IT system can vary globally or within localized areas, on timescales of minutes to hours or days, driven by effects coming from both above and below this layer. *Below,* atmospheric processes occur over scales that are relatively small, reaching continental-scale at the largest; while *above*, processes can occur over multiple scales, with the global system being affected by frequent magnetic storms that can change the entire structure of the upper atmosphere in a matter of a few hours, drastically affecting the technology on which we depend.

The GDC mission will meet the critical observational needs of the complex IT system by employing a multi-satellite architecture sufficient to cover the relevant temporal and spatial scales, thereby transforming our understanding of this critically-undersampled region.

Our society's reliance on global navigation satellite systems such as GPS is ever increasing. Signals from these satellites traverse our near Earth plasma environment where their paths can be altered dramatically by ionospheric scintillations and large magnitude density gradients, potentially causing significant errors in positioning knowledge. Meanwhile, above our heads, 20,000+ objects orbit in the near Earth region of space, including the International Space Station and a wide variety of weather, communications, and other operations satellites, with this number increasing every year, particularly as launchers become more economical. Predicting and mitigating satellite collisions is of paramount importance to our nation and the world. Further, new regulatory entities require accurate environmental specification in order to produce realistic and effective orbit management,

The thin envelope of our upper atmosphere remains a mysterious region. (Credit: NASA)

spectrum usage, and launch regulations. To accomplish this, we must understand variations in the thermosphere neutral density which directly affect these orbits, and which are tied to the dynamics of the thermosphere and ionosphere, especially during periods of solar and geomagnetic storms.

The Geospace Dynamics Constellation (GDC) mission will unravel complex mysteries in the combined and interacting ionized and neutral gases of the IT system by using an array of satellites. It is anticipated that GDC will be comprised of several satellites in different orbital planes that will be capable of measuring, for the first time, both the large-scale and localized dynamics of the interaction between the upper atmosphere and the near-Earth space plasma environment. The data will provide measurements of both the neutral and plasma dynamics at more than one local time and will also enable spatial/temporal effects to be distinguished. The proposed constellation concept will focus on the regions where the ions and neutrals are significantly and efficiently coupled and driven, and where key space weather effects, such as ionospheric scintillations and satellite drag, are most profound.

The GDC mission will dramatically change our understanding of how the upper atmosphere reacts to energy input from above, below, and within by addressing two overarching science goals with specifically actionable objectives:

1. **Understand how the high latitude ionosphere-thermosphere system responds to variable solar wind/magnetosphere forcing.**
2. **Understand how internal processes in the global ionosphere-thermosphere system redistribute mass, momentum, and energy.**

The Objectives for GDC recommended here have been established as the driving questions at the forefront of IT science. Goal 1 is advanced through achieving four Objectives that focus on high latitudes, where the coupling to the solar wind/magnetosphere has the most profound consequences. Achievement of these Objectives will resolve long-standing puzzles of how this connection accelerates winds and creates density structures in the ionized and neutral gases of the IT region, and how tides and atmospheric gravity waves act to influence these responses. Goal 2 is advanced by accomplishing six Objectives that concentrate on the global system, including low- and mid-latitudes where internal IT processes are key determinants of behavior. These Objectives explore the vital pathways that create and dissipate IT structures under a spectrum of influences from magnetic storms and propagating atmospheric tides and gravity waves, as well as the dissipative effects of radiative cooling and winds. Goal 2 is also furthered by determining the effects that hemispheric asymmetries have on the IT system. Achievement of these Objectives constitutes the basis for deriving the GDC mission requirements.

As a Living With a Star (LWS) mission, GDC follows NASA's Solar Dynamics Observatory and Van Allen Probes, providing the first ever measurements of the global-scale dynamics of the ionosphere-thermosphere system. GDC will revolutionize our understanding of the global IT system and the causes of its variations, allowing for dramatic improvements in our space weather models, ultimately leading to the mitigation of the negative effects on the space technology upon which we rely daily.

The original discoveries that will be facilitated by GDC will extend beyond the Earth system. The vast majority of the observed matter in the universe exists in a state known as plasma, an ionized gas that is affected by magnetic and electric fields. The dynamics of systems of plasmas are influenced by extremely complex processes that occur in almost all areas of NASA science: from stellar evolution, to Io's interaction with Jupiter, to understanding why Mars lost its atmosphere. GDC will grant us new insights into the fundamental dynamics of the solar system.

The Geospace Dynamics Constellation (GDC) Science and Technology Definition Team (STDT) has outlined a science-focused mission concept that will revolutionize our understanding of the dynamics that take place within the ionosphere/thermosphere system. The STDT has defined various mission implementation scenarios that are feasible, effective, and allow for the evolution of the system to be tracked across a range of temporal and spatial scales. The mission concept fully addresses the requirements specified by NASA in the STDT charter while also ensuring alignment with the recommendations of the 2013 National Academy of Sciences Committee on a Decadal Strategy for Solar

and Space Physics. GDC represents the beginning of an exciting new chapter in geospace exploration, promising to significantly advance our knowledge and understanding of our planet.

Global Scale

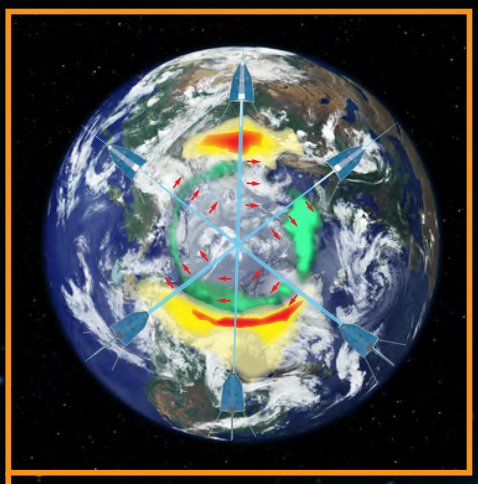

GOAL 1

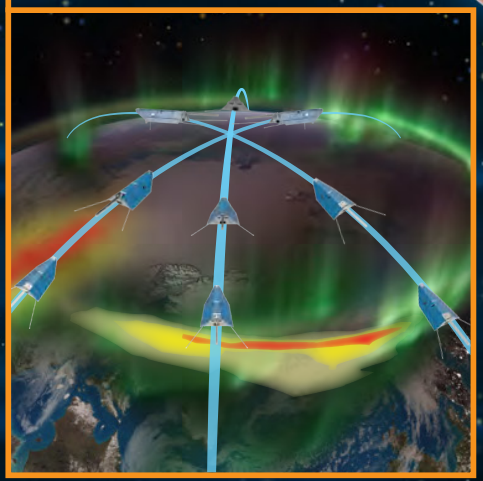

Regional Scale

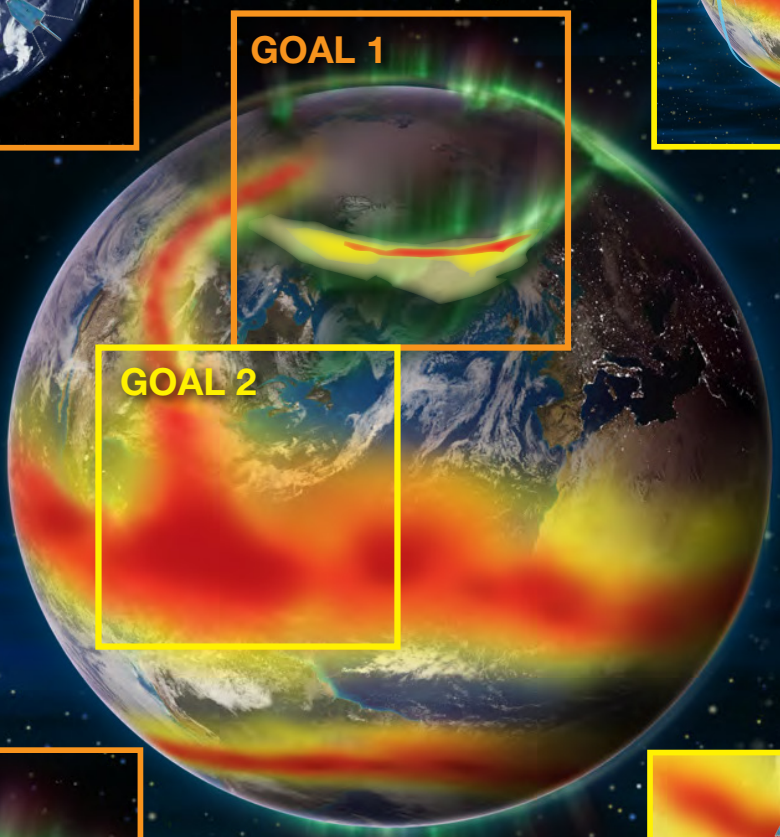

Global Scale

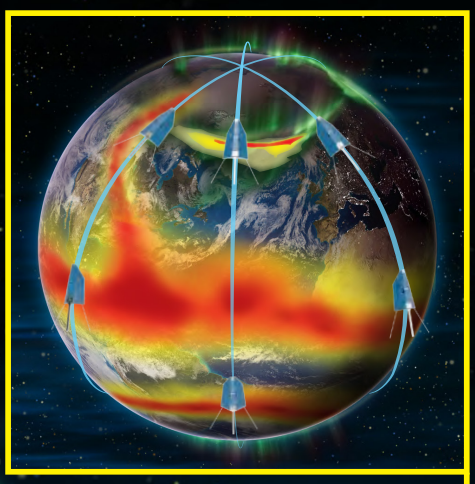

GOAL 2

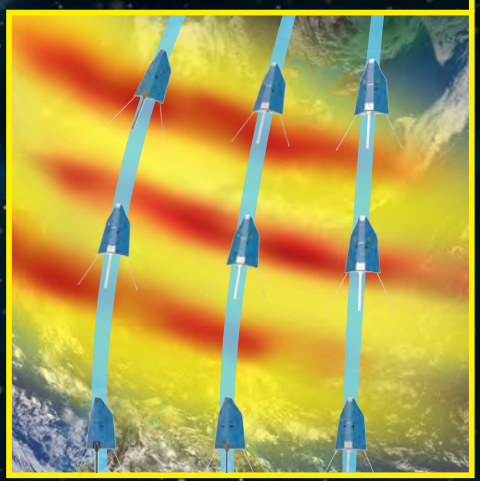

Regional Scale

1 INTRODUCTION

The Geospace Dynamics Constellation (GDC) is a strategic, Living With a Star (LWS) mission that will accomplish breakthroughs in fundamental understanding of the processes that govern the dynamics of the Earth's upper atmospheric envelope that surrounds and protects the planet. This layer resides in the nearest region of geospace and is comprised of an ionized component (the ionosphere) and a neutral component (the thermosphere) that co-exist above ~80 km altitude with the peak ambient ionospheric density occurring between 200-450 km. This region is where the transition to space literally occurs: below about 100 km altitude, the atmosphere is controlled primarily by neutral fluid dynamics, while above about 200 km, the atmosphere is strongly driven by electromagnetic forcing resulting from the dynamic interaction of the solar wind with the Earth's magnetosphere. The dynamics of the upper atmosphere at any time is the result of balancing the strength of each of its drivers, with the solar wind and magnetosphere electrodynamically driving huge impulsive changes with global-scale consequences, while the lower atmosphere continuously drives the thermosphere and ionosphere with tides, planetary, and gravity waves, shaping the global changes imposed by the magnetosphere. This constant tension between fluid dynamics and electrodynamics makes the upper atmosphere an extremely important and highly compelling region of scientific exploration. Most important, GDC will provide multipoint observations of both the energy inputs and the ionosphere-thermosphere (IT) system response with sufficient spatial and temporal resolution to finally unravel the physical processes underlying the observed system-level dynamical responses.

During the last half century, with the deployment of both short-lived and long-lived satellite missions, as well as rockets and ground facilities, society has gained some understanding of the general characteristics of, and the many physical processes inherent to, the climatology of the ionosphere and thermosphere. This knowledge has been pieced together using disparate sets of observations, often extremely limited in measured parameters, duration or coverage, providing primarily the climatological response of the IT system to its drivers. Due to a crippling lack of global, comprehensive observations, an understanding of IT system-level dynamics and their specification and prediction remains elusive. New comprehensive measurements are critically needed to elevate understanding of the upper atmosphere from a collection of distinct parts to a system that acts and reacts as a whole. New theories of processes that describe the coupling of the IT system with the solar wind and magnetosphere from above and the lower atmosphere from below have been proposed. Sophisticated models have pushed the boundaries of current understanding and have predicted the dynamical responses to a wide variety of drivers. Yet no data exist to evaluate or substantiate these theories, nor are there data to help define how local and regional processes influence the dynamics of the global-scale system, and ultimately progress models to where predictions are reliable. **The Geospace Dynamics Constellation is the mission that will achieve this breakthrough, providing the critical measurements needed to radically transform the understanding of the Earth's global upper atmosphere system.**

This report contains the GDC Science and Technology Definition Team (STDT) formulation of science Goals, Objectives, and Measurement Requirements that address compelling ionosphere-thermosphere system science, and that are consistent with, though not identical to, the recommendations of the 2013 National Academy of Sciences Committee on a Decadal Strategy for Solar and Space Physics. The science Objectives have been ranked in priority order by the STDT. The Objectives and physical parameters that must be observed for each one are described in Chapter 2. A variety of recommended implementation scenarios that provide the necessary measurements to achieve closure of the stated Objectives are included in Chapter 3, allowing flexibility in mission design. While this STDT report outlines a focused science mission that specifically increases the scientific understanding of how the upper atmosphere dynamically reacts to external and internal drivers, the measurements provided by GDC will also enable NASA to contribute to other national interests, detailed in Appendix B.

1.1 History of NASA IT Missions

Scientific knowledge and the basic understanding of Earth's coupled ionosphere and thermosphere climatology have advanced considerably since the earliest days of space research, led primarily by ground-based and space-based observations in concert with extensive data

analysis and advances in theory and modeling. Much of the fundamental, early knowledge of the ionosphere/thermosphere system was gathered from space-based observations using primarily *in situ* measurements on NASA's Atmosphere-Explorer satellites, launched in the 1970's, and NASA's Dynamics Explorer-2 (DE-2) satellite launched in 1981. In particular, DE-2 provided measurements of the ionized and neutral gas states in the ionosphere/thermosphere system simultaneous with measurements of high-latitude electrodynamic forcing, resulting from magnetosphere-solar wind coupling.

While the DE-2 mission revealed some of the phenomenology resulting from ion-neutral interactions, the combination of a single elliptical orbit, a restrictive power system which resulted in a very low duty cycle, and a short mission life led to an inability to reveal the spatial and temporal scales over which different processes operate. One of the main purposes of the GDC mission is to explore those scales and, for the first time, obtain the critical, missing information that will enable a comprehensive physical description of the coupling between the magnetosphere and the ionosphere-thermosphere system including the dynamic feedback between the charged and neutral species.

For example, measurements made by DE-2 allowed the determination of the ion-neutral velocity difference and to use local plasma and neutral density measurements to determine the momentum exchange and frictional heating rates [*Killeen et al.*, 1984a]. However, reconciling these local rates with the evolution of the system as a whole requires knowledge of the spatial scales and the persistence time of events which could not be obtained from 18 months of a single satellite dataset with its limited data-taking capabilities. GDC will remove this lack of knowledge, which has been a significant barrier to understanding the system-level response to external drivers.

DE-2 provided tantalizing glimpses into the climatology of ionospheric convection and the complex interplay between the charged and neutral species at high latitudes. In the intervening years, the increased sophistication of computational models of these interactions has revealed how important they are to understanding each of the constituents. New measurements, such as the Global Position Satellites' (GPS) Total Electron Content (TEC), and High Frequency (HF) radars' plasma drift velocities, have provided a more continuous description of the large scale behavior of the ionosphere. The ionosphere-thermosphere system is now appreciated as an active element in coupling to the magnetosphere; yet the ability to describe and explain the observed

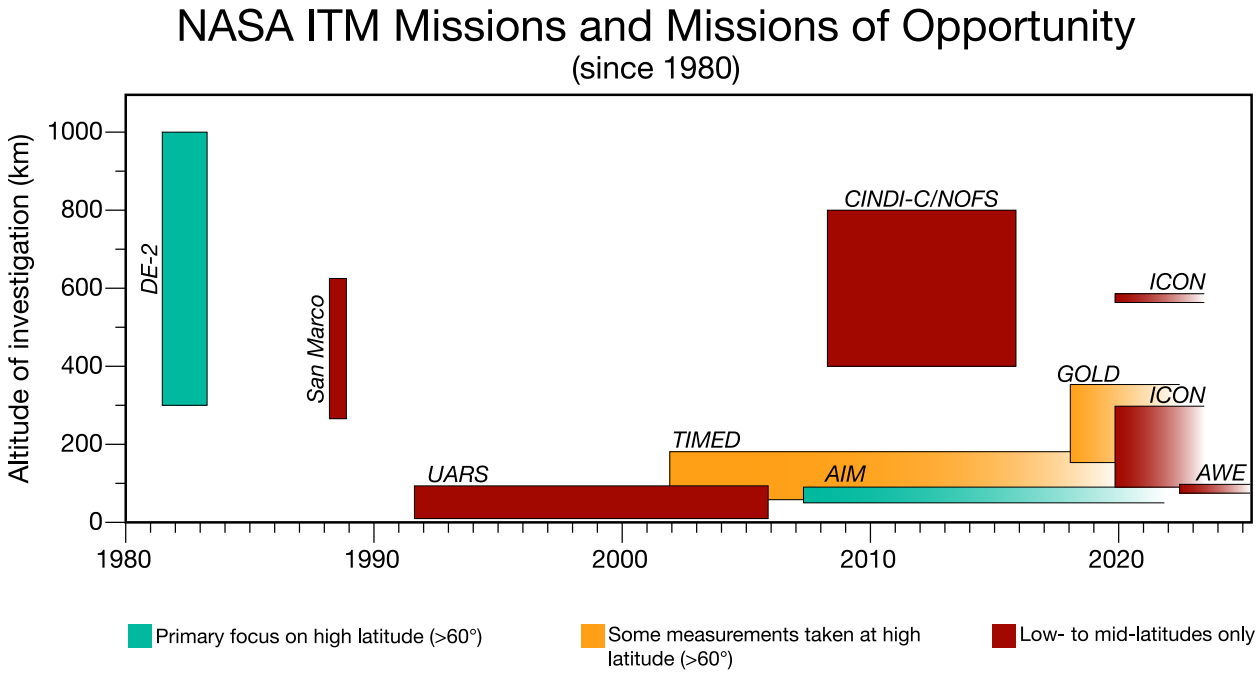

Figure 1.1. History of NASA ITM missions. The multi-scale constellation capabilities of GDC will enable science that goes well beyond what was possible with previous missions, as shown here in time-line vs. altitude format. The majority of these missions covered low- to mid-latitude science, and thus could not address the fundamental high-latitude-focused goals of GDC.

phenomenology is limited due to the inability to describe the prevailing dynamics of the charged and neutral species and the spatial and temporal scales that have the greatest influence. GDC is the right mission at the right time to provide these much-needed measurements.

Since DE-2 re-entered the atmosphere over 35 years ago, in early 1983, remote sensing measurements have been at the forefront of NASA's dedicated ITM missions, including the UARS, TIMED, and AIM satellites, which focused on the stratosphere, mesosphere, and lower thermosphere. NASA recently launched the GOLD mission, which gathers remote full disc imaging and limb profiles of the low- and mid-latitude thermosphere to measure integrated O/N2 ratios on the dayside and electron densities on the nightside. The ICON mission, expected to launch soon, will remotely measure altitude profiles of winds and temperatures at low and mid-latitudes with simultaneous *in situ* ion drifts measured along the satellite orbit. Figure 1.1 gives an historical perspective of NASA's ITM missions launched since 1980. Included are the approximate altitude and latitude regions that pertain to the data collected by each mission.

As can be seen in Figure 1.1, NASA has not launched a high-latitude ITM mission that has focused on the key ionosphere/thermosphere region between 300-450 km since DE-2. The high latitudes at altitudes above 100 km is where significant magnetospheric energy is deposited, where efficient ion-neutral coupling creates a complex interplay of ion and neutral dynamics, and where many critical ionosphere/thermosphere space weather effects originate. This region is a major focus area of the recommended GDC mission, as described herein. The science that GDC investigates cannot be addressed by missions currently in operation or development, such as GOLD, ICON, and AWE, since these missions do not measure quantities at high latitudes or the physical parameters required to address even a subset of the Objectives described in this report. For example, GOLD remotely senses the atmosphere from geosynchronous orbit, providing measurements every 30 minutes of mid- and low-latitude composition and temperature during the day and electron density at night. It does not provide measurements of high latitude drivers, nor the winds that are critical to understanding the dynamics of the system. AWE will remotely sense the atmospheric gravity wave structure around 90 km altitude at night within approximately +/-55° geographic latitude. It will not measure any thermospheric or ionospheric quantities at all. ICON does measure the neutral winds, but with an inclination of only 27°, it can address neither any of the effects of magnetospheric forcing on the neutral winds at high latitudes, nor any aspects of the dynamics of the environment, since it is a single satellite with a 90-minute orbital period. It is only with a dedicated constellation mission that measures key parameters of the thermosphere and the drivers of the system in the polar region that significant progress can be made in understanding how the upper atmosphere dynamically reacts to energy input.

Because the dynamics of Earth's combined ionosphere-thermosphere are global in nature, it needs to be understood as a system: energy added to the system in one location both creates localized perturbations, and also creates responses that have the potential to propagate across the globe, altering the state of the entire system. In order to make significant progress on understanding this complex, dynamical system, comprehensive, systematic measurements of the key physical parameters need to be gathered across the globe in concert with measurements of the driving energy and momentum sources from both the magnetosphere and lower atmosphere. Such a system level approach requires not only globally distributed measurements but also coordinated measurements of regional and localized processes across a variety of scales.

For these reasons, the Decadal Survey called for the next Heliophysics Living with a Star mission to be a multi-probe measurement approach with a distributed array of satellites to transform scientific understanding of the fundamental dynamics of the ionosphere/thermosphere system. Such a distributed system has the power to provide a network of global, synchronized measurements and an array of closely-spaced satellites that enable spatial and temporal variations to be distinguished and various cross-scale coupling processes to be understood for the first time. This mission is GDC.

1.2 Physics of the Upper Atmosphere

The ionosphere and thermosphere consist of the intermingled ionized and neutral gases that coexist above ~100 km and form the outer boundary of the Earth's atmosphere with the space environment beyond.

The two components strongly interact with each other via collisions and charge exchange and are coupled with the magnetosphere above and the atmosphere below. Understanding the state of the upper atmosphere requires the understanding of the individual gases, their dynamics, electrodynamics, and their complex interactions with drivers from above and below. It is the closest, richest, and largest atmospheric and space plasma laboratory that humans have the opportunity to study with multi-point observations. It is also a region of Earth's atmosphere that can influence many parts of technological systems, for example, by causing drag on orbiting satellites, altering pathways for over-the-horizon communication systems for the military and commercial aviation, and causing errors in autonomous location devices used in self-driving cars, construction, and farming equipment. Improving scientific understanding of this region of Earth's atmosphere is critical for making significant progress in the ability to specify, predict, and mitigate the effects of space weather.

In this section, some of the important basic processes that occur within the upper atmosphere are reviewed. The significant unknowns associated with these processes are discussed to better understand the motivation for the GDC mission.

1.2.1 The Importance of Neutral Winds

Of primary importance in increasing scientific understanding of the dynamics of the upper atmosphere is the measurement of the neutral winds. The global-scale wind structure in the upper thermosphere is strongly driven by the day-to-night pressure gradient, with winds blowing from mid-day towards pre-dawn. The winds are believed to be roughly constant above about 200 km altitude, strongly influenced by atmospheric tides, planetary, and gravity wave structures also controlled by viscosity, ion drag, and the Coriolis forces [*Forbes,* 2007]. At low latitudes, the ions are essentially at rest compared to the neutral winds, so ion drag slows down the winds. At high latitudes, plasma convection is usually significantly stronger than the neutral winds, so ion drag tends to accelerate the neutrals. At the same time, viscosity tends to reduce altitudinal gradients in the horizontal winds, forcing the neutrals to be slower than the ions [*Rishbeth*, 1977]. As the neutral wind is accelerated, the Coriolis force tends to cause the winds to rotate. If the vorticity of the ion convection is in the same direction as the Coriolis force, the winds can be accelerated strongly, while if they oppose each other, the winds do not follow the plasma convection This creates a strong dawn-dusk asymmetry in climatological patterns of the neutral winds [*Richmond et al.*, 2003].

Plasma convection is more complicated with significantly sharper gradients, as it is strongly controlled by stresses on magnetic field lines associated with electric fields. Because ions and electrons gyrate around magnetic fields, their motion can be best described as having a parallel and perpendicular component. Along the magnetic field line, the ion flow is strongly driven by collisions with the neutrals, where the neutrals tend to impart momentum to the ions [*Hanson and Moffett,* 1966]. The winds drag ions along field-lines, which often means up and down in altitude, since mid-latitude field-lines are tilted. Perpendicular to the magnetic field, winds, ion-neutral collisions, and internally and externally driven forces (associated with electric fields) strongly control the ion velocity. The resulting plasma convection can arise due to forces involved in the solar wind-magnetosphere interaction, or due to neutral winds at mid and low latitudes, including the neutral wind dynamo at altitudes below about 150 km altitude [*Richmond*, 2016]. Because the driving winds and electric fields change dramatically from the equatorial region to the polar region, the plasma velocity (parallel and perpendicular to the magnetic field) can be extremely complicated and is strongly dependent on both external driving conditions and internal neutral motions, which are controlled by both EUV heating as well as lower atmospheric forcing.

Understanding the control of neutral wind dynamics has been hampered by a lack of measurements. This can be illustrated by exploring the data that was used to make the Horizontal Wind Model [*Drob et al.*, 2015], and newer models of the wind [*Dhadly et al.*, 2017, 2018]. These models combined decades of different satellite and ground-based observations to produce very simple climatological maps that are only dependent on location and F10.7 (i.e., solar EUV), even though modeling studies have shown a strong dependence on many other drivers. Climatological studies of the neutral winds at specific locations have shown a strong dependence on solar wind conditions [*Killeen et al.*, 1984; *Lu et al.,* 1995], but these studies did not have enough data to empirically describe global patterns of winds. These

simple relationships result from large statistical studies or modeling studies, since the availability of neutral wind measurements in the auroral and polar region has been quite limited. Dynamically, the neutral winds are believed to react sluggishly to changes in the ion flows; however, recent work has shown that this may not be the case. *Kiene et al.*, [2018] and *Zou et al.*, [2018] showed that the neutral winds can have time-scales of less than 30 minutes when the aurora increases dramatically. Finally, *Harding et al.* [2019] showed a global model of the thermosphere could not capture the "weather", or day-to-day variability, of the system. It is unclear what drives this variability, since measurements were not available to describe the dynamics of the winds.

What is the neutral wind dynamo?

Above about 150 km altitude, both the ion and electron plasma convection is strongly controlled by magnetic field motion, as described through electric fields. Below this altitude, the collision frequency between the ions and neutrals cause the ion convection to be deflected from the ExB direction, whereas electrons still ExB drift as there are very few collisions between the neutrals and the electrons. This difference in the ion and electron convection drives currents in the lower ionosphere. In particular, at mid and low latitudes, the winds set up a global system of "atmospheric dynamo" currents in the lower ionosphere. Because there are gradients in the winds, conductivities, and magnetic field structure, there can be strong convergence and divergence of horizontal currents. This causes motion of the entire field-line (equivalent to setting up internal electric fields to maintain a divergent free current), modifying the plasma convection above 150 km altitude.

To be able to describe the neutral wind reaction to a geomagnetic storm, a disturbance model was developed that describes in rough terms how the neutral winds change when the activity level increases, but include no dynamics [*Dhadly et al.*, 2018]. There has not been enough data collected to differentiate phases of a storm or anything more subtle than "disturbed" or "not disturbed". Figure 1.2 describes simulated mid- to low-latitude winds resulting from a geomagnetic storm adding energy at high latitudes. This figure shows that the winds are typically directed towards the equator after a storm, since the pressure is increased at high-latitudes which results in a reversal of the normal equator-to-pole pressure gradient. There have been only a few measurements of these disturbance winds [e.g., *Xiong et al.*, 2015], and recent studies using ground-based measurements have noted that contamination may cause confusion in the interpretation of large equatorward winds observed after storms [*Harding et al.*, 2017].

In addition to controlling the dynamics of the thermosphere, the neutral wind directly affects the amount of heating at high latitudes. Frictional heating between ions and neutrals results from their velocity

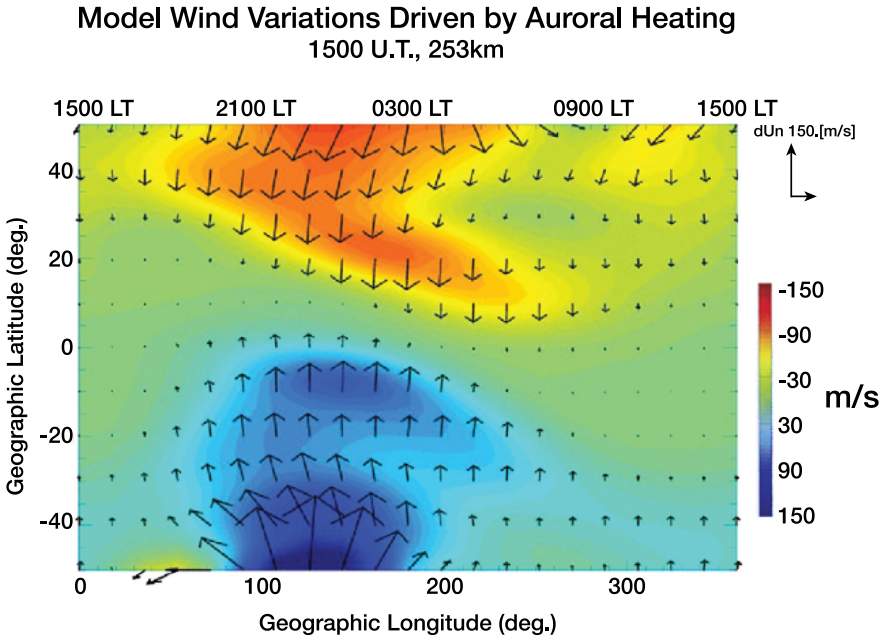

Figure 1.2. Modeled disturbance neutral winds resulting from energy being added at high latitudes. After *Fuller-Rowell* [2008].

difference, and can become the dominant source of energy in the upper atmosphere during geomagnetic storms [e.g., *Thayer et al.*, 1998; *Lu et al.*, 2009; *Prölss,* 2011]. This heating is extremely structured, because both the ion velocities and auroral precipitation, which drive the ion densities in the high-latitude region, are highly structured and their relationship is quite complex [e.g., *Codrescu et al.*, 1995; *Cosgrove and Codrescu,* 2009]. In addition, when there is significant heating, the ions accelerate the neutrals rapidly, reducing the velocity difference and therefore the heating. The balance between all of these factors is extremely complicated. Because there have not been adequate measurements of the neutral winds, scientific understanding of the heating of the IT system has not been possible.

Neutral winds control almost all dynamics within the thermosphere and ionosphere system. The winds advect and redistribute density, momentum, and energy both horizontally across the globe as well as vertically, changing both the composition and temperature of the system in localized regions. In addition, convergent and divergent winds can increase or decrease the temperature and density within the system. To develop a complete understanding of the thermospheric behavior and how this drives change in the ionosphere, the neutral winds must be measured with enough resolution and at a high enough cadence. This has never been done, and is critical to discover the processes that drive the dynamics of the upper atmosphere.

1.2.2 The Importance of Internal Processes

The primary heating source of the thermosphere is the solar extreme ultraviolet (EUV) irradiance, which both directly heats the neutrals and ionizes a portion of them to create the ionosphere. Adding to this energy, sources from below, the atmospheric tides, planetary, and gravity waves within the troposphere, stratosphere, and mesosphere control the density, temperature, and wind structure of the thermosphere below about 150 km. From above, the IT system is driven by solar wind-magnetosphere interactions which add density, momentum, and energy at high latitudes. Each of these processes have different spatial and temporal scales. For example, the EUV and high-latitude forcings are somewhat periodic as the sun evolves in its 11-year cycle and rotates every ~27 days. The EUV heating is global-scale, while the high-latitude drivers have structure across scales from kilometers to thousands of kilometers.

Atmospheric tides, planetary, and gravity waves deposit their momentum in the lower thermosphere, impacting the mean circulation of the upper atmosphere and driving wind-dynamo electric fields in the ionosphere (see side bar), redistributing plasma, and modulating the IT response to the energy input from the solar wind and magnetosphere. Through poorly characterized mechanisms, atmospheric waves influence ion-neutral coupling and therefore coupling to different latitudes and altitudes, and serve to redistribute energy within the IT system. The temporal and spatial scales over which atmospheric waves impact the response of the IT to magnetospheric inputs are not well understood and vary temporally from minutes to interannual and spatially from kilometers to global.

The background EUV input and the drivers from below are punctuated with periods of intense activity caused by solar flares that can last for an hour or two and by geomagnetic storms that can last for a day to a week. During storm periods, the variability in the IT system can transition from being dominated by lower atmospheric drivers to being totally controlled by the solar wind's interaction with the magnetosphere. The dynamics associated with this transition in forcing are not understood because measurements needed to study the dynamics have not been made. Obtaining these measurements and understanding this transition and the internal dynamics within the system during storm periods is one of the main goals of the GDC mission.

1.2.3 The Importance of Composition

The lower boundary of the thermosphere (near 100 km) is close to the homopause, below which the atmosphere is well mixed with all its constituents moving roughly as a single fluid. Within the thermosphere, however, the neutral atmospheric constituents are free-flowing and separate, with their altitudinal profiles differing according to their individual scale heights. The dynamics of the thermosphere are not just controlled by the neutral number or mass density but also strongly by the composition and its dynamics at different altitudes. In addition, the heating and ionization are strongly dependent on the composition, causing altitudinal structuring of the ionosphere.

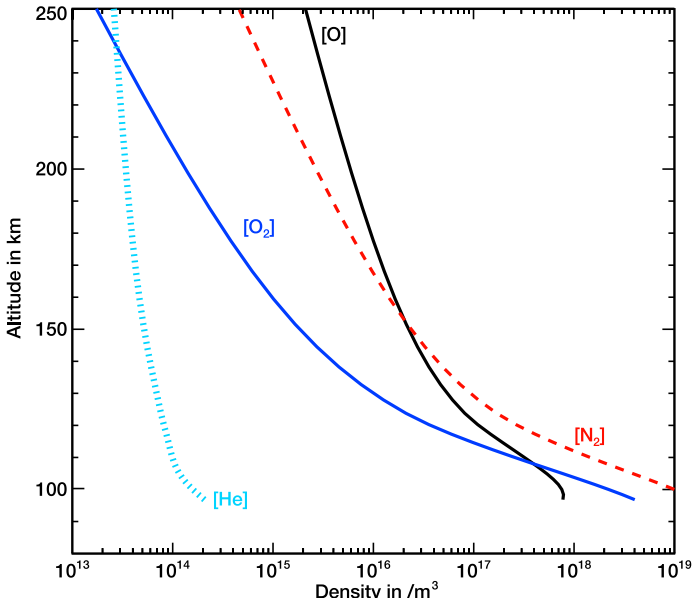

Figure 1.3. An example of the thermospheric composition as a function of altitude from the model presented in *Picone et al.*, [2002].

As shown in Figure 1.3, molecular nitrogen (N_2) is the most abundant constituent in the lower thermosphere. As measurements by the AE satellites showed in the 1970s, above 150-200 km, atomic oxygen (O) takes over, and helium (He) becomes dominant at altitudes well above 500 km [*Bruinsma and Forbes*, 2010a; *Thayer et al.*, 2012]. During geomagnetic storms, the composition is theorized to change dramatically, as shown by remote sensing measurements of dayside airglow, with the column integrated O/N_2 ratio decreasing due to the possible upwelling of molecular species [*Prolss*, 1997]. The composition changes were shown by measurements from DE-1 as well the GUVI instrument on the TIMED satellite [*Meier et al.*, 2005]. In addition, as measurements made by accelerometers on CHAMP, GRACE, and GOCE have shown, the thermospheric mass density increases at a constant altitude during large geomagnetic storms [*Sutton et al.*, 2009]. Such changes could be due to hydrostatic expansion of the thermosphere due to increased temperature, or due to compositional changes, or a combination of the two [*Lei et al.*, 2010a]. Without in situ compositional measurements, the contribution of each is uncertain.

Understanding these compositional changes is important for specification, prediction, and understanding of the ionospheric density. For example, in the ionosphere, the E-region peaks around 105 km altitude and is dominated by NO^+ and molecular oxygen (O_2^+), while the peak of the ionospheric density occurs around 200-450 km altitude and is dominated by atomic oxygen (O^+). The composition of the neutral upper atmosphere is critical in determining the density of the ionosphere, since the atomic oxygen controls the production rate of ions, while the molecular nitrogen controls the loss rate.

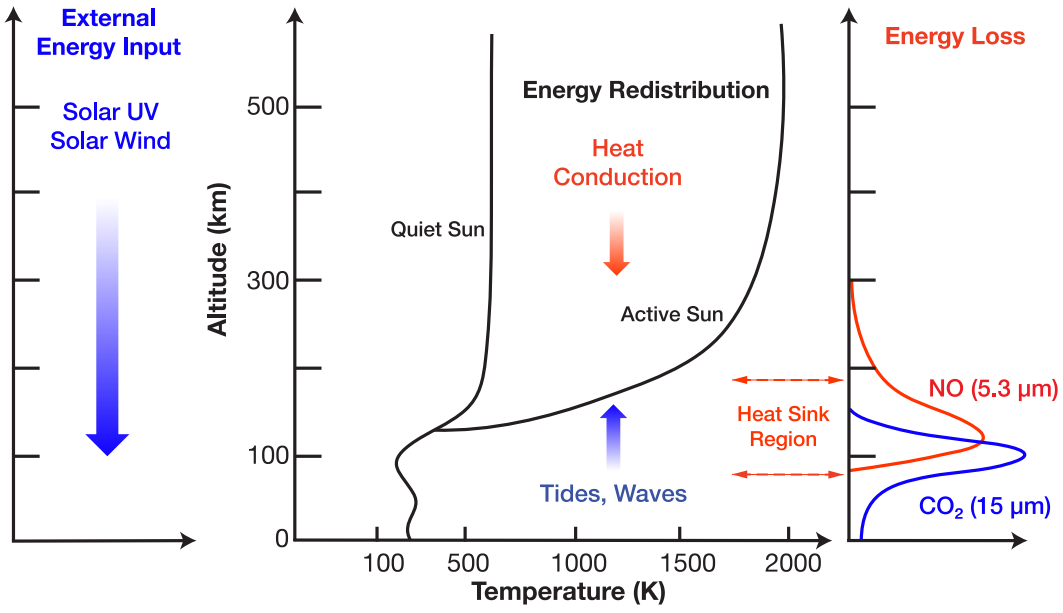

Figure 1.4. The simplified energetics of the thermosphere. The primary source of heat in the thermosphere is solar EUV irradiance (left), high-latitude driving (left), and waves from below (middle). Energy is redistributed with height by heat conduction (middle), and dissipated through radiative cooling by NO and CO_2 (right). After *Mlynczak et al.* [2018].

In addition, the primary loss mechanism of the energy in the upper atmosphere is through Nitric Oxide (NO) and Carbon Dioxide (CO_2) radiative cooling. While the CO_2 density is relatively stable on a day-to-day basis, the NO density is highly variable and chemically active in the thermosphere, and its density depends on solar EUV flux and auroral/high-energy electron precipitation. As such, the radiative cooling by NO is one of the most difficult processes to understand and to predict accurately. During geomagnetic storms, the density of NO increases dramatically, due to the increased precipitation. This increased density radiatively cools the atmosphere, even as more energy is being added. Any imbalance in the energy causes the thermosphere to heat or cool at different rates. Understanding the dynamics of the heating and cooling of the atmosphere is highly dependent on knowing how much energy is entering the system (i.e., high-latitude forcing) and how much energy is leaving the system (i.e., radiative cooling). Without obtaining an accurate assessment of the energy inputs or outputs, it is almost impossible to capture the dynamical reaction of the thermosphere to energy inputs, and scaling factors are typically added to models to compensate for this lack of understanding [e.g., *Deng and Ridley,* 2007].

Due to the lack of composition observations, except for short-term observations during the 1960s-1980s, and remote sensing of column integrated compositional values (which can be difficult to interpret), scientific understanding of compositional change in the thermosphere is severely limited. **GDC will advance the understanding of how compositional changes in the thermosphere control both the ionospheric density as well as the heating and cooling rates during geomagnetic storms.**

1.2.4 The Importance of Structuring of the Energy Input

The magnetosphere and solar wind are coupled to the ionosphere at high latitudes via the geomagnetic field. Energy resulting from the solar wind-magnetosphere interaction is deposited there and becomes the dominant driver of the upper atmospheric system during large geomagnetic storms. This linkage provides a pathway for particle, momentum, and energy coupling between the magnetosphere and upper atmosphere [e.g., *Kelley,* 2009; *Knipp et al.*, 2004; *Prölss,* 2011]. Particles are exchanged in the form of electron and ion precipitation into the thermosphere, with ion outflow adding mass to the magnetosphere. Electron precipitation drives significant ionization in the high-latitude region, while magnetic stresses due to the solar wind-magnetosphere interaction drive plasma convection within the ionosphere, imparting momentum and energy to both ions and neutrals, influencing the neutral winds and temperatures at high latitudes. The existing paradigm for how energy input from the solar wind-magnetosphere interaction influences the global IT system is based on empirical climatological patterns that show a uniformity that does not exist during geomagnetically active times. Studies have shown that energy input at high latitudes is delivered over multiple spatial and temporal scales, which elicit dramatically different responses in the IT system [*Codrescu and Cosgrove*, 2005]. Due to a severe lack of measurements, understanding of how structuring of the energy input drives the local, regional, and global IT dynamics is extremely limited. In order to make significant progress on understanding the dynamics of the system, new measurements of the multi-scalar drivers and response must be made.

1.2.5 The Importance of Energy Transport Through the Global IT System

Energy input into the IT system at high latitudes alters the ambient temperature, density, composition, and wind structure. When the energy input increases dramatically, the responses are communicated to the global atmosphere via large-scale horizontally propagating waves called Traveling Atmospheric Disturbances (TADs), for the neutral gas, and Traveling Ionospheric Disturbances (TIDs), for the plasma [e.g., *Bruinsma and Forbes*, 2007; *Lei et al.*, 2008, 2010b]. Due to a lack of measurements at adequate temporal and spatial resolution, the dynamics of TAD/TID formation, evolution, and decay are not understood. It is not known if the amplitudes and propagation characteristics of these waves are dependent on local time, season, energy input, or background atmospheric structure caused by, for example, tides and gravity waves. It is also unclear whether structures observed in the polar cap are driven by local energy input or propagating waves. Finally, it is unclear whether waves, structure, and variability observed throughout the global IT system are driven by waves from the lower atmosphere or internally generated

waves at high-latitudes that propagate to lower latitudes. The relationship between TIDs or TADs is not currently understood, although they are typically assumed to be the manifestation of the same trigger in the two different gases of the IT. GDC will globally measure both TIDs and TADs, providing for the first time the capability to understand energy transfer simultaneously through the gases, the origin of the structures, the propagation direction, and the evolution and decay of the structures. GDC will dramatically increase scientific understanding of these processes.

1.3 On the Scale Sizes In the Thermosphere and Ionosphere

The GDC mission goals and objectives demand a description of the coupled I-T region at all latitudes between the magnetic poles in both hemispheres. The sampling strategy to achieving the goals is most easily visualized by the acquisition of latitudinal profiles of the key parameters, with a resolution that allows the most important gradient scales to be identified. In the ionosphere the smallest gradient scale lengths are associated with plasma irregularities and can be just a few centimeters. In the neutral atmosphere the viscous scale lengths are much larger. In order to bound the science objectives and measurements required to meet them, we have specified latitudinal resolutions of 0.1° (~10 km) and 0.25° (~25km) for the key state variables describing the plasma and the neutral gas respectively. Using this approach, the latitudinal extent of a particular region to be studied is not a driver of the sampling strategy. However, the need to sample the same latitude range, almost simultaneously, over a range of local times or longitudes defines the azimuthal extent of the investigation as global, regional or local. For example, the need to simultaneously sample latitudinal profiles of the neutral wind distributed in local time between 0 and 24 hours, defines a global strategy with latitude profiles largely spaced in local time. Describing the cusp, which may occupy a local time extent of less than 4 hours demands a regional strategy with more closely spaced local times. Separating the spatial and temporal ambiguity in a small auroral emission region requires a local sampling strategy for which almost the same local time is repetitively sampled.

These different sampling strategies for a satellite constellation, local, regional and global scale, will be a theme throughout the different sections of the report, since it is critical to understand how the IT system responds to both smaller scale energy inputs and as a global system.

1.4 Summary

The Geospace Dynamics Constellation mission will dramatically improve scientific understanding of how the upper atmosphere reacts to energy input from above and below by addressing two overarching science Goals:

1. **Understand how the high latitude ionosphere--thermosphere system responds to variable solar wind/magnetosphere forcing.**

2. **Understand how internal processes in the global ionosphere/thermosphere system redistribute mass, momentum, and energy.**

GDC will accomplish this by having a constellation of satellites in multiple planes measuring the dynamic evolution of both the drivers and the response of the system to those drivers. It will be the first Heliophysics mission to adequately track how the upper atmosphere absorbs and processes energy and momentum to produce structuring in the atmosphere across a variety of temporal and spatial scales. GDC will revolutionize current understanding of the upper atmosphere by providing a multi-point, evolving perspective on the system as a whole.

Ionosphere-Thermosphere Space Weather Processes Addressed by GDC

The ionosphere-thermosphere system is the site of a number of critical space weather phenomena with direct societal relevance. Each of these, discussed below, will be mitigated with improved models based on the data collected by the GDC mission.

Atmospheric Drag, Collision Avoidance, and ISS Orbit Maintenance

The uncertainty in the current knowledge of the neutral atmosphere and its variations, particularly in response to solar EUV changes and those associated with solar variability and magnetic storms, poses a major dilemma for engineers who need to carry out both orbit and attitude maintenance of spacecraft assets. GDC is poised to provide unprecedented measurements of how the neutral density varies as a function of latitude, longitude, local time, season, and solar EUV. Knowledge of the neutral density is also important to predict the effects of space "debris" in orbit, including meteoritic material (Figure 1.5).

Scintillations That Disrupt Radio Wave Navigation (GPS), Communication, and Radar Systems

Radio waves propagating through the ionosphere can be altered dramatically or even disrupted due to strong gradients in the plasma density. These signals originate from satellites, such as GPS and commercial geosynchronous communication satellites, and high frequency systems on the ground, such as those used to track satellites and those used for over the horizon communications. These include systems utilized by the Department of Defense, commercial aircraft, maritime assets, and a wide variety of other systems that are coming online, given the ubiquity of GPS. Understanding both the cause and the nature of the plasma density variations and their structure, including the unstable spectrum of density waves that scatter and disrupt radio waves, is an anticipated result of the GDC mission. Such irregularities also include those associated with traveling ionospheric disturbances (TIDs) and traveling atmospheric disturbances (TADs) that abound within the IT system.

Induced Currents in Power Grids

Long, ground-based conductors, such as power grids and pipelines, have induced electric fields caused by rapidly varying high-latitude currents in the ionosphere associated with solar variability and magnetic storms. These induced currents can cause corrosion of pipelines and disrupt the electrical power grids. GDC will provide important information regarding how these currents originate and evolve in time.

Rapid Ionospheric Plasma Density Variations and Severe Spatial Gradients During Magnetic Storms

During magnetic storms, the ionospheric plasma density can vary by orders of magnitude and on short time scales (< few hours). In some cases, the entire ionosphere is driven to altitudes of many hundreds of km above its normal height. The abrupt changes in the plasma density and its associated severe spatial gradients during magnetic storms affect radiowave communication and over-the-horizon radars. GDC will enable better predictions of the response of the ionosphere to magnetic storms, including local time, altitude, and longitude variations.

The Ionosphere-Thermosphere and Solar Variability

The neutral and plasma density within the ionosphere/thermosphere are both dependent on solar EUV variability. They also respond dramatically to solar flares and subsequent magnetic activity which result in sustained, impulsive, and unpredictable consequences in the near-earth region of space. Subsequently, all of the processes listed above are affected by these solar driven variations. In this manner, the sun's unpredictable "temperament" is at the core of many of the ionosphere/thermosphere space weather processes and illustrate the need to gather comprehensive IT measurements in concert with measurements of the sun and its variations.

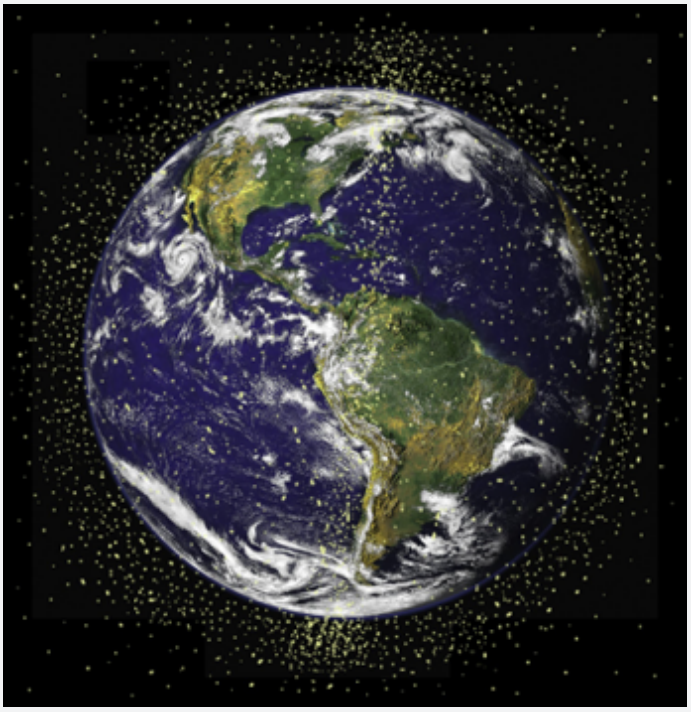

Figure 1.5: Illustration of identified and tracked objects in low-Earth orbit. [Credit: NASA]

2 GDC MISSION SCIENCE

2.1 GDC Science Goal Overview

The complex physical processes creating and dominating the dynamics of the ionosphere-thermosphere (IT) system are driven by multiple sources ranging from solar EUV to solar wind/magnetosphere coupling at high latitudes to atmospheric tides and gravity waves that propagate into the system from below. The close coupling of the neutral components and plasma in the near-Earth environment is unique in that, depending on the time, location, and scale-size, either the ionospheric or thermospheric processes may dominate and drive the other.

Understanding the IT system and its response to external forcing has been, to date, limited by sparse, non-coordinated measurements of IT parameters and drivers. The Geospace Dynamics Constellation (GDC) mission is designed to provide simultaneous, global observations of IT parameters and their drivers that will enable critical new science research to mature IT system models for more reliable understanding of space weather and its effects that meet humanity's emerging space needs.

Goal 1 focuses on fundamental interaction processes inherent in the coupling of magnetospheric energy inputs to the **high latitudes**, a dominant driver of global dynamics in the IT system. Understanding these key interactions is essential if we are to accurately parameterize the interaction physics in models as needed to improve space weather nowcasting and forecasting.

Goal 2 focuses on fully understanding the role of fundamental processes inherent to the **global IT system** with a particular emphasis on understanding the global response to magnetic activity and storms. To this end, the Objectives seek to understand how the IT system departs from a baseline state, and how these significant departures produce space weather impacts with societal consequences.

Detailed descriptions of each Objective are presented in the following sections, with lists of scientific parameters and physical measurements necessary to achieve closure. The measurement requirements for each Objective are explicitly discussed independent of the other Objectives. This introduces some redundancy into the text, but allows readers to evaluate all of the Objectives on their own merits. Two summary tables that capture all of the physical parameter requirements and spatial and temporal requirements are included in Section 2.6.

As described in Chapter 1, GDC has two focused science goals, with closable Objectives:

Goal 1: Understand how the high latitude ionosphere-thermosphere system responds to variable solar wind/magnetosphere forcing.

Obj. 1.1: Determine how high-latitude plasma convection and auroral precipitation drive thermospheric neutral winds.

Obj. 1.2: Determine how localized, coherent plasma density features arise and evolve.

Obj. 1.3: Determine how neutral winds, auroral precipitation, and collisional heating drive high-latitude neutral density structures.

Obj. 1.4: Determine how atmospheric tides and gravity waves influence the IT response to magnetospheric inputs.

Goal 2: Understand how internal processes in the global ionosphere-thermosphere system redistribute mass, momentum, and energy.

Obj. 2.1: Determine the relative importance of penetration electric fields and disturbance winds in driving plasma density variations at mid- and low-latitudes during geomagnetic storms.

Obj. 2.2: Identify the processes that create and dissipate propagating structures within the ionosphere and thermosphere during active and storm conditions.

Obj. 2.3: Determine the connections between winds and neutral density/composition variations at mid- and low-latitudes during geomagnetic storms.

Obj. 2.4: Characterize the spatial and temporal variability in IT parameters that results from the transfer of momentum and energy from atmospheric tides and gravity waves.

Obj. 2.5: Quantify the roles of radiative cooling and neutral winds in dissipating thermospheric energy.

Obj. 2.6: Determine how hemispheric asymmetries in the Earth's magnetic field, seasonal variations, and magnetospheric input affect the IT system.

2.2 Science Goal 1 and Objectives

Goal 1: Understand how the high latitude ionosphere-thermosphere system responds to variable solar wind/ magnetosphere forcing.

The four Objectives each focus on understanding the dynamical high latitude response to energy input from the magnetosphere above and the atmosphere below into the IT system. Each Objective focuses on a different aspect of the response to the drivers, allowing a systematic approach to understanding the non-linearly coupled dynamics.

Each of these Objectives are described in detail below.

Objective 1.1: Determine how high-latitude plasma convection and auroral precipitation drive thermospheric neutral winds.

Understanding the drivers of thermospheric neutral winds is critically important to being able to describe the dynamics of the global geospace system. The neutral winds influence nearly every aspect of the coupled thermosphere-ionosphere-magnetosphere system:

- the winds advect gradients in density, composition, momentum, and energy in the thermosphere;
- convergence and divergence in the winds drive changes in density, composition, momentum, and energy;
- neutral winds act to drag ions up and down inclined field lines, changing the density of the ionosphere;
- neutral winds in the lower thermosphere drag ions across field lines, driving ion flows in the F-region ionosphere, thus altering the plasma density structure dramatically; and
- the winds non-linearly regulate coupling between the magnetosphere, ionosphere, and thermosphere through ion drag and frictional heating, which serves as a primary energy sink in the near-Earth space environment.

For these reasons, understanding the evolution of the thermospheric neutral wind is of critical importance for determining how the global system reacts to energy inputs and even its day-to-day variability.

At high latitudes, the magnetospheric interaction with the solar wind imposes a two-celled convection pattern on the ionosphere plasma, which can be highly distorted depending on the solar wind IMF [e.g., *Weimer*, 2005; *Cousins and Shepherd*, 2010]. This plasma circulation sets the neutral upper atmosphere in motion via ion drag. Hence, as it is controlled by magnetospheric forcing, the ion drag is quite dynamic and is influenced by both plasma convection and the ion density, which itself is partially determined by auroral precipitation. In addition, because the ion drag both changes and is dependent upon the speed of the winds, the forcing is dependent on the persistence of the ion convection features. The forcing is complicated by the fact that the neutral density is approximately 1000 times larger than the ion density, so it takes a long time to accelerate the neutrals. The time constants of neutral wind change are uncertain, with new studies, using a network of Scanning Doppler Interferometers [*Conde et al.*, 2018], casting doubt on the long-held view of ~3-hour time-scales [*Kiene et al.*, 2018; *Zou et al.*, 2018].

An important consequence of neutral and ionized gas motions is the frictional or Joule heating. This heating depends linearly on the plasma density and on the square of the relative motion of the gasses. Pressure gradients resulting from localized Joule heating drive winds that contribute to the neutral flows already set in motion by ion drag and are an important component of the physical processes responsible for the ambient neutral flow patterns and their relation to the external drivers [e.g., *Thayer et al.*, 1995; *Thayer*, 1998, 2000; *Strangeway*, 2012]. Joule heating may be significantly increased by structured electric fields or plasma drifts compared to the neutral gas motions, as shown by *Codrescu et al.* [1995] and others. In addition, heating by particle precipitation can cause gradients in pressure that drive strong flows. The systematic contribution of Joule and auroral precipitation heating to the ambient flow patterns has not been adequately determined with measurements, since the gradients in pressure need to be measured in order to describe the forcing on the neutral winds, and these measurements have not been made. For example, balloon-based measurements of the neutral winds near the cusp show flows that are in the opposite direction as predicted by models [*Wu et al.*, 2012]. This

indicates that the models are not including the correct heating, whether it is Joule or particle precipitation, in the cusp region in order to capture the gradients in pressure and the resulting winds.

To illustrate how the plasma motions driven by the magnetosphere in the high latitude ionosphere set the neutral upper atmosphere in motion via ion-neutral collisions, the left side of Figure 2.1 shows simultaneous measurements of the ion drifts and the neutral wind measured by the Dynamics Explorer-2 (DE-2) satellite as it transited the polar region near 350 km altitude [*Killeen et al.*, 1984]. The neutral winds essentially track the ion drifts in the evening sector and within the polar cap, yet diverge considerably in the morning sector. Where the two vectors are not aligned is where Joule heating and compositional changes occur, as shown on the right hand side of Figure 2.1, which displays other measurements gathered in situ by instruments on the DE-2 satellite during this same event. Notice that after about 23:36 UT, the ion temperatures increase as the drifts diverge. This is also a region where compositional changes were observed; most likely caused by thermal expansion. Whereas such DE-2 data are extremely valuable for "case studies", the available data were extremely limited.

The influence of magnetic activity on high latitude winds is dramatically illustrated in Figure 2.2, which shows DE-2 satellite cross-track wind data (i.e., winds available in the plane perpendicular to the satellite motion) plotted alongside the AE index and the IMF Bz and By components [Killeen and Roble, 1988]. Here, available passes are every 2nd or 3rd orbit, or 3-4.5 hour spacing. Notice that, in general, two-celled structures appear in the passes during quiet periods, before 9 UT but the patterns and wind amplitudes change dramatically when the IMF Bz turns negative around 10 UT. This results in strong anti-sunward flow. That the change in the interplanetary magnetic field has such a remarkable effect on the winds **illustrates the close connection of the upper atmosphere to the driving solar wind/magnetosphere and underscores our need to understand, with systematic, comprehensive measurements, how these coupling processes work.** While DE-2 provided tantalizing results such as these, the dynamics of the system and much of the detail was lost because of remeasurement times of 3-4.5 hours.

Despite the importance of the neutral winds, our knowledge base is extremely limited, as is our understanding of how the winds are coupled to large scale plasma convection features of magnetospheric origin. This is primarily because we have not had extensive measurements of the neutral winds, especially

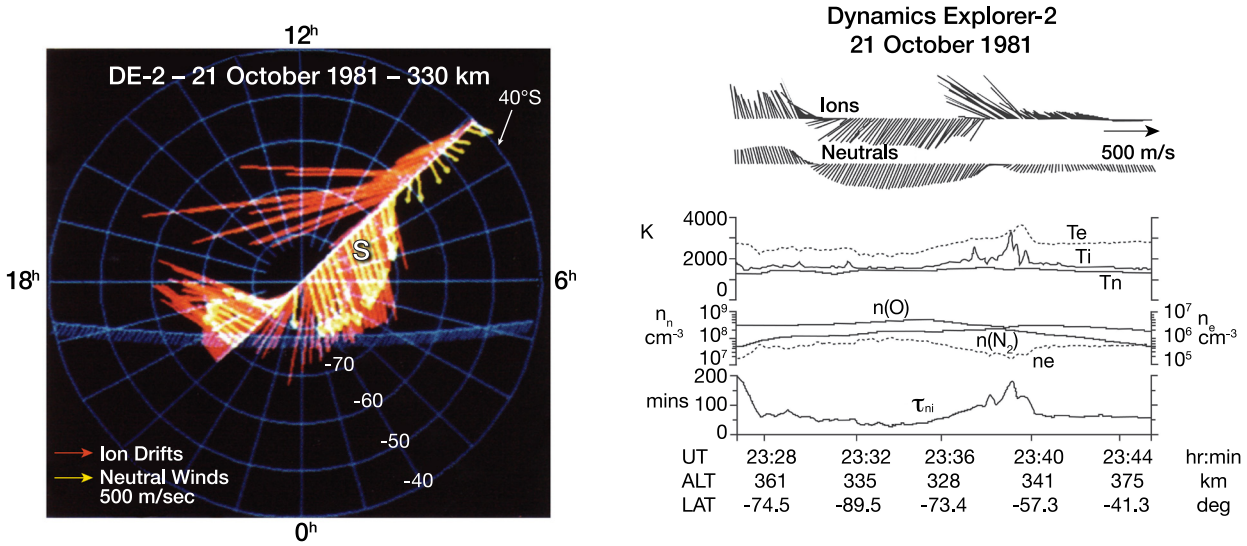

Figure 2.1. DE-2 observations of colocated neutral and plasma observations during a single pass through the high-latitude region. **(left)**: The neutral wind and ion drift vectors measured by Dynamics Explorer-2 on a perigee pass over the southern polar region, plotted in geographic polar coordinates. The neutral winds are coded by the yellow arrows, and the ion drifts are coded by the red bars. The curved blue line represents the location of the solar terminator. **(right)**: Measurements along the track of DE-2 during the orbit shown on the left side. The ion drifts and the neutral winds are shown in the top two traces. The second panel shows the electron, ion, and neutral temperatures measured along the track, and the third panel shows the atomic oxygen and molecular nitrogen number densities (left-hand scale) and the electron density (right-hand scale). The bottom trace shows a model ion-neutral coupling time constant. After *Killeen et al.* [1984].

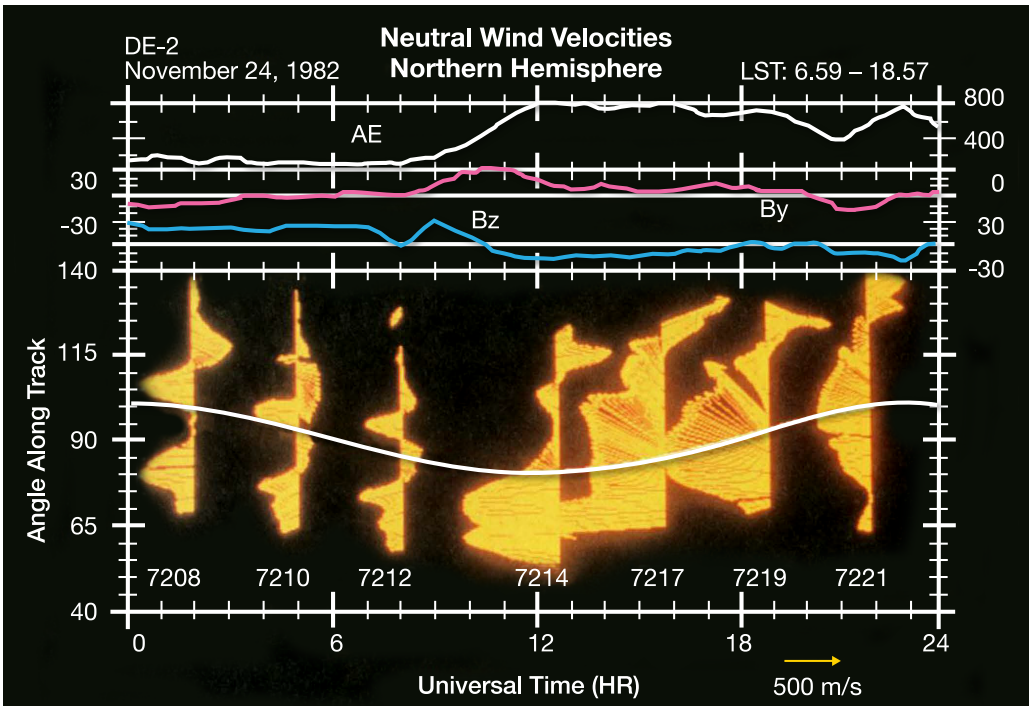

Figure 2.2. Neutral wind observations (yellow arrows) made on the seven referenced DE 2 orbital passes over the northern hemisphere polar region just prior to and following the major geomagnetic disturbance of November 28, 1982. The winds are plotted as a function of angle along the track (equivalent to latitude; north pole at 90° angle along track) and UT. Top panels show the variations of the AE index and the IMF Bz and By components during this period. The neutral winds are plotted such that the sunward direction is toward the right of the figure and dusk toward the top. From *Killeen and Roble* [1988].

with measurements that would support understanding of what controls the dynamics of the winds, such as plasma convection, ion density, and neutral temperature. While the DE-2 satellite had these types of measurements, the mission was limited in sample space and duration. Researchers are forced to combine large databases of disparate (in time, location, and instrument type) wind measurements to create statistical patterns of the high-latitude winds, describing roughly the climatology, but not the dynamics nor even the relationship with the drivers. As an example, an empirical fit of almost all neutral wind data available in the northern polar region above 200 km altitude gathered from both ground-based and satellite instruments over more than 30 years was produced by *Dhadly et al.* [2017a,b]. These studies only included about 650,000 measurements of the winds in total over the 30 years and over the northern and southern polar regions, and is roughly equivalent to only a single measurement every 20 minutes. **This is a data-starved region.**

Given the extreme lack of measurements, researchers have turned to global models of the coupled ionosphere and thermosphere to understand the drivers of the winds. *Killeen and Roble* [1984] showed that the winds

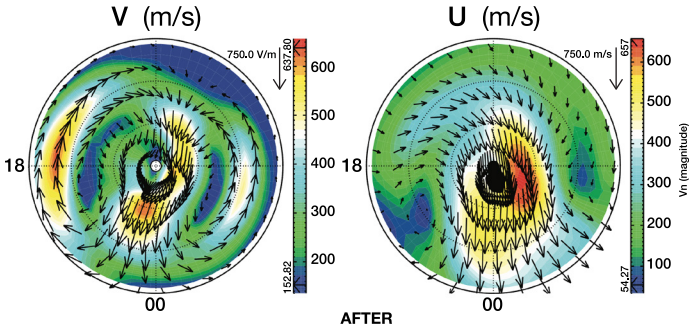

Figure 2.3. GITM simulation results for plasma convection (left) and winds (right) over the northern hemisphere at 400 km altitude. After *Deng and Ridley* [2006].

are driven primarily by four forces: pressure gradients, ion drag, Coriolis, and viscosity. *Deng and Ridley* [2006] showed similar dependencies for the winds. These four forcing terms are all dynamic and interdependent. For example, when the plasma convection changes dramatically (such as at the start of a geomagnetic storm), the ion drag increases dramatically over the other three forces. But, at the same time, the difference in ion and neutral velocities drives strong heating, which changes the pressure distribution in the thermosphere, causing winds to be driven by the gradient in pressure. Thus,

because the neutral winds increase to follow the ion flow, the ion drag term decreases in importance, while the Coriolis term, which is dependent on the wind speed, increases. This dynamic interplay between the different forcing terms continues until the ion convection changes again, which can be a few minutes to a few hours later. If the ion convection stays strong for long periods of time (~3 hours or more) the neutral winds can reach a significant fraction of the plasma convection speed [e.g., *Deng and Ridley*, 2006]. If the ion forcing is turned off, or dramatically reduced (due to a change in the configuration of the magnetosphere), the winds can drive the plasma convection. This is termed the flywheel effect [*Deng et al.*, 1991] and can drive energy from the ionosphere back towards the magnetosphere, as shown through a negative Poynting flux [*Kelley et al.*, 1991].

Physics-based model results of the ion convection (left) and neutral winds (right), shown in Figure 2.3 indicates that the neutral winds roughly follow the ion drifts across the pole and have some return flow towards the dayside on the dusk side, but no return flow on the dawn side. Thus the model shows that while the ion convection is roughly symmetric from dawn to dusk, the neutral winds are not, due to the vorticity combined with the Coriolis force. When the neutral winds from the physics model are compared to the empirical model, significant differences exist: the flow over the pole is much too strong in the model, the return flow near dusk is stronger in the empirical model, and the dawn-side flow has an extremely strong day-to-night pattern in the empirical model compared to the physics-based model.

These differences indicate that even on a climatological scale, we do not understand the connections between the thermospheric winds and the major drivers. It is unclear whether this is due to insufficient data describing the wind field, from the driving of the model with poorly specified ion convection pattern and auroral precipitation patterns, or whether there are physical processes that the models are not including. This lack of knowledge has significant ramifications for our understanding the entire system, since, as described in many of the other Objectives, the neutral winds drive density, composition, and temperature changes that can dramatically alter the thermosphere and ionosphere both.

The dynamical evolution of the neutral winds is critically important for our understanding of how the globally coupled ionosphere-thermosphere system evolves during active time periods, and measurements made by GDC will dramatically improve our understanding of these processes. With multiple satellites in different orbit planes, GDC will reveal the evolution of the neutral winds and its dependence on the external drivers, revolutionizing our understanding of the upper atmosphere.

To determine how the high-latitude convection and auroral precipitation drive thermospheric winds, the different forcing terms that control the neutral momentum must be measured. The terms are:

- Ion Drag: The ion drag includes the ion and neutral velocities, the ion density and composition, the neutral density and composition, and the ion and neutral temperatures to determine the ion-neutral collision frequency.

- Pressure Gradient: The pressure gradient includes the neutral density and temperature. Gradient scales of 0.5° in latitude and 15° in longitude are directly comparable with the outputs of coupled model capabilities [e.g. *Ridley et al.*, 2006; *Lei et al.*, 2018; *Liu et al.*, 2018], while global maps of the pressure and the neutral wind can be used to establish the relative importance of this force.

- Coriolis: The Coriolis force is dependent on the neutral wind velocity, the rotation rate of the Earth, and the position at which the measurements are taken.

- Viscosity: The viscosity is dependent on the vertical profile of the neutral wind. The horizontal wind is often assumed to be constant above about 200 km altitude. Occasional measurements at two different altitudes simultaneously will determine whether this approximation is appropriate and under what conditions it is violated.

The forcing terms, and therefore the winds, will be highly dependent on latitude, longitude and local time through the influence of solar zenith angle, auroral precipitation, ion convection, and Coriolis effects. Therefore, measurements distributed in local time will allow simultaneous exploration of the forcing terms in a global-scale mode.

Remeasuring a 15°-longitude region within 30 minutes will allow newly-observed short evolution times to be examined [*Conde et al.*, 2018].

Scientific Measurements *Obj. 1.1*

Forcing Physical Parameters: plasma velocity vector, neutral wind vector, cold plasma density, fractional ion composition, neutral density, neutral composition, neutral temperature, electron auroral characteristics, vertical ionization and heating rate profile, electromagnetic energy flux

Response Physical Parameters: neutral wind vector

Measurement Characteristics:

- Timescales: From 30 minutes (rapid local evolution) to several days (global storm evolution); different seasons and activity levels;
- Local time coverage: capture differences on global scale (0-24 hrs/3 hr res.); gradients in local time on regional scales (6 hrs/2 hr res.).
- Latitudinal coverage: poleward of 45° latitude, 0.25° res.
- Altitudinal coverage: measurements above 250 km but below approximately 500 km are desired; occasional measurements that are co-located but altitudinally separated by less than 2 scale heights (approximately 100 km)

Objective 1.2: Determine how localized, coherent plasma density features arise and evolve.

The high-latitude F-region ionosphere is home to a number of localized plasma density features, typically appearing as regional-scale structures (i.e., with horizontal scale sizes ranging from 100 km to 1000 km), confined either in latitude only or in both latitude and local time. These features are associated with energy transfer from the solar wind and magnetosphere and with the regulation and re-organization of high-latitude dynamics. Due to the long life-times of the F-region plasma, the density structures that arise continue to evolve in response to variations in external forcing and interaction with the background IT system, including effects of ion-neutral coupling [e.g., *Crowley et al.*, 2000].

Although the persistent plasma density features of interest to us here are observed to extend to lower latitudes, the primary driving processes are currently understood to originate at high latitudes. The fact that energy enters the system in the form of auroral particle precipitation, which drives ionization, and that the F-region plasma is strongly influenced by the ever changing convection leads to strong structuring of the plasma within this region.

One such feature is called Storm-Enhanced Density (SEDs) structures which are observed to extend poleward from mid- to high-latitudes during the recovery phase of a storm [*Foster et al.*, 2002]. SEDs have been observed to be associated with expanded and enhanced plasma convection in the ionosphere from mid to high latitudes. They have been topologically mapped to the plasmaspheric erosion plume during times of strong magnetospheric driving and convection [*Foster et al.*, 2002], but the physical mechanisms that generate them are not understood. While different processes have been discussed and modeled to create SED features [*Heelis et al.*, 2009; *Lin et al.*, 2005; *Zou et al.*, 2014] there are presently insufficient observations to verify the existence of variable convection patterns and storm induced wind systems that might be the drivers. One feature that is thought to strongly influence the creation of SEDS are Sub-Auroral Polarization Streams (SAPS), resulting from magnetosphere ionosphere coupling, which are latitudinally narrow structures that persist for several hours, evolving with the storm phase [*Foster and Vo*, 2002].

Walsh et al. [2014], using simultaneous in situ and ground observations, showed that an SED, evidenced by a TEC tongue of ionization (as shown in Figure 2.4), matched the location of a plasmaspheric erosion plume and correlated with the bursty generation of polar cap patches (SEDs that have been broken up into isolated plasma density enhancements). They argued that the cold plasma from the plume eroding toward the magnetopause modified the reconnection rate there, creating bursts of reconnection that generated the polar cap patches within the cusp region that subsequently moved across the polar cap. In addition, auroral precipitation can produce high plasma density inside the cusp [*Walker et al.*, 1999], thermal ion upflow in the cusp [*Burchill et al.*, 2010], hot polar cap patches [*Zhang et al.*, 2017], and traveling ionospheric disturbances [*Lyons et al.*, 2019] which are all manifestations of plasma density structures reflecting the changing convective history of the plasma. Such dense plasma signatures can decay as a result of

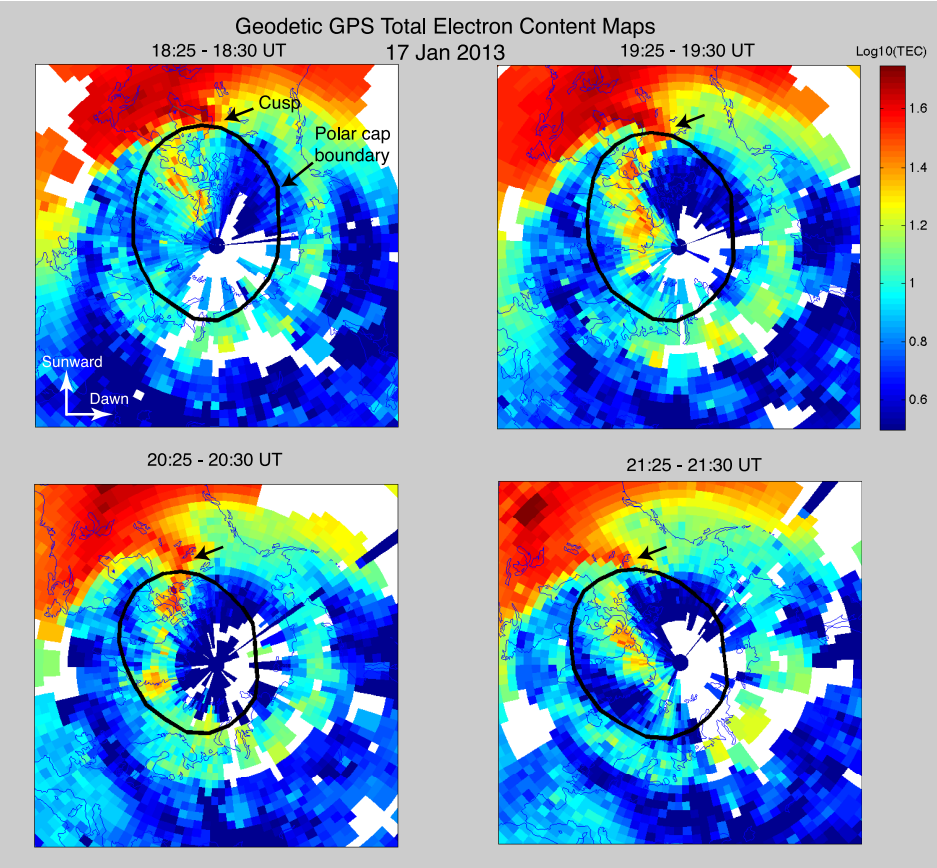

Figure 2.4. GPS TEC maps showing temporal evolution of the SED plume at noontime cusp. The color scale shows TEC units (TECU) where 1 TECU = 10^{16} electrons/m^2. The plots are oriented so that local noon is up in each panel. The plume persists for a number of hours; the black arrow indicates the position of the cusp signature in the TEC data. After *Walsh et al.* [2014].

the ionosphere – thermosphere interaction through ion-neutral interactions or by recombination [*Hosokawa et al.*, 2011], or they can travel significant distances in the form of traveling ionospheric disturbances [e.g., *Jonah et al.*, 2018].

The impact of SEDS and SAPS on the thermosphere is also poorly understood despite the importance of feedback between the thermosphere response and the ionosphere. If the SAPS flow appears as a latitudinally narrow feature with flow speeds exceeding 2000 m/s then strong frictional heating occurs and changes in ion and neutral composition result from the changing chemistry [*Zhu et al.*, 2016]. The existence of strong spatial gradients in the plasma density and velocity associated with SED and SAPS have significant impacts on space-based navigation and communication signals [*Coster et al.*, 2007].

The polar cap region also features plasma density structures that can be caused by enhancements in F-region ionization created by particle precipitation and variations in the convective flow through the cusp, or SEDs that are drawn into the polar cap by periodically changing convection. An example is shown in Figure 2.4. These enhancements, referred to as plasma patches, frequently exhibit plasma density increases of a factor of 10 or more and subsequently convect across the polar cap, representing a significant local enhancement of the ion drag force on the neutral gas [*Gardner and Schunk,* 2008]. The impact of these regional-scale structures on the neutral atmosphere may extend well beyond the localized plasma enhancement, but this has not been investigated. Because the plasma density increases and decreases significantly across these regions, the collisional coupling between the ions and neutrals also changes, possibly driving regions of intensified or reduced heating, depending on the change in plasma density. The formation, evolution and impact of these structures has not previously been fully explored due to the difficulties associated with observing the dynamically evolving moving structures.

In order to understand the physical processes that generate and evolve plasma density features, the connections between these features and magnetospheric processes, and the impact of these features on the thermosphere, we must measure the large-scale reconfiguration of convection and neutral winds. Understanding the formation of plasma patches requires determining the temporal evolution of plasma and ionization features at smaller scales. The possible relationships between these two processes must be further investigated.

Several forcing terms need to be measured to understand how regional-scale plasma structures originate and evolve:

- Plasma Convection Velocity: Transport perpendicular to the magnetic field moves plasma across vast distances and can drive structuring when the convection changes. Transport parallel to the magnetic field changes the recombination rate by moving the plasma into regions of different neutral density and composition.

- Horizontal neutral wind velocity: The neutral wind can drive plasma along the magnetic field line. Measuring the winds would provide a physical understanding of what is driving the field-aligned plasma convection.

- Vertical ionization altitudinal profile: The plasma density will increase directly in regions of auroral precipitation producing spatial gradients that can be advected by convection orthogonal to the auroral region.

- Ion, electron, and neutral temperatures: Changes in the ion, electron, and neutral temperatures lead to changes in chemical reaction rates, which increase or decrease plasma density. These changes in temperature are often associated with particle and electromagnetic energy inputs from the magnetosphere.

- Neutral composition: thermospheric compositional changes can lead to changes in plasma densities by altering the balance between source and loss terms. These are typically captured by the densities of O and N_2, which are the most important neutral species in determining the source and loss terms.

Structures in the ionosphere typically develop on time-scales of order 30 minutes to several hours. The spatial scales that need to be measured are diverse, since the features have varying characteristics. Ionospheric structures are often narrowly aligned, reflecting the configuration of the plasma convection. In the trough, the alignment is in longitude / local time, so they are narrow in latitude. SEDs are aligned in latitude primarily, so they are narrow in longitude / local time. Patches can be much more diverse and therefore could be narrow or elongated in either direction. Narrow scale sizes can be as small as 10s of kms, while the elongated direction can be as wide as 1000s of kms. The enhanced or diminished plasma density can be an order of magnitude or more above or below the background density.

Scientific Measurements *Obj. 1.2*

Forcing Physical Parameters: plasma velocity vector, neutral wind vector, neutral density, neutral composition, ion, electron, and neutral temperature, electron auroral signatures, vertical ionization and heating rate profile, electromagnetic energy flux

Response Physical Parameters: cold plasma density, plasma composition

Measurement Characteristics:

- Timescales: from 30 minutes to several hours; different seasons and activity levels
- Local time coverage: 4-8 hours of local time coverage with spacing between 1-2 hours; coverage and separation can vary to explore scale sizes and gradients
- Latitudinal coverage: poleward of 45° latitude, 0.1° res. for plasma/fields and 0.5° res. for neutrals
- Altitudinal coverage: measurements between 200-450 km desired; vertically aligned measurements occasionally to verify altitude profile assumptions.

Objective 1.3: Determine how neutral winds, auroral precipitation, and collisional heating drive high-latitude neutral density structures.

Neutral densities at altitudes of 150-500 km are known to be highly variable in time and space. For example,

large-scale cellular structures of density minima and maxima have been observed over the polar region. These structures, or cells, were first noticed in the NCAR-TGCM atmospheric models [*Crowley et al.*, 1989] and studied in the high-latitude region, particularly [*Schoendorf et al.*, 1996a; *Crowley et al.*, 1996; *Guo et al.*, 2019]. Recent missions like CHAMP and GRACE have shown direct evidence of significant regional-scale structures in neutral mass density, i.e., from 100 km to 1000 km in size [e.g., *Schlegel et al.*, 2005].

Neutral density anomalies (defined as mass density enhancements more than 50% above the ambient mean density) have been found in the high latitude thermosphere by *Lühr et al.* [2004]. Average CHAMP neutral density data are shown in Figure 2.5 [*Liu et al.*, 2005]. Here, the variations of the averaged data reveal that structures in the neutral density do not only appear in the cusp (as discussed by *Lühr et al.*, 2004, and many subsequent studies) but also are present on the nightside near local midnight. Furthermore, such enhancements could be occurring locally within smaller spatial scales across the high/latitude polar cap as isolated events are washed out in average plots and must be examined in conjunction with the driving sources of energy. This figure also shows how the averaged structures are different between the northern and southern hemispheres, as discussed in Objective 2.6 below. *Clausen et al.* [2014] described the statistical temporal evolution of the thermosphere during over 2,000 substorm events by using a superposed epoch analysis of several years of CHAMP data. They showed only an approximately 4% density increase on the nightside (similar in shape as the nightside enhancement in Figure 2.5) during the average substorm, but this is most likely an underestimate because of the use of only a single satellite and the averaging.

Some studies [e.g., *Huang et al.*, 2014] interpreted polar density structures as evidence that the polar thermosphere is a direct sink of geomagnetic storm energy input via Poynting flux and particle precipitation. Others [e.g., *Lu et al.*, 2016] have argued that the features are a result of propagating large-scale atmospheric gravity waves causing density changes across the globe, including those that move from the auroral zone into the polar cap.

The relationship between the density anomaly

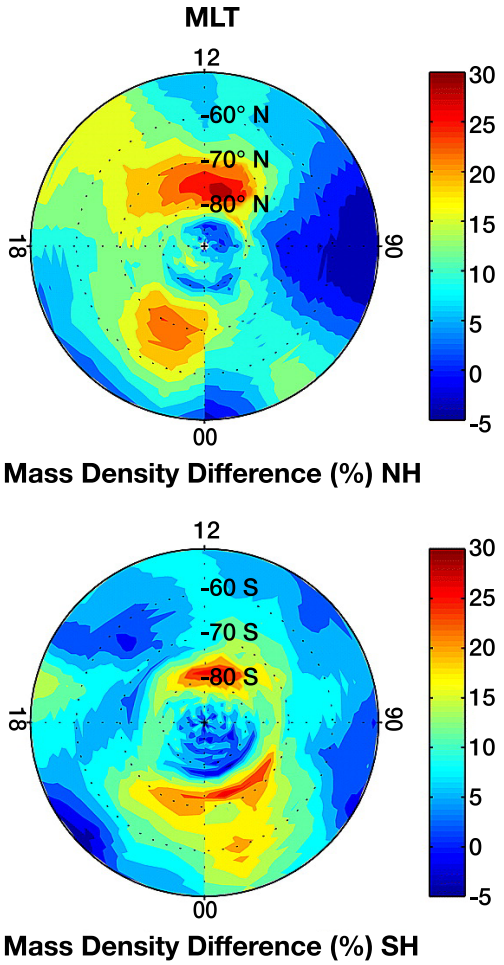

Figure 2.5. Distribution of the percent difference between the thermospheric mass density from CHAMP and MSIS90 in the northern hemisphere (NH) and southern hemisphere (SH) polar regions during quiet conditions. Large differences are seen in the cusp and midnight sector. From *Liu et al.* [2005].

structure and local energy dissipation, whether particle precipitation, frictional heating, smaller-scale variability in the drivers, or a combination of all of these, remains elusive. Some of these structures are accompanied by enhanced collisional heating as represented by Alfvenic waves which drive variable ExB drifts [*Lühr et al.*, 2004], but nearly one half of the observed density anomaly events are not [e.g., *Liu et al.*, 2010]. In particular, the cusp is a well-established region of low energy particle precipitation [e.g., *Newell and Meng*, 1992] and strong Joule heating [*Knipp et al.*, 2011] in the upper thermosphere, and there are many uncertainties in what actually drives these density enhancements [e.g., *Deng et al.*, 2013; *Clemmons et al.*, 2008]. The scale sizes of plasma and neutral structures can also be very different, with plasma structures possibly being much smaller, due to the electrodynamic forcing as well as the plasma interaction with the magnetic field

allowing significant cross-field structuring, while the inherent diffusion in the thermosphere quickly reduces horizontal gradients. In addition, we do not understand how plasma density structures (SAPS, SEDs, Polar cap patches, trough) impact the neutral density and whether the plasma structures are also reflected in neutral density structures. This is primarily because there are not reliable simultaneous measurements that describe the driving mechanisms along with the measurements of the plasma or neutral density enhancements. From both a basic understanding of plasma physics and our atmosphere, as well as a practical consideration, it is important to understand the drivers of neutral density structures and their relationships to plasma density structures.

Several physical processes may contribute to the observed thermospheric density structures [e.g., S*choendorf et al.*, 1996b], with different mechanisms possibly working across different scales: vorticity in the neutral winds driving pressure changes, enhanced Joule/collisional heating bringing neutral gases to higher altitudes through thermal expansion or upwelling; pressure gradients associated with impulsive collisional heating and auroral energy dissipation generating gravity waves propagating equatorward as well as poleward, driving neutral density variability globally; and neutral air parcels being transported vertically through converging and diverging neutral winds. Figure 2.6 shows modeling results of the polar cell of low density driven by vorticity in the neutral winds [*Guo et al.*, 2019].

Past missions (e.g., AE, DE-2, TIMED, CHAMP, GRACE, GOCE) have uncovered the general behavior of these density structures. However, due to the lack of simultaneous observations of both the energy inputs and the resultant thermospheric response, the relative importance of the different physical processes in driving thermospheric density structures remains largely unknown. We also do not know how geomagnetic storms are tied into these processes, although evidence suggests that stronger driving leads to stronger density anomalies [*Liu et al.*, 2010] as well as asymmetries between northern and southern hemisphere (see Objective 2.6). Extreme vertical winds (>100 m/s) in the auroral oval region have been observed both by the DE-2 satellite [*Spencer et al.*, 1982] and ground-based Fabry-Perot measurements [*Rees et al.*, 1984; *Price et al.*, 1995], yet we still do not know how localized those large winds are, and if they cause significant localized density structures. In addition, the complete lack of observations with re-measurement times over the same region less than ~100 mins (a typical LEO satellite orbital periods) has severely limited our ability to determine the relationships between local and global energy inputs and to separate locally driven responses from globally propagating responses.

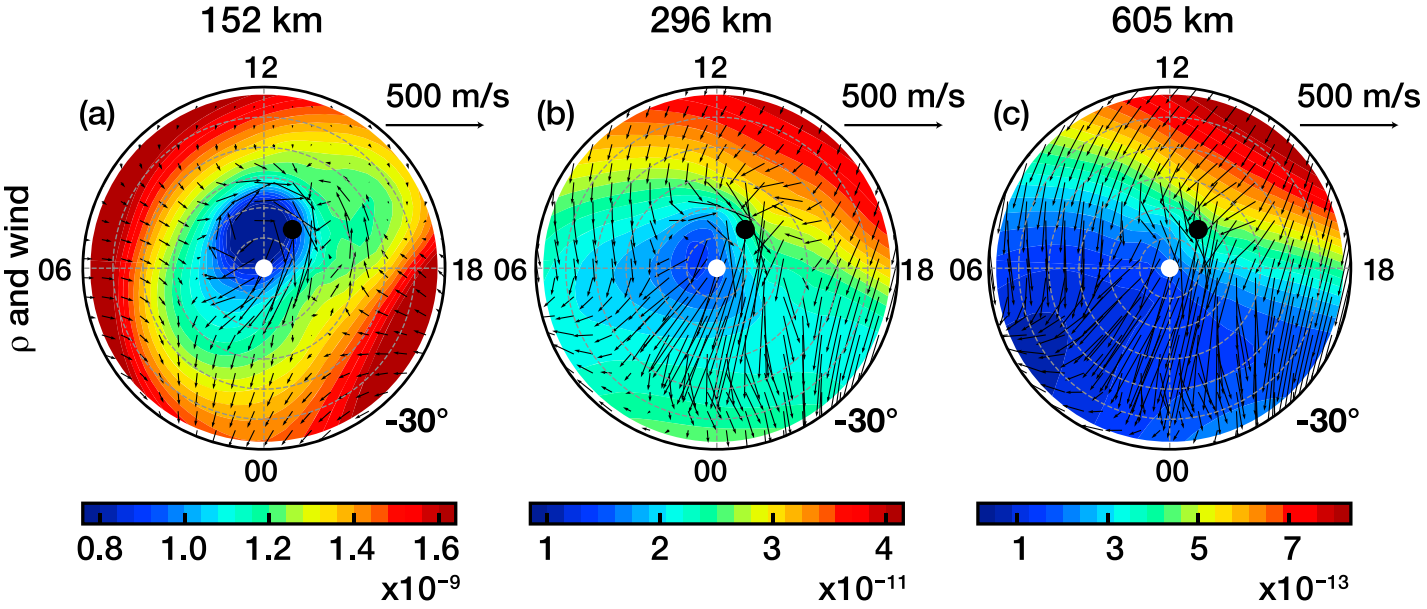

Figure 2.6. Modelled thermospheric mass density and neutral winds for the southern polar region at three different altitudes. A large density depletion exists at altitudes around 150-300 km, but fades above this. The depletion is primarily driven by clockwise flowing winds that are accelerated by ion drag. From *Guo et al.* [2019].

In order to fully understand how high-latitude neutral density structures form and evolve, it is critically important to measure the forcing terms that drive them:

- Collisional heating: Collisional heating drives upwelling in the thermosphere, which causes neutral density change at a constant altitude. Collisional heating, the dominant mechanism for dissipation of the electromagnetic energy flux, includes frictional heating, which is proportional to the difference between the ion and neutral velocities squared and the thermal heat transfer between ions and neutrals, which is proportional to the difference between the ion and neutral temperatures; the cold plasma density and composition, and the thermospheric mass density, which is dependent on the neutral density and composition. Finally, structure in the electric field at small spatial scales is an additional frictional heating source that can be applied to the IT at larger scales.

- Auroral precipitation: The auroral precipitation deposits energy directly into the system producing heat and ionization that drive both thermospheric expansion and increased collisional heating.

- Neutral winds: Thermospheric neutral winds advect gradients in the neutral density, drive density increases and decreases through convergence and divergence, respectively, and can drive pressure changes through changes in vorticity.

The electrodynamic environment, including the plasma convection and auroral precipitation, at high latitudes can evolve rapidly, reconfiguring significantly over 15-20 minutes. In order to capture the rapid evolution of the plasma environment and the possibly rapid response of the neutrals that may respond to changing electrodynamics with buoyancy waves, remeasurement should be at time-scales less than 10 minutes. Over larger spatial scales, the neutrals evolve over the course of 30-180 minutes, allowing remeasurement times of 30 minutes to be used.

The forcing terms will be highly dependent on latitude, longitude and local time through the influence of solar zenith angle, auroral precipitation, ion convection, and Coriolis effects. Therefore, measurements distributed in local time will allow simultaneous exploration of the forcing terms in a global-scale mode.

Scientific Measurements *Obj. 1.3*

Forcing Physical Parameters: plasma velocity vector, neutral wind vector, cold plasma density, plasma composition, neutral density, neutral composition, ion temperature, neutral temperature, electron and ion auroral signatures, vertical ionization and heating rate profile, electromagnetic energy flux

Response Physical Parameters: neutral density, neutral composition

Measurement Characteristics:

- Timescales: from 6 minutes for small-scale rapid evolution, to 30 minutes to several hours for global-scale evolution; different seasons and geomagnetic activity levels
- Local time coverage: 4-8 hours of local time coverage with spacing between 1-2 hours to explore the longitudinal extent of the structures; local time coverage and separation can vary to explore scale sizes
- Latitudinal coverage: poleward of 45° latitude, 0.1° res. for plasma/fields and 0.5° res. for neutrals
- Altitudinal coverage: measurements between 200-450 km desired, vertically aligned measurements occasionally to verify altitude profile assumptions to explore hydrostatic assumptions.

Objective 1.4 Determine how atmospheric tides and gravity waves influence the IT response to magnetospheric inputs.

Planetary waves, tides, and gravity waves (GWs) that propagate up from the lower atmosphere are all sources of momentum and energy in the IT system. As the waves deposit their momentum, they impact the mean circulation and generate dynamo electric fields, redistributing plasma and modulating the IT response to energy inputs from the solar wind and the magnetosphere. These waves are ubiquitous features of the Earth's thermosphere and ionosphere, and their imprints are found in nearly all types of IT parameters including the thermospheric wind, temperature, pressure, density, and plasma density and convection. Specifically, these waves precondition the IT system by (a) driving the E-region neutral wind dynamo at altitudes

of between 100-150 km [e.g., *Richmond,* 2016]; (b) imprinting horizontally travelling wave features that originate from upward-propagating GWs at altitudes between 100-400 km [e.g., *Miyoshi et al.*, 2018]; (c) causing hemispheric and longitudinal asymmetries that reflect the land-sea distribution of the Earth's surface and other stratospheric and mesospheric phenomena at altitudes between 100-400 km [e.g., *Siskind et al.*, 2003, 2018]; and (d) affecting seasonal variations of the IT system, including compositional mixing and general circulation at altitudes between 100-400 km [e.g., *Qian et al.*, 2009; *Yue et al.*, 2019]. Through poorly characterized mechanisms, atmospheric waves influence ion-neutral coupling and therefore coupling to different latitudes and altitudes and redistribute energy within the IT system as the waves are attenuated. The temporal and spatial scales over which atmospheric waves impact the response of the IT system to magnetospheric inputs are not well understood and vary from minutes to interannual and from kilometers to global [e.g., *Fritts and Lund*, 2011; *Laštovička*, 2006].

At high latitudes these waves influence coupling between the magnetosphere and ionosphere through their ability to modulate the electric field and conductivity by driving the neutral wind dynamo as well as modifying the plasma density. In spite of its importance, the role of the neutral wind dynamo in ionosphere-magnetosphere coupling is not well understood [*Peymirat et al.*, 1998; *Ridley et al.*, 2003]. Tides and GWs deposit momentum and energy at high latitudes and structure the IT system on spatiotemporal scales that are comparable to the scales of magnetospheric inputs. Semi-diurnal tides are expected to peak at 40°-65° latitude, at altitudes near 110-120 km [*Smith*, 2012]. A Semidiurnal Westward one non-migrating component is known to peak at even higher latitudes of 75°-80°, with zonal and meridional wind amplitudes as high as 100 m/s [*Hagan and Forbes,* 2003; *Wu et al.*, 2011; *Oberheide et al.*, 2011].

Neutral winds below 160 km have a more complex relation to ion convection than in the upper thermosphere above 200 km, as shown by in-situ and remote-sensing observations [*Heppner and Miller,* 1982; *Richmond et al.*, 2003]. There is significant nonlinear interaction between semidiurnal tides and IMF-dependent neutral wind pattern driven by ion convection [*Mikkelsen and Larsen*, 1991]. Chemical release rocket experiments [*Larsen*, 2002; *Zhan*, 2007] and meteor radar and lidar experiments [*Oppenheim et al.*, 2009, 2014; *Liu et al.*, 2016; *Yue et al.*, 2010] have repeatedly revealed the presence of strong horizontal winds ranging from 100 to 200 m/s with large vertical shears at altitudes between 90 and 140 km. Recent whole atmosphere modeling work suggests that the large buoyancy frequency just above the mesopause sets up dynamically stable conditions that support large vertical shears, and that upward-propagating GWs contribute significantly to these large shears [*Liu*, 2017]. At the same time, strong winds and large vertical shears can be generated by magnetospheric inputs, and these neutral winds can significantly influence the Joule heating estimation [*Sangalli et al.*, 2009]. Figure 2.7 shows an attempt to model the neutral winds measured by chemical tracers during the JOULE-II sounding rocket experiment [*Deng et al.*, 2017]. Below about 120 km, the model misses the wind structure, since the shears at these altitude are not included properly within the model. Instead, the large-scale, climatologically smoothed tidal structures are included, while the strongly vertically structured wave are ignored, since their spatial representation is not adequately understood enough to be represented.

GWs at high latitudes can penetrate far up into the thermosphere before breaking and depositing momentum, and middle atmosphere disturbances such as sudden stratospheric warmings can enhance these effects [*Yigit et al.*, 2014]. It is also possible for GWs to alter the neutral winds below about 150 km altitude,

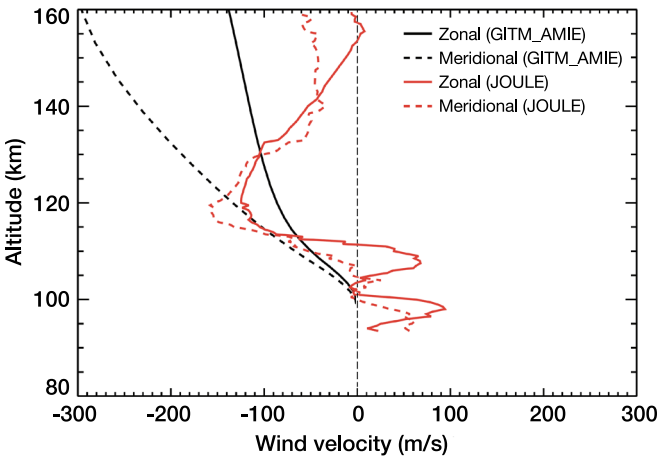

Figure 2.7. The comparison of the neutral wind profiles between JOULE rocket observations and GITM simulations along the downleg portion of trajectory. The black lines are for the GITM simulations and the red lines are for the JOULE observations. The solid lines represent the zonal winds and the dashed lines represent the meridional winds. From *Deng et al.* [2017].

which can drive small-scale changes in the neutral wind dynamo. The role of this effect with respect to observed small-scale (< 50 km) variability in the plasma convection is largely unexplored [*Matsuo and Richmond*, 2008; *Bristow et at.*, 2016; *Cousins and Shepherd*, 2012; *Yigit et al.*, 2014]. This momentum and energy deposition is highly dependent on geographical location, season, and state of the stratosphere, which complicates how the IT system responds to magnetospheric inputs at a given geomagnetic latitude and local time.

To fully understand how the high latitude IT responds to solar wind and magnetosphere forcing in quiet and disturbed conditions, it is imperative to determine the role of atmospheric waves in preconditioning the system's dynamical and electrodynamical responses to magnetospheric inputs. The wave-induced perturbations in neutral winds, plasma convection, and plasma density can impact the neutral wind-dynamo, conductivity and magnetosphere-ionosphere coupling through ionospheric current closure, Joule heating, and the fly-wheel effect. Some of the causes of seasonal and longitudinal dependence, and hemispheric asymmetry in magnetosphere-ionosphere coupling can be traced back to wave forcing from the lower atmosphere [Yigit et al., 2014].

To understand how the lower atmosphere winds drive change in the high-latitude thermosphere and ionosphere, it is necessary to estimate the plasma motions induced by the dynamo action of the neutral wind and contrast them with the large-scale convective motion of the plasma. To do this, GDC must measure:

- Neutral wind dynamo forcing: The neutral wind dynamo is most effective in the altitude region between 100 and 150 km. Ideally, the ion density and the neutral density and composition will be measured within this region, but this can be a challenging task from an orbiting platform. However, models can be used to specify the plasma density given auroral precipitation characteristics and solar EUV drivers. In situ ion measurements at multiple altitudes, as well as ground-based measurements, can be used to verify model assumptions. The neutral density and composition can be extrapolated with an in situ measurement of the neutral density, composition, and temperature at higher altitude. There is no easy way to measure or estimate the winds in this region except through remote sensing on an orbiting platform.

- Plasma convection: The plasma convection above 150 km is the main signature of neutral wind dynamo forcing. Thus, measurements of the plasma convection must be made and analyzed in such a way that tides, gravity, and planetary wave structures can be extracted. In order to capture the small-scale effects that are possibly driven by gravity waves, the E-field spatial structure amplitude should be measured.

Waves from the lower atmosphere can have time-scales ranging from the buoyancy frequency (~12-16 minutes)

Scientific Measurements *Obj. 1.4*

Forcing Physical Parameters: neutral winds between 100-150 km, high latitude plasma convection, cold plasma density and composition, auroral electron and ion characteristics, vertical ionization/heating rate, neutral density and composition, neutral temperature

Response Physical Parameters: plasma convection and electric field spatial structure amplitude, neutral winds

Measurement Characteristics:

- Timescales: from approximately 12 minutes to several weeks; different seasons;
- Local time coverage: for small-scale waves, 2-6 hours of local time coverage with spacing between 1-2 hours; for tides and planetary waves, complete coverage of local time with 3-4 hours of separation is needed; coverage and separation should vary to explore scale sizes
- Latitudinal coverage: poleward of 45° latitude, 0.1° res. for gravity waves and 1° res. for tides and planetary waves
- Altitudinal coverage: neutral winds need to be measured between 100 and 200 km altitude, while other parameters can be measured between 200-350 km and extrapolated to lower altitudes, vertically aligned measurements occasionally to verify altitude profile assumptions.

for gravity waves, to several weeks for planetary waves. Similarly, gravity waves (at 100 km altitude) can have scale sizes from less than 10 km to 100 km, while planetary waves can have scales of greater than 1000 km. Atmospheric tidal structures have local time, longitudinal, and universal time dependence, requiring measurements at different local times and longitudes to resolve. The winds between 100-150 km altitude have vertical wavelengths from approximately 10-20 km to 50-70 km.

2.3 Science Goal 2 and Objectives

Goal 2: Understand how internal processes in the global ionosphere-thermosphere system redistribute mass, momentum, and energy.

Goal 2 of the GDC mission is complementary to Goal 1, providing a comprehensive view of the global ionosphere-thermosphere system's internal processes that are influenced by the coupling between regions. This includes the propagation of density, composition, wind, and temperature changes from high latitudes to equatorial latitudes, the impact of regional-scale structures on the global system, northern/southern hemisphere symmetries, how low- and mid-latitude plasma and density structures develop and evolve, and the interaction and feedback between plasma and neutral dynamics. Goal 2 focuses on six Objectives selected to highlight the global IT internal processes as they are influenced from surrounding regions. Each of these Objectives are described in detail below.

Objective 2.1 Determine the relative importance of penetration electric fields and disturbance winds in driving plasma density variations at mid- and low-latitudes during geomagnetic storms.

When the interplanetary convection electric field increases (with IMF Bz turning southward and/or By increasing) the plasma flow across the polar regions increases, and its direction varies depending on the IMF orientation. These flows are associated with an enhancement in the region-1 field-aligned currents (FACs), which directly respond to changes in the solar wind. In the inner magnetosphere, the plasma distribution that controls the region-2 FACs takes an hour or more to readjust to the enhanced flow pattern. During this adjustment time there exists an imbalance between the strength of the region-1 and region-2 FACs resulting in convection electric fields that extend beyond the auroral oval to the equatorial region [e.g., *Spiro et al.*, 1988]. These are the so-called prompt penetration electric fields, which drive mid-latitude disturbance fields, the sub-aurora polarization streams (SAPS) [*Foster and Burke*, 2002; *Foster and Vo,* 2002], and which at the equator can drive upward plasma drift on the dayside, resulting in enhanced equatorial anomalies (the two enhancements in F-region plasma density just north and south of the magnetic equator) [e.g., *Ma and Maruyama*, 2006; *Abdu*, 2012]. If the penetration electric fields become large enough, as they do during large geomagnetic storms, the equatorial anomalies can move poleward by significant distances, resulting in a largely depleted equatorial ionosphere [e.g., *Klimenko and Klimenko*, 2012; *Tsurutani et al.*, 2008., *Huang et al.*, 2006]. The penetration electric fields rapidly increase as the region-1 FACs increase, and then slowly decrease as the plasma in the magnetosphere readjusts to the new convection pattern, driving a new pressure balance and increasing the region-2 FACs. This increase and decrease can take place in approximately an hour.

The enhanced high latitude plasma flows, associated with the increased region-1 FACs, also drive significant energy deposition. This causes heating, which can result in large pressure gradients from high latitudes towards the equator, ultimately driving equatorward neutral winds, often referred to as "disturbance winds". The disturbance wind is defined as the difference between the quiet time wind and the wind during a storm. Therefore, while the "disturbance wind" may be directed equatorward, the actual (total) wind could simply be less poleward. While these winds can drive density and composition change, as described in other Objectives, they can also cause significant changes in the ion density: the horizontal winds impart momentum to the ions, which move easily along the field lines, and because those field-lines are tilted at mid-latitudes, this results in either upward or downward motion of the ions. At mid-latitude, poleward directed winds drive ions down field-lines, resulting in reduced ion densities, while equatorward directed winds, as exist during geomagnetic storms, drive ions up field lines, and cause density enhancements. The disturbance winds at altitudes above about 200 km affect the winds below this altitude through viscosity, driving change in the dynamo current system between 100-150 km altitude.

This further modifies the plasma drifts in the F-region ionosphere.

The large-scale variations of the ionospheric plasma density during magnetic storms and their association with magnetospheric energy sources controlled by the solar wind and IMF represents a fundamental aspect of magnetosphere-ionosphere-atmosphere coupling for which much of the basic causal processes are not known. Consider the CHAMP satellite measurements of TEC gathered on three consecutive passes (spaced 90 minutes apart) at mid and low latitudes near noon LT during the October 30-31, 2003 superstorm, shown in Figure 2.8 [*Mannucci et al.*, 2005]. Here, the total electron content increases by 900% over the normal values, suggesting that a penetration electric field had elevated the entire ionosphere to higher altitudes than that of the CHAMP orbit at 400 km. Furthermore, as discussed by *Rishbeth et al.* [2010], the result of this "super fountain" effect is to transport the plasma in the poleward direction as well. This would account for the fact that the equatorial "crests" or anomalies shown in the TEC data in Figure 2.8 that typically occur near 15° (see blue trace corresponding the TEC just prior to the storm) are abruptly shifted to latitudes of ~30° during the storm.

It is not clear how the elevated plasma density and the "push" of the equatorial anomalies to higher latitudes (Figure 2.8) result from a combination of electric fields and disturbance winds and whether the forces associated with these processes reinforce or oppose each other. Multi-point measurements of the neutral winds and plasma drifts from GDC will allow researchers to disentangle these processes to determine each of their effects on the globally coupled IT system.

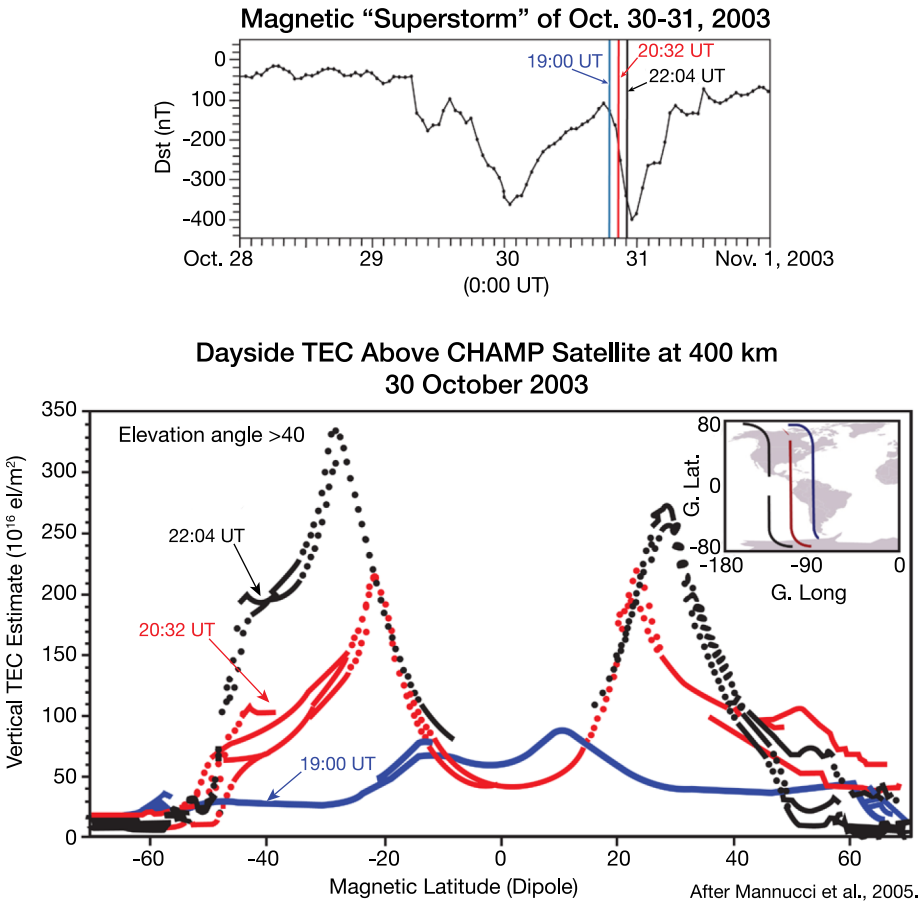

Figure 2.8. Integrated electron content (corresponding to total electron content or TEC) as measured by the GPS instrument on the CHAMP satellite for altitudes above the CHAMP altitude of 400 km (*lower panel*). Data are shown for three orbits plotted as a function of magnetic latitude which correspond to times just prior to (*blue*) and after (*red and black*) the onset of a magnetic storm on October 30, 2003, as shown in the plot of Dst in the *upper panel*. The locations of the CHAMP orbits are shown in the upper right corner of the lower panel. The local times of these orbits range from 1230–1330 LT for latitudes within ±60°. Points missing near the anomaly trough are due to the elevation angle cut-off. After *Mannucci et al.* [2005].

At low latitudes, density "holes" are created during the daytime due to the large plasma uplift. These holes are gradually replenished over a few hours by photo-ionization due to solar EUV irradiance at the lower altitudes, creating a "new" ionosphere [*Balan et al.*, 2008]. The associated electrodynamics with such newly created regions of high conductivity associated with the density enhancements are not known.

Due to a lack of simultaneous and multi-point observations of plasma drifts and neutral winds along with the global electric field structure during low and high geomagnetic activity periods, we do not understand the conditions under which different physical processes dominate the creation of density variations or how long they persist. They are likely functions of local time and storm phase, and ultimately how the incoming magnetospheric energy is transported and processed through the IT system. Global, and multi-point measurements are needed to explore and understand these fundamental processes.

To fully understand how changes in the ionospheric density at mid- and low-latitudes result from penetration electric fields and disturbance winds, it is critically important to measure the forcing mechanisms and the response:

- Plasma velocity vector: The plasma velocity perpendicular to the magnetic field will transport plasma azimuthally and latitudinally and should be measured at sub-auroral and equatorial latitudes to assess the impact of penetration fields.

- Auroral Zone Precipitation Signatures: The equatorward boundaries of the regions of ion and electron precipitation are critical to identifying the spatial relationship between sub-auroral drifts and the location of the aurora.

- Field-Aligned Current Signatures: The boundaries of the region 2 current system should be identified to understand the storm-time evolution of penetration fields.

- Disturbance winds: Horizontal neutral winds at mid- and low-latitudes are greatly enhanced due to significant energy input at high latitudes and drive plasma motion up or down field-lines depending on the direction and magnitude of the wind and the magnetic field.

- Cold plasma density: Changes in the plasma density are the main result of the drivers described above. Changes in composition may indicate lifting or descent, as structuring of the ionosphere is heavily dependent on whether the ions are molecular or atomic.

- Plasma Chemistry: The plasma density is also affected by chemical losses dependent on the neutral composition, primarily O and N2, as well as the neutral, electron, and ion temperatures.

Penetration electric fields are transmitted across the globe almost instantly, but it can take 15 minutes or more for the magnetospheric drivers and ionospheric plasma density to evolve. In order to determine whether a change in plasma convection is driven by changes in high-latitude forcing, measurements of the plasma convection need to be made approximately simultaneously at high latitudes and low/mid-latitudes. Dynamo winds take several hours to develop. The effects of the penetration electric fields, through the plasma convection, and the winds on the plasma density take approximately an hour to several hours to produce a significant change.

Scientific Measurements *Obj. 2.1*

Forcing Physical Parameters: plasma velocity vector, neutral wind vector, neutral wind vector, auroral electron signatures, magnetic field perturbations, ion temperature, electron temperature, neutral density, neutral composition

Response Physical Parameters: cold plasma density

Measurement Characteristics:

- Timescales: To test the simultaneity of the plasma drift changes at different locations across the globe, measurements from different locations should be within 5s of each other. The plasma drift takes 15-20 minutes to change at high latitudes (i.e., would get full penetration in about 15-20 minutes), with the decay time of the penetration fields having a time-scale of 60 minutes. The disturbance neutral winds take approximately 3 hours to ramp up. Different seasons and activity levels need to be explored.

- Local time coverage: Complete coverage of local time would allow exploration of how the balance between winds and penetration electric fields affect the plasma density. The scale-sizes in local time and the local time dependence are not clear at all for the penetration electric fields or the disturbance winds, Thus, both closely spaced and more broadly spaced local times will allow the sequential exploration of specific processes as well as a systematic global description of the phenomena.

- Latitudinal coverage: Global, with simultaneous sample volumes at low/middle latitude and at higher latitudes. This Objective is exploring more large-scale structures, so a resolution of approximately 100 km would allow closure.

- Altitudinal coverage: Measurements between 200-450 km. Vertically aligned measurements occasionally to further explore the vertical motion of the plasma density. In cases where the plasma has risen above the altitude of the measurements, the penetration electric fields and neutral winds measurements can be related to local absence of plasma.

Secondary Measurements

Ground-based GPS measurements of total electron content (TEC) easily capture the increase or decrease of plasma density above a given location on the Earth's surface. With nearly world-wide coverage, these measurements can put the GDC measurements in a global context.

Objective 2.2: Identify the processes that create and dissipate propagating structures within the ionosphere and thermosphere during active and storm conditions

The IT system transports energy inputs away from the entry point via large scale wave structures termed Traveling Atmospheric Disturbances (TAD) and Traveling Ionospheric Disturbances (TID) for the neutral and plasma gases, respectively. TADs and TIDs can have wavelengths from 100's of meters to a few 1000's km (periods of 10 to 30 min) and they propagate with typical velocities of a few 100s of m/s. They can last for hours and cover a significant portion of the Earth longitudinally while they propagate both poleward and equatorward [Prölss, 2011]. Near the equator, the TADs from the northern and southern hemispheres meet and may continue into the opposing hemisphere [e.g., *Brunisma and Forbes*, 2007]. While TADs result from almost any energy input, such as flares or storms [e.g., *Prols*, 2011; *Bruinsma and Forbes*, 2007; *Lei et al.*, 2010; *Sutton et al.*, 2009], the intent of this Objective is to quantify and understand the high-latitude generation, propagation, and dissipation of large scale, horizontally-propagating ionosphere and thermosphere density structures (TIDs and TADs) and to determine the relationship between the driving energy sources, and their spatial sizes, local time dependencies, propagation speeds and distances travelled.

In a fashion similar to that of TADs, large-scale ionospheric disturbances are generated at high latitudes during geomagnetic storms and are observed to be propagating both poleward and equatorward as well. These TIDs are observed in mid and low latitude ground-based radars and all-sky imagers as well as in the total electron content (TEC) measurements from ground-based GPS receivers [e.g., *Saito et al.*, 2001]. TIDs may be seeded by TADs and their relationship to neutral winds and electric fields suggest that they may be electrified TADs, but separating the energy source from the troposphere or the magnetosphere has not always been possible [*Prolss*, 2011; *Vlasov et al.*, 2011].

Despite the apparent widespread appearance of TADs within the earth's upper atmosphere, there has been little advance in our understanding of this topic due to the lack of multipoint observations or remeasurements times faster than the orbital period of LEO satellites like CHAMP and GRACE. In particular, it is unclear how

TADs change as they propagate. With multiple platforms and higher temporal resolution measurements, the dynamic morphology of the TAD can be determined, including how these large scale wave structures change and dissipate.

There has been disagreement in the community about whether density enhancements observed within the polar cap during storms are due to direct energy input from solar wind - magnetosphere coupling [*Huang et al.*, 2016, 2017] or the result of poleward propagating TADs [*Lu et al.*, 2016]. While the former has been argued with observations the latter has only been shown via modeling. The conflicting interpretations cannot be resolved due to a lack of appropriate measurements.

Further, it is unclear how much of the atmospheric disturbances are due to pressure or number density changes and how much is due to composition changes. Recent studies have started to explore the role of helium in the neutral atmosphere at altitudes of approximately 500 km, and how the reaction of the lighter species to storms can be very different from the reaction of heavier species [e.g., *Sutton et al.*, 2015]. Without direct measurements of mass composition, it is impossible to verify the role of helium, let alone distinguish how the subsequent propagation and evolution of TADs to lower latitudes is driven by compositional changes compared to pressure or number density changes.

The energy source of TADs can be gravity waves generated in the lower thermosphere or mesosphere, or magnetospheric energy during geomagnetically active events in the forms of Joule/frictional heating and auroral particle precipitation. Lower atmospheric waves can trigger TADs all over the globe, while the latter originates at high latitudes only. It is generally assumed that TADs and TIDs are likely the neutral atmosphere and ionosphere equivalent responses to the same energy trigger, but there have never been sufficient simultaneous observations with wide enough coverage to capture and understand whether or not the creation, propagation, and dissipation of TADs and TIDs is simultaneous.

Distribution of ground instrumentation allows continuous tracking of TIDs, so more is known about TIDs than about TADs. For example, the sudden appearance of strong TIDs are observed in association with magnetospheric disturbances as shown in Figure 2.9 [*Jonah et al.*, 2018], which shows their propagation from high latitudes to mid latitudes. In addition, instruments gathering simultaneous observations in both the northern and southern hemispheres sometimes observe similar behavior in TIDs, leading to the idea that the structures could exist along the same magnetic field-lines [e.g., *Otsuka et al.*, 2004]. However, the lack of concurrent plasma and neutral gas observations has severely limited our understanding of how the energy is transported within the IT system and the physical mechanisms that may link TIDs and TADs.

In order to understand TADs and TIDs creation, evolution, and dissipation during different geomagnetic conditions, as well as their relationship with each other, it is important to measure several aspects of these processes:

- Heating rates: The creation of TADs and TIDs within the high-latitude region can be driven by different types and levels of energy input that should be captured. The collisional heat transfer between the ions and neutrals, commonly referred to as Joule or frictional heating, includes both the ion and neutral velocity difference (squared) and the temperature difference between ions and neutrals as well as both the ion and neutral density and composition. Plasma drifts, required to determine the local heating rate can be resolved perpendicular and parallel to the magnetic field allowing the remote dynamo action of winds to be distinguished from local collisional interactions. The vertical profile of the ionization and heating rate is specified by the auroral precipitation characteristics. Further, the electromagnetic energy flux can be used to specify where the magnetospheric energy is being added in at the top of the atmosphere.

- Neutral Winds: Winds can modify the densities through horizontal advection of density gradients, through convergence or divergence of flows driving increases or decreases in the density respectively, or through vertical flows driving upwelling that increases the density or downwelling that decreases the density. Wind features may propagate away from regions of heating and drive plasma up and down magnetic field lines to create local differences in the plasma loss rate.

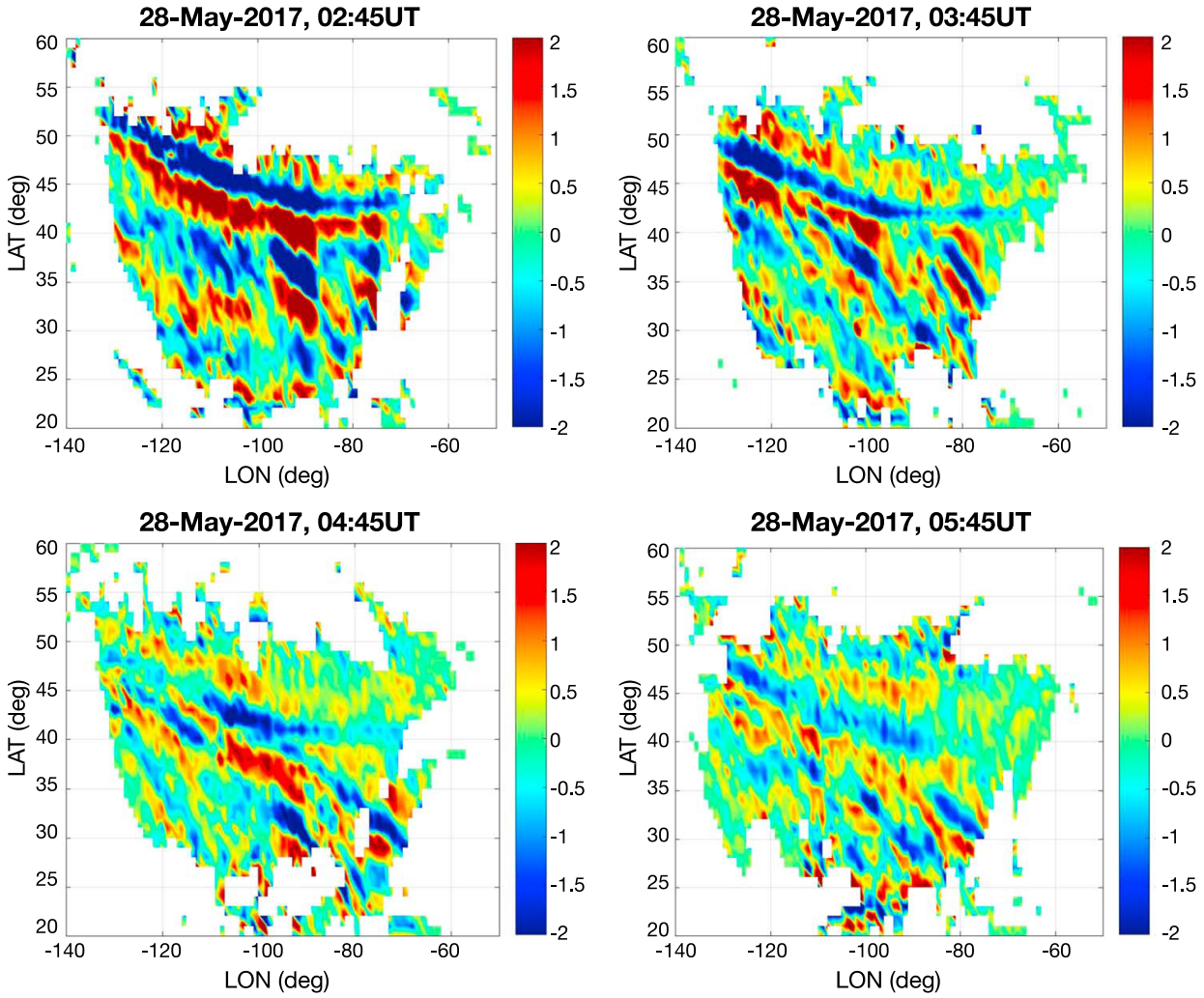

Figure 2.9. Two-dimensional maps of traveling ionospheric disturbances over North America at 1 hour intervals during the main phase of a geomagnetic storm on May 28, 2017. From *Jonah et al.* [2018].

- Plasma density and composition: In order to capture TIDs, the plasma density needs to be captured, since TIDs are manifestations of plasma density fluctuations. In addition, the plasma density and composition are both needed to describe the ion-neutral coupling (ion drag, Joule heating) that may serve to create or inhibit TADs.

- Neutral density and composition: By definition, the TADS are neutral density changes. The composition is needed to fully describe the makeup of the TAD, whether it is driven by some composition changes or only number density changes. Further, the composition is needed to describe the collisional coupling between the ions and neutrals, as described above.

TADs and TIDs develop over the course of approximately 10 minutes and can take a few hours to propagate from high latitudes to the equatorial region. To capture the source region of a TAD or TID, the remeasurement time needs to be fast enough to distinguish whether the perturbation arose in the given location or whether it was advected from a different location. On a more global-scale, the remeasurement time needs to be fast enough (~30 minutes or less) to track changes in the density. The scale size of TADs is relatively large, on the order of 1,000 km or more, although much smaller neutral density waves exist. The density perturbation within a TAD can be more than 50% of the ambient neutral density. The scale size of TIDs can be very small - less than 1 km, but the regional-scale TIDs are on the order of 100 km in size. These perturbations can be increases or decreases by an order of magnitude in strong TIDs.

Scientific Measurements *Obj. 2.2*

Forcing Physical Parameters: plasma velocity vector, vertical ionization/heating rate, neutral wind vector, ion temperature, neutral temperature, neutral density, neutral composition, cold plasma density, plasma composition

Response Physical Parameters: neutral density, neutral composition, cold plasma density, plasma composition

Measurement Characteristics:

- Timescales: from 5 minutes for regional-scale development to several hours for propagation characterization; different seasons and activity levels;
- Local time coverage: Complete coverage of local time would allow exploration of how different background conditions allow for the development, propagation characteristics (latitudinal and local time), and dissipation mechanisms for TADs and TIDs. Neither the scale-sizes in local time, nor the local time dependence, are at all clear for TAD/TID generation, propagation, or dissipation. Thus, both closely spaced and more broadly spaced local times will allow the sequential exploration of specific processes as well as a systematic global description of the phenomena.
- Latitudinal coverage: Global, 0.1° res. for ions and 0.5° for neutrals. Remeasurement needs to be done with times less than 5 minutes to investigate regional-scale structures and development of the TADs/TIDs, while remeasurement of ~30 minutes will be adequate to track the propagation of the TADs/TIDs.
- Altitudinal coverage: measurements between 200-350 km desired; vertically aligned measurements occasionally to verify altitude profile assumptions

Secondary Measurements

- High density global ionosphere measurements such as TEC, height and density of the F-region peak, in order to image large scale TIDs. This would have to be limited to land masses.
- Ground-based all-sky images in wavelengths that provide TID motion.
- Additional neutral wind measurements at ground-based observatories to allow more rapid temporal scales and higher resolution spatial scales to be observed.

Objective 2.3: Determine the connections between winds and neutral density/composition variations at mid- and low-latitudes during geomagnetic storms.

Above about 100 km the neutral atmosphere constituents are usually in a state of hydrostatic equilibrium in which the constituent species decrease in density according to their mass. At high latitudes energetic particle energy and electromagnetic energy are deposited into the atmosphere at different altitudes producing horizontal and vertical circulation in the neutral gas. The vertical circulation lifts the heavier masses and displaces the lighter masses at a given altitude so that a redistribution of the composition with altitude results. This change in the latitude and altitude distribution of the mass density, changes the plasma-neutral chemistry and the thermal balance in the thermosphere. The impacts of the neutral circulation on the neutral composition and the thermal balance of the thermosphere must be adequately understood in order to describe the flow of energy through the system.

During geomagnetic activity, different species have different upwelling rates, making minor species dominant in the dynamics during a storm. There are three specific examples of this. The first is Nitric Oxide. Even though NO is very minor in its concentration ($< 10^{-4}$), it is an efficient radiator of heat at infrared wavelengths, making it the major cooling agent of the thermosphere. In fact, recent work has suggested that the role of NO is of primary importance in the thermospheric heat budget during strong geomagnetic storms [*Knipp et al.*, 2017]. The second example is molecular nitrogen. As described in several of the Objectives above, the ionospheric loss rate is strongly dependent on N_2, since the fastest loss of O^+ in the F-region occurs when O^+ charge exchanges with N_2, then NO^+ combines with an electron and dissociates. Therefore, when N_2, a minor species in the F-region, is uplifted during strong driving, it will increase the charge exchange rate with O^+, reducing the density of the ionosphere. Finally, helium is a very light, minor species at altitudes of around 400 km, and as such, the relative concentration of helium can change in unexpected ways during geomagnetic storms. This is due to how vertical diffusion works for light and minor species. If this change in concentration of helium is not accounted for properly, it is difficult to accurately specify the drag on satellites at these altitudes because the mass density will be incorrect, and helium and

oxygen interact with the surface of satellites in different ways, making the drag coefficient dependent on the concentration of the different species. It is therefore important to understand the ratios of helium to oxygen during different driving conditions.

During active conditions and particularly during magnetic storms, dramatic variations in the neutral composition of the upper atmosphere have been recorded at mid and low latitudes. The cause of these variations has not been well established, nor has the association of the neutral composition changes with those of the various ion species or even the total ionospheric plasma number density. In situ measurements of neutral composition in the thermosphere have been limited to sparse observations from rocket and satellite missions between 1969 - 1983. These data have shown that the heavier (molecular) species are enriched and the lighter (atomic) species are depleted during storms, at least in the thermosphere above about 300 km [e.g., *Prölss*, 1982, 1997, 2011; *Burns et al.*, 1991, 1995; *Fuller-Rowell et al.*, 1994]. A significant portion of our knowledge of large scale variations in neutral composition during magnetic storms comes from remote sensing measurements of the integrated column density of the oxygen to molecular nitrogen (O/N_2) ratio. This appears in the far ultraviolet band of imagers such as those flown on DE-1, Polar, TIMED, and IMAGE [e.g., *Prölss*, 1987; *Strickland et al.*, 2001; *Zhang et al.*, 2004] and most recently, since the fall of 2018, on the GOLD mission. These emissions

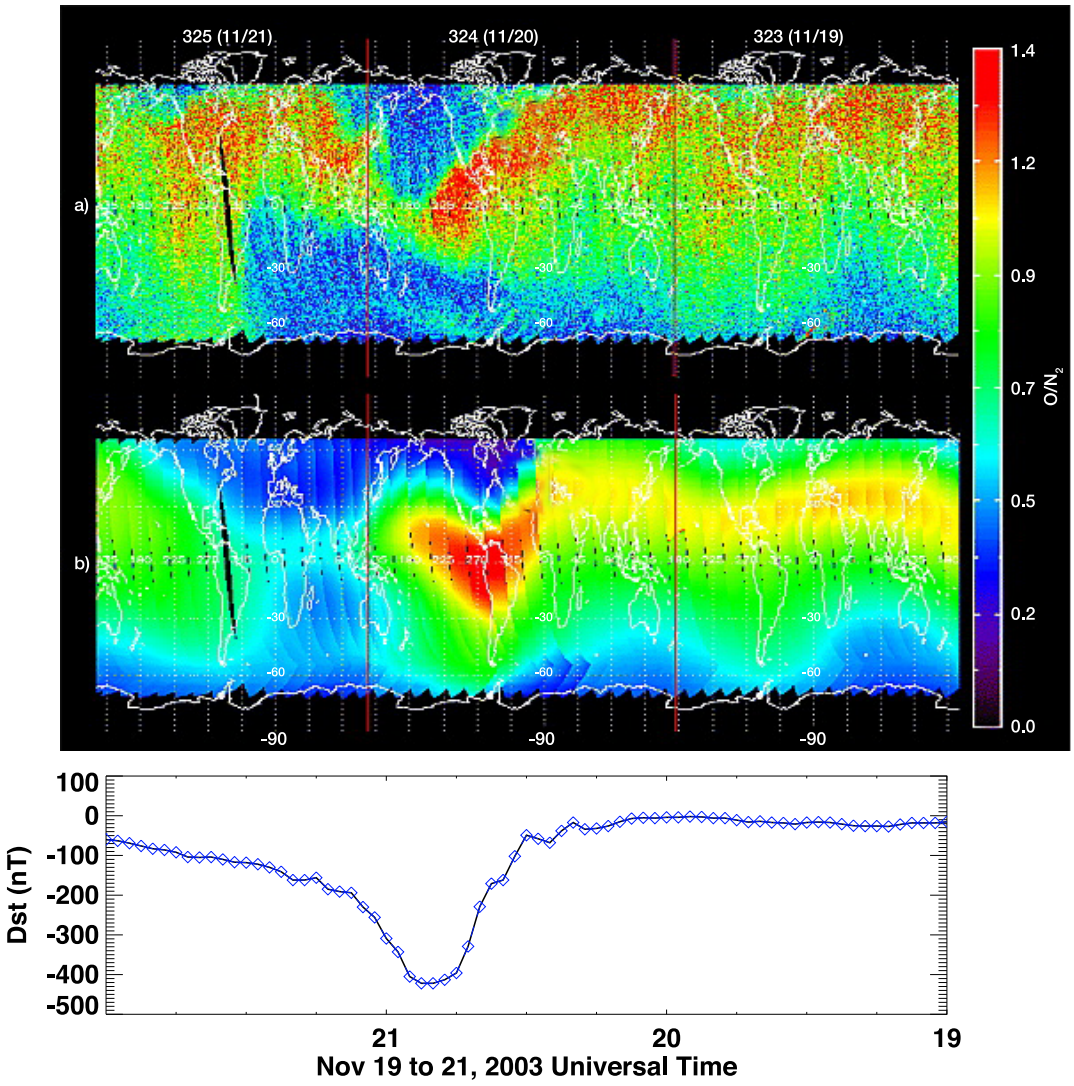

Figure 2.10. Comparison of observed and modeled variation in thermospheric densities during a geomagnetic storm. Top: Comparison of GUVI and TIEGCM O/N2 for November 19–21, 2003. Bottom: Dst for November 18-22, 2003. UT runs backwards (from right to left) within each plot and the panel boundaries are near 0000 UT for the bottom two plots. After *Meier et al.* [2005].

are only visible on the dayside and originate primarily from the altitude range of 140 to 250 km.

While the general concept of composition change during storms is thought to be relatively well understood (i.e., heating in the high-latitudes causes upwelling and disturbance winds, which change the composition of the high-to-mid latitude region [e.g., *Prölss*, 1997; *Crowley and Meier*, 2008]), there are many aspects that are not well understood. For example, very few, if any, studies have explored all compositional changes together, so it is unclear how changes in NO, N_2, and He are related during heating events. Because the NO acts as a cooling agent, while N_2 drives the loss of the ionosphere, which subsequently reduces the Joule/frictional heating, these both act to change the energy balance in the thermosphere in the same way, but through very different mechanisms. Both are extremely dynamic and very hard to simulate properly due to the multi-step processes that must occur in order to change the composition in a realistic way.

Impeding our understanding is the lack of in situ composition and wind measurements during storms, forcing the community to rely heavily on the use of models that may be inconsistent with the application of storm time drivers [e.g., *Richmond et al.*, 1992; *Fuller-Rowell et al.*, 1996; *Meier et al.*, 2005; *Crowley et al.*, 2006b; *Maruyama et al.*, 2007; *Fedrizzi et al.*, 2008; *Lei et al.*, 2008]. Because different models use different drivers and have different physics, it is extremely difficult to determine whether the drivers are incorrect or the physical approximations in the models are incorrect. Most of these models are hydrostatic, which means that they cannot accurately capture the vertical motion in the auroral zone, which is thought to be an important source of the compositional changes at higher latitudes. There is very little wind data (both horizontal or vertical) to validate the wind results from the models. Given the decades of progress with numerical simulations and models designed specifically to understand how and why the thermospheric composition changes during storms, the main impediments to our understanding are basic measurements of the composition and drivers, preferably at more than one local time simultaneously. Figure 2.10 [after *Meier et al.*, 2005]), shows a comparison between GUVI measurements of the O/N2 ratio (middle) during a geomagnetic storm and simulation results of the same storm (bottom), illustrating and example of both partial success and failure of models. While the model captures some of the variations, such as the daily variations in the southern hemisphere, it misses significant dynamics in the northern hemisphere, including the second intensification of O/N_2 ratio changes during the storm. It is not clear why the model fails in this regard, since the measurements were not comprehensive enough to give insights as to the model limitations. For example, if the plasma convection, neutral winds, or actual densities of oxygen and molecular nitrogen were measured in different local times, the dynamical response of the IT system to the storm could have been evaluated and compared to the global model results. Instead only a single orbit plane could be compared with height-integrated values.

With NO, the situation is also complicated, since the chemistry and dynamics that control the NO density are difficult to accurately capture with models. The density of NO is strongly controlled by EUV radiation, auroral precipitation, and Joule heating, with EUV responsible for mostly seasonal changes and the precipitation and Joule heating affecting how the thermosphere NO reacts to magnetic activity at high latitudes [e.g., *Mlynczak et al.*, 2008; *Lu et al.*, 2010]. Furthermore, NO created during geomagnetic activity can spread out to lower latitudes due to its long lifetime [*Siskind et al.*, 1989; *Barth et al.*, 2009], changing the energy balance of the local region. NO chemistry is dependent on the excited states of atomic nitrogen, which are challenging to simulate. NO also lasts a very long time in dark conditions, so correctly modeling the background conditions of the NO density in winter is difficult for models. This is because for long lasting species, tiny errors in vertical transport integrated for long periods (i.e., weeks to months) can cause large density errors. This is what happens with NO descending into the mesosphere and stratosphere in the winter polar cap [e.g., *Randall et al.*, 2005; *Newnham et al.*, 2018]. When the background state of NO is not correct, it is unclear whether the transport mechanisms that occur during a storm are capturing the dynamics correctly, or the background state is correct but the dynamics are incorrect. Wind and composition measurements are needed to evaluate these issues.

Simulation studies have shown that the helium in the thermosphere reacts quite differently from the major species during storms, which is contradictory to

empirical models. This was discovered by comparing mass density measurements from the CHAMP and GRACE data, which were at different altitudes. When these measurements were "corrected" to the same altitude, there were differences that could not be easily explained without allowing for more helium to have been present at GRACE altitudes. Without composition measurements, it is almost impossible to validate the modeling results and understand the dynamics of the minor species during geomagnetic storms. Following helium will facilitate tracking of a non-reactive tracer constituent, which will allow for a mapping of the flow throughout the thermosphere as well as a more accurate specification of the neutral mass density and its impact on LEO vehicles [*Sutton et al.*, 2015].

In order to fully understand how compositional changes are driven by winds at mid- and low-latitudes, it is critically important to measure the possible sources of the compositional changes:

- Upwelling: Changes in neutral composition and density are associated with vertical neutral winds and the differing neutral species scale heights. Thus, measured changes in the vertical wind must be reconciled with the assumption of hydrostatic equilibrium, which additionally requires knowledge of the neutral temperature.

- Horizontal advection: After upwelling, it is theorized that equatorward directed winds will transport molecular species from the high latitudes to mid-latitudes. In this case, the horizontal wind and gradients of the density and composition must be measured, most importantly in the north/south direction.

- Horizontal divergence/convergence: Changes in density/composition can also be driven by convergence or divergence in the winds. Because the background density is different for each of the species, the relative change in the composition can be modified greatly for convergent or divergent flow. For this to be investigated, the density and composition must be measured as well as the gradients in the winds, especially the latitudinal gradient in the north/south wind.

While compositional changes take place over several hours, the uplifting process can take place over a few minutes, since it is quite difficult to maintain strong vertical winds in the thermosphere. In addition, regions of strong upwelling may be quite isolated in longitude. Thus causal mechanisms (specifically upwelling and divergence) require temporal remeasuring on scales of order 5 minutes with longitude separations of ~15°-30°. To examine temporal evolution at larger spatial scales, remeasuring sub-auroral latitudes between 40°-60° geographic, where the gradients in the composition can be maximized, at times greater than 30 minutes and local times separated by 3 hours is appropriate. In addition, having local times span the full range from 0 to 24 hours will allow investigation of how the background conditions in solar irradiance affect the dynamics of the transport.

Scientific Measurements *Obj. 2.3*

Forcing Physical Parameters: vertical and horizontal neutral winds, neutral density, neutral composition, neutral temperature

Response Physical Parameters: neutral density, neutral composition

Measurement Characteristics:

- Timescales: vertical upwelling can occur on timescales of 5-10 minutes, global-scale advection can occur on timescales from 30 minutes to several hours; different seasons and activity levels

- Local time coverage: for longitudinal gradients of the winds, 3-6 hours of local time coverage with spacing between 1-2 hours are needed; for global-scale dynamics, the coverage and separation can vary to explore scale sizes in the longitudinal direction;

- Latitudinal coverage: approximately global latitudinal coverage is needed with less than 0.5° res.

- Altitudinal coverage: measurements between 200-450 km desired; vertically aligned measurements occasionally to verify altitude profile assumptions in the density and composition

Objective 2.4: Characterize the spatial and temporal variability in IT parameters that results from the transfer of momentum and energy from atmospheric tides and gravity waves.

In order to fully understand the impact of magnetospheric drivers and the evolution of structures within the IT system, it is necessary to determine the baseline state and the baseline variability of the IT system [*Forbes et al.*, 2000; *Rishbeth and Mendillo*, 2001]. During geomagnetically quiet conditions, the variability of the upper atmosphere may be dominated by tidal and gravity waves entering the IT system from below [*Pancheva and Mukhtarov*, 2012; *Liu*, 2016]. Atmospheric waves represent a key dynamic process of energy transfer in the horizontal and vertical directions, and are important sources of variability in the IT system [*Liu*, 2016]. A comprehensive understanding of how tides, planetary, and gravity waves affect the global IT system requires first and foremost knowledge of how the global wave spectrum evolves temporally and spatially in the thermosphere.

Transfer of momentum and energy from atmospheric waves can be manifested in the IT system on a large variety of temporal scales, from several minutes to 2-3 hours for atmospheric and ionospheric disturbances and 8, 12, 24 hours for tides [*Yigit and Medvedev*, 2015; *Liu,* 2016]. Furthermore, multi-day and multi-week changes in temperature, wind, composition, and electron density can be related to wave dissipation [*Jones et al.*, 2014]. A large variety of gravity waves and non-migrating tides also leads to a complex latitudinal and longitudinal variation in the IT behavior. Figure 2.11 [*Lin et al.*, 2007] shows an example of the longitudinal variation of total electron content between 400-450 km from COSMIC observations. This variation is enhanced during daytime hours and is manifested as a 4-peak structure in the low-latitude ionosphere. The 4-peak longitudinal pattern is attributed to the influence of non-migrating eastward

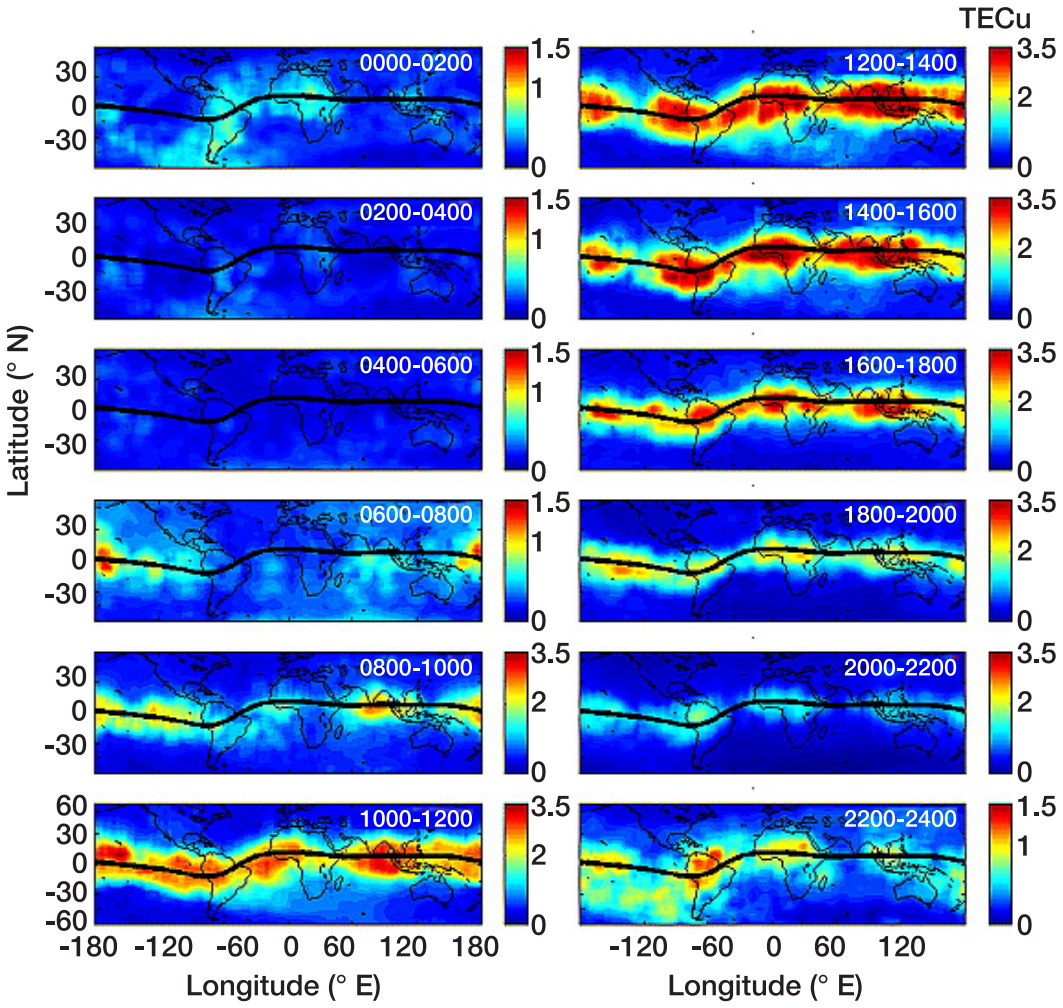

Figure 2.11. Temporal variations of the four-peaked longitudinal structure of integrated TEC (1TECu = 10^{12} electrons/cm^2) between 400 and 450 km in two hour segments. The color contour levels vary in different subplots in order to clearly show the four-peaked structure. From *Lin et al.* [2007].

propagating diurnal tide DE3 which is generated by solar heating of tropospheric clouds. Figure 2.12 shows large differences in electron density at two neighboring longitudes corresponding to a peak and a minimum in the longitudinal structure. Although significant progress has been made in understanding low-latitude ionospheric effects of the non-migrating eastward propagating diurnal tide [*Immel et al.*, 2006; review by *England*, 2012], the effects of other atmospheric tides are not well known, though they could be even more important. For example, semidiurnal tides have longer vertical wavelength and reach higher amplitudes than diurnal tides, potentially leading to a higher impact on the IT system, but the extent of the impact is not known due to the lack of observations. Short-term (~1 day to multi-day) variations of amplitudes and phases of different tidal modes and gravity waves are in particular not well understood, although they can significantly contribute to day-to-day variations of the IT system.

Planetary waves are generally not expected to propagate above ~100 km, however, they do modulate tides and gravity waves, which then impose planetary wave periodicities on the IT system well above 100 km. Numerical models have only limited success in reproducing tidal variations in the mesosphere-lower thermosphere [*Pedatella et al.*, 2014], and related variability in the F-region ionosphere [*Pedatella et al.*, 2016].

The altitude region from about 100 to 200 km is particularly important for understanding how atmospheric waves affect the response of the IT system to magnetospheric input, since this is where the vertically propagating tides and gravity waves are dissipated and the E-region dynamo electric fields are generated. Both migrating and non-migrating semidiurnal tides reach their maximum amplitudes at altitude 110-120 km, but can remain significant even above 300 km [*Häusler and Lühr,* 2009; *Forbes et al.*, 2009; *Oberheide et al.*, 2009].

GW waves and tides affect the IT system through two different pathways. One of these pathways (indirect effect) includes wave propagation to the E-region only, generation of E-region dynamo currents, which drive F-region drifts, and finally modify the F-region electron density through vertical advection. The second pathway (direct effect) includes propagation and dissipation of waves in the F1-F2 regions, where they can directly affect

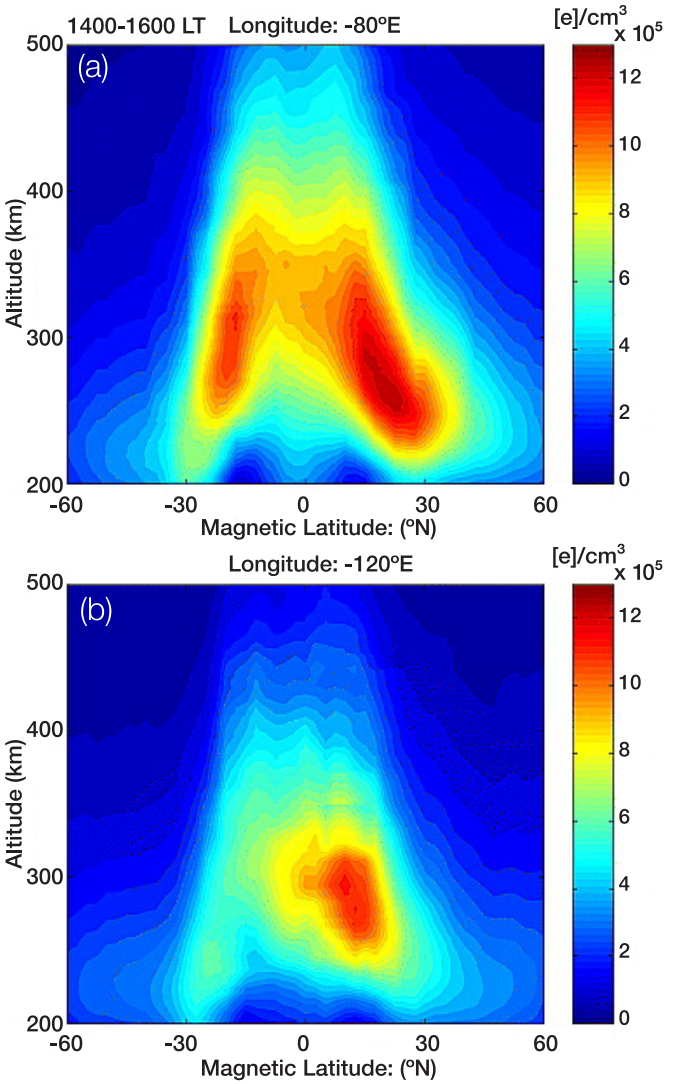

Figure 2.12. Cross-section plots of the equatorial ionization anomaly in longitude regions where it is stronger (80° E) and weaker (120° E) at 1400–1600 LT. These plots show that the anomaly has significant structure due to longitudinal variability From *Lin et al.* [2007].

temperature, winds, and thermospheric composition. In order to separate these pathways, observations are needed at different altitudes within the IT system with sufficient altitude resolution.

Our knowledge of tidal and GW variations at altitudes between 100-200 km is particularly limited. Ionospheric waves are ubiquitous and omnipresent throughout the entire ionosphere, and some of these waves are generated by atmospheric gravity waves. Upward propagating gravity waves cause turbulent mixing and small-scale plasma variations. Dissipation of gravity waves is expected to create secondary and tertiary gravity waves and generate perturbations in thermospheric wind and density, but serious discrepancies exist between

observations and theory [*Vadas and Crowley*, 2017]. Though TIDs are often seen propagating equatorward from high latitudes, they are not well correlated with magnetospheric energy inputs, but instead are well correlated with middle atmospheric phenomena like the polar vortex [*Frissell et al.*, 2016].

This Objective aims to quantify contributions from atmospheric waves to the variability of IT parameters (for example, temperatures, winds, neutral densities, neutral composition, plasma drifts, and electron densities) on global to regional spatial scales and on hourly to seasonal temporal scales. This Objective will address when and where (in latitude, longitude, and altitude) contributions from tides and GW have significant impacts on the IT parameters. The intent of this Objective is to establish the baseline variability of the IT system as controlled by atmospheric tidal and gravity waves entering the IT system from below in order to assess their relative importance as compared to the magnetospheric inputs.

Current understanding of wave-induced IT variations is based on limited data from ground-based observations or highly averaged data from UARS, TIMED, CHAMP, GRACE, and COSMIC, with most of the measurements pertaining to altitudes below 110 km or above 350 km. Due to the scarcity of available data, current understanding is limited to climatological features (i.e., 60-100 day average). It is not known how the global IT system responds to day-to-day variability of tides or how it responds to gravity wave forcing, although theory and modeling suggests both of the above effects to be profound.

In order to fully understand how much influence planetary, tidal, and gravity waves have on the baseline state and day-to-day variability of the thermosphere and ionosphere, it is critically important to measure various neutral and plasma parameters simultaneously:

- Plasma velocity vector: Underlying wave signatures in the plasma motion perpendicular to the magnetic field indicate the presence of dynamo currents driven by neutral wave motions. Underlying wave signatures in the plasma motion parallel to the magnetic field can be compared with horizontal wind motions to reveal the presence of local collisional forcing of the plasma by the neutral gas.
- Altitude profiles of cold plasma density: Wave signatures in the height and density of the F-peak are indicative of wave forcing
- Neutral density: Neutral density variations will reveal the presence of local wave motions in the neutral gas.
- Neutral composition: Propagating waves in the neutral gas will present signatures with different phases in the neutral composition.
- Altitude profiles of neutral wind: The horizontal wind variation with altitude will reveal the horizontal and vertical wavelength of wave features.
- Altitude profiles of neutral temperature: The neutral temperature profile will reveal changes in the neutral pressure and the heat balance produced by wave motions.

Planetary waves have time-scales of days to weeks, while gravity waves can have periods from 10-12 minutes to several hours. Tidal amplitudes and phases can possibly change on a day-to-day basis. Gravity waves can be quite localized, with scale sizes of 10s of km, while tides have wavelengths in the longitudinal direction that are dependent on their wave number, which means that the spacing of measurements in local time / longitude will determine which tides can be tracked over a given time period. For example, to capture the diurnal tide, two local times need to be measured; to capture the semi-diurnal tide, four local times need to be measured; etc.

Scientific Measurements *Obj. 2.4*

Forcing Physical Parameters: altitudinal profiles (100-200 km) of horizontal neutral winds, altitudinal profiles (100-200 km) neutral temperatures

Response Physical Parameters: plasma velocity vector, neutral density, neutral composition, altitude profiles (near 200-300 km) of cold plasma density

Measurement Characteristics:

- Timescales: from ~10 minutes to several days; different seasons and activity levels;
- Local time coverage: 2-6 hours of local time coverage with approximately 1-3 hours of spacing to investigate gravity waves; global local time coverage with spacing between 3-4 hours (considering both ascending and descending nodes); coverage and separation can vary to explore scale sizes and gradients
- Latitudinal coverage: all latitudes, 0.1° res. for plasma/fields and 0.5° res. for neutrals
- Altitudinal coverage: measurements between 100-300 km desired with ~1/2 scale height altitude resolution (~10 km in the lower thermosphere to 20+ km in the upper thermosphere) to resolve vertical wavelengths

Objective 2.5: Quantify the roles of radiative cooling and neutral winds in dissipating thermospheric energy

Energy added to the thermosphere is almost completely dissipated in the form of radiative cooling by nitric oxide and carbon dioxide at altitudes below about 150 km [*Maeda et al.*, 1989, 1992]. Most of the energy is not dissipated at the same location in which it is added, so three processes serve to move energy from one location to another - namely transport of existing temperature gradients , adiabatic heating and cooling , and thermal conduction . Ultimately, when investigated over global scales and longer time periods, these three processes don't tend to dissipate energy, but move it from one location to another. The winds tend to move the energy horizontally across the globe, while vertical conduction tends to move the energy to lower altitudes, where radiative cooling dissipates the energy [*Barth et al.*, 1988].

This simplistic description works on a global scale over long time periods, but during time periods when significant energy is added to the system, such as during geomagnetic storms, the amount of energy added to the system overwhelms the ability to move or dissipate energy [*Knipp et al.*, 2013; *Knipp et al.*, 2017]. This leads to massive heating at high latitudes, and the creation of equatorial directed winds. These winds both advect the strong temperature gradients as well as adiabatically cool the high latitudes . In addition, auroral precipitation generates NO at low altitudes, which increases the radiative cooling [*Mlynczak et al.*, 2003], allowing the thermosphere to recover faster to storms than expected. Further, as described in Objective 2.3, NO can be upwelled and advected to lower latitudes, allowing enhanced radiative cooling to take place in those locations.

Therefore, the thermospheric temperature and density response to energy input is extremely sensitive to the balance between winds and radiative cooling. In order to understand the dynamical response of the system to energy input, this balance must be determined.

In order to better understand the energy balance in the thermosphere during active time periods, it is important to understand both the sources and sinks of energy. Because NO is considered to be a critical cooling agent in the thermosphere, it is important to understand what is controlling its production and loss. NO radiative cooling, in fact, has been measured for the past 18 years by the SABER instrument on the NASA TIMED satellite [e.g., *Mlynczak et al.*, 2018]. However, there are no thermospheric composition or temperature profile data from the TIMED mission. Thus the infrared output has been very well characterized but the behavior of the thermosphere that generates this output, and the overall thermosphere response, is still unknown.

An example of how NO radiative cooling increases during a magnetic storm is shown in Figure 2.13 from the SABER instrument on TIMED [*Mlynczak et al.,* 2018]. It is difficult to understand this storm-generated increase in NO production, and hence accurately model it, because of its complicated chemistry and it remains one of the outstanding uncertainties on the energetics of a storm. For example, *Knipp et al.* [2017] showed that the structure of a coronal mass ejection (CME), specifically whether or not it contained a shock, greatly influenced the temperature and density of the thermosphere during

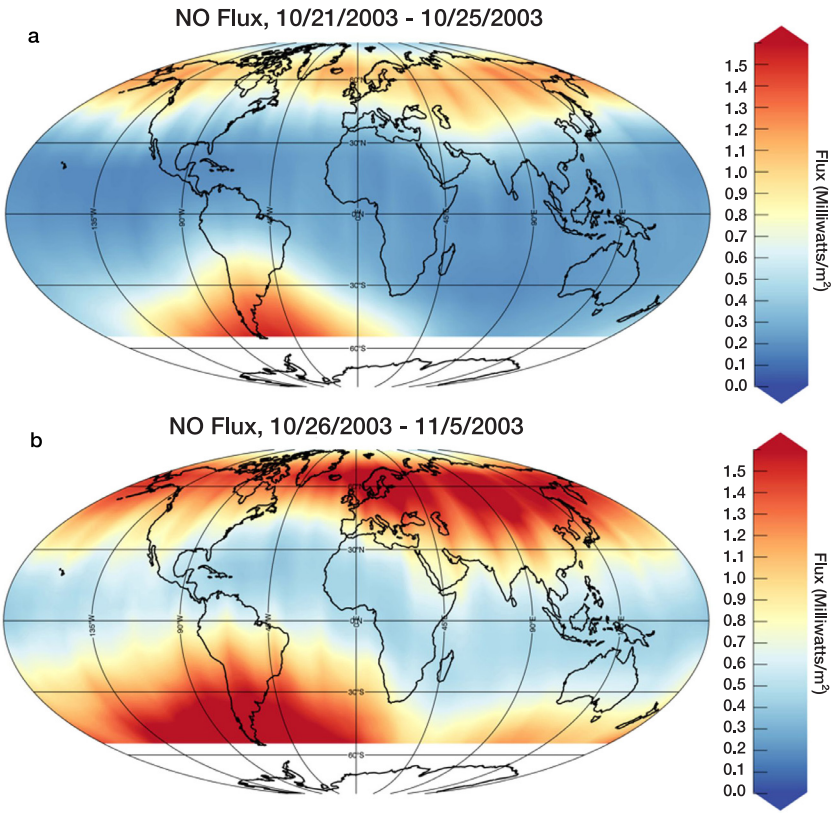

Figure 2.13. A demonstration of the dramatic increase in NO radiative cooling observed by Sounding of the Atmosphere using Broadband Emission Radiometry (SABER) during the 2003 Halloween storm. (a) Prestorm fluxes (mW/m^2) of infrared radiation from nitric oxide (NO) observed by SABER between 21 and 25 October 2003. (b) Fluxes (mW/m^2) of infrared radiation from NO during storm conditions from 26 October to 5 November 2003. From *Mlynczak et al*. [2018].

a geomagnetic storm. They discovered that some storms that should have had an extremely large thermospheric temperature and mass density increase (as measured by CHAMP) did not. The differentiation between smaller than expected responses and expected responses had to do with the auroral particle precipitation and the generation of significant NO density in the high latitudes. Storms with smaller than expected responses had significantly more NO produced than the other storms. Thus in addition to the complexities of the internal chemistry of the thermosphere, the forcing mechanism itself strongly determines the cooling response.

Because there are very few measurements of the neutral winds, especially on a global scale, the role of winds in moving energy across the globe during geomagnetic storms is very unclear. Simulation results highlight the disturbance winds, but their role in energy balance is not discussed often, since it is not at all clear whether the simulated winds are correct. **Neutral wind measurements are critical for resolving the dynamical evolution of the energy within the thermosphere.**

In order to fully understand the dynamic energy balance of the thermosphere during active time periods, it is important to measure various physical parameters of the system:

- Determining the amounts of NO and CO_2 in the thermosphere observationally is quite challenging. Their infrared emissions are readily measured [*Mlynczak et al.*, 2005], but they are dependent on the temperature and atomic oxygen density. The temperature dependence of the infrared emission is non-linear. For NO in particular, model calculations must get the NO density, the O density, and the neutral temperature reliably in order to compute the correct cooling rates. Measurements of NO density, temperature, and atomic oxygen will greatly advance the ability to verify model physics and chemistry for computing the critical rates of radiative cooling. Changes in the composition at higher altitudes will provide a quantification of how the densities of radiative coolers change during and after heating events.

- Horizontal advection: Once energy is added to the high latitude region, equatorward directed winds transport enhanced temperatures from the high latitudes to mid- and low-latitudes. The horizontal gradients of the temperature must be measured, especially in the north/south direction. In addition, the winds, especially in the north/south direction, need to be measured.

- Horizontal divergence/convergence: Changes in temperature can also be driven by convergence or divergence in the winds. For this to be investigated and quantified, the temperature must be measured as well as the gradients in the winds, especially the northward gradient in the north/south wind.

Objective 2.6: Determine how hemispheric asymmetries in the Earth's magnetic field, seasonal variations, and magnetospheric input affect the ionosphere-thermosphere system

In the IT system, the solar irradiance differences between the seasons drives first-order hemispheric asymmetries in the temperatures, densities, composition, and winds in the thermosphere. The winter hemisphere receives less sunlight, and therefore is colder and less dense in the neutral atmosphere. This sets up a circulation pattern that roughly flows from the summer hemisphere to the winter hemisphere. From this circulation, one would then expect that there should be a simple maxima in the neutral density in the summer hemisphere with a minima in the winter hemisphere, but this is not observed at all altitudes [*Bruinsma and Forbes*, 2010] or latitudes [*Zesta et al.*, 2016]. There is a much more complicated dependence, with maxima occurring sometimes during the equinox seasons [*Liu et al.*, 2007; *Qian et al.*, 2009; *Zesta et al.*, 2016]. This may be the result of the hemispherical differences impacting the creation and evolution of the upward propagating tides and gravity waves, the complex feedback between the thermosphere and ionosphere, or most likely a combination of the two. At this time, the causes of these differences between the hemispheres remains unclear.

The Earth's approximate dipole magnetic field is additionally tilted and offset from the geographic axis, producing further hemispheric asymmetries in the plasma density and dynamics. The varying tilt of the Earth's dipole field also alters the magnetospheric coupling with the solar wind and interplanetary

Scientific Measurements *Obj. 2.5*

Forcing Physical Parameters: NO and CO_2 cooling rates, neutral density and composition, horizontal neutral winds. Altitude profiles (from approximately 50 km to 150 km) of neutral temperature and oxygen density are needed to estimate the cooling rates.

Response Physical Parameters: neutral temperature

Measurement Characteristics:

- Timescales: Both the changes in neutral densities that drive increased radiative cooling, and the changes in the neutral winds occur over the time-scales of an hour or more. The NO density enhancements driven by geomagnetic storms can last for at least a day or two after the storm is finished. Therefore measurements with a remeasurement time of approximately 30 minutes to several hours are acceptable; different seasons and activity levels need to be investigated;

- Local time coverage: The longitudinal/local time scale size of the meridional wind is expected to be large, so all local times need to be covered, but with relatively coarse resolution (4-6 hours) to allow for a comparison between the different driving in different local times; determining the scale-size in local time could be investigated by allowing orbital plans to vary in spacing.

- Latitudinal coverage: global coverage is needed with < 50 km res. for neutrals;

- Altitudinal coverage: measurements of the neutral winds and temperatures are needed between 200-450 km, since these states are roughly constant in altitude in this region. Vertically aligned measurements occasionally to verify altitude profile assumptions. In order to estimate the NO and CO_2 cooling rates, the temperature and oxygen density from approximately 50 km to 150 km with approximately 1/3 scale height resolution (approximate 3 km).

Modeling Studies

The vertical thermal conduction is extremely difficult to measure, since it relies on having a vertical profile of the temperature and thermal heat conduction coefficient, which can't be measured. Modeling of events to explore the role of thermal conduction in moving energy from higher altitudes to the region of radiative cooling will assist in addressing the Objective. In addition, to more fully understand the NO and CO_2 cooling rates, how those relate to the NO and CO_2 density changes during and after a heating event, and how the energy is lost from the system through radiation, models will be needed to complete the radiative transfer.

magnetic field reflected in changes in the ion convection velocity in the ionosphere. Because the high-latitude forcing of the ionosphere is most strongly influenced by the magnetic field, the rotation of the magnetic pole around the geographic pole drives a UT dependence in both the drivers (i.e., ion convection and aurora) and the background conditions (solar EUV driven thermospheric structure), and this UT dependence is different in the northern and southern hemispheres [*Perlongo et al.*, 2016].

The structure of the magnetic field is different between the two hemispheres, with the northern hemisphere having two "peaks" in the magnetic field dip angle, and the southern hemisphere having a strong longitudinal dependence in the strength, but a single peak in dip angle near the pole (see Figure 2.14). This hemispheric asymmetry in the magnetic field is thought to drive differences in ion drifts through many different mechanisms reviewed by *Laundal et al.*, [2017]. The ionospheric conductivities (both Pedersen and Hall) are dependent on the strength of the magnetic field, [e.g., *Richmond,* 1995; *Cnossen et al.*, 2011; *Cnossen et al.*, 2012] with associated effects on the plasma drifts that are dependent on them [e.g., *Ridley et al.*, 2004; *Tanaka*, 2001; *Lotko et al.*, 2014; *Tu et al.*, 2014]. There are large longitudinal differences in the magnetic field and those longitudinal differences are quite different between the two hemispheres. Thus, the hemispheric asymmetry in the ionospheric conductivities in the region where strong flows driven by substorms exist, may be UT dependent [e.g., *Laundal*, 2010a,b]. Studies of the high latitudes cross polar cap potential (CPCP) have shown that the magnitude CPCP on average is 5-10% stronger in the southern hemisphere [e.g. *Pettigrew et al.*, 2010; *Papitashvili and Rich*, 2002; *Förster and Haaland*, 2015]. *Förster and Cnossen* [2013] use a global MHD code to show that with asymmetric magnetic fields, they could get stronger flows with weaker magnetic field values. Other studies have shown that there are systematic differences in the ion drifts between the hemispheres when the IMF By is large [*Knipp et al.*, 1994; *Forster et al.*, 2008]. *Laundal et al.*, [2017] showed with a mathematical model that with the same CPCP, the northern hemisphere had a larger UT variation in the plasma drifts and larger drift speed the majority of the time, but during some UTs, the southern hemisphere drifts would be larger.

Advances in our understanding of hemispheric asymmetries in the IT behavior require simultaneous observations of the key drivers and responses in northern and southern hemispheres over for all seasons. Most important will be the identification of spatial features in the plasma density and neutral wind that evolve for similar driving conditions and a description of the hemispheric differences that may be related to magnetic field structure and or land-sea distributions.

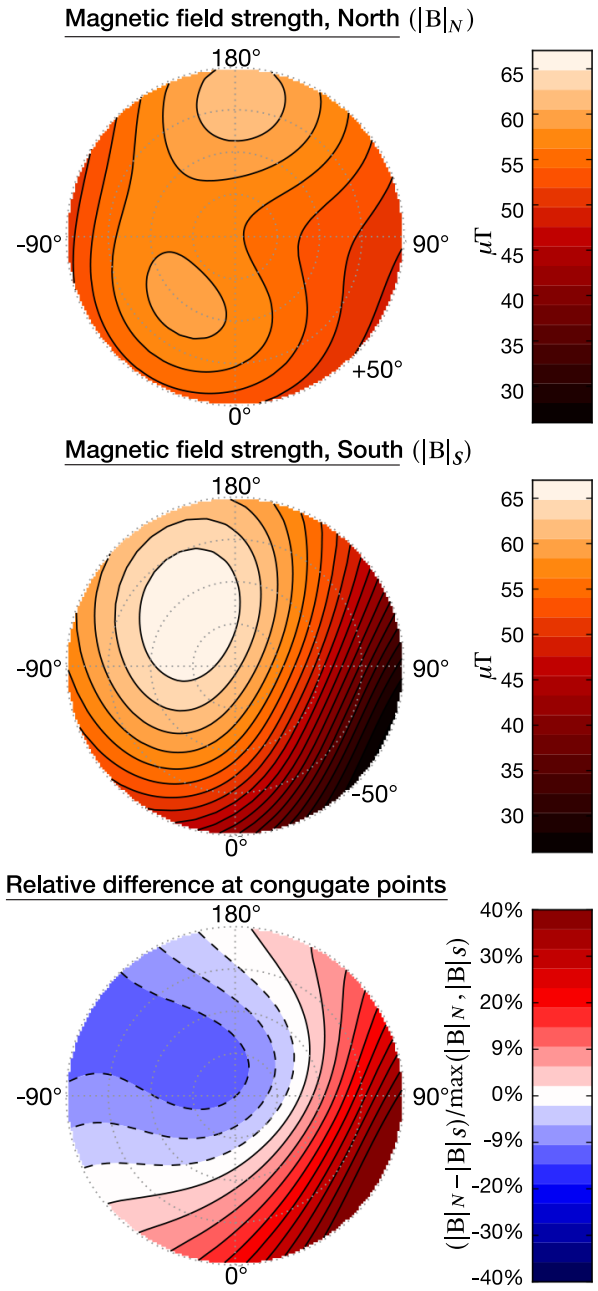

Figure 2.14. Magnetic field strength in apex coordinates in the northern hemisphere (top) and southern hemisphere (middle). From *Laundal et al.* [2017].

Differences in the IT system between the two hemispheres are complicated due to intrinsic asymmetries in Earth's magnetic field, seasonal effects, land-sea distribution, hemispherically asymmetric coupling between the magnetosphere and the solar-wind, and non-linear feedback between the magnetosphere and ionosphere in controlling the drivers of the IT system. Electron densities, plasma velocities [e.g. *Yakymenko et al.*, 2018; *Liu et al.*, 2018], neutral wind velocities, and composition have all been observed to statistically exhibit hemispheric asymmetries [*Barlier et al.*, 1974; *Forster et al.*, 2011] and these asymmetries are often enhanced during geomagnetic disturbances [e.g. *Zhang et al.*, 2017]. Hemispheric asymmetries may be responsible for the semi-annual oscillation, in which the thermospheric density does not oscillate in magnitude as expected during the seasons [*A et al.*, 2012], and is not easily predictable, making satellite drag and therefore collisions, more difficult to predict.

In the ionosphere, there are large differences between the hemispheres when smaller-scale ionospheric structures are investigated [*Spicher et al.*, 2017]. For example, the magnetic pole offset allows the convection throat in the southern hemisphere to extend to lower latitudes during certain times of day as compared to the northern hemisphere, which should drive stronger tongues of ionization in the southern hemisphere as seen in modeling studies [*Liu et al.*, 2017]. However, observations show tongues of ionization appear to be strongest over the continental US, although this may be due to the southern hemisphere having significantly worse coverage in ionospheric measurements than the northern hemisphere [e.g. *David et al.*, 2016]. It is unclear why the northern hemisphere would have a larger amplitude ionization structuring. Measurements from GDC will help address whether this is indeed true, and will allow researchers to understand the driving mechanisms that cause different structuring in the northern and southern polar regions.

With respect to neutral density variations, there are also significant differences between the northern and southern hemispheres, as shown previously in Figure 2.5. This is also apparent in the response to geomagnetic storms, as shown in Figure 2.15 [*Sutton et al.*, 2009]. Here, CHAMP data shows significant increases in neutral density in the northern hemisphere during a geomagnetic storm in July 2004 believed caused by variations in Joule heating. Although the stronger solar EUV in the northern hemisphere in July could account for some of this variation (as well as some differences in the CHAMP satellite geopotential height, described by *Sutton et al.* [2009]), the large hemispheric differences

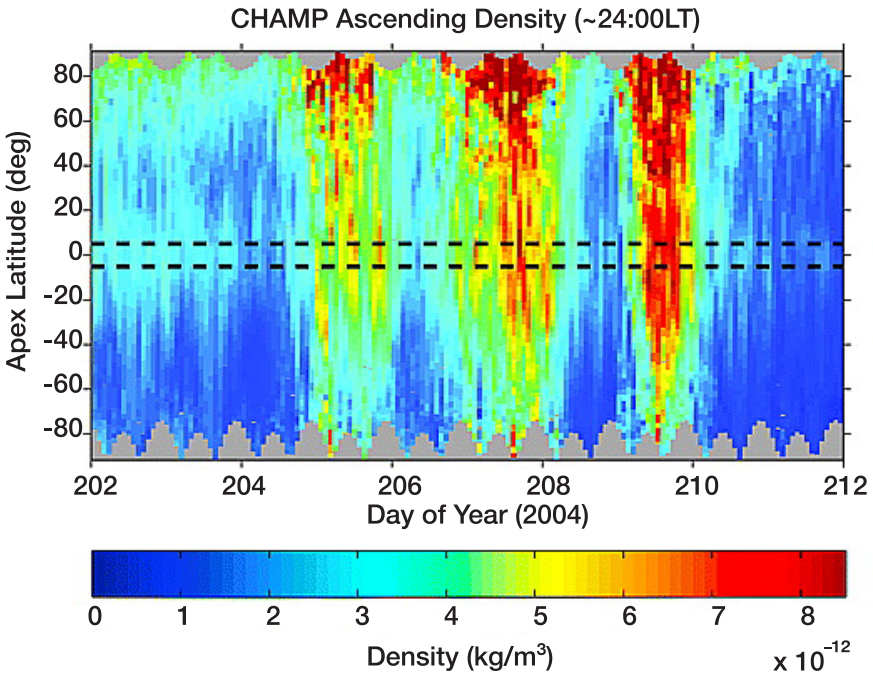

Figure 2.15. Neutral density measured during the ascending portions of CHAMP's orbits (2400 LT) given in magnetic coordinates during 20–29 July 2004. From *Sutton et al.* [2009].

in energy injection during storms and the subsequent response of thermosphere need to be understood.

In order to fully understand what controls hemispheric asymmetries in the thermosphere and ionosphere, it is critically important to measure various neutral and plasma parameters simultaneously:

- Background magnetic field: The magnetic field structure controls the ion drift and the auroral precipitation in each hemisphere. The magnitude of the field influences the strength of the plasma convection, while the angle of the magnetic field with respect to the ground controls the vertical component of the plasma convection, which will drive the loss rate of the ion density and the amount of drag with the neutrals. These quantities also influence the intensity of the auroral precipitation into the hemisphere - a weaker field allows more particles to enter the atmosphere where they collide and deposit energy into the hemisphere. These attributes can be quantified with both statistical studies that can tease apart the effects of local time, longitude, and hemisphere, and with event studies that quantify the reaction to energy input with measurements in different local time sectors and different hemispheres. While the magnetic field of the Earth is relatively stable, it does change over periods of several years. European missions such as CHAMP, GOCE, and Swarm have measured these changes in the past, and it is unclear whether they will continue these measurements into the future. Finally, it is extremely unlikely that measurements will be very often taken at exactly conjugate points (i.e., at both ends of the same magnetic field line), since conjugate points move rapidly due to currents in the magnetosphere and slowly due to changes in the background field. Therefore, analysis techniques will have to take these changes into account, perhaps using models to assimilate data or using multi-point measurements to increase the probability of having two observations that are closer to conjugate locations.

- Magnetospheric drivers: The plasma convection and auroral precipitation need to be measured to determine the degree to which the drivers of the system are asymmetric. The difficulty in obtaining conjugate measurements, makes measurements in different local time sectors crucial for describing the large-scale drivers.

- Background state of the system: In order to quantify how the dynamics of the system are asymmetric, the climatology of the background state needs to be quantified. This means that maps of the density, composition, temperature, and wind in both the thermosphere and ionosphere need to be created. These maps need to be created with enough resolution and temporal granularity that they can reveal any asymmetries in the system. For example, longitudinal structure for each local time and season needs to be captured. Having measurements in different local time sectors will greatly facilitate the creation of these maps (i.e., less time will be needed to build statistics, allowing better differentiation between drivers, driving down ambiguity).

- Reaction to energy input changes: The asymmetric dynamics of the system can be captured by measuring the system response to changes in magnetospheric energy input (plasma convection and auroral precipitation). It is often observed that the reaction to energy input is asymmetric (for example, Figure 2.10 illustrates that compositional changes in the northern and southern hemisphere are quite different). It is unclear whether this is due to background winds, or initial states, or whether the reaction is different at different local times / longitudes. Therefore, it is important to have measurements of the thermospheric dynamics at different local times in order to quantify and understand the origins of asymmetric reactions within the system. This reaction will also be reflected in the thermospheric density, composition, wind, and temperature.

In order to capture the global-scale dynamics of the thermosphere, a remeasurement time of approximately 30 minutes is needed, since neutral wind, density, and compositional changes occur over periods of a couple of hours. Because it will be impossible to systematically measure conjugate points, the scale-sizes of the processes that can be explored are more global in scale, so creating maps of different background states in the thermosphere with resolutions in latitude of 100+ km and 200+ km in longitude / local time is sufficient.

Scientific Measurements *Obj. 2.6*

Forcing Physical Parameters: plasma velocity vector, ion density and composition, auroral ionization and heating vertical profiles, ion and electron temperatures

Response Physical Parameters: neutral density, neutral composition, neutral wind velocity, and neutral temperature

Measurement Characteristics:

- Timescales: from 30 minutes to several hours; different seasons and activity levels;
- Local time coverage: global coverage with spacing between 4-6 hours; Coverage and separation can vary to explore scale sizes and gradients; need different longitudinal measurements in the same local time sector;
- Latitudinal coverage: approximately global coverage needed (<80° latitude), 0.1° res. for plasma/fields and 0.5° res. for neutrals
- Altitudinal coverage: measurements between 200-450 km desired; vertically aligned measurements occasionally to verify altitude profile assumptions.

2.4 Prioritization of Objectives

Outlined above are ten Objectives that, when completed, will enable a breakthrough in our understanding of how the thermosphere and ionosphere react to, and internally process, energy that comes from the magnetosphere and the lower atmosphere. While these Objectives describe a highly focused Living With a Star mission, prioritization is needed in order to help guide programmatic decisions in a budget-constrained environment. Here, we describe three levels of prioritization: Core, Core Comprehensive, and Core Enhancing, and specify which Objectives should be placed in each category. This prioritization was reached as an STDT group consensus.

Core

As described throughout this document, a systematic understanding of the dynamics of the thermosphere and ionosphere is the core of the mission. The IT dynamics cannot be addressed without a deep understanding of what drives the thermospheric neutral winds, as outlined in Objective 1.1. Therefore,

Objective 1.1: *Determine how high-latitude plasma convection and auroral precipitation drive thermospheric neutral winds.*

is elevated above all others. This is primarily because there is a realization that no progress can be made without measurements of the neutral winds - there is such a huge gap in our understanding of the climatological wind patterns, the variability in the patterns, and the ***dynamical evolution*** from quiet to disturbed conditions, that very little progress can be made in the field without these measurements gathered in conjunction with the associated high latitude drivers.

Core Comprehensive

While an understanding of what controls the high latitude neutral winds is of critical importance to determining how the thermosphere and ionosphere dynamically react to energy input from above and below, there are other important Objectives that provide a more comprehensive description of the coupled IT. These Objectives focus on how the neutral winds drive structures and changes within the system.

Objective 1.2: *Determine how localized, coherent plasma density features arise and evolve.*

Objective 1.3: *Determine how neutral winds, auroral precipitation, and collisional heating drive high-latitude neutral density structures.*

Objective 2.1: *Determine the relative importance of penetration electric fields and disturbance winds in driving plasma density variations at mid- and low-latitudes during geomagnetic storms.*

Objective 2.2: *Identify the processes that create and dissipate propagating structures within the ionosphere and thermosphere during active and storm conditions.*

Objective 2.3: *Determine the connections between winds and neutral density/composition variations at mid- and low-latitudes during geomagnetic storms.*

Core Enhancing

Finally there are Objectives that enhance the core by including a more expansive description of the intrinsic

variability in the background state of the IT and how it regulates the flow of energy through it.

Objective 1.4: *Determine how atmospheric tides and gravity waves influence the IT response to magnetospheric inputs.*

Objective 2.4: *Characterize the spatial and temporal variability in IT parameters that results from the transfer of momentum and energy from atmospheric tides and gravity waves.*

Objective 2.5: *Quantify the roles of radiative cooling and neutral winds in dissipating thermospheric energy.*

Objective 2.6: *Determine how hemispheric asymmetries in the Earth's magnetic field, seasonal variations, and magnetospheric input affect the ionosphere-thermosphere system.*

2.5 Use of Modeling to Specify Measurement Requirements

To support the analysis described in this section, NASA Headquarters tasked the Community Coordinated Modeling Center (CCMC) at NASA Goddard Space Flight Center, and flight dynamics engineers at NASA Goddard Space Flight Center and Applied Physics Laboratory, the Johns Hopkins University. The CCMC ran global IT models to examine the March 16-18, 2015 storm, and executed analysis guided by the STDT and NASA. For simplicity, this analysis assumed in situ, space-based measurements, and this section's discussion reflects that assumption even though the resulting measurement requirements are method-agnostic. The spacecraft trajectories used were provided by the flight dynamics support and assumed spacecraft in circular orbits at 400 km altitude and at 82° inclination taking measurements with no errors.

The STDT investigated and quantified key configuration requirements for achieving the science objectives. Specifically, to bound the spatial resolution for measured parameters and the remeasurement time between successive observations of local, regional or global parameters; and define temporal and spatial gradients of IT parameters.

This report has stressed the current severe lack of observations of the IT system on local, regional, and global scales. Thus, the analysis of IT global models, applied quantitatively to specific multi-platform event data, informed the science measurement requirements and implementation considerations. This analysis focused on the following three questions:

1. What is the optimal number of satellites in an orbit plane to recover latitudinally dynamic structure during geomagnetically active events, like storms?
2. What is the optimal number of orbit planes to reconstruct regional and global dynamics during geomagnetically active events, like storms?
3. What are the relevant temporal and spatial gradients in regional-scale phenomena?

The symmetric-H (SYMH) component of the disturbance storm time (Dst) index for the March 16-18, 2015 (Figure 2.16) had two separate onsets: one with a minimum SYMH of ~ -80 nT (onset at ~0620 UT), and one with a minimum SYMH of ~-230 nT (onset at ~1201 UT).

CCMC Models run for the March 17, 2015 storm

TIEGCM:
1. grid resolution 2.5° latitude by 2.5° longitude
2. spin-up time: 20 days
3. scale height: 1/4

GITM:
1. grid resolution 1° latitude by 4° longitude
2. spin-up time: 1 day
3. scale height: 1/3

CTIPe:
1. grid resolution 2° latitude by 15° longitude
2. spin-up time: 4 days
3. scale height: 1

(All models were run for the March 15-20, 2015 time period with 1 minute output.)

2.5.1 Question 1: What is the optimal number of satellites in an orbit plane to recover latitudinally dynamic structure during geomagnetically active events, like storms?

The full-resolution, global model simulation results were used as the "ground truth" for each IT parameter. Simulated

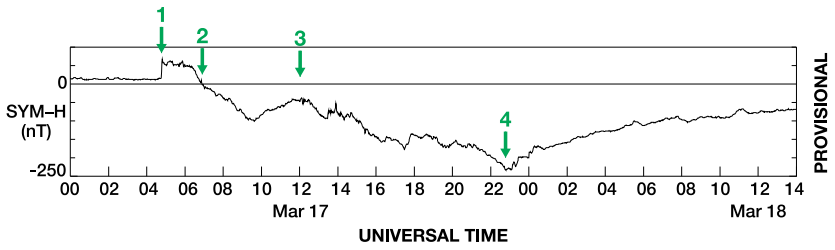

Figure 2.16. SYMH for the March 16-17, 2015 double storm. The first onset occurred at 0620 UT and the second onset occurred at 1201 UT.

spacecraft were "flown" in circular low-Earth orbit (LEO) paths at different local time meridians, "measuring" the IT parameter. For multiple spacecraft in the same orbit plane, the single trajectory was used and the spacecraft were spread out along it.

Four simulations were completed at CCMC for this analysis: the global ionosphere thermosphere model (GITM) and the coupled thermosphere ionosphere plasmasphere electrodynamics (CTIPe) model each run in standalone mode and with high-latitude driving from SWMF. The thermosphere ionosphere electrodynamics general circulation model (TIEGCM) was not used in this analysis. For each of the four simulations, "ground truth" was obtained from the simulation results by taking a single LT cut at 2° latitudinal resolution each minute from 03/17 0000 UT - 03/19 0200 UT. This was carried out for 00, 06, 12, and 18 LT meridians.

Figure 2.17 shows the GITM model ground truth for neutral mass density, along the 12 local time meridian for the full two day and two hour time period identified above. Significant events for the modeled storm (shock impact, onsets, and storm maximum) are identified with vertical green arrows at the top of the plot. The ground truth simulations show a series of high-latitude responses to the shock impact and the two different storm onsets, as well as series of TADs propagating equatorward.

Figure 2.18 illustrates the reconstruction procedure. Panel A is the ground truth extracted from the model run (shown in more detail in Figure 2.17). Panels B1 and B2 are the reconstructions of latitudinal dynamics by a single satellite and by 3 equidistant satellites, respectively.

The reconstructions used interpolations of the satellite

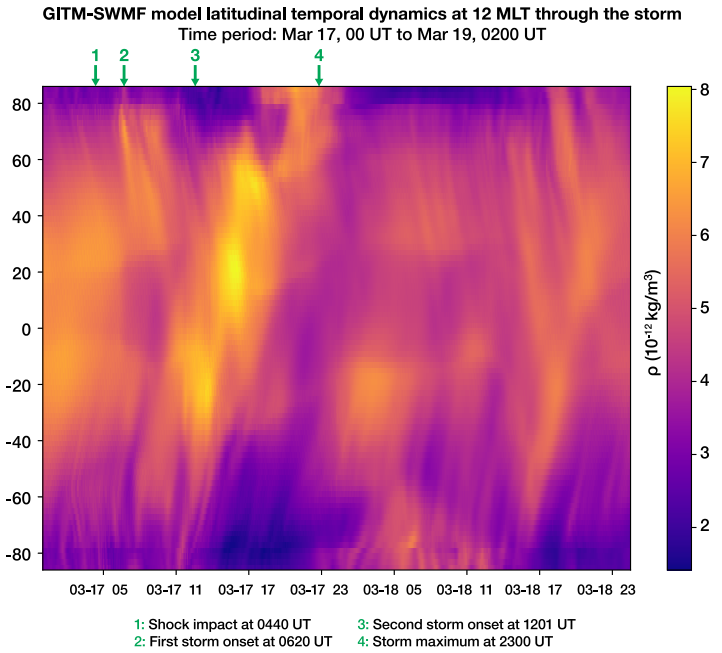

Figure 2.17. Model output of 'ground-truth' IT neutral mass density from the GITM-SWMF simulation for the March 17-18, 2015 storm, shown for 12 MLT. Green arrows at the top of the figure mark times of note in this period of activity.

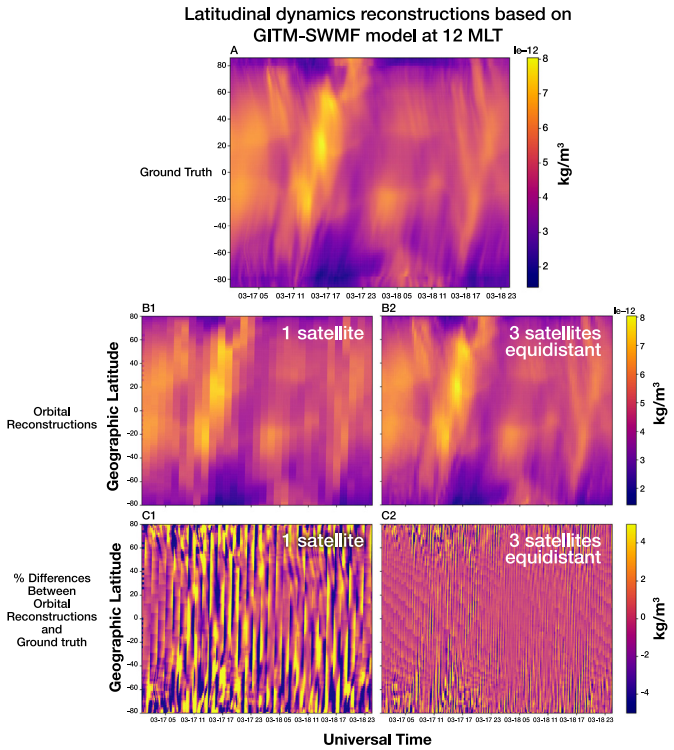

Figure 2.18. GITM-SWMF model ground truth of mass density and reconstructions in the 12 magnetic local time meridian for multiple satellite constellation configurations. Panel A shows the model ground truth. Panel B1 shows the reconstruction using one satellite; panel B2 shows the reconstruction using three equidistant satellites. Panel C1 shows the difference between the reconstruction and the ground truth; panel C2 shows the difference between the reconstruction and the ground truth. All panels show the same time and latitude range.

observations onto the model grid of 2° of latitude by 1 minute of time, covering all latitudes in a particular local time meridian for the entire storm period. Figure 2.17 shows the results along the 12 MLT meridian. By visual inspection alone, the 3 equidistant satellites reproduce the latitudinal dynamics significantly better than the single satellite along the same orbit. For example, the 3-satellite configuration better captures the TADs and their equatorward propagation, as well as the timing of different enhancements at different latitudes. Panels C1 and C2 show this improvement more quantitatively with the difference between the reconstructions and the ground truth; the 3-satellite configuration has smaller differences overall and the largest differences are restricted to the regions of finer structure rather than being more evenly spread throughout the reconstruction.

In order to remove potential biasing of the results by a spacecraft passing through a particular strong and/or complex feature, this analysis was conducted at multiple longitudes, with different spacecraft spacings, and with different initial starting latitudes. Specifically: 1) The reconstructions were performed at the 00, 06, 12, and 18 MLT meridians; 2) spacecraft trains were examined for both equidistant and uniform, 5-minute spacings; and 3) the spacecraft starting latitude was varied throughout the entire orbit path.

This analysis was run with the GITM and CTIPe models, both in a stand-alone mode and driven by the SWMF high-latitude dynamics. There was an impressive consistency between the two different models and good general agreement between the stand-alone runs and those driven by SWMF. All examples shown here are from the SWMF-driven GITM model for two reasons: 1) the SWMF run models showed better detail in dynamics and better enabled the quantification of reconstruction quality, and 2) the GITM model better produced regional cusp activity, which was used for the analysis of Question 3 below. In every other aspect, the results from the two models were impressively similar.

This analysis examined the statistical distribution, using the 2° latitude by 1 minute time grid, of the following properties: of the difference and error distributions using the differences between the reconstructed dynamics and the ground truth; the RMS error of these differences, and the bias of the differences. To separate

the different types of dynamics, the analysis separated the meridians into three different latitude regions: 1) northern high latitudes (50° to 80°); 2) southern high latitudes (-50° to -80°); and 3) mid and low latitudes (-50° to +50°).

Figure 2.19 shows the key results of this analysis for the 12 MLT meridian. The left column shows the median difference for the north (blue), south (orange) and equatorial (green) regions with respect to the number of satellites in the orbit. The top panel shows the median differences for equidistant satellites, and the bottom panel shows the median differences for satellites with 5-minute spacing. The middle column (difference RMS error) and the right column (different bias) are similarly structured.

For equidistant satellites, both the difference and the RMS error drop sharply up to 3 satellites, drop at a much slower rate for between 3 and 6 satellites, and level off after 6 satellites. These identified transition points have been marked on the plots with vertical black lines. The first transition point identifies the minimum number of satellites along one orbit that are required in order to reliably reproduce the global latitudinal dynamics; the second transition point is the number beyond which there are significant diminishing returns. The bias analysis (right column) shows large oscillations for fewer than 3 satellites, but those oscillations drop below +/- 0.1% after 3 satellites and level off to zero after 6 satellites; although the character of these variations are different than the difference and RMS error, the ideal range of spacecraft train length is consistent with them.

For satellite trains with 5-minute spacing, the median of the differences does not level off after 12 satellites, the RMS error does not drop to below 1% until 15 satellites, and the bias does not approach zero for fewer than 15 satellites. Considering that, for a 90-minute orbit (the orbit period at ~400 km altitude), inter-spacecraft spacing of 5 minutes requires 18 satellites to equidistantly cover the orbit, an orbit configuration with multiple, closely spaced satellites are not able to reliably capture global latitudinal dynamics at an adequate level of detail. However, the closely spaced configuration would be suited to the study of fast-varying regional-scale structure, as will be shown in the analysis for Question 3 below.

Conclusions

The optimal satellite configuration for recovering the global latitudinal neutral mass density dynamics in a given meridian requires a minimum of 3 equidistant satellites in the same orbit plane. There is quantifiable improvement for up to 6 equidistant satellites, but a marginal benefit for more than 6 satellites.

2.5.2 Question 2: What is the optimal number of orbit planes to reconstruct regional and global dynamics during geomagnetically active events, like storms?

This analysis was based on GITM simulations of 17-18 March 2015. The model outputs were re-gridded into a resolution of 2° x 2° in latitude and longitude. Global 2D maps of neutral density at ~400 km altitude with the 2° x 2° grid were used as the ground truth. The examples shown here were derived from the 2D maps of 18:00 UT on 17 March, 2015, and of 12:00 UT on 18 March, 2015. The ground truth maps were sampled for different satellite orbital configurations with an 82°-inclination orbit and a varying number of orbital planes. The separation of orbital planes is defined by a constant longitudinal increment so that the orbital planes are evenly separated over 360° at the ascending node of the orbits. The reconstructed density maps assume that the ground truth density distributions were stable over a typical orbital period of 90 minutes, i.e., the reconstruction is done for a single-instance map. This was done so that the question of how many different orbital planes are needed for spatial/longitudinal global reconstruction is isolated and answered. For the same reason, each simulated orbit contained a single spacecraft and the only thing changing was the number of orbits used to accomplish the reconstruction.

The reconstruction was performed by first collecting the "observations" along the orbits at 1 min sampling. Then the simulated satellite observations were binned into a 1° x 1° latitude and longitude grid. The 1° binning was finer than that of the ground truth in order to minimize the smearing of the satellite observations into larger bins. After binning, a simple interpolation scheme was used to fill in the latitude and longitude bins containing no satellite data. The interpolation was done in longitude

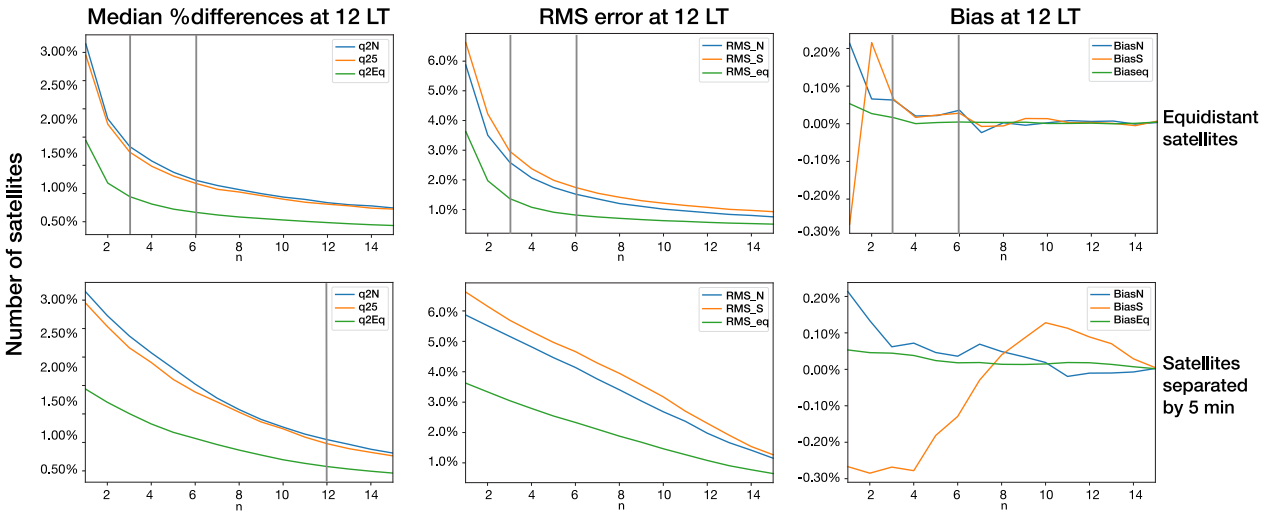

Figure 2.19. Reconstruction analysis for satellite trains in a single orbit path in the 12 MLT meridian. Each column shows a different aspect of the analysis between the reconstruction and the model ground truth: median difference (left), RMS error of the difference (middle), and bias of the difference (right). All analysis are split by the northern high latitudes (blue), southern high latitudes (orange), and mid/low latitudes (green). Vertical black lines mark identified distribution transitions.

first, then in latitude. After the interpolation, the results was smoothed over 4 degrees of latitude to eliminate the banding that emerges from the sparse latitude spacing. The interpolated values were rebinned into a 2° x 2° grid to be directly compared with the ground truth. The smoothing in latitude was necessary because of the rather coarse 1-min sampling used in the simulation.

Figure 2.20 shows the ground truth and reconstructions for the global neutral density map of 18:00 UT on 17 March, 2015. Panels 2.19(a)-(c) show the high latitude ground truth with 5 equidistant orbital paths for indication of coverage, the reconstruction with two satellite orbits, and the reconstruction with five satellite orbits, respectively. Panels 2.19(d)-(f) show the same properties but for the mid and low latitude range.

The accuracy of the reconstruction was quantified by taking the average of the absolute value of the percent difference between the model (ground-truth) values and the reconstructed densities for all the bins within the covered latitude region. Note the poor reconstruction from just two orbits and the significant improvement from 5 orbits. This is also manifested by the reduction of the average percent difference in Figure 2.20 from the 2-orbit reconstruction to the 5-orbit reconstruction.

The simulation was performed using 1 to 15 orbit planes and for satellite orbits that offset in longitude by 0, 30, 60, and 90 degrees. The longitude offsets demonstrate the effects of shifting the sampling locations of the simulated satellite data. The results would vary depending on the local time of the orbital meridians with respect to the features of neutral density and their spatial scales.

The quantitative analysis of the differences between ground truth and reconstructions are shown in Figure 2.21. The left two panels are for the northern high latitudes, and the right two panels are for the latitude range from -50° to +50°. Each panel displays the average percent difference between the ground-truth and the reconstructed values for the four different longitudinal offsets as indicated by the different symbols.

Figure 2.21 demonstrates that in all cases the relation between the number of satellite orbit planes and the accuracy of the reconstruction is a nonlinear function. The accuracy of the density reconstruction becomes nearly constant when the number of satellite orbital planes is increased to 6 in both the high-latitude and low-latitude region, although the first significant change of the slope occurs at 4 satellite orbital planes. With fewer orbit planes, the accuracy deteriorates rapidly. Note also that the longitudinal shift of the orbital planes from 0 to 90 degrees provides variable results only up to four orbital planes and the four curves overlap after that.

The STDT examined one storm and 4 different instances

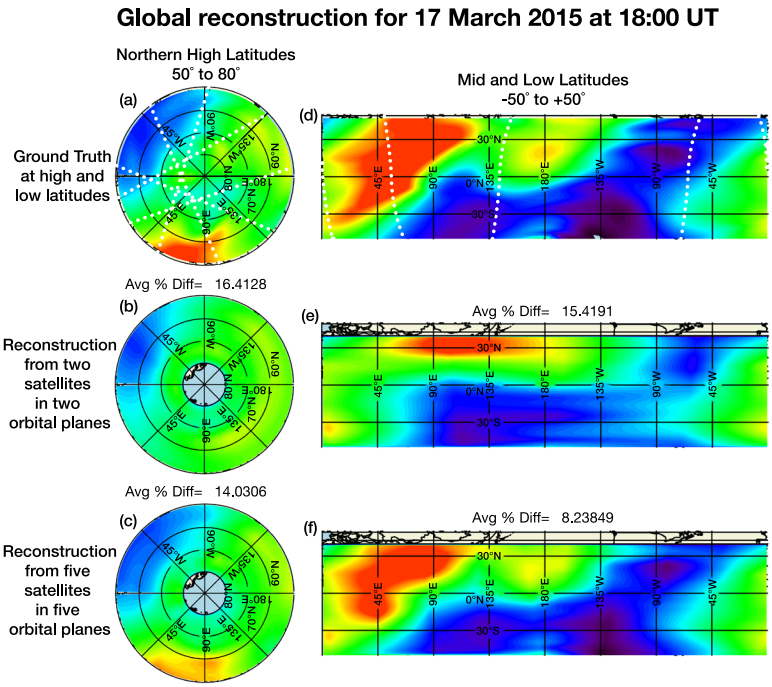

Figure 2.20. Global reconstruction example results. Ground-truth density maps (top). The solid lines indicate the projected orbits that are used for the reconstruction. Reconstructed density maps with 2 satellites (middle). Reconstructed density maps with 5 satellites (bottom).

during the storm, selected for their global feature variation. The results for all these instances (examples for two of them shown) are consistent even though the features are different for each instance. In future mission pre-formulation efforts to follow this report, this methodology should be extended to more storms for a more statistically supported result.

In conclusion, for recovering the global spatial structure of neutral density features during a storm, the optimum mission configuration requires a minimum of 4 orbital planes whose ascending nodes are evenly distributed over 360°. There is some quantifiable improvement for up to 6 orbital planes and no identifiable benefit for more than 6 orbital planes.

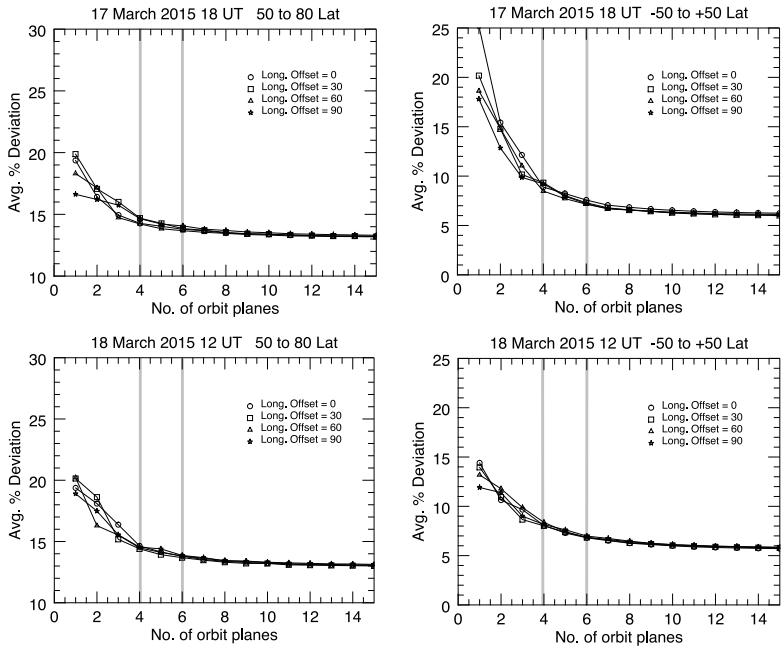

Figure 2.21. Average percent deviation of the reconstructed neutral density from the ground-truth density values as functions of the different number of orbit planes used in the reconstruction. The different symbols represent the longitude offset of the sampling meridional plane.

2.5.3 Question 3: What is the magnitude of temporal and spatial gradients that need to be observed in regional-scale phenomena?

Observing and understanding local and regional IT features is a key focus for GDC to accomplish on a global scale with a comprehensive set of measurements. This focus is addressed by almost all of the science Objectives. To quantify the expected gradients in these features, this part of the modeling analysis focused on the cusp feature that manifests as an enhanced neutral density after shock impulses or storm onsets [*Shi et al.*, 2017], but can also be a more "regular" feature under cusp precipitation [*Luhr et al.*, 2005; *Liu et al.*, 2010; *Clemons et al.*, 2008]. In order to explore this in more detail, the study focused on the time period from 0540 to 0800 UT on 17 March 2015, just after the shock impulse and first storm onset, as identified in Figure 1.

For this period of time, Figure 2.22 shows four representative instances of cusp activity that start as localized perturbations (0550 UT image) and spread to regional enhancements. Neutral density is shown in Figure 1, but the structure of electron density (Ne), horizontal plasma convection (Vi), and horizontal and vertical neutral winds (U_H and U_{UP}, respectively).

The northern hemisphere region between 60° and 80° latitude and from 13 to 17 LT was binned by 2° in latitude and 5° in longitude. For every bin and for every minute (t) from 0540 UT to 0800 UT, the change in mass density ($\Delta\rho(t)$) was calculated by subtracting the mass density at time zero ($\rho(t_0)$, where t_0 = 0540 UT). This produced the neutral mass density change for each bin in time in $\Delta\rho$ units.

The left panel in Figure 2.23 shows the neutral mass density change distribution. The thick black line is the median and the two dashed lines are the 1st and 3rd quartile distributions. The middle panel shows the average percent change of the mass density in a similar format. Similar distributions (not shown here) are present for the electron density, the horizontal plasma convection, and the horizontal and vertical neutral wind. These analyses then quantify the change in these IT parameters at key times after the onset of activity, t_0.

Table 2.1 reports the IT parameter variability at 10, 30, 45, and 90 minutes after t_0. It is important to note that within 10 minutes of the onset of cusp activity, all IT parameters, except for the upward wind, have varied by measurable amounts that support the requirement accuracy and precision identified in the requirements Table 2.4. The strongest change, in all parameters, is

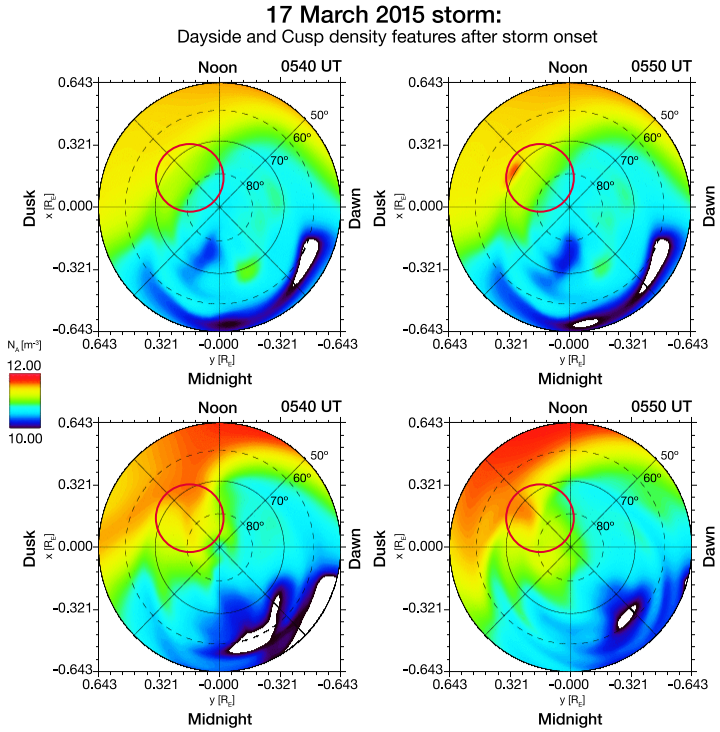

Figure 2.22. Average percent deviation of the reconstructed neutral density from the ground-truth density values as functions of the different number of orbit planes used in the reconstruction. The different symbols represent the longitude offset of the sampling meridional plane.

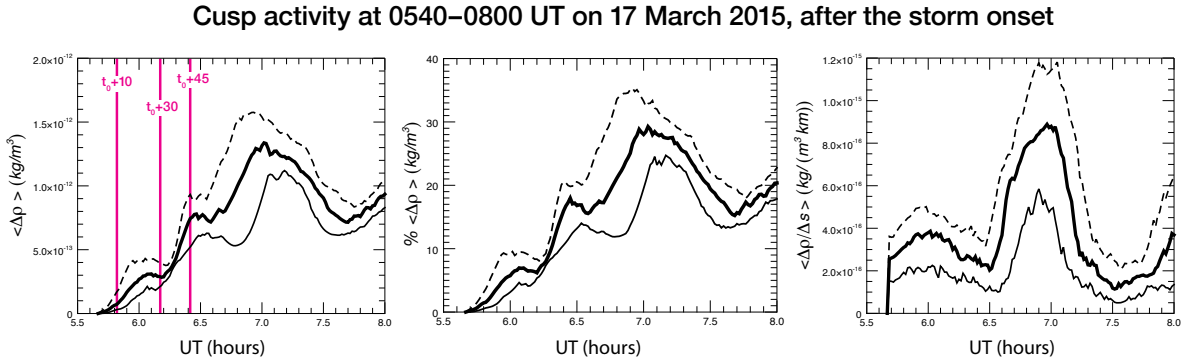

Figure 2.23. Neutral mass density change in time for the cusp activity event. The average neutral mass density change (left). The percentage average neutral mass density (center). The average longitudinal gradient of neutral mass density (right). All plots start at t_0, the cusp activity event onset, and show the median (black line) and the 1st and 3rd quartiles (dashed lines). All plots use model output between 60° and 70° latitude (a subset of the full 60° to 80° range).

observed by 45 minutes, and those parameters begin returning to their pre-activity levels by 90 minutes after onset. **These results indicate that, for cusp regional features, measurements should be at intervals faster than 45 or 30 minutes, likely on the order of 10 minutes in order to capture the dynamics.**

The right panel in Figure 2.23 shows the distribution (median with 1st and 3rd quartiles) of the longitudinal gradients of the mass density through the 2 hours and 20 minutes of cusp activity. Longitudinal gradients are calculated as follows:

- For each instance (160 1-min maps through the studied time period), binned in latitude (described above), the differences were calculated between bins separated in longitude. Specifically, along the same latitude row and starting from the first bin near the 13 LT meridian, differences were calculated between the initial bin and bins that are at later local times by progressive distances of 5, 10, 15, 20, 25, and 30 degrees (or from 1/3 hr to 2 hr distances) in longitude. These differences were divided by the arc distance between the two bins, creating comparable gradients in longitudinal space.
- This analysis is conducted only for initial bins up to 15 LT, because this is the last bin for which all spatial distances from 1/3 hr to 2 hrs of LT can be calculated within the region of interest.
- For each instance, the distribution of the gradients is calculated from all latitude bins and all longitude bins from 13 to 15 LT based on distances up to 2 hrs of LT;

The right panel in Figure 2.23 is the plot of these distribution functions. This plot demonstrates that for the neutral density, the highest gradients occur 30 minutes after the first storm onset, and also shows there is a smaller peak that occurs after the shock impact before the storm onset.

This gradient calculation then identifies the longitudinal separation over which measurable differences can be

Table 2.1. IT parameter variability after the onset of cusp activity.

Time after t0=0540 UT (min)	$<\Delta\rho>$ (kg/m^3)	<ΔNe> (/cc)	<ΔVi> (m/s)	$<\Delta U_H>$ (m/s)	$<\Delta U_{UP}>$ (m/s)
10	$0.5x10^{-13}$	$0.9x10^{4}$	15	10	0
30	$3.0x10^{-13}$	$4.9x10^{4}$	250	17	0
45	$7.5x10^{-13}$	$1.07x10^{5}$	590	52	13
90	$8.0x10^{-13}$	$1.35x10^{5}$	340	44	2

Table 2.2. IT parameter variability after the onset of cusp activity.

Property	<Δρ/Δs> (kg/m³/km)	<Δρ> (kg/m³)	<ΔNe> (/cc)	<ΔVi> (m/s)	<ΔU_H> (m/s)	<ΔU_{UP}> (m/s)
Max gradient over 1 hr LT	$8.7x10^{-16}$	$5.0x10^{-13}$	$1.0x10^{4}$	125	31	6
Max gradient over 1/2 hr LT		$2.5x10^{-13}$	$0.5x10^{4}$	63	15	3
Min gradient over 1 hr LT	$2.0x10^{-16}$	$8.0x10^{-14}$	$0.85x10^{4}$	6	8.5	0
Min gradient over 1/2 hr LT		$4.0x10^{-14}$	$0.42x10^{4}$	3	4.2	0

discerned. This provides guidance on the longitudinal separation over which the mission may need to acquire synchronized observations in order to understand regional phenomena and their spatial structure.

Figure 2.24 shows the longitudinal gradient distributions during the time period of cusp activity for the following IT properties: electron density, horizontal plasma convection, horizontal neutral winds and upward neutral winds. The purpose of this exercise was not to focus on the physical meaning behind the features in the figure, but to accept that this would be the type of structure in regional features that GDC will need to understand.

Table 2.2 shows the differences over ½ hr (285 km) and 1 hr (570 km) of LT separations at 70° latitude for the maximum and minimum of the mean gradient shown in Figures 2.22 and 2.23. The maximum gradients provide an indication of whether there is a need for close spacing in longitude mission configuration (if the gradients are large enough). The minimum gradients over those distances (the bottom two rows of Table M.2) provide guidance for the precision requirement for the measurement of the IT parameters; for GDC to reliably resolve these cusp structures, the different spacecraft longitudinally separated must be capable of identifying these gradients. For reference, the actual maximum and minimum gradients for the mass density are provided, but not the other four IT parameters.

From Table 2.2, it is apparent that there are significant longitudinal gradients over separations of 1 hr in LT and even over 1/2 hr of local time. **This finding indicates that a mission architecture should be considered that will allow for at least some time, a closely spaced orbit configuration in order to study local-scale phenomena.**

The final aspect of this analysis provides insight for the sensitivity requirement for the IT parameters. To derive that requirement, this analysis uses an inverse cumulative distribution. This curve shows the value that is met or exceeded by a specified percentage of the distribution, and thus is an indicator of the minimum gradient that must be resolved in order to identify these features in the physical system. For this analysis, the 80% value is chosen to guide the measurement requirement. Because the real physical features are likely to have higher differences than observed in the simulation (where the features tend to be relatively smooth), the model's 80% value is likely to capture a larger percentage of the real differences, and thus is a reasonable limit for the IT parameter accuracy requirement here.

Figure 2.25 shows this distribution for the mass density measurement. The vertical magenta line marks the 80% distribution value, ~4e-13 kg/m³. Similar inverse cumulative distributions have been derived for the other IT parameters, but are not plotted here. The 80% percentile values are shown in Table 2.3.

Table 2.3. 80% values for IT parameter inverse cumulative distributions.

<Δρ> (kg/m³)	<ΔNe> (/cc)	<ΔVi> (m/s)	<ΔU_H> (m/s)	<ΔU_{UP}> (m/s)
$4.0x10^{-13}$	$2x10^{4}$	5	4	2

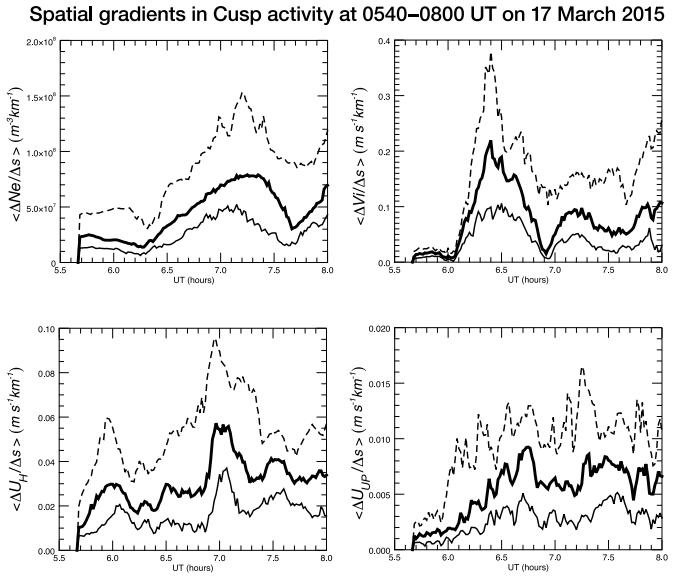

Figure 2.24. Gradients observed in each of the IT parameters.

2.6 Measurement Requirements

The GDC Objectives described above identify key focused approaches in understanding how the IT system behaves in global, regional and local scales. They also describe the challenges, as yet unconquered, that must be resolved by GDC. Finally, the Objectives isolate the most important parameters that, when measured under the defined requirements, allow closure to be achieved. While each Objective above has listed required physical parameters, a complete description of all the required physical parameters and their contribution to the GDC Science Goals is given at the end of this chapter in Section 2.7 to provide a comprehensive reference.

Table 2.5 shows the list of all the needed IT physical parameters and outlines their measurement requirements in terms of their measurable range, and the accuracy and precision for each of the parameters.

Altitude Specifications

The altitude of the GDC measurements is driven by many competing factors. Although the Objectives embrace a large region of the ionosphere-thermosphere system, the key physical processes associated with the core Objectives and core-comprehensive Objectives (1.1., 1.2, 1.3, 2.1, 2.2, and 2.3) largely operate within the altitude range of 300-400 km. This is the region where the ions and neutrals are significantly and efficiently coupled and where key space weather effects, such as ionospheric scintillations and satellite drag, can be profound. Furthermore, this altitude region is sufficiently high such that precipitating particle energy and energy flux can be measured before significant deposition occurs and sufficiently low such that the neutral density is adequately dense to sustain the ion-neutral interactions that are the subject of the Objectives as well as to ensure suitable detection in space. Hence this altitude region is considered the "optimum balance" to enable closure of the GDC core and core comprehensive Objectives. An important consideration for the altitudes of interest for GDC is that of solar activity. While the 300-400 km altitude is notional, this could be adjusted based on the solar activity conditions near the time of launch, with higher activity requiring a slightly higher altitude.

While the energy exchange between the ion and neutral gases maximizes in the 100-150 km altitude range, most forcing terms are divided by the thermospheric mass density, which decreases exponentially with altitude. For example, although the Joule/frictional heating energy exchange maximizes at an altitude of approximately 120-140 km, the associated temperature change rate maximizes between 250-350 km altitude, in the F-region. This is true for all terms in which the mass density must be considered, such as energy and momentum exchange.

In the thermosphere, for the vast majority of the time, the vertical profile of neutral density/composition and temperature can be described by hydrostatic equilibrium below about 500 km altitude, at least during quiet conditions. Measurements at more than one altitude enable this assumption to be thoroughly tested.

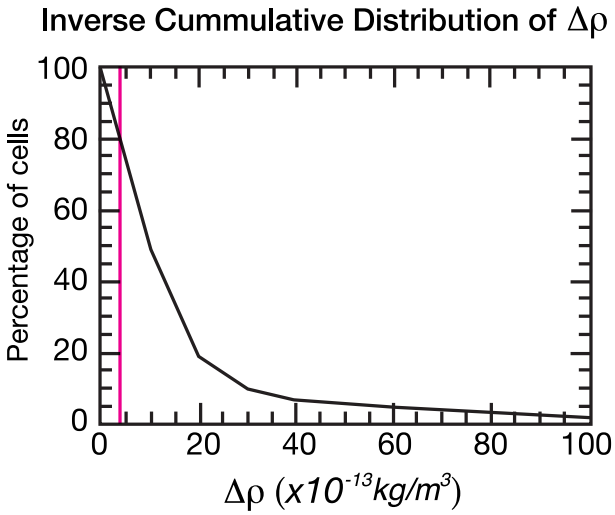

Figure 2.25. Inverse cumulative distribution of the model-derived IT parameters. The Δρ measurements are made between all combinations of cells (as described above) in the region of interest during the 0540 – 0800 UT period. The vertical magenta line marks the 80% point in the distribution.

Table 2.4. List of all needed IT physical parameters and outlines their measurement requirements in terms of their measurable range, and the accuracy and precision for each of the parameters.

Objective	Physical Parameters	Latitude Range	Scale	Remeasurement Time (min)[a]	Nominal Number of Measurements in Succession	Local Time Range (hrs)[b]	Local Time Spacing (hrs)[c,d]	Synchronicity[e]	Altitudinal Resolution (km)
1.1	1, 2, 3, 4, 7, 9, 10, 11, 12, 13, 14, 15	Poleward of +/- 30°	Global	30	3	24	4	30 min	n/a
			Regional	6	3	6	3	3 min	
			Local	6	3	2	1	10 sec	
1.2	1, 2, 3, 4, 5, 6, 7, 9, 10, 11, 12, 13, 14, 15	Poleward of +/- 30°	Global	45	2	24	3	45 min	n/a
			Regional	10	2	4	2	1 min	
			Local	< 10	2	2	0.67	10 sec	
1.3	1, 2, 3, 4, 5, 7, 8, 9, 10, 11, 12, 13, 14, 15	Poleward of +/- 30°	Global	45	2	24	4	45 min	n/a
			Regional	10	2	6	3	3 min	
			Local	1	2	2	1	10 sec	
1.4	1, 2, 3, 4, 7, 8, 9, 11, 12, 13, 14, 15, 16, 19	Poleward of +/- 30°	Global	90	1	24	3	90 min	10 km
			Regional	6	2	6	2	3 min	
			Local	< 6	2	2	0.67	10 sec	
2.1	1, 2, 3, 5, 6, 7, 11, 12, 13, 14, 17	-80° to +80°	Global	30	3	24	6	30 min	n/a
			Regional	20	3	4	4	1 min	
2.2	1, 2, 3, 4, 5, 9, 11, 12, 13, 14, 15	-80° to +80°	Global	30	3	24	4	30 min	n/a
			Regional	10	3	6	3	3 min	
			Local	< 6	3	2	1	1 min	
2.3	11, 12, 13, 14, 15	-80° to +80°	Global	30	3	24	3	30 min	n/a
			Regional	20	3	6	2	3 min	
2.4	1, 2, 13, 14, 18, 19, 20	-80° to +80°	Global	90	1	24	3	90 min	10 km
			Regional	6	2	6	2	3 min	
2.5	11, 13, 14, 15, 18, 21, 22	-80° to +80°	Global	90	2	24	4	90 min	3 km
2.6	1, 2, 3, 4, 5, 6, 9, 11, 12, 13, 14, 15	-80° to +80°	Global	30	3	24	4	30 min	n/a
			Regional	6	3	6	3	3 min	

[a] Remeasurement time is an idealized spacing, with +/- some time (for example, 30 min +/- 5 min)
[b] Local time range assumes ascending and descending nodes for global coverage
[c] Local time spacing is inclusive, so 6 hours range with 2 hours spacing, implies measurements at 0, 2, 4, and 6 LT
[d] Local time spacing is measurement agnostic. For ground based, it holds; but, for inclined planes, this is the average local time spacing at the equator.
[e] Synchronicity is defined in detail in the text, but means the simultenaity of measurements in different local time sectors, but the same latitude.

In the high latitude ionosphere in the presence of electron or ion precipitation, the height profile of the ionization rate, and the subsequent plasma density, can be derived using a combination of modeling and measurements of auroral precipitation (whether in situ or remotely sensed). The densities at altitudes between 100 km and 180 km are relatively straightforward to derive, since the ions are in chemical equilibrium. Above this altitude, advection becomes important. Fortunately, the plasma parameters will be measured at the satellite altitude in the F-region, such that a height profile can be approximated using models and assimilation techniques.

Beyond the core and core-comprehensive Objectives, some Objectives require the acquisition of parameters at altitudes below 300 km:

- Objective 1.4 requires vertical profiles of the neutral winds between 100 - 200 km with altitudinal resolution of approximately 10 km, consistent with the vertical wavelength of propagating features in the lower thermosphere and 10-20 km in the middle thermosphere.
- Objective 2.4 requires measurements of some parameters between 100-300 km.
- Objective 2.5 requires measurements of some parameters in the altitude range of 50 -250km.

Latitude Specifications

The derived physical parameters are easily separated into those that originate from measurements of the plasma or fields and those that originate from measurements of the neutral gas. Parameters originating from plasma or field measurements should be derived with a latitudinal resolution of 0.1° or better, unless otherwise noted. Parameters originating for neutral gas measurements should be derived with a latitudinal resolution of 0.25° or better, unless otherwise noted. Many of the Objectives focus on high latitude processes and have the need for auroral precipitation measurements. Because of the offset between the geographic and geomagnetic pole, the roughly average location (in both hemispheres) of the auroral oval is around 75° geographic latitude. Thus, latitude profiles should be obtained up to latitudes beyond 80° to examine influences poleward of the auroral zone.

The time over which a latitude profile should be obtained and temporal simultaneity with which points at different latitudes should be measured, varies among the different Objectives. This report describes the remeasurement times and the time scales to be considered by noting the range of nominal evolution times within the IT system.

Local Time/Longitude Specifications

For the purposes of mission requirements, three groups pertaining to local time scales to be covered have been specified:

- Global Scale: 9-24 hours local time distribution with 3-4 hour local time resolution. When considering both the ascending and descending nodes of orbital planes, the 24 hours can be covered by both nodes, requiring only half the planes. For example, to cover 24 hours of local time with 3 hours separation, planes with ascending nodes at 00, 03, 06, and 09 are needed, since these planes will have descending nodes at 12, 15, 18, and 21 local time.
- Regional Scale: 2-9 hours local time distribution with 2 to 3 hour local time resolution
- Local Scale: less than 2 hours local time distribution with less than 1 hour local time resolution. It is expected that the structure within the neutral parameters will have spatial scales larger than this, such that measurements taken with this spacing may be approximated as being within the same region.

Unless otherwise noted, Objectives do not require measurements in specific local time sectors or specific timing. Measurements should cover all local time sectors and seasons during the course of the investigation.

One of the considerations in specifying satellite spacing in an orbit plane with multiple orbit planes, is how aligned they are in latitude. For example, when one satellite in one plane passes through the equator, what is the time delay before a satellite in another orbit plane passes through the equator? This is considered the synchronicity time. It is important to discuss this because when regional and local scales are explored, the constellation is acting in synchronicity to make maps that can be used to take gradients. If the satellites in the different planes are not aligned, then they cannot be used to create such maps, since the system may evolve too much. In considering the global scale, this is important because using the ascending node and descending node of the same satellite may cause too much delay to be considered “simultaneous”, which

Table 2.5. A summary of the physical parameters, spatial, and temporal requirements for each Objective.

Number	Physical Parameter	Profile	Altitudes Assumed	Range	Accuracy[(b)]	Precision	Objectives
1	Plasma velocity perp. to B	Latitudinal	>200 km	+/- 5000 m/s	20 m/s	10 m/s	1.1, 1.2, 1.3, 1.4, 2.1, 2.2, 2.4, 2.6
	Electric field perp. to B			+/- 250 mV/m	1 mV/m	0.5 mV/m	
2	Plasma velocity parallel to B	Latitudinal	>200 km	+/- 2000 m/s	20 m/s	10 m/s	1.1, 1.2, 1.3, 2.1, 2.2, 2.4, 2.6
3	Cold plasma density	Latitudinal	200-500 km	10^2 - 10^7 cm^{-3}	10%	1%	1.1, 1.2, 1.3, 1.4, 2.1, 2.2, 2.3, 2.4, 2.6
4	Fractional ion composition	Latitudinal	400 km	1 - 40 AMU: 0 - 100%	5%	5%	1.1, 1.2, 1.3, 1.4, 2.2, 2.6
5	Ion temperature	Latitudinal	300-500 km	500 - 5000 K	10%	5%	1.2, 1.3, 2.1, 2.2, 2.6
6	Electron temperature	Latitudinal	300-500 km	500 - 10000 K	10%	5%	1.2, 2.1, 2.6
7	Auroral electron signatures:	Latitudinal	400 km				1.1, 1.3, 1.4, 2.1
	total energy flux (0.03 - 35 keV)			0.1 - 100 mW/m^{2} [(a)]	15%	10%	
	average energy			0.03 - 35 keV	20%	10%	
8	Auroral ion signatures:	Latitudinal	400 km				1.3, 1.4, 2.1
	total energy flux (0.03-200 keV)			0.1 - 50 mW/m^{2} [(a)]	15%	10%	
	average energy			0.03 - 200 keV	25%	10%	
9	Particle precipitation:	Latitudinal / Altitudinal	400 km				1.1, 1.2, 1.3, 1.4, 2.2, 2.6
	ionization rate			0 - 10^4 $ions/cm^3/s$	25%	10%	
	heating rate			0 - 0.5° K/s	25%	10%	
10	Electromagnetic energy flux	Latitudinal	400 km	0.1 - 100 mW/m^{2} [(a)]	10%	10%	1.2, 1.2, 1.3
11	Horizontal neutral wind	Latitudinal	>200 km	+/- 1500 m/s	15 m/s	5 m/s	1.1, 1.2, 1.3, 2.1, 2.2, 2.3, 2.6
12	Vertical neutral wind	Latitudinal	>200 km	+/- 150 m/s	5 m/s	3 m/s	1.2, 1.3, 2.2, 2.3
13	Neutral density	Latitudinal	300-400 km	10^6 - 10^{10} cm^{-3}	10%	2%	1.1, 1.2, 1.3, 1.4, 2.1, 2.2, 2.3, 2.4, 2.6
14	Neutral composition	Latitudinal	> 200 km	1 - 40 AMU: 0 - 100%	5%	5%	1.1, 1.2, 1.3, 2.1, 2.2, 2.3, 2.4, 2.6
15	Neutral temperature	Latitudinal	> 200 km	400 - 2000 K	10%	2%	1.1, 1.2, 1.3, 1.4, 2.2, 2.3, 2.5, 2.6
16	Electric field spatial structure amplitude (0.1 - 25 km)	Latitudinal	>200 km	+/- 500 mV/m	10%	1%	1.1
17	Magnetic field perturbation	Latitudinal	300-500 km	+/- 4000 nT	4 nT	1 nT	2.1
	(e.g., to estimate field aligned currents)			+/- 10^{-5} A/m^2	$3x10^{-7}$ A/m^2	10^{-7} A/m^2	
18	Neutral temperature	Latitudinal / Altitudinal	100-200 km	170 - 500 K	3 K	3 K	1.4, 2.4, 2.5
			200-400 km	400 - 2000 K	20 K	10 K	
19	Neutral wind horizontal vector	Lat./Alt.	100-150 km	+/- 1500 m/s	5 m/s	5 m/s	1.4, 2.4, 2.5
20	Cold plasma density	Lat./Alt.	100-150 km	10^2 - 10^7 cm^{-3}	10%	5%	1.4, 2.4
21	NO cooling rate	Lat./Alt.	100-300 km	0 - 10^{-8} W/m^3	5%	5%	2.5
22	CO_2 cooling rate	Lat./Alt.	80-150 km	0 - 10^{-8} W/m^3	5%	5%	2.5

[a] 1 mW/m^2 is equivalent to 1 $erg/cm^2/s$

[b] Many of the quantities are derived, and so have accuracies that are for the (roughly) mid-point values. For example, the particle measurements.

drives a requirement for multiple satellites in an orbit plane to measure the same latitude, at a local time offset by 12 hours, within a given time.

Temporal Specification for Remeasuring Global, Regional, and Local Scales

The temporal specifications for re-measuring the global, regional, and small scale groups defined above are:

- Global Scale: In order to capture the global-scale dynamics as described by many of the Objectives, a remeasurement time of approximately 30 minutes is needed. This allows the evolution of the neutral winds as well as plasma motions, plasma and neutral densities, and other parameters to be captured.
- Regional Scale: In order to capture the regional-scale dynamics described by many of the Objectives, a remeasurement time within the range of 6-30 minutes is needed. Six minutes is roughly half of the buoyancy wave period. This allows the evolution of mesoscale features to be captured, such ionospheric parameters and the waves in the neutral gas.
- Local Scale: Some Objectives call for sampling of local scale phenomena, which would require remeasurement an area within about 6 minutes or faster, allowing the evolution of plasma structures to be explored.

Summary

Table 2.4 presents the latitude and local time scales, ranges, resolution and remeasurement times required by each Objective discussed above. This material is based on the discussion presented in the text for each Objective, current understanding of the physical processes inherent to each Objective, as well as on modeling input, where appropriate. All the scales specified are used to distinguish the primary requirements of each Objective. The measurement requirements should be further refined as a Phase-A activity, when the capabilities of the measurement platforms and instrumentation are specified.

The measurement space is described in altitude, latitude and local time, while recognizing that it is also necessary to resolve longitude variations driven by the orientation and magnitude of the Earth's magnetic field and by energy sources that are fixed with respect to Earth's surface.

The spatial and temporal distribution of the parameters should be optimized to complete the science Objectives in the most efficient manner.

Not all parameters are required to address the questions associated with a single Objective and the table below identifies those that are considered to be the minimum required to accomplish the stated Objective. The constraints provided in the table are derived from the best available knowledge but could evolve in time as refinements to the knowledge base are made.

2.7 Description of the physical parameters of the IT system

Magnetic Fields

The earth's magnetic field is a fundamental parameter that organizes plasma flow and serves as a conduit for energy and momentum exchange between the ionosphere and magnetosphere. The earth's dipole magnetic field is offset and skewed from the geographic pole, it also contributes to longitude variations and asymmetries between hemispheres. In the region of 300-400 km altitude at high latitudes, the earth's field strength varies from +/- 60,000 nT. Knowledge of the magnetic field is needed for every objective. It can be acquired via measurements or a model.

Plasma Velocity Perpendicular to B or Electric Field Perpendicular to B

Plasma convection refers to the plasma flow perpendicular to the magnetic field which may be equivalently represented by the electric field: E = -VxB. In the region in which there are few collisions with neutrals, i.e., above about 200 km, both the ions and electrons execute the same E x B drifts. Below this altitude, the ion drift velocity is impeded by collisions with the neutral gas. However, the electron E x B drifts represent unobstructed plasma convection throughout the lower ionosphere as they are not affected by neutral collisions until below 100 km. The ion convection acts as a driver to the neutral atmosphere via ion-neutral collisions. The plasma drifts or electric fields are critical indicators of the electrodynamics associated with the distribution of currents and auroral emissions controlled by magnetosphere-ionosphere interactions. Because magnetic field lines are equipotentials, the magnitude of the electric field (plasma convection) can be scaled along the magnetic field. At high latitudes where the magnetic field direction is mostly vertical, the exact altitude of the measurement is not critical. At mid and lower latitudes,

the altitude becomes very important, as the magnetic field lines are much more inclined, becoming horizontal at the magnetic equator.

Plasma Velocity Parallel to the Magnetic Field
In addition to plasma velocity perpendicular to the magnetic field, the ion drift component parallel to the magnetic field is also important for many objectives. The parallel flow component is required to reveal signatures of frictional heating at high latitudes (as a driver) and magnetic field-aligned motions produced by momentum coupling between the plasma and neutral gas (as a resultant).

Cold Plasma Density
The cold or "thermal" plasma density determines the effectiveness of the collisional coupling between the neutral atmosphere and the ionosphere in both momentum and energy as both a forcing term and a resultant. It is also a critical measure of ionospheric response of being redistributed under the influence of plasma convection and motion along the field-line.

Fractional Ion Composition
In the altitude range 300 km to 400 km, it is expected that the ion composition will be dominated by O^+. Expansion of the plasma due to heating and transport, as well as changes in local chemistry dependent on temperature, can make it desirable to know the fractional ion composition, particularly the contributions of H^+, He^+ and molecular species. The composition is important for determining the collisional coupling between ions and neutrals in both directions. Local measurements of the composition can be extended in altitude with reasonable model assumptions.

Ion Temperature
The cold plasma ion temperature is primarily driven by a balance between frictional (Joule) heating with neutrals and heat exchange with the neutrals [*Thayer and Semeter*, 2004; *Zhu et al.*, 2016]. Therefore, the ion temperature is important in an assessment of energy exchange and momentum transfer between the ions and neutrals as well as driving the ion density and composition, since many reaction rates are dependent on the ion temperature.

Electron Temperature
The cold plasma electron temperature is responsive to photoelectron heating from solar radiation, from precipitating particles, and from a heat flux from the magnetosphere. Heat conduction is so effective that the electron temperature is responsive to the heat input almost independently of the altitude at which it is deposited. It is important in an assessment of the total thermal balance between the ionosphere and thermosphere and, because many reaction rates are dependent on the electron temperature, it controls the ion density and composition.

Auroral Electron Signatures
Aurora electron signatures (30 eV to 35 keV) are used in studies of ionosphere-magnetosphere coupling and how the electron precipitation energizes the atmosphere. The energetic electrons are important in specifying both the heating and ionization in the thermosphere and to identify field aligned current carriers. The signatures are also used to tie ionospheric locations to those in the magnetosphere such as the magnetopause, the boundary layer and the plasma sheet. Models use the energetic electron spectra observed above about 300 km to infer the electron density and hence the conductivity at lower altitudes (see below).

Aurora Ion Signatures
Aurora ion signatures (30 eV to 200 keV) at ionospheric altitudes above 300 km are used primarily in studies to identify boundaries as well as the cusp location and energy input due to solar wind particles that directly enter the earth's ionosphere. These measurements also identify contributions to ionospheric conductivity from precipitating energetic ions.

Particle Precipitation: Ionization Rate and Heating Rate
In order to determine the role of the auroral precipitation in driving the thermosphere and ionosphere, the ionization and heating rate profile due to the auroral precipitation must be determined. The ionization and heating rate profiles drive both ion and neutral dynamics. While the ionization profile is difficult to measure with direct instruments on satellites, the auroral precipitation characteristics can be measured, and when combined with models, can be used to determine the altitude profile of the ionization and heating rate [*McGranaghan et al.*, 2015; *Thayer and Semeter*, 2004]. Precipitation characteristics are typically measured as electron energy distribution functions from ~30 eV to 35,000 eV or remotely sensed radiances which are then inverted to determine the auroral precipitation spectrum, with many assumptions. The altitude of each profile occurs between 100 and 400 km altitude, with nominal auroral precipitation energies (~3 keV) causing an ionization peak around 120 km altitude.

Electromagnetic Energy Flux:
The electromagnetic energy flux specifies the total amount of electromagnetic energy that is being exchanged between the magnetosphere and the upper atmosphere including both kinetic and thermal energies. The electromagnetic energy is controlled by magnetosphere-solar wind coupling, internal processes within the magnetosphere, and magnetosphere-ionosphere coupling. While the energy flux acts as a driver for many of the Objectives, the thermospheric reaction to energy and momentum forcing serves to regulate this term.

Horizontal Neutral Wind:
Determination of the neutral wind vector is fundamental to closure of almost all science Objectives of GDC. At high latitudes, the neutral wind is responsive to the momentum transfer from the plasma and for influencing the effective collisional coupling processes between the ions and neutrals. It is responsive to changes in the neutral pressure distribution produced by frictional and particle heating as well those induced by solar heating and propagating disturbances from below. It is therefore a resultant for many of the Objectives. At low and middle latitudes, however, the winds may influence the distribution of the plasma through the production of dynamo currents and mechanical forcing parallel to the tilted magnetic field-lines. It also drives changes in the neutral density and composition. Therefore, it is a driver in other Objectives. Measurements of the winds in the altitude range 300 km to 400 km can be utilized with measurements of neutral and plasma density in the plasma dynamics to estimate the wind to altitudes down to ~200 km.

Some Objectives require the horizontal component of the neutral wind to be measured in the altitude range from 80-200 km altitude. The winds below 200 km are known to sometimes be highly variable with large shears with altitude [e.g., *Larsen*, 2002]. In this region, changes in the neutral wind influence the current flow and the energy exchange between the ionosphere-thermosphere and magnetosphere.

Vertical Neutral Wind:
The horizontal winds are significantly stronger than the vertical component, due to the gravity and gradient in pressure acting rapidly to reduce wind speeds. The dynamics of the vertical winds are largely unknown, since it is very difficult to measure them accurately. They are typically believed to be small (e.g., < 10 m/s) in magnitude across the globe, but may exceed 100 m/s in isolated regions in the auroral zone.

Neutral density:
Knowledge of the neutral density is of primary importance, since it controls almost all aspects of the thermosphere and coupling to the ionosphere. The mass density controls the inertia and specific heat of the gas in the momentum and energy coupling between the ions and neutrals. The gradient of the neutral density acts as a forcing term on the winds. At a constant altitude, the density is responsive to heating from particle precipitation and friction from ion-neutral collisions due to thermal expansion. The structure of the density determines the altitude of energy deposition from solar EUV and auroral precipitation. With models and approximations the number density of the gas and the mass density can be derived from each other if only one is known. During relatively steady time periods, the thermosphere can be approximated to be in hydrostatic equilibrium, so that the neutral density can be extrapolated to different altitudes. During active times, this approximation may break down.

Neutral Composition:
Energy inputs from the magnetosphere, applied continuously or impulsively at high latitudes, will induce bulk motion and travelling disturbances in the neutral gas. Such vertical and horizontal motions are associated with changes in the neutral composition that additionally affects the ion chemistry. Dissipation of vertically propagating tides also leads to significant changes in the neutral composition [*Jones et al.*, 2014]. It is particularly instructive to know when and where changes in the atomic oxygen and nitrogen molecules (as well as the O/N_2 ratio) and helium occur. These quantities are both resultants of the system forcing and drivers of the thermosphere-ionosphere interaction.

Neutral temperature:
The neutral temperature is responsive to the frictional and particle heating and directly contributes to the neutral gas pressure that acts as a driver of the neutral winds. It further helps to control both the collision rate between the neutrals and ions and the reaction rates between the two. The thermosphere above about 200 altitude is isothermal the vast majority of the time, so measurements of the temperature at one altitude can be directly compared to measurements at a different altitude, unless waves are present, and then measurements at different altitudes can be compared to determine the vertical wave structure.

For some Objectives, the temperature in the altitude range

between 80 and 300 km is needed. In this altitude range, the minimum of the temperature occurs around 100 km altitude.

Infrared Radiative Cooling

Thermospheric energy is dissipated through the radiative cooling of NO and CO_2, and therefore these cooling rates need to be determined. As described in the Objectives, the cooling maximizes in the lower thermosphere and upper mesosphere respectively. Because the process of transference of temperature to the NO and CO_2 is dependent on collisions with O and the temperature of the system, in order to determine the cooling rate, the oxygen density and temperature must be measured.

E-Field Spatial Structure Amplitude (0.1 - 25 km)

Structure in the electric field, and therefore the ion convection, is expected to significantly contribute to heating of the thermosphere and to be a driver for plasma structuring. Because the structuring is often quite dynamic, it is the magnitude of the variability that is often important, especially in determining the contribution to the heating of the thermosphere, and therefore the determination of the spatial distribution of the electric field is not as critical. The magnitude of the variability can be scaled along the magnetic field line, so that measurements at one altitude can be directly compared to other altitudes.

Magnetic Field Perturbation

Magnetic field perturbations typically represent the presence of field-aligned currents or electromagnetic waves, indicative of electromagnetic energy input into the upper atmosphere. Some Objectives require that the boundaries in the field-aligned current regions be identified and that changes in the current intensity be associated with changes in the drivers and/or responses of the system. At high latitudes in the altitude range between 300-400 km, magnetic field perturbations are mostly associated with field-aligned currents, so they can be scaled along the magnetic field. The field-aligned current can be crudely estimated with measurements of the magnetic field by making assumptions about the structure of the current. This approximation is reasonable for GDC, since it is the location of the FACs that are of importance to closing Objectives.

3 IMPLEMENTATION

3.1 Introduction

The combined Goal of the GDC mission is to understand the response of the global ionosphere/thermosphere system from its reaction to geomagnetic driving forces, to the internal processes that redistribute mass, momentum, and energy. Thus, simultaneous globally-distributed measurements are required, which necessitate a constellation of satellites rather than a single spacecraft. A multi-spacecraft approach is needed to disambiguate between variations in time and space, a critical requirement that other missions, such as DE-2, have not provided. The Objectives in Chapter 2 focus on several types of features and processes with scale-sizes ranging from 10's to 1000's of km. A satellite constellation mission concept will provide the needed flexibility to observe the full range of these scale-sizes.

The number of different constellation architectures that may address the GDC Objectives is only limited by feasible orbital maneuvers and imagination. The purpose of this chapter is to demonstrate both the benefits and limitations of several general constellation concepts as related to addressing GDC's Goals and Objectives. This chapter will not recommend a specific architecture, but rather provide information that can be used and referred to during future GDC mission architecture formulation.

The following chapter explores four types of potential orbital architectures for the GDC mission concept. Several assumptions are made in order to easily compare the architecture types. As discussed in Chapters 1 and 2, the main altitude focus region for the "Core" and "Core comprehensive" GDC Science Objectives is 300-400 km. A baseline initial circular orbit at 400 km altitude for science operations has been chosen for this trade study for ease of comparisons. It should be noted that the four types of potential architectures examined here will have orbit altitudes that vary from this baseline. Orbital drag and reboost capabilities will enable altitudes within the 300-400 km range to be sampled by some of the architectures present here. Additionally, one or more architectures can be stitched together with varying altitudes throughout multiple mission phases, a consideration we don't expand upon in this analysis. A baseline inclination of 82° is used since GDC Goal 1 focuses on high latitude features and coupling to the magnetosphere as well as the fact that precession induced by this inclination provides good local time coverage during all seasons. Finally, while a 3-year nominal mission is assumed in order to provide nominal local time and seasonal coverage, as well as varying geomagnetic conditions, it should not be considered as the final mission duration, but again is a bound for this trade study. This 3-year mission length also provides the minimal time for the various constellation phases to form (during which measurements are gathered). No specific instrumentation is assumed on any individual satellite. Each satellite may host a variety of in-situ and/or remote sensing instruments and is outside the scope of this trade study. This Chapter's focus is on architectures that will observe the spatial and temporal scale-sizes required to close on the GDC Science Objectives.

The four architectures considered are 1) M x N where M is the number of satellites in each of N orbit planes, 2) high and low circular orbits (High/Low), 3) coordinated pairs of elliptical orbits (Over/Under), and 4) a constellation of Motherships and CubeSats. Each of these architectures can have different variations and they can be combined in various ways. For example, one architecture could be a SmallSat constellation consisting of both high and low altitude circular orbiting satellites. For each of the architecture types, three to four variations, or scenarios, were selected that span the architecture trade space and are described in terms of their ability to meet GDC Goals and Objectives as well as orbital and launch characteristics. An orbital primer is presented in Appendix C should the reader require more context for the subsequent sections.

3.2 Orbit Dynamics Relevant to GDC

This section provides details on some of the parameters relevant to dynamics of satellites in low Earth orbit (LEO). A more general overview of multiple orbital dynamics parameters is provided in Appendix C. Several baseline parameters have been selected for the potential architectures discussed in this section, reflecting the approximate altitude and latitude coverage required to address the GDC Science Objectives. The orbit altitudes are limited to LEO (i.e. < 2000 km altitude) with a baseline circular orbit altitude of 400 km and inclination of 82°. This baseline is a reference from which the limits of each architecture are explored, and is not meant to be a final implementation prescription. The potential

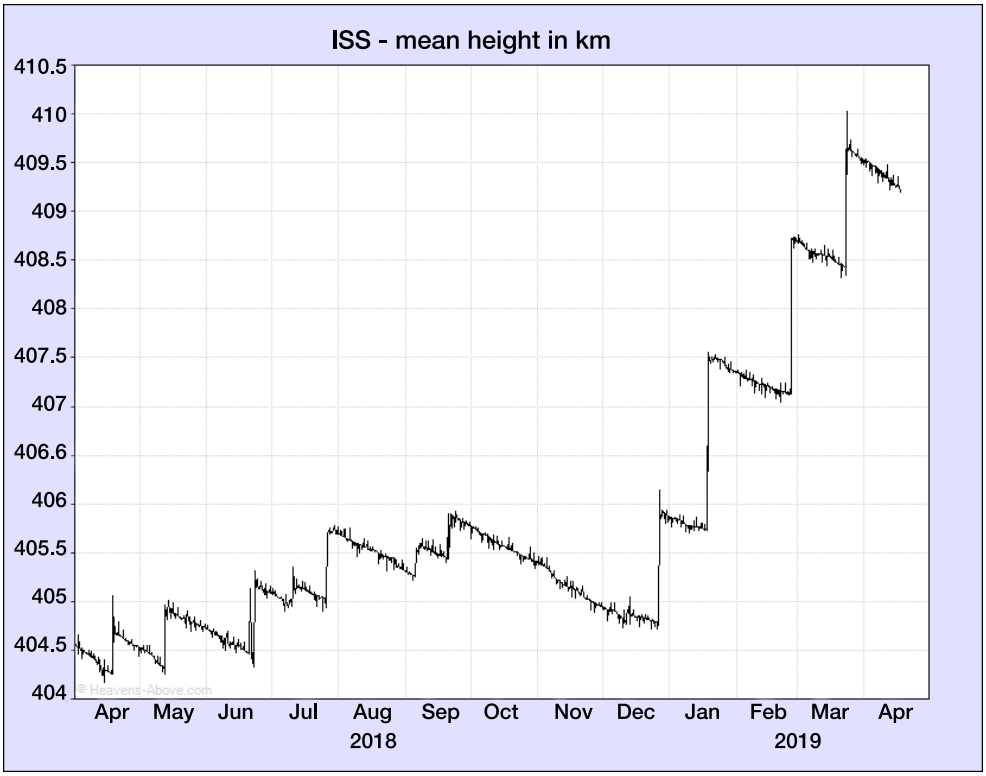

Figure 3.1. The altitude of the International Space Station as a function of time during 2018 and early 2019. The decay of the orbit due to drag is illustrated as slow decreases in the altitude, while the orbit raising maneuvers are indicated step-changes in the altitude. [From https://www.heavens-above.com/IssHeight.aspx]

architectures' orbital characteristics and resources are described in terms of three F10.7 conditions: 80 (quiet), 110 (moderate), and 150 (high) to indicate the sensitivity to average thermospheric densities.

Drag: Satellites in low-Earth orbit are affected by drag since the satellites orbit speeds are fairly high (~7500 m/s cf. Figure C.1) and because the atmospheric densities, although very low, are not zero and increase exponentially with decreasing altitude. The drag force causes the satellites to lose altitude over time. The orbit decay rate for a given orbit altitude is controlled by the satellite's mass-to-area ratio, with a larger area causing the satellite to decay faster and a larger mass causing it to decay slower.

When planning a satellite mission in low-Earth orbit, the orbit decay needs to be accounted for, since each orbit-raising maneuver requires delta-V, or fuel. Without these maneuvers, the satellite's orbit would decay until the satellite burned up in the atmosphere. Figure 3.1 illustrates the orbit decay and periodic orbit-raisings by showing the altitude of the international space station (ISS) as a function of time. In the case of a mission such as GDC which seeks to explore a range of altitudes, particularly 300-400 km, orbit decay can be used as a natural way to sample a range of altitudes, providing there is propulsion on board to provide periodic "re-boosts" as shown in the example in Figure 3.1. Ultimately, a balance must be struck between the ideal measurement regime and the amount of fuel available to the satellite, particularly for a mission such as GDC that is meant to measure regions of relatively low altitude. If the satellites are placed at a higher altitude, the maneuvers are needed less often, but the measurements may not be obtained in the needed altitude range. If the satellites are placed at a much lower altitude, frequent maneuvers may be needed and the fuel required to meet the mission lifetime requirement may exceed the available payload launch mass capability. These trades and others are discussed below relative to each of the possible configurations.

Spacing within an Orbital Plane: Some missions require several satellites separated within an orbital plane, referred to as 'pearls on a string'. When satellites are deployed into a single orbit plane, some type of orbital maneuvers will be required to achieve the desired spacing. Because along-track separations between satellites with slightly different orbit periods accumulate with time, along-track separations can be managed with

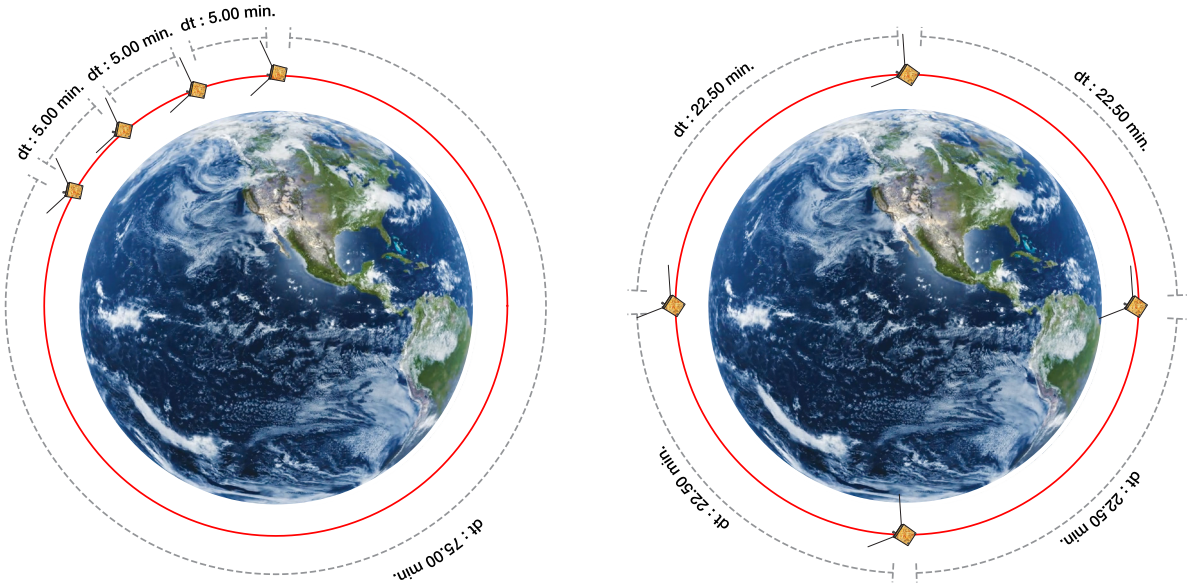

Figure 3.2. An illustration of revisit times for two basic configurations of four satellites in one orbit plane: closely spaced (left) and evenly space (right).

very small changes in along track speed by changing the orbital altitude, which can be done either via differential drag or small propulsion maneuvers. (More details are provided in Appendix C.)

Revisit Time: An extremely important consideration with satellites that are in the same orbit plane is the revisit time, the amount of time between measurements at roughly the same location along an orbit plane. (Note: by "location", we are referring to revisiting the same local time and latitude, since the earth is continuously rotating beneath the orbits.) Figure 3.2 illustrates this concept for two spacings of 4 satellites. In the first (left), the satellites are spaced roughly 20° apart around a circular orbit. As the first one passes over the north pole, the next one will pass over it 5 minutes later, giving a revisit time of 5 minutes. The third one will pass 5 minutes after the second, and the fourth will pass 5 minutes after the third. It will then take about 90 minutes (a typical LEO orbit period, cf. Figure C.1) for this to repeat. Therefore, the revisit times within this orbit plane would be 5, 5, 5, and 75 minutes. In the second (right), the satellites are evenly spaced around the orbit at 90° angular separations giving a uniform revisit time of 22.5 minutes. The revisit time does not correspond to measuring the same geographic location, since the Earth rotates under the orbit. It is more accurate to state that succeeding satellites return to the same latitude and local time. This concept is encompassed by 'remeasurement' constraint within the STM.

Orbital Plane Spacing: It is anticipated that a mission such as GDC will require a constellation of satellites distributed in multiple orbit planes. The most straightforward way to accomplish such orbital plane spacing is via separate launch vehicles. However, it is often not cost effective to have multiple launches into different orbit planes. Thus, it is important to consider the most effective technique for constellation missions to start from a single orbit plane with clustered satellites and then disperse the satellites into distinct local time planes with different separations within orbit planes. There are three considerations for determining the best method for separating the orbit planes: (1) the amount of fuel required to complete the maneuver (measured in terms of delta-V); (2) the length of time to move the orbit plane; and (3) the ability of the satellite to conduct science operations while the orbit planes are being reconfigured. With these three considerations in mind, differential precession is the most fuel-efficient way to separate orbit planes.

The concept for differential precession is based on the local time node precession rates shown in Figure C.5 since the precession rate varies with both circular orbit altitude and inclination. The relative precession is implied by the slopes of the curves in Figure C.5 at the baseline orbit, 82° inclination and 400 km altitude. For this orbit, the node precession rate varies by +0.1391°/day per degree of inclination departure from 82°. That is, an orbit with an inclination of 83° will precess eastward by 0.1391°/day relative to the baseline orbit. Since one

hour of local time is 15° in longitude, this corresponds to a time of 108 days for the orbits to separate by one hour in local time. The cost to achieve this separation rate is 133 m/s delta-V to achieve the 1° inclination difference. Note that after the desired orbital plane separation were achieved, it would be necessary to expend delta-V to then stop the separation to maintain a given orbital plane separation. However, as the separation is slow, another consideration would be to simply let the orbital planes continue to drift back to more closely spaced configurations. Finally, we note that the launch vehicle could be used to help enable solutions for achieving the orbital plane spacing to save propulsion. For example, it could release a number of satellites at one inclination and then slightly change inclination before releasing the remaining satellites.

Another consideration would be to use the precession rate dependence on altitude. For the baseline orbit, the node precession rate varies by +0.005788 deg/day eastward per 10 km altitude departure from 400 km. A circular orbit at 650 km altitude and 82° inclination precesses -0.13345 deg/day eastward relative to the baseline orbit, yielding a one hour separation between orbit planes in 112 days. The cost to boost to a 650 km altitude circular orbit from 400 km altitude is approximately 138 m/s, with the same delta-V needed to bring the satellite back down to 400 km. (Alternatively, the launch vehicle could be used to achieve the initial, higher altitude orbits saving propellant.) A significant disadvantage of this approach is that measurements at lower altitudes (400 km and below) would not be acquired during the long periods when the orbital planes were being separated. This could be alleviated somewhat if elliptical orbits were used instead (e.g., 250 km by 1000 km) although this would invoke strong apsidal precession during this period.

In summary, the propulsion needs for these different approaches are comparable. The main discriminator between these approaches depends on whether data at low altitudes are gathered during the long local time precession drift phase. Other considerations include how the propulsion is distributed between satellites, and whether one needs to stop the precession or allow it to continue after the desired orbital plane separation is achieved.

3.3 Implementation Architectures

Four basic architectures are considered to illustrate possible orbit configurations and satellite distributions that can be reasonably employed to address the GDC Science Objectives. Whether a given architecture can address the GDC Science Objectives or whether support from models and other data sources are needed is shown in the measurement requirements tables (Tables 2.4 and 2.5) in Chapter 2. The first architecture considered is an array of M satellites in each of N orbit planes (Section 3.3.1: MxN Architecture). Even though the MxN architecture may not provide closure on all of the GDC Science Objectives, it is a framework upon which variations can be built, developed, and tuned at different mission phases to support all of the GDC Science Objectives. This architecture discussion does not prescribe the platform size, specific instrumentation, accommodation, or satellite nominal orientation/ operations. These considerations are appropriate for mission design studies which are not the subject of the science implementation analysis. Nonetheless, generally recognized capabilities of different classes of satellites were considered.

Because some GDC Science Objectives benefit from near-simultaneous observations at more than one altitude, the second and third architectures discuss techniques to achieve these observations. The second architecture considers the dynamics of satellites at two different altitudes in an orbit plane (Section 3.3.2: High/ Low Circular). The third discusses a different approach to achieve multiple altitude observations where a pair of satellites are in slightly eccentric orbits in the same orbit plane with apogees at opposite locations within their elliptical orbits (Section 3.3.3: Over/Under Elliptical). These architectures demonstrate that the multiple altitude requirements can be achieved in several ways utilizing a mix of the MxN architecture with the high/ low or over/under configurations.

Another consideration is the trade between numerous identical payloads and resolution of global coverage of IT parameters. The desire to populate multiple altitudes and local times while maintaining revisit times shorter than LEO orbit periods motivates consideration of novel approaches to increase the number of in-situ platforms employed in GDC. Recognizing recent developments in satellite and instrumentation miniaturization, the MxN

architecture may also be enhanced by using CubeSats in various ways to dramatically increase the measurement locations. For example, a variant of the MxN architecture might include smaller satellites carrying different instrumentation, to decrease the spatial separations and revisit times. The fourth architecture therefore considers options for achieving much higher in-situ sampling density for a set of selected parameters by using multiple CubeSats in addition to a smaller number of more conventional satellites (Section 3.3.4: Mother Ship/CubeSat Constellation). It should be noted that CubeSats may also host remote sensing instrumentation which would further enhance the constellation.

In this discussion, it was assumed that the satellites in the MxN configuration will be no smaller than so-called SmallSats (50 - 100 kg), that is, substantially larger than CubeSats (6U, ~10 kg).

A major consideration in any architecture is the configuration of the orbit planes, which in turn depends on the local time scales associated with the GDC Science Objectives. Different GDC Science Objectives require different longitude spans and revisit times.

Table 3.1. High-level overview of system local time spatial and temporal revisit scales of primary (P) relevance to GDC Science Goals.‡

Scales (local time and temporal) vs GDC Science Objectives	Local† (<2 hr LT; 6 min)	Regional† (2-9 hr; 6-30 min)	Global† (9-24 hr;30-90 min)
1.1. High-latitude driving of neutral winds.	P	P	P
1.2. Localized, coherent plasma density.	P	P	P
1.3. Winds, precipitation, heating and high-latitude neutral density structures.	P	P	P
1.4. Influence of Tidal and gravity waves and tides on IT response.			P
2.1. Penetration electric fields/winds and mid- to low-latitude plasma densities.		P	P
2.2. Origins of propagating IT structures.	P	P	
2.3. Winds and mid- low-latitude storm-time density/composition variations.		P	P
2.4. Variability due to tidal and gravity waves.		P	P
2.5. Radiative cooling and winds in dissipation.			P
2.6. Hemispheric asymmetries.		P	P

‡ Scales are based on the Measurement Requirements described in Table 2.4 and 2.5

† All scales are important for fully closing each GDC Science Objective, but the Primary (P) designation indicates the minimum sub-set of scales required to make major advances.

The Measurement Requirements identified three longitude scales with the following approximate definitions. The range of revisit times follow from each spatial scale identified in the Measurement Requirements Table 3.2.

Local scale corresponding to <2 hours in local time and a revisit time of 6 minutes or less.

Regional scale corresponding to 2 to 9 hours in local time with a revisit time in the 6 to 30 minute range.

Global scale corresponding to >9 hours in local time with a revisit time of 30 to 90 minutes.

An approximate mapping between these scales and GDC Science Objectives is given in Table 3.1. These scale identifications should be recognized as a broad guide since there is considerable overlap between scales. Addressing all GDC Objectives requires observations at all three scales, but it is not essential that all scales be sampled simultaneously, so a sequential approach is envisioned.

For Objectives primarily requiring regional- and local-scale measurements, observations need to be made at all local times (though not simultaneously), requiring a local time precession of the orbit. Only a 12-hour local time precession is needed since each orbit plane samples two local times approximately 12 hours apart. For the baseline orbit this corresponds to ~85 days (cf. Figure C.5) or less than three months.

Since seasonal dynamics (especially solar illumination at high latitudes) governs key aspects of IT structure, tides, heating, and conductance, observations spanning all seasons are highly desirable for each scale. The relatively rapid pace of local time precession means that minimum 9-month period is required for complete coverage in local time spanning summer, equinox, and winter seasons. Since hemispheric differences between vernal and autumnal equinox conditions may be significant, a full calendar year within each of the three scale regimes is highly desired, yielding a minimum of a three-year baseline mission.

3.3.1. M x N

The first GDC architecture is a configuration of M satellites in each of N orbit planes, denoted "MxN" requiring a total of M times N satellites. The same number of satellites in each orbit plane is not essential, but is assumed for simplicity. We also assume a single launch vehicle.

The MxN architecture illustrates several aspects of orbital dynamics governing how spacecraft can be configured/arrayed to address GDC Science Objectives. The MxN configuration naturally facilitates multiple science measurements from each satellite at several simultaneous latitudes and longitudes, providing global scale coverage of multiple geophysical parameters. To address different Objectives, the MxN orbital planes may be closely spaced and/or satellites within an orbit plane may be clustered (cf. Figure 3.2). Moreover, the configuration can be adjusted during the mission to optimize the observations for different Objectives. Thus, multiple scale-sizes in both revisit time and longitude can be probed throughout the mission. While there is a trade between revisit time and coverage, the MxN architecture analysis provides a quantitative assessment of the relationships between resolution/re-sampling cadence and coverage.

To assess the range of Objectives that could be addressed with different numbers of satellites, three MxN scenarios were examined. For each scenario, the ability to address the Science Objectives is assessed in terms of orbital requirements, mission lifetime, launch logistics, and propulsion requirements. The analysis considers configuration of the planes and satellite spacing to achieve measurement requirements. The MxN constellation scenarios employ either 3, 4, or 8 total satellites in 2, 3, 4, or 8 planes.

MxN-1: nx4: 1 or 2 satellites in 4 evenly spaced planes;

MxN-2: nx2: n satellites in 2 planes;

MxN-3: 1xn: 1 satellite in n planes;

Techniques to adjust orbits between different configurations are discussed along with timeline and propulsion requirements. Comparing the scenarios demonstrates the relative trades and capability limits of the MxN configuration.

Scenario MxN-1: n Satellites x 4 Planes

The first MxN scenario consists of n = 1 or 2 satellites in each of 4 planes. To span all of the longitude scales required given a single launch, the orbit planes must be separated efficiently and for this purpose differential nodal precession is considered. Assuming a single launch vehicle, the satellites' orbit planes will initially be coincident and differential precession can be used to separate the planes in local time. There are two basic approaches to cover the longitude scales required for GDC: local to global or global to local. Only the first approach, local to global, is feasible, given reasonable delta-V constraints.

The local-to-global-scale approach adopted executes an initial small inclination change to achieve a total span between orbit planes of 2-hours local time (30° in longitude, 10° between planes) at the end of the first year of science observations. A second inclination change maneuver will increase the drift rate resulting in the orbit planes spanning 9-hours in local time at the end of the second year of observations (135° in longitude, 45° between planes). At this point the constellation is in position to conduct global-scale observations since a span of 9-hours corresponds to 24-hour local time coverage, considering both ascending and descending nodes. This sequence of gradually separating orbit planes for four planes with two satellites in each orbit plane is illustrated in Figure 3.3. In these figures, the orbits gradually separate to 36° longitude. Because of the baseline 82° inclination, the coverage at high latitudes is somewhat distorted relative to that at the equator. For this discussion these differences are ignored, but would need to be considered in the formal mission design.

To achieve smaller scale (local) measurements, the local time span of the four planes needs to remain below 2 hours, or 30° in longitude for the first year of science observations. A reasonable scenario follows: At the start of science observations, 90 days after launch (a commissioning period), the total span between the leading and trailing orbit planes would be 4.2° or just about 16.8 minutes in local time with a plane separation of 1.4° or 5.6 minutes. At the end of the first year of science observations, the nearest orbit planes will be 10° apart in longitude and the orbit plane configurations for this phase pass from the $\Delta\varphi = 6°$ panel in Figure 3.3 to the $\Delta\varphi = 12°$ panel. At the equator these correspond to longitudinal separations of 165 km between planes and a total span of 496 km. By conducting science observations throughout the year, the local scale phase of the mission would explore cross-track scales at the equator from under 200 km to 1200 km while sampling spans of 600 km to 3600 km later in the mission. The spatial separations at high latitudes would be smaller (cf. Figure 3.3).

The along-track separations for the local-scale mission phase should achieve revisit times down to 10 minutes and not longer than ½ an orbit period, or 45 minutes. The along track separations can be configured in various ways with little propulsion cost. For example, an along track relative orbit phase drift of 5.5° per day can be achieved for 2.5 m/s so that a drift of half an orbit, 180° phase difference, would accrue in 33 days. Another 2.5 m/s could be used to stop the phase drift. If each plane were to have the satellites aligned with each other with the satellites in each plane separated by 180°, the resampling time would be 46.2 min. If, instead, the satellites between the planes were staggered to provide uniform resampling times (i.e., satellite 1 from plane 1 passes through an area, then satellite 1 from plane 2, then satellite 1 from plane 3, etc.), the resampling time would be 11.6 min. This assumes that all the planes are close enough together that they sample the "same" region of the atmosphere. The revisit times could be enhanced even more by utilizing dynamic models driven by solar wind/IMF measurements and constrained by GDC satellite data. This configuration, with at least 2 satellites in each of four planes and offset satellite groupings, would then provide complete closure for the local-scale science.

The second mission phase would address regional-scale phenomena. The orbit separation at the end of phase 2 would span 9 hours or 135° in longitude (+/- 67.5° relative to the center). Given the relative drift of 15° achieved in the first year, this corresponds to an additional relative drift of 52.5° in longitude, corresponding to a drift rate in year 2 of 0.144°/day. To achieve this increase in drift rate, a net inclination difference of 1.03° or an inclination difference increase of 0.780° is needed, translating to an additional delta-V of 104 m/s. The orbit plane configurations for phase 2 are represented by the $\Delta\varphi = 12°$, 20°, and 36° panels of Figure 3.3. The longitude spacings between orbits are under 2 hours for the first ~7 months of phase 2 and are

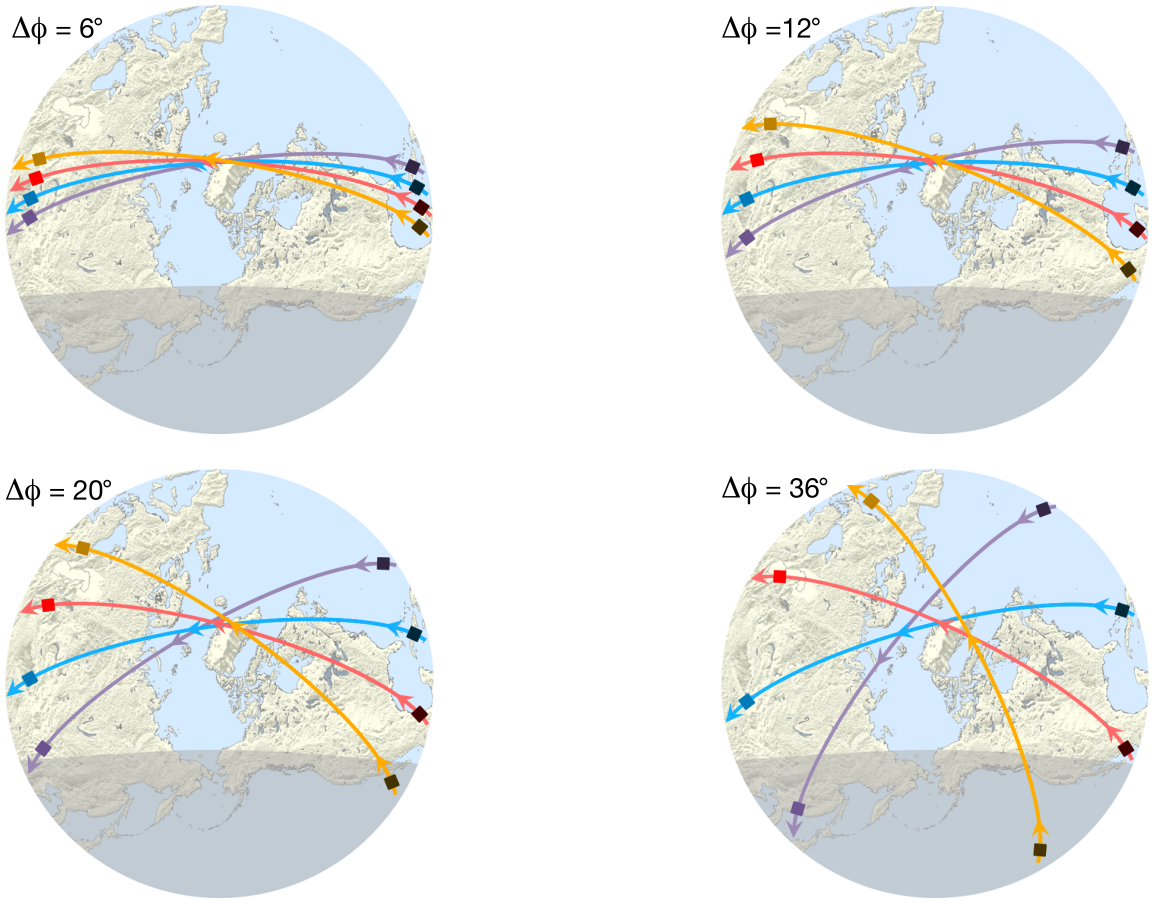

Figure 3.3. Illustration of 2x4 GDC configuration with longitudinal precession between orbit planes. Panels show configuration of 8 satellites in 82° inclination orbits for longitudinal plane separations, Δφ = 6°, 12°, 20°, and 36°. Earth view shows the terminator at 110 km altitude for equinox conditions at 1200 UTC.

below 3 hours for the entire phase. Most of the GDC Objectives related to regional-scale features requires resampling at 6-30 minutes. With two satellites per plane, the shortest uniform satellite separation time is ½ orbit, or 46.2 min. To reduce the satellite separation to 6-30 min will require having the two satellites closer together, providing one desired resample time and one longer time (see Figure 3.2). At the end of phase 2, the orbit separations are configured for the global scale observations, although small inclination changes will be required to keep a stable configuration (if desired). Table 3.2. provides a summary assessment of the ability for the 2x4 scenario described above along with several other MxN variations to address the Objectives in terms of required coverage, resolution, and revisit times. It is important to note that the scenarios of the MxN architecture provide limited altitude coverage since the orbit will decay at a rate dependent on solar cycle activity. Alternate architectures that can address more extensive and repeatable altitude coverage are discussed in Sections 3.3.2 and 3.3.3.

The total 275 m/s delta-V cost for the orbit plane configuration changes described above are well within the capabilities of prior NASA missions. Assuming a reasonable propulsion mass fraction of 30% for GDC provides an available delta-V just under 800 m/s provides adequate resources for not only the MxN but also the high/low and over/under architectures. Note the delta-V of 275 m/s for orbit plane adjustment is substantially less than the orbit boost delta-V required to achieve the global configuration in one year (not including the required de-boost maneuver which would bring the total to about 800 m/s).

The propulsion budget for maintaining a 400 km altitude orbit can be estimated using the high F10.7 limit (150 SFU) for the mass to area ratio of 150 kg/m2 and the drag coefficient of 2.2. The time to decay 25 km from 400 km altitude is 74.9 days implying the need for 16 re-boost maneuvers over the three year plus 90 day commissioning mission. The delta-V cost to boost from 375 km altitude to 400 km altitude is 14.18 m/s bringing

Table 3.2. The extent to which measurements from the MxN scenarios, supplemental data, and models can address the GDC Objectives based on nominal measurement requirements (See Table 2.2 Measurement Requirements). Dark Green: GDC satellites only, Light Green: GDC combined with model support and other data sources, Grey: Objective not closed.

Based on Nominal Measurement Coverage Requirements										
	Goal 1				Goal 2					
Sats x planes (total)	1.1	1.2	1.3	1.4	2.1	2.2	2.3	2.4	2.5	2.6
2x4 (8)										
1x4 (4)										
3x4 (12)										
4x2 (8)										
2x2 (4)										
1x8 (8)										
1x3 (3)										
3x3 (9)										

the total delta-V required to maintain the 400 km altitude orbit to 227 m/s. Thus, the total delta-V budget for the envisioned 2x4 architecture is 502 m/s. This is summarized in Table 3.3 which lists the delta-V and type of maneuver for this notional mission architecture. Allowing a margin of about 298 m/s for other orbit maneuvers to achieve lower altitude sampling (dipping) and/or changing the orbits to sample multiple altitudes. For this case study only, a 25 km orbit decay is used. However, allowing the orbit to decay to 300 km will greatly enhance the ability of GDC to address a number of the science questions and should be considered if a similar architecture is selected.

In summary, the 2x4 scenario can address all of the longitude spans and resolution requirements to meet the GDC Science Objectives' nominal measurement requirement in a three-year mission (plus 90 day commissioning period) with reasonable spacecraft design parameters, but relies on modeling to assist with some of the Objectives to meet the temporal resampling requirement. While the scenario meets the upper limit of the revisit times requirement, it will result in a somewhat degraded closure of the Science Objectives. Progressing from local to global scales (i.e. 10 minutes to ½ orbit), can only be addressed by varying the spacing between the two satellites from 6 to 46 minutes. The global- and regional-scale nominal measurement requirements require revisit times of 30 minutes or greater which could never be continuously achieved in the 2x4 scenario. Further, the GDC science would be almost entirely dependent on models or other observations to constrain the auroral energy and high-latitude convective forcing inputs. Even with these limitations, the 2x4 scenario is used as the reference architecture to explore MxN variations and other architectures in order to assess the impact on science closure as a function of number of spacecraft, satellite distribution, and multiple continuous orbit altitudes. The 3x3 scenario also allows closure of all objectives using modeling, but is deficient in the number of orbit planes needed to meet the measurement requirements for some Objectives. The inclusion of an additional satellite in each plane (3x4) will eliminate the issues described above providing closure on all objectives.

Table 3.3. Propulsion usage for the 2x4 GDC Architecture with three mission phases addressing local-, regional-, and global-scale Science Objectives in each of three mission years.

Mission Phase	Days	dV inclination (m/s)	Number boosts	dV boosts (m/s)	Total dV (m/s)
Commissioning	0-90	34	1	14	48
Local scale	91-455	0	5	71	71
Regional scale	456-820	104	5	71	175
Global scale	821-1185	137	5	71	208
				Total dV	502*

* For reference, a nominal propulsion mass fraction of 31%, comparable to that achieved for each MMS spacecraft, yields a total delta-V of 800 m/s for Hydrazine 220. Higher specific impulse propellants (BiProp 285 or 310) yield delta-V capabilities in excess of 1000 m/s for comparable mass fractions.

Scenario MxN-2: n Satellites x 2 Planes

The second MxN scenario consists of n = 2 or 4 satellites in two orbit planes, equivalent to the leading and trailing precession drift planes of the 2x4 scenario. This scenario is well-suited to local scale coverage with a local time span of less than 2 hours and comparable local time resolution (in this case identical). An advantage of 4x2 is the potential for a continuous 23.1 minute revisit time, requiring minimal trade between revisit time and duty cycle. However, this scenario will not address the nominal global- and regional-scale longitude requirements for the majority of the GDC Objectives. The ability of the 4x2 scenario to meet nominal measurement requirements is shown in Table 3.2. This scenario's assessment shows its usefulness as an alternative configuration during the local scale mission phase to ensure continuous rapid revisit times during this phase. The modest additional delta-V required to increase or slow down the differential precession to convert from a 4x2 to 2x4 configuration would be readily accommodated. For completeness, a row for a 2x2 scenario is included in Table 3.2.

Scenario MxN-3: 1 Satellite x n Planes

The final MxN scenario has each satellite in a separate orbit plane, with n = 3, 4, or 8. This provides a distinct difference from the earlier scenarios such that the satellites orbit more or less in parallel, crossing the same latitudes and simultaneously sampling more local times. The most significant disadvantage of a 1x8 scenario is its inability to provide revisit times shorter than one orbit period, which is required for the majority of the GDC Objectives. A smaller delta-V than that described in scenario MxN-1 is needed to achieve a slightly broader local time span between planes at the start of phase 2 (regional-scale) since the initial 9-hour span achieves global coverage already. A simple delay of the stop-hold delta-V to the early part of phase 1 (global scale) will achieve uniform plane spacing. The local time sampling is finer than required in any one Objective and partially addresses a number of Objectives. However, the measurement requirements for at least 3 Objectives involving revisit times of less than one orbit would never be met without significant modelling and/or other dataset support. The coverage relative to the requirements drops in the 1x4 case as can be seen in Table 3.2. A 1x3 scenario along with a 3x3 variation are also included in the table since the modelling assessment has shown that combining a three-orbital plane mission with model support is capable of addressing some GDC Objectives.

In the following sections, variations on the MxN architecture are explored to assess other measurement capabilities including: multiple (at least two) altitude coverage; higher altitudes more appropriate for remote sensing; very low (below 300 km) altitudes; and applications of new technologies in miniature satellites (CubeSats) to increase the number of multi-point measurements.

3.3.2 High/Low Circular

The second architecture, referred to as "High/Low", consists of at least one satellite at a different orbit altitude than other satellites in a given plane and can be considered a variation on the MxN architecture. High/Low could be implemented in any or all of the N orbit planes. Figure 3.4 illustrates two pairs of satellites in a High/Low orbit configuration. The high-fliers have a longer orbital period than the low-fliers, thus the vehicle pairs are only in conjunction (along a nadir line of sight) at a period (in days) which is dependent upon the high and low altitudes. The time between conjunctions is a function of the altitudes. For example, if the high satellite is at 700 km with a ~99 min period and the other is at the 400 km baseline orbit with a ~92 min period, the lower satellite laps the higher once every ~1 day. A pair of satellites in this configuration would sweep through all revisit times between ½ orbit to < 6 minutes every day in ~ 6 minute steps (~92 min per orbit divided by 15 orbits per day).

Taking advantage of the lapping process, one or more high-fliers can be combined with one or more low-fliers at appropriate altitudes to satisfy the nominal GDC measurement requirements' revisit and sampling rates. However, note that thermospheric measurements above about 450 km may be sub-optimal for neutral species measurements, making more closely spaced orbit altitudes more appropriate for some Objective requirements.

The altitude separation between circular orbits is not independent of the orbit plane separation used to span different scales during the mission (cf. Table C.1), since circular orbits with different altitudes will separate in local time over time. The differential node precession

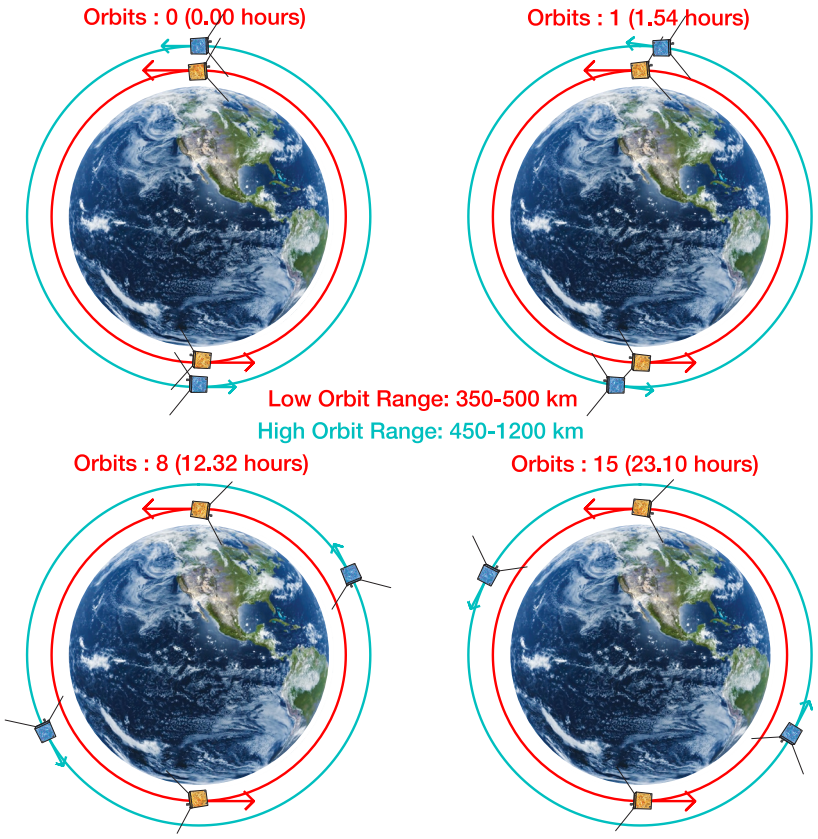

Figure 3.4. Illustration of the High/Low architecture with a single pair of satellites.

between 400 km and 700 km altitude orbits is 0.158°/day, leading to an orbit plane local time separation of four hours in local time over a one-year mission phase (cf. Table C.1), exceeding the desired plane separation span of the local scale phase. With orbits of 375 km and 425 km, the differential precession rate leads to a slower local time separation of one hour in 520 days. Nonetheless, the separation of High/Low orbit planes would imply that conjunctions would devolve to latitude conjunction only after the first year.

The High/Low architecture also provides a means to combine remote sensing and in situ observations. For example, remote sensing of auroral precipitation has historically been conducted from 700 km altitudes or higher whereas in situ neutral density structures and composition are typically conducted below ~500 km altitude. Providing higher altitude platforms to optimize remote sensing while allocating a greater number of platforms for lower altitude in situ observations may facilitate reaching closure on several science Objectives.

Two particular scenarios that combine the High/Low configuration with the MxN scenarios of Section 3.3.1 are discussed in detail. They are assessed in terms of orbital requirements, launch logistics, and ability to address the GDC Objectives' measurement requirements. A summary of the assessment is shown in Table 3.4.

H/L-1: One or more satellites per orbit plane raised to 700 km altitude orbits with the remaining satellites in the baseline 400 km altitude orbit.

H/L-2: Pairs of satellites with orbit altitudes of 375 and 425 km (delta from 400 km altitude baseline).

Table 3.4 summarizes the performance relative to the Objective measurement requirements for a combination of in situ and remote sensing observations, denoting the first High/Low scenario as 700(1), 400(1) x 4. Similar to the earlier discussion of the 1x4 scenario, the revisit times at 400 km are low. However, the situation is improved by the 700 km altitude satellite being lapped by the lower satellite once every day resulting in some revisit times less than 20 minutes. Assuming that the remote sensing thermospheric observations complement the in situ observations and meet the Objectives of the revisit sampling, this scenario is actually superior to the 2x4 scenario in the increased effective cadence of observations so that all Objectives are met in a comprehensive way. The scenario offers a substantial additional advantage in that it also provides orbit period cadence observations with altitude information and potentially provides information on scales smaller than the longitude sampling between orbit tracks via remote sensing. This configuration is therefore regarded as a significant upgrade relative to the **MxN-1** scenario even though in the table it shows the same assessment.

The second variation assumes two orbit planes with 4 satellites distributed in altitude, with three at a lower altitude and one at a higher altitude. In this case, the revisit times meet many of the Objectives, but the longitude distribution of two orbit planes fails to meet several Objectives requiring global measurements. The other Objectives require more than two orbit planes, and thus are only partially met although the remote sensing helps mitigate the missing orbit planes to some degree. However, it should be noted that some of the Objectives can be met with modeling support.

The last High/Low scenario considered has two satellites in each orbit plane of altitudes 25 km lower than the baseline orbit and 25 km higher. This was selected such that two in situ observations separated by approximately a scale-height in altitude was obtained, which represents an important piece of information for understanding a variety of phenomena. As discussed above, the altitude separation introduces a modest differential precession drift resulting in a 2.5 hour longitude separation between the two altitudes.

The configuration assumed has one satellite at 375 km and another at 425 km altitude, denoted 375(1)x425(1) x 4 planes with eight total satellites. This configuration has identical performance relative to the Science Objectives as the MxN-1 scenario (the 2x4 scenario) and is reflected in Table 3.4.

3.3.3 Over/Under

The third architecture, another variation on the MxN architecture, is referred to as "Over/Under" and consists of one or more pairs of elliptical orbit satellites oriented such that the apogee of one corresponds to the perigee of the other. Similar to High/Low, this architecture could be implemented in any or all of the N orbit planes described in Section 3.3.1 with either a single or pair

Table 3.4. Summary of the Objectives addressed by the High/Low scenarios.
Illustrates the extent that measurements from the High/Low scenarios, supplemental data, and models are capable of addressing the GDC Objectives in terms of measurement requirements (See Table 2.2 Measurement Requirements). Dark Green: GDC satellites only, Light Green: GDC combined with model support and other data sources, Grey: Objective not closed.

Based on Nominal Measurement Requirements										
	Goal 1				Goal 2					
Satellite Pairs x Planes Orbit alt. (#), Orbit alt. (#) [Total sats]	1.1	1.2	1.3	1.4	2.1	2.2	2.3	2.4	2.5	2.6
700 (1), 400 (1) x 4 [8]										
700 (1), 400 (3) x 2 [8]										
375 (1), 425 (1) x 4 [8]										

of satellites in a plane. Figure 3.5 illustrates two pairs of satellites in an Over/Under orbit configuration at LEO. The satellites in the figure have elliptical orbits with an apogee between 500 - 1200 km and perigee between 250 - 500 km (covering the full range of trade space examined). The top left panel shows the initial configuration with the two pairs of satellites in the same plane with a ½ orbit separation. Each pair is located at their respective apogee/perigee and has an orbit period of ~120 min. As the satellites progress 1/6 of an orbit (top right), the individual satellites within the pair are separated both in altitude and along track. At the ⅓ orbit point (bottom left), each pair's orbits have crossed, and the individual pairs have exchanged relative altitude position (i.e. the higher of the pair is now the lower of the pair). After ½ orbit (bottom right) the two pairs are located at their respective apogee/perigee, but at opposite positions from the beginning of the orbit.

For the Over/Under architecture, elliptical orbits with a baseline apogee/perigee of 550/250 km were selected for further study. This configuration will provide measurements over the altitude range of greatest interest for most of the GDC Science Objectives. Assuming the pairs are released from the same launch vehicle, a similar deployment process to the **MxN-1 scenario** will occur with several additions. At the point in the orbit of the desired apogee/perigee (pole), one of each satellite pair will be boosted to an apogee of 550 km using a delta-v of 42 m/s. A half of a circular orbit later (~45 min), the second satellite will be boosted to an apogee of 550 km. Even though the first satellite will be trailing, the separation distance is so small (< 3 km) compared to any of the spatial measurement requirements, another adjustment is not necessary. If no further maneuvers are performed the line of apsides will precess 3.6° per day resulting in the apogee/perigee moving to the equator in 25 days. This means that there will not be continuous altitude-aligned high latitude observations for many days every month. While this does not prevent closure to some of the Objectives, it does mean that models and other data sets will be required to supplement GDC science during those times. There is an additional complication: the low altitude perigee associated with significant drag will result in a relatively quick circularization of the orbit and the delta-V required to maintain the elliptical orbit must be included in the overall delta-V budget. The delta-V for elliptical orbit maintenance is not included here, but will be determined in future GDC mission architecture formulation activity.

There are several advantages to the Over/Under architecture. First, each satellite will sample a range of altitudes in the ionosphere/thermosphere over each

orbit. Second, each pair of satellites will provide 2 simultaneous altitude points throughout an orbit. Two altitude points, although limiting, will provide invaluable information regarding the extent and propagation of features and the variation of parameters as a function of altitude. The most significant advantage of this architecture is the ability to observe the lower altitude conditions that influence the ionosphere/thermosphere system including compositional changes, atmospheric tides and gravity waves. This will be especially useful for distinguishing energy input from the magnetosphere from the lower atmosphere. Even though dipping to 250 km (or lower) during each perigee will provide invaluable information, modeling support will still be required to close most Objectives.

The Over/Under architecture does have very specific limitations and challenges. The most significant scientific challenge is resolving horizontal vs. vertical features due to the horizontal and altitude separation of the pair of satellites for most of the orbit. Another limitation is the type of sensors that may be hosted with some sensors potentially requiring a circular orbit or substantial thermospheric density for nominal operations (although this is not elaborated on in this report).

Like the previous architectures, there are many options that may be pursued related to the Over/Under architecture. Some options include multiple pairs in a single orbit plane, satellite pairs in different orbit planes, and each pair with apogee/perigee at different locations (i.e. 1 at pole, 1 at equator). Several variations utilizing MxN configurations are examined in terms of the orbital requirements, launch logistics, and ability to address the Science Objectives. The three scenarios are:

O/U-1: 1 pair (apogee/perigee 550/250 km) x 4 planes
O/U-2: 2 pair (apogee/perigee 550/250 km) x 2 planes
O/U-3: 1 pair (apogee/perigee 550/250 km) x 3 planes

The first Over/Under scenario consists of a pair of elliptical satellites with a final apogee/perigee of 550/250 km (+/- 150 km from 400 km reference orbit) in each of 4 orbital planes (i.e. MxN-1). Table 3.5 summarizes the ability of the O/U-1 scenario to address measurement requirements for the Science Objectives. The O/U-1 scenario is equivalent to the 2x4 **MxN-1 scenario** in terms of regional- to global-scale coverage and revisit times. Both of the following variations decrease the orbital coverage such that alone they only address a subset of the Science Objectives.

The second Over/Under scenario doubles the numbers in each plane while reducing the number of planes to two. It is similar to 2 x 4 **MxN-2** scenario in terms of maneuvers with three phases to address local, regional-, and global-scale coverage. Its ability to address measurement coverage requirements is the same as **MxN-2**. However, it is considered a significant improvement since a more continuous altitude coverage occurs.

The final Over/Under scenario is a variation on the **MxN-3** scenario with a pair of satellites in three different planes. While the O/U-3 assessment in Table 3.5 is the same as the **MxN-3,** it is still considered a significant improvement because of the continuous altitude coverage.

3.3.4 Mothership/CubeSat Constellation

The final potential GDC mission architecture involves a constellation consisting of at least 1 Mothership and 5 or more CubeSats in a number of different orbit planes (nominally, 2, 3, or 4). As described in the National Academy of Sciences report on CubeSats [2016], CubeSats have now become important measurement platforms for conducting scientific investigations.

In this strategy, the Motherships are larger, but may be a SmallSat (<100 kg), with a more comprehensive suite of instruments or larger instruments that require more resources. The CubeSat portion of the constellation could be comprised of different platforms (e.g. 1U, 3U , 6U, etc.). While CubeSats are smaller and typically less capable than larger satellites, they can be used to target specific measurements. This heterogeneous constellation of satellites would allow more measurements in different volumes of space. The CubeSats would augment the main Mothership satellites within the constellation in order to target specific regions and scale-sizes within the IT system.

There are a number of unique advantages to a Mothership/CubeSat constellation. The most obvious is that a much larger number of simultaneous measurements may be obtained at multiple locations, providing improved resolution of global patterns and dynamics of measured

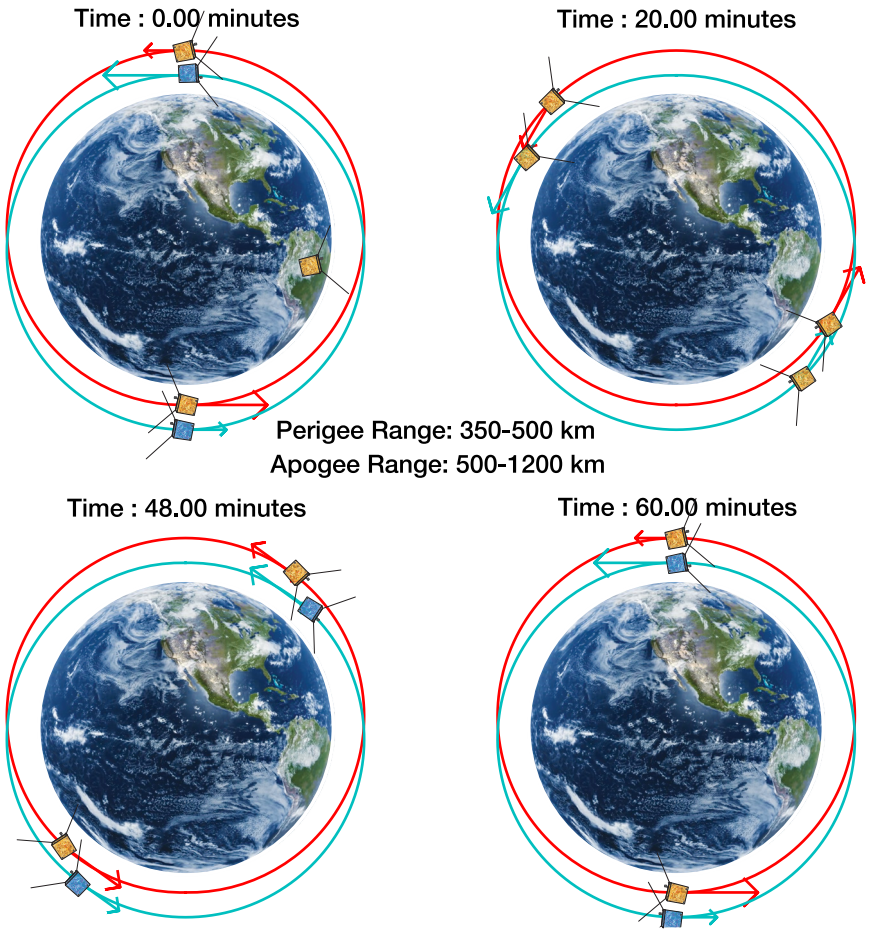

Figure 3.5. Illustration of 2 pairs of over-under satellites in the same orbital plane.

geophysical quantities. This would address the GDC Objectives that are more focused on understanding the evolution of the IT system. There are a number of advantages related to the relatively lower size and complexity of CubeSat production, especially compared to a Mothership. First, a variety of CubeSats could be developed with different instruments, providing an array of possibilities in augmented measurements. Second, having a large number of CubeSats provides the flexibility of different deployment altitudes potentially providing altitude profiles of geophysical quantities. Finally, CubeSats may be deployed at lower altitudes with short lifetimes since they can be considered somewhat disposable and be replenished with additional CubeSats. This would provide measurements in undersampled altitude regions without sacrificing the lifetime of the Motherships or requiring propulsion for orbital maneuvers.

There are many potential advantages to utilizing a Mothership/CubeSat constellation, but there are also several disadvantages. Having a heterogeneous constellation with both a Mothership and CubeSats significantly increases the overall complexity of the mission in terms of bus development, instrument testing and validation, operations, etc. This will be even more complicated if CubeSats of differing sizes with various types of payload are used. It can be argued that having a more comprehensive set of measurements at fewer locations may be better at achieving some Science Objectives rather than a less comprehensive set of measurements at a larger number of locations.

While there are a wide variety of possible scenarios for Mothership/CubeSat constellations, three are highlighted here in order to examine the orbital requirements, launch logistics, and ability to address the Science Objectives. As a baseline, 3 orbit planes with 1 mothership per plane and 5 CubeSats per mothership is assumed. It is also assumed that 3 CubeSats equates

Table 3.5. Illustrates the extent that measurements from the Over/Under scenarios, supplemental data, and models are capable of addressing the GDC Objectives in terms of measurement requirements (See Tables 2.4 and 2.5). Dark Green: GDC satellites only, Light Green: GDC combined with model support and other data sources, Grey:

Based on Nominal Measurement Requirements										
	Goal 1				Goal 2					
Sat Pairs x Planes (apogee/perigee, total sats)	1.1	1.2	1.3	1.4	2.1	2.2	2.3	2.4	2.5	2.6
1 x 4 (550/250, 8)										
2 x 2 (550/250, 8)										
1 x 3 (550/250, 6)										

in measurement capability to 1 Mothership. The three scenarios of Mothership/CubeSat constellation types are:

M/C-1: CubeSats deployed from Motherships
M/C-2: Mothership and CubeSats launched on the same vehicle
M/C-3: Mothership and CubeSats launched on different vehicles and at different times

It is clear that the CubeSats would not have as comprehensive of a measurement suite as the Motherships. For these scenarios, it is assumed that the CubeSats are capable of measuring a subset of the physical parameters, while the three Motherships contain instrumentation that will provide measurements of the full complement of physical parameters.

The first scenario assumes that each mothership would carry a certain number of CubeSats which would then be deployed at one or more altitudes as the Mothership's orbit evolved. Releasing more than one CubeSat per altitude would provide more measurements in the given orbit plane and at a given altitude. Without propulsion, the CubeSats would lose altitude and would sample different regions of the thermosphere and ionosphere as they descend. Because they would be at a lower altitude than the Mothership, they would have repeated conjunctions with the Mothership, enabling measurement of one or more parameters along an altitude profile. If the CubeSats carried propulsion, they could maintain an altitude lower than the Motherships for a given amount of time, allowing a specified altitude distribution of measurements.

Pros:

1. The CubeSats would be, by definition, moved to the same orbit plane as the Mothership before deployment, so there could be Mothership/CubeSat constellations in different local time planes.
2. The timing of the deployment of the CubeSats could be carried out to target different activity levels or seasons or phenomena.
3. Altitude profiles of different physical parameters would be commonplace, since conjunctions between CubeSats and Motherships would occur quite frequently.

Cons:

1. Deployment of CubeSats from a Mothership complicates the Mothership design and adds significant infrastructure to each Mothership.
2. Each Mothership would have more mass, requiring more delta-V to achieve the mission.

The second scenario assumes that the CubeSats would be launched from a wide variety of launch vehicles. For example, CubeSats could be deployed from the ISS, as secondary payloads on launches of opportunity that occur on a very regular basis now, or from dedicated launch vehicles that have the capability to send very small payloads into low-Earth orbit.

Pros:

1. The CubeSats are deployed semi-randomly around the globe, allowing for a wide variety of orbit planes and altitudes to be sampled, with a baseline minimum of 2 CubeSats per orbit plane.
2. The launches can be spaced out in time, allowing for a regular revitalization of the constellation.
3. With dedicated, inexpensive launch vehicles, the GDC mission could target specific areas with different CubeSats. For example, the cusp is an area of interest for Objectives 1.2 and 1.3. Because the cusp is centered around noon, it might make sense to have a few CubeSats in a noon-midnight sun-synchronous orbit continuously targeting this region.

Cons:

1. The cost of the extra launches/deployments may be prohibitive in terms of the base launch costs, the costs of maintaining the satellites on the ground, integrating them into deployers, tracking the satellite launches, and commissioning the different CubeSats in different orbit planes. This has been done by many different commercial vendors at this point, though.
2. The resulting orbit planes and altitudes would be dependent on launch availability, which would be harder to plan for, and the data analysis techniques of the community may have to be adapted.

In the final scenario, the launch vehicle would deploy both the Motherships and the CubeSats, resulting in a heterogeneous constellation of satellites immediately. There are two options for deployment. First, the Motherships and CubeSats could remain in the same orbit plane. The Science Objective assessment would be the same as for **M/C-1**. The second option has the CubeSats remaining in their orbit plane, while the Motherships move to different orbit planes. The Objective assessment for this variation option would be the same as **M/C-2**. Thus, **M/C-3** is not listed separately in Table 3.6.

Pros:

1. This is relatively simple to implement, since standard deployers could be used to deploy the CubeSats.
2. The CubeSats would start contributing to the mission immediately.

Cons:

1. All of the CubeSats would be in a single orbit plane, unless the CubeSats had a large enough amount of propulsion sufficient to change inclinations, which is unlikely given current technologies.
2. The CubeSats would not be deployed at different times, meaning that they would all be used as a single-use constellation. For the assessment, it is assumed that the CubeSats have the same mission life as the Motherships.

3.4 Balance Between Instrument Techniques

The core goals of the Geospace Dynamics Constellation mission are to understand the dynamical response of the upper atmosphere to external drivers. This produces some natural challenges to the observational strategies to be employed. Understanding the processes that couple the charged and neutral gases are best served with simultaneous observation of all the state variables in the plasma and the neutral gas in a local volume, while a study of the global response of the system is best served with a spatial distribution of observing platforms. Satisfying both these desires with identically instrumented platforms can drive a satellite constellation requiring resources that exceed reasonable expectations for cost and launch mass.

These issues become more complex by recognizing that the coupling between the plasma and the neutral gas is a strong function of altitude, with radically different behaviors at altitudes below 200 km and above 250 km. Observations at all altitudes cannot be made simultaneously in a volume threaded by the magnetic field, as is most desirable. Thus, to unravel the connections between the charged and neutral gases and the vertical coupling between the different regions of interaction, it is necessary to gather the data contemporaneously and utilize physics-based models to connect them.

While evolving technologies and observing strategies will continue to make regions at lower altitudes more accessible, the core GDC science objectives are focused on those that can be addressed with a simultaneous characterization of the auroral heating and ionization profiles and common volume measurements most readily accomplished at altitudes above 300 km. In this region measurements of the neutral gas density,

Table 3.6. Illustrates the ability of different Mothership/CubeSat scenarios to address GDC Science Objectives. Note: The variations follow the MxN scenarios with the Motherships as the M satellites with 5 CubeSats for every Mothership. Dark Green: GDC satellites only, Light Green: GDC combined with model support and other data sources, Grey: Objective not closed.

Based on Nominal Measurement Requirements										
	Goal 1				Goal 2					
Mothership x Planes (# CubeSat, CubeSat Deployment)	1.1	1.2	1.3	1.4	2.1	2.2	2.3	2.4	2.5	2.6
M/C-1&3: 2 x 4 (10, Mothership)										
M/C-1&3:4 x 2 (20, Mothership)										
M/C-1&3: 1 x 4 5, Mothership)										
M/C-1&3: 1 x 3 (5, Mothership)										
M/C-2&3: 2 x 4 (10, Launch vehicle)										
M/C-2&3: 4 x 2 (20, Launch Vehicle)										
M/C-2&3: 1 x 4 (5, Launch Vehicle)										
M/C-2&3: 1 x 3 (5, Launch Vehicle)										

temperature, major composition and wind velocity can be used in evolving physics based data assimilation schemes to describe the global distributions of these same parameters above 250 km. Likewise point measurements of the plasma density, composition, temperature and velocity together with a specification of the height and magnitude of the F-peak density, can also be used to specify the global distributions of these parameters above 250 km.

There are several technologies that are being developed that will assist in reducing this natural tension:

- The first is the miniaturization of instruments that is occurring due to the creation of small satellites. This revolution has pushed researchers to push technologies towards new methods of measurements and to shrink existing instruments to fit on smaller platforms. While some remote sensing techniques will always require long baselines to accomplish the measurements, other techniques have been developed to allow measurements that have never occurred before. It is not clear what techniques will be developed in the next few years that will enable relatively low-resource remote sensing measurements of the thermosphere between 100-150 km altitude.
- The development of CubeSats enables development of relatively inexpensive satellites that can be used to probe altitude in which the main satellites are not able to reach. These CubeSats could be treated as disposable, such that limited measurements, in terms of parameters and time, could be made periodically through the mission.
- Finally, the development of data assimilation techniques allow for this tension to be addressed head on. First, using simulated observations,

it is possible to determine whether there is enough information in a type of measurement to provide insight into either a science question or a different type of measurement. For example, the thermospheric density and temperature are highly correlated. Using a data assimilation scheme, with only measurements of the density, for example, the simulated temperature will directly respond in a physically consistent way with the density measurements. Further, data assimilation schemes can quantify this influence (or observability), so that any given measurement type can be tested to determine its unique influence on the solution. For example, assimilation schemes may show that in order to determine how gravity waves entering the thermosphere from below deposit energy into the system, the temperature and winds in the region from 100-150 km need to be measured, while determining how tides deposit energy may be addressed using measurements of the temperature and winds at 300 km, since signatures of the tides may penetrate to this altitude, so tides at 100 km may be observable with measurements at 300 km. Finally, once the mission is launched, assimilation schemes can be used to better describe the dynamical evolution of the system, since these schemes fuse both first principle models of the environment with measurements of the system. Using assimilation schemes to address measurement requirements and better describe the global system is quite common in the atmospheric (Earth) science community, but is in its infancy within the Heliophysics community. In order to better address the ties between science objectives and measurement requirements, as well as optimize the usefulness of the measurements, development of assimilation techniques should be encouraged.

3.5 Implementation Logistics

3.5.1 Calibration, Validation, and Verification Efforts

Calibration, validation, and verification (CVV) activities for the payloads are critical to the success of GDC science. This is especially true because of the constellation nature of the GDC mission. CCV activities are often conflated, but at the most basic level they occur at different phases of the mission. Calibration activities are dependent on the individual sensor and may occur prior to spacecraft integration or launch as well as during early orbit payload checkout. Validation occurs after launch when initial sensor calibration is completed. The verification involves determining whether the measurements meet the science requirements as specified in the STM. It is critical that CVV be considered early on in the mission, both during sensor selection and satellite build phase. Planning, adequate scheduling, and resources for CVV activities must be provided to ensure GDC's ability to reach closure on the science goals

Since GDC is a constellation mission, likely with multiple sensors of several types, sensor calibration activities will require extensive planning and time. Calibration is highly dependent on the type of sensor and its particular features. Laboratory calibration is likely required for each individual sensor. Additionally, inter-calibration among the same type of sensor in the laboratory should be undertaken.

Required on-orbit calibration activities include both inter- and cross-calibration of sensors. Inter-calibration occurs between identical instruments on different vehicles and cross-calibration between instruments that measure the same physical parameter and overlap in range. Both are crucial to the success of a constellation mission like GDC.

A number of lessons related to calibration activities have been learned from recent NASA constellation missions such as Van Allen Probes, Magnetospheric MultiScale, CYGNSS, and ESA constellation missions such as Swarm. First, generous time and planning must be dedicated to pre-flight testing of instrumentation so that individual sensor and full inter-calibration will be completed. Both ground and space inter-calibration implementation is straightforward since the same institution typically provides multiple copies of a sensor; however adequate personnel and facility resources must be available to minimize cost and schedule impacts.

Regardless of the success of pre-launch calibration activities, unexpected calibration issues will occur on-orbit, thus it is recommended that the same sensor team members of the pre-flight calibration teams remain available as part of the on-orbit calibration activities and general data support.

The most important lesson learned regarding cross-calibration involving multiple sensor types is to ensure adequate understanding of each sensor's performance and lab calibration response prior to launch. Otherwise duration of on-orbit calibration activities significantly increases, delaying validation and verification activities as well as the onset of nominal mission operations.

Validation compares on-orbit measurements of a subset of parameters with so-called 'ground truth'. These exercises are inherently difficult, depending on measurement technique, although every effort should be made toward validation of measurement platforms. Validation may be performed using lab activities, or by comparison to other on-orbit or ground-based assets. Each measurement technique will have different sources for ground truth. For example, TIMED/GUVI used digisondes to validate on-orbit measurements of electron densities [*DeMajistre et al.*, 2007]. Validation should be performed following completion of any calibration activity throughout the mission life, when possible.

Verification refers to ensuring that the sensor measurements will fulfill the sensor-specified STM requirements and bring closure to the Science Objectives. Verification occurs at two different points in the mission lifecycle. First verification will occur at the individual sensor level prior to pre-ship reviews. The second verification occurs after completion of initial calibration and validation activities.

3.5.2 Technology and Software Considerations

In addition to defining the number of satellites to use and their orbital characteristics, the GDC mission architecture includes all related infrastructure including satellite subsystems, communication networks, data processing tools, analysis software, and data centers. This section identifies potential enabling technology and mission areas that may require further development or planning.

While traditional satellite bus and sensor technologies are well developed, the increasing use of CubeSats has required technology development in several areas. In recent years, miniaturization of multiple types of payloads, improved power systems, and more precise attitude control systems are just a few of the areas that are now mature and can support science missions. However, there remains a few areas that will benefit from on-going development including radios, constellation flying, component reliability, and ground infrastructure. For example, most early CubeSats operated in the amateur radio band using UHF/VHF radios which limited downlink volume and their science capability. Recently, several S-band and X-band commercial radios have been developed for Cubesat/NanoSat applications. In the near-term both Ka-band and optical communication technology is being developed that may benefit GDC. While precise constellation flying may not be required for GDC, the associated technology developed to control large numbers of Cubesats would be a benefit. One of the greatest benefits of CubeSats is their rapid deployment and refresh capability. Since a long mission life is not necessarily a priority, this is partially achieved through the use of readily available non-space rated commercial components. However, if CubeSats are to be considered for mission lifetimes greater than 1-year, such as a part of GDC, an awareness must be maintained of the on-going research into the utilization of more robust components. The other aspect of GDC architecture that may require additional technology development is the ground infrastructure. This includes satellite communication ground sites, data processing algorithms and tools, analysis software, and data centers. For a dedicated science mission consisting of a constellation of CubeSats, a more formalized and possibly dedicated array of ground stations will be required. This may mean further investment in building and standardizing CubeSat compatible ground stations or the utilization of commercial communication satellites.

Post-data processing analysis software is a key component to spacecraft missions and the final aspect of ground infrastructure.

Analysis software is a combination of data visualization tools and data repository. It is key for allowing the scientific community uncomplicated access to the mission data and facilitates ease of use for all stakeholders. There are distinct advantages to deciding on a software path early on in a mission schedule. Instrument teams can work out data packaging earlier in their design, and share with other team members for inter- and cross-

calibration efforts. Missions sometimes will decide on a preferred analysis package and allocate effort for support of that package. The public data can still be delivered in CDF file format, but users can access, visualize and analyze higher level data products easily using these programs with built-in functions specific to the mission data.

3.6 Complementary and Required Implementation Resources

Ideally, GDC's Objectives will be satisfied by measuring all relevant parameters at every place and time. Technology limitations and resource constraints do not provide for such a comprehensive approach, however, and a large portion of this document is devoted to discussing the optimum approach to achieving the most fruitful approximation to this ideal within the limitations and constraints. In this way the present report is similar to those that have gone before in the pursuit of other scientific Objectives, and this section follows that paradigm in developing recommended requirements for ground-based measurements and physical models as a way to help meet Objectives in a cost-effective manner.

3.6.1 Ground-Based Measurements and Data Sets

Focused measurement paradigms

While many of the Goals for GDC are global in nature, not all of the Objectives discussed above require a high-density set of global measurements. Many of the phenomena of interest, especially those that are dominated by regional or even local behavior, can be well-characterized by focusing on smaller-than-global domains. Many phenomena also have limited durations or even a cyclical time dependence that can be measured effectively through short-term or occasional monitoring.

Ground-based measurements

GDC also relies on measurements made by facilities on the ground to improve sampling and expand the GDC domain beyond that available to the flight segment. Several aspects of such measurements are particularly well-suited for contributing to the achievement of the GDC Objectives. Such facilities can observe regions in the GDC realm for long durations in comparison to the time it takes for a satellite to pass. Thus requirements on revisit times for the constellation can be relaxed in some cases. Several types of ground-based measurements also sample large volumes with multiple measurement points, which can help relax constellation spacing requirements. While these aspects of ground-based measurements represent excellent enhancements to the overall capabilities of GDC, perhaps the most significant role played by ground-based measurements is the extension of the domain in the vertical dimension. The augmentation of the mission by several types of ground-based measurements helps alleviate this difficulty through techniques that yield vertical profiles or even simply sample altitudes that are not accessed by the constellation. Examples of ground-based vertical profiling instruments include incoherent scatter radar and ionosondes. Other examples (non-exhaustive) of ground-based instruments that may be quite helpful in augmenting the science accomplished with GDC include all sky imagers, Fabry-Perot Interferometers and Scanning Dopper Interferometers, GNSS receivers, and LIDARs.

3.6.2 Modeling

The capabilities of several general classes of physical models are required to fulfill the GDC Science Objectives. They allow for interpretation of measurements in a larger context as well as extending the effective domains and sampling capabilities of the GDC constellation. The following types of models are needed to accomplish the mission Objectives:

Global circulation models (GCMs)

GCMs specify the behavior of the I-T system on a global basis. These physics-based models approximate the known processes and interactions within the I-T system to give an indication of how the system will respond to various changes in boundary conditions and forcing influences, such as changes in solar input or gravity wave flux. They typically sample the entire system at scales of 1° in latitude and longitude, a fraction of a neutral gas height in altitude, and several minutes temporal resolution, and they can span many days in duration. Not only will GDC data be used to greatly improve existing models, the updated models will, in turn, be used to interpret, test, and validate the measurements gathered by GDC within the larger physical context.

Local models

Local models predict the behavior of the I-T system on local, or smaller-than-global, scales. They have the

advantage of focusing on small- and medium-scale phenomena, and can include processes that evolve rapidly. Typical spatial sampling is at the kilometer scale, and system evolution is determined on time scales of order one second. These models will be utilized by GDC to test physical ideas for the development of localized structures using the measurements from the constellation and the ground.

Transport models (electron, gravity waves, tides, cooling)
Transport models apply accepted physical principles to translate measurements made in one location to approximate the conditions at another location. A typical use is to translate measurements of particle fluxes made at one point to be propagated along field lines through collisions with thermospheric species to approximate the flux at an unmeasured location. These models can specify things such as heating and ionization rates, which will be critical for achieving the science specified in this document. GDC will require these models to extend the effective domain of a given measurement.

Empirical models
Empirical models are a mainstay in the I-T research and applications communities. They produce approximations to the behavior of various aspects of the system based on previous decades of measurements. Mature models exist to describe the behavior under a range of geomagnetic and solar conditions. These include specification of neutral density and composition throughout the thermosphere; horizontal wind fields; the structure and composition of the ionosphere; the Earth's magnetic field; electric potentials, and auroral precipitation. GDC will use these models in order to provide bases for interpreting GDC measurements in the context of measurements made previously.

Electrodynamic models
Electrodynamic models specify many of the processes that occur in magnetosphere-ionosphere-thermosphere coupling. For example, the electric potential can be calculated from the field-aligned currents of magnetospheric and neutral-wind dynamo origin as well as the conductivities. The auroral precipitation is also part of the coupling, so specification of the electron and ion precipitation can be done through these models.

Assimilative models
Assimilative models combine sets of measurements with models of the system to approximate the state and evolution of the I-T system, or a subset of the I-T system, in a best-fit fashion. One class of models is based primarily on empirical foundations, sometimes with evolution schemes based on Kalman-filter-like propagation concepts, while others incorporate physical principles into the approximation formulation. These models will be used by GDC in a manner similar to the way the empirical models are used, but have the advantage of specifying the system much better given the measurements during a given event in contrast to being tied to the much larger ensembles of measurements that have gone into creation of the empirical models. They are thus required by GDC when unusual conditions are encountered or understanding a given phenomenon requires smaller uncertainties throughout a modeled domain.

Development of many of these model types will be needed to address the Objectives described in Chapter 2.

3.6.3 Lab Measurements

Beyond the non-flight requirements discussed above, other measurements are highly desired to achieve GDC's Objectives. These measurements generally support analysis of the GDC data, especially in the context of models. While these measurements are needed by GDC, they generally can be performed in the lab under simulated conditions in space. Here, we provide a partial list of some important lab measurements that would greatly benefit the GDC mission.

Physics of particle collisions
A key element of the physics of the ionosphere-thermosphere system is the collision between particles of the various constituent species. Collisions between charged and neutral species are particularly important due to the differing behavior of these two fluids in a given environment. The processes of momentum and energy exchange depend in a detailed manner on the microphysics of how particles collide with one another. Thus understanding this process, usually codified as energy-dependent collision cross sections, is very important for achieving GDC's Objectives.

Rates of charge- and species-changing reactions
A process inherent to ionosphere-thermosphere

coupling that is strongly related to the physics of particle collisions is that of rates of charge- and species-changing reactions. These reactions generally proceed in the context of particle collisions, and in some cases non-binary collisions are involved. Incorporating these chemical changes adequately is important for accurate understanding of how the I-T system works and achieving GDC Objectives.

Excited-state lifetimes

The dynamics of the I-T system leads to production of a wide variety of molecular, atomic, and ionic excited states. Their behaviors differ from those of ground-state species in many aspects, most significantly in their ability to radiate. This radiation is the principal observable in many I-T measurement techniques, both in space and on the ground. Understanding the lifetimes of these excited states, especially in a collisional environment that causes some emissions to be quenched to various degrees, is then an important element in understanding how these measurements can be used to determine densities, temperatures, and other physical parameters. Knowledge of the lifetimes of excited states, especially in a collisional environment, is an essential aspect of the GDC mission.

3.7 Summary

This purpose of this chapter on GDC implementation is to provide a foundational discussion of potential types of architectures including their reasonableness in terms of launch and orbit resources, ability to address GDC Science Objectives, and the role of models and supplemental data.

> While no one implementation architecture is specifically recommended, it is important to reinforce the point that ***only with a constellation of satellites*** can the GDC Science Objectives be addressed.

In order to discuss and compare relative aspects of several potential architectures, assumptions are made. The selected baseline orbit is 400 km with an 82° inclination and the nominal mission life is 3-years. It is anticipated that via orbital drag and reboosting capabilities, the GDC platforms will gather measurements at lower altitudes, for example between 300-400 km. For a given individual satellite, no specific instrumentation is assumed. Each satellite may host a variety of in situ and/or remote sensing instruments with the exception of CubeSats due to their limited size. Four general architecture types are examined: 1) M x N where M is the number of satellites in each of N orbit planes, 2) high and low circular orbits (High/Low), 3) coordinated pairs of elliptical orbits (Over/Under), and 4) a constellation of Motherships and CubeSats. The M x N architecture, which is more traditional, used either 3, 4, or 8 total satellites for assessment. The number of selected satellites provides a reasonable upper bound and allows for a clear assessment of which Objectives require supplemental support (i.e. models and/or ground observations) in addition to the constellation observations. Each subsequent architecture discussion built upon the defined M x N architectures for assessment.

There are four major findings of the GDC implementation study:

1. The GDC Science Goals and Objectives can be addressed by a satellite constellation utilizing currently demonstrated technologies. This is extremely important since it implies that minimal new instrument, satellite, ground infrastructure technology must be developed.
2. A multi-year mission is required in order for the constellation to observe the local- to global-scale features as required by the GDC Objectives. This can be achieved through reasonable orbital maneuvers of a multi-plane constellation (See MxN scenario) within 3-years. However, note that observations spanning all seasons for each scale size is highly desirable and may require more than a nominal 3-year mission.
3. Even with a very large number of satellites in multiple orbital planes, closure of all GDC Objectives will require modeling support and will benefit from supplemental observational data. This is primarily due to unobservable quantities being needed, such as collision frequencies and auroral energy deposition. Usage of models in data assimilation techniques and supplemental data sets, such as from ground-based facilities, will allow closure of the Objectives to take less time and may offer significant scientific insights beyond the Objectives described here.
4. Non-traditional mission concepts such as those that utilize CubeSats may offer significant advantages

and should be considered. While CubeSats are typically not capable of hosting the same number of instruments as more traditional satellites, the ability to build large numbers and distribute them in space provides an unprecedented ability to measure local- and regional-scale IT features that would be invaluable to closing GDC Science Objectives.

4 GDC SYNERGIES WITH OTHER SCIENCE MISSIONS AND NON-SCIENCE SPACECRAFT

4.1 GDC Synergies with Recent (or Future) NASA ITM Missions

NASA ITM missions that were recently launched or being prepared for launch have science Objectives that complement the GDC objectives. Here, briefly, are their science Objectives, their current status at the time of this report, and their expected synergy with the GDC Objectives.

TIMED NASA's Thermosphere, Ionosphere, Mesosphere, Energetics, and Dynamics mission, which has been continuously operating since 2001, was designed to investigate and understand the energetics of the Earth's atmosphere from about 60 to 180 km in altitude. The measurements of TIMED provide data defining the basic states of the Mesosphere and Lower-Thermosphere/Ionosphere (MLTI) region and its thermal balance, including determination of the temperature, density and wind structure in the MLTI region and the relative importance of the various radiative, chemical, electrodynamical, and dynamical sources and sinks of energy to provide an understanding of the thermal structure of the MLTI. At the present time, all of the TIMED instruments continue to collect data. The SABER instrument has established an unprecedented database of how the energy balance in the mesosphere including measurements of nitric oxide in the upper atmosphere. TIMED and GDC have some overlap within Objectives 2.4 and 2.5, but TIMED is missing a very large amount of the correlative measurements needed to close these Objectives.

GOLD NASA's Global-scale Observations of the Limb and Disk mission was launched on January 25, 2018 as part of a commercial communications satellite, SES-14. GOLD is investigating the dynamics of Earth's upper atmosphere in the mid- and low-latitudes and consists of an imaging FUV spectrograph that creates full disk images of the earth from its geostationary vantage point above the Western Hemisphere. The FUV images, gathered approximately every 30 minutes, provide continuous measurements of the upper atmosphere neutral temperature (from N_2 LBH rotational structure) and composition (via daytime O/N_2 column density ratios) and how they vary as a function of solar EUV and magnetic activity. These emissions arise primarily in the lower thermosphere between 140 and 250 km. It also measures the peak electron density during the night from radiative recombination of O^+. From limb measurements, it measures O_2 density profiles from stellar occultation and determine the exospheric neutral temperature during the day. GOLD and GDC have some overlap with Objective 2.3, but GOLD is missing a very large amount of the correlative measurements needed to close this Objective.

ICON NASA's Ionospheric Connection Explorer mission has a goal of understanding the interplay of the neutral and ionized gases at the interface between the atmosphere and the ionosphere at low- and mid-latitudes. ICON is expected to be launched in late 2019 into an orbit with a 27° inclination and an altitude of 575 km, measuring properties of the low- and mid-latitude IT system that both influence and result from the dynamical and chemical coupling of the atmosphere and lower ionosphere. ICON will achieve these goals by combining remote optical imaging and in situ measurements of the plasma. ICON's remote sensing MIGHTI instrument observes the temperature and speed of the neutral atmosphere, gathering line-of-sight Doppler information of neutral winds between 95-300 km in the daytime and between 90-105 km and 200-300 km altitude at night. It also provides neutral temperatures in the altitude range of 95-105 km. The EUV imager gathers limb scans from 100 to 500 km that will reveal O^+ density during the daytime. The FUV imager provides limb scans from 130 to 450 km, revealing O/N_2 ratios during the day and O^+ density during the night. The FUV instrument measures the density of the ionosphere at night, tracking how it responds to weather in the lower atmosphere. During the day, FUV measures changes in the chemistry of the upper atmosphere -- the source for the charged gases found higher up in space. In addition, ICON includes an in situ instrument, an ion drift meter, which directly measures the velocity of the ionosphere plasma through which the satellite flies. ICON and GDC have some overlap with Objectives 2.2 and 2.4, but ICON will have no measurements at high latitudes, so will not be able to close these Objectives.

AWE NASA's Atmospheric Waves Experiment mission will fly on the International Space Station (ISS) in

August 2022. AWE will study the effects of both solar activity and terrestrial weather on the upper atmosphere by monitoring airglow in that region. AWE will gather airglow measurements originating in the mesosphere at night to study the characteristics of atmospheric waves propagating up from below, within the ISS inclination of 52 degrees. AWE and GDC have some overlap with Objective 2.4, but AWE is missing high latitudes, tides, planetary waves, and all of the other measurements needed.

AIM NASA's Aeronomy of Ice in the Mesosphere mission includes remote sensing instrumentation to study noctilucent clouds (NLC) which form in the polar regions of the upper mesosphere near 80-85 km. Launched in 2007, this small Explorer mission has had its mission life extended and continues to gather data relevant to gravity waves at all latitudes, in addition to NLC-related cloud particles including aerosols and ice at high latitudes. AIM and GDC have no direct scientific overlap.

SDO NASA's Solar Dynamics Observatory mission is the first Living With a Star satellite. It gathers continuous measurements of the sun at high cadence in order to understand its variability and how it affects space weather on earth. In addition to detailed measurements of solar activity, of particular interest for ionosphere/thermosphere research is the EUV Variability Experiment (EVE) on SDO. EVE measures the EUV irradiance with high resolution in order to study, among other things, how irradiance variations affect both the heating and ionization of the upper atmosphere. SDO will provide EUV measurements to GDC, if still in operation.

4.2 GDC Synergy with Current or Projected Non-NASA ITM Missions Expected to be Operating at the Same Time as GDC

ESA SWARM The SWARM constellation mission consists of two satellites flown "side by side" with circular orbits at 450 km separated by 1°-1.5° (east-west) with a third satellite varying within 0° to 135° in longitude of the other pair at 530 km altitude. Although the main motivation for the multi-satellite configuration for SWARM is to determine detailed knowledge of the magnetic and gravitational anomalies deep within the earth as well as in the crust, precision magnetometers on the SWARM satellites continue to provide important advances in our understanding of field-aligned and horizontal currents within the earth's upper atmosphere region. Other measurements include plasma density and temperature gathered with Langmuir probes and the plasma drift velocity gathered with thermal ion imagers. The SWARM satellites are presently expected to remain operational beyond 2023. SWARM and GDC have some overlap with Objectives 1.2, 1.3, and 2.2, but SWARM is missing a great deal of the correlative measurements, so will not be able to close any of these Objectives.

ESA/Chinese Smile The joint ESA-Chinese Smile mission includes a Canadian-led Aurora imager (soft X-ray and UVI) that will gather images of the aurora from large distances that will include prolonged views of Earth's northern auroral region. In addition to the images, the data provides the total and mean energy of the precipitating auroral energy. The images will provide high latitude context for the GDC high latitude studies, including the polar cap/magnetosphere boundary as well as the location of the cusps. It is expected to be launched in 2023. If Smile launches, it may provide some global context to the GDC mission, but will not be able to close any of the GDC Objectives.

COSMIC-2 The joint Taiwan/US Constellation Observing System for Meteorology, Ionosphere, and Climate mission includes 6 satellites launched in low-inclination orbit (24 degrees) in final circular orbits of 520-550 km. The satellites include GPS receivers from which to obtain plasma density profiles at low latitudes. The satellites also include RF beacon experiments and ion drift meters provided by the US Air Force. The satellites were launched on June 25, 2019 and are planned to operate for at least 5 years. COSMIC-2 and GDC have some overlap with Objectives 2.1 and 2.2, but COSMIC-2 is missing a great deal of the correlative measurements, and is a low latitude mission, so will not be able to close any of these Objectives.

DMSP The US Air Force Defense Meteorological Satellite Program (DMSP) are a series of polar-orbiting spacecraft at 850 km that are essentially locked in dawn-dusk, sun-synchronous orbits. Although their

primary mission is to observe the tropospheric weather, they include a secondary mission to monitor the space environment. Currently, three DMSP satellites are in operation (F16, F17, and F18). As long as the tropospheric weather instruments are operating, it is believed that DMSP will continue to operate. DMSP and GDC have some overlap with Objectives 1.2, 2.1, and 2.3, but DMSP is missing a great deal of the correlative measurements, and does not have the needed number of satellites to measure the dynamics of the system, so will not be able to close any of these Objectives.

Iridium Next Data from avionics magnetometers on the Iridium satellites have been applied for scientific study of Earth's magnetosphere-ionosphere interaction under the NSF-sponsored Active Magnetosphere and Planetary Electrodynamics Response Experiment (AMPERE) [cf. Anderson et al., 2000; Waters et al., 2001; Anderson et al., 2014; Coxon et al., 2018]. The Iridium constellation consists of 66 active satellites in six orbital planes in 780 km altitude circular orbits and 86.4°inclination providing continuous global allows for global coverage. The system provides re-sampling of the large-scale (2 hr local time by 1.5° in latitude) Birkeland field-aligned currents every ten minutes. AMPERE science data began in January 2010 and have been applied to a wide range of M-I coupling science questions [cf. Coxon et al., 2018] including: determinations of storm-time ionospheric electrodynamics [e.g. Wilder et al., 2012; Lu et al., 2014], development of the large-scale current system [e.g. Anderson et al., 2018], substorm dynamics [e.g. Clausen et al., 2012, 2013], and validation comparisons with global simulations [e.g. Merkin et al., 2013]. The original satellites, launched in 1997-1998 have recently been replaced with the new Iridium-NEXT satellites and AMPERE products derived from NEXT data are 2 to 3 times more precise than from Block 1. A total of 75 Iridium-NEXT satellites were deployed in eight launches from 2017 to 2019 and have a projected mission life of at least 15 years, ensuring services will be extended to at least 2030. Risk mitigation to ensure constellation operations are achieved with nine on orbit spares in orbit in addition to the 66 active constellation satellites. The main expected contribution to GDC science is the globally distributed, continuous magnetometer data from which measurements of field-aligned currents can be obtained to observationally constrain the high-latitude driving electrodynamics on ten-minute scales.

4.3 Relevance to Space Working Groups and Collaborations

The CEDAR and GEM workshop groups, under the auspices of NSF, are both expected to be actively engaged in GDC research. Synergistic activities such as Focus Groups related to IT science with more of a GDC focus would be ideal. Anticipated modeling research would be expected to be carried out during the lead-up to GDC, which can predict observations and lead to more mature models that are ready to ingest GDC data once they become available. Coordination with CISM, CCMC, and others is imperative. This ramp-up in simulation and modeling efforts will help ensure significantly improved science return once GDC is on-orbit.

There are various small working groups which currently study IT science including secondary science topics that complement GDC's main Science Goals and Objectives. These groups may be part of ISSI (International Space Science Institute), LWS (Living With a Star) sub-groups, potential upcoming Heliophysics DRIVE centers, or other independently-formed associations. Such communities constitute the current state of knowledge on many aspects of the system science which GDC will be exploring.

The European Space Agency (ESA) has many synergistic activities that will be relevant to GDC science. Beyond the SMILE and potential Daedalus missions, there are numerous groups supported by ESA that explore IT-related science from whom it would be useful to leverage experience and science expertise.

References

A, E., A. J. Ridley, D. Zhang, and Z. Xiao (2012), Analyzing the hemispheric asymmetry in the thermospheric density response to geomagnetic storms, J. Geophys. Res., 117, A08317, doi:10.1029/2011JA017259.

Abdu, M. A., (2012) Equatorial spread F/plasma bubble irregularities under storm time disturbance electric fields, J. Atmos. Solar Terr. Phys., 75, 44-56,doi:10.1016/j.jastp.2011.04.024.

Anderson, B. J., K. Takahashi, and B. A. Toth (2000), Sensing global Birkeland currents with iridium® engineering magnetometer data, Geophys. Res. Lett., 27, 4045-4048, doi:10.1029/2000GL000094.

Anderson, B. J., C. N. Olson, H. Korth, R. J. Barnes, C. L. Waters, and S. K Vines (2018), Temporal and spatial development of global Birkeland currents, J. Geophys. Res., 123, JGRA54317, doi:10.1029/2018JA025254.

Balan, N., S. V. Thampi, K. Lynn, Y. Otsuka, H. Alleyne, S. Watanabe, M. A. Abdu, and B. G. Fejer (2008), F3 layer during penetration electric field, J. Geophys. Res., 113, A00A07, doi:10.1029/2008JA013206.

Barlier, F., P. Bauer, C. Jaeck, G. Thuillier, and G. Kockarts (1974), North-south asymmetries in the thermosphere during the last maximum of the solar cycle, J. Geophys. Res., 79(34), 5273– 5285, doi:10.1029/JA079i034p05273.

Barth, C. A., W. K. Tobiska, D. E. Siskind, and D. D. Cleary (1988), Solar-terrestrial coupling: Low-latitude thermospheric nitric oxide, Geophys. Res. Lett., 15, 92–94, doi:10.1029/GL015i001p00092.

Barth, C. A., G. Lu, and R. G. Roble (2009), Joule heating and nitric oxide in the thermosphere, J. Geophys. Res., 114, A05301, doi:10.1029/2008JA013765.

Bristow, W. A., D. L. Hampton, and A. Otto (2016), High-spatial-resolution velocity measurements derived using Local Divergence-Free Fitting of SuperDARN observations, J. Geophys. Res. Space Physics, 121, doi:10.1002/2015JA021862.

Bruinsma, S. L., and J. M. Forbes (2007), Global observation of traveling atmospheric disturbances (TADs) in the thermosphere, Geophys. Res. Lett., 34, L14103, doi:10.1029/2007GL030243.

Bruinsma, S. L., and J. M. Forbes (2010a), Anomalous behavior of the thermosphere during solar minimum observed by CHAMP and GRACE, J. Geophys. Res., 115, A11323, doi:10.1029/2010JA015605.

Bruinsma S. L., and J. M. Forbes (2010b), Large-scale traveling atmospheric disturbances (LSTADs) in the thermosphere inferred from CHAMP, GRACE, and SETA accelerometer data, J. Atmos. Solar-Terrestrial Phys., 72(13), 1057-1066, doi: 10.1016/j.jastp.2010.06.010.

Burchill, J. K., D. J. Knudsen, J. H. Clemmons, K. Oksavik, R. F. Pfaff, C.T. Steigies, A. W. Yau, and T. K Yeoman (2010) Thermal ion upflow in the cusp ionosphere and its dependence on soft electron energy flux, J. Geophys. Res., 115(A5), CiteID Ao5206, doi:10.1029/2009JA015006.

Burns, A. G., T. L. Killeen, and R. G. Roble (1991), A theoretical study of thermospheric composition perturbations during an impulsive geomagnetic storm, J. Geophys. Res., 96(A8), 14153–14167, doi:10.1029/91JA00678.

Burns, A. G., T. L. Killeen, G. R. Carignan and R. G. Roble (1995), Large enhancements in the O/N2 ratio in the evening sector of the winter hemisphere during geomagnetic storms, J. Geophys. Res., 100(A8), 14661–14671, doi:10.1029/94JA03235.

Clausen, L. B. N., J. B. H. Baker, J. M. Ruohoniemi, S. E. Milan, and B. J. Anderson (2012), Dynamics of the region 1 Birkeland current oval derived from the Active Magnetosphere and Planetary Electrodynamics Response Experiment (AMPERE), J. Geophys. Res., 117, A06233, doi:10.1029/2012JA017666.

Clausen, L. B. N., J. B. H. Baker, J. M. Ruohoniemi, S. E. Milan, J. C. Coxon, S. Wing, S. Ohtani, B. J. Anderson (2013), Temporal and spatial dynamics of the region 1 and 2 Birkeland currents during substorms, J. Geophys. Res., 118, 3007-3016, doi:10.1002/jgra.50288.

Clausen, L. B., S. E. Milan, and A. Grocott (2014) Thermospheric density perturbations in response to substorms, J. Geophys. Res. Space Phys., 119(6), 4441–4455, doi:10.1002/2014JA019837.

Clemmons, J. H., J. H. Hecht, D. R. Salem, and D. J. Strickland (2008), Thermospheric density in the Earth's magnetic cusp as observed by the Streak mission, Geophys. Res. Lett., 35(24), CiteID L24103, doi:10.1029/2008GL035972.

Cnossen, I., A. D. Richmond, M. Wiltberger, W. Wang, and P. Schmitt, (2011), The response of the coupled magnetosphere-ionosphere-thermosphere system to a 25% reduction in the dipole moment of the Earth's magnetic field, J. Geophys. Res., 116, A12304, doi:10.1029/2011JA017063.

Cnossen, I., A. D. Richmond, and M. Wiltberger (2012), The dependence of the coupled magnetosphere-

ionosphere-thermosphere system on the Earth's magnetic dipole moment, J. Geophys. Res., 117, A05302, doi:10.1029/2012JA017555.

Codrescu, M. V., T. J. Fuller-Rowell, and J. C. Foster (1995), On the importance of E-field variability for Joule heating in the high-latitude thermosphere, Geophys. Res. Lett., 22(17), 2393–2396, doi:10.1029/95GL01909.

Conde, M. G., W. A. Bristow, D. L. Hampton, and J. Elliott (2018), Multi-instrument studies of thermospheric weather above Alaska, J. Geophys. Res. (Space Physics), 123(11), 9836–9861, doi:10.1029/2018JA025806.

Cosgrove, R. B., and M. Codrescu (2009), Electric field variability and model uncertainty: A classification of source terms in estimating the squared electric field from an electric field model, J. Geophys. Res., 114, A06301, doi:10.1029/2008JA013929.

Coster, A. J., M. J. Coerico, J. C. Foster, W. Rideout, and F. Rich, (2007) Longitude sector comparisons of storm enhanced density, Geophys. Res. Lett., 34(18), CiteID L18105, doi:10.1029/2007GL030682.

Cousins, E. D. P., and S. G. Shepherd (2010), A dynamical model of high-latitude convection derived from SuperDARN plasma drift measurements, J. Geophys. Res., 115, 12,329, doi:10.1029/2010JA016017.

Cousins, E. D. P., and S. G. Shepherd (2012) Statistical characteristics of small-scale spatial and temporal electric field variability in the high-latitude ionosphere, J. Geophys. Res., 117(A3), CiteID A03317, doi:10.1029/2011JA017383.

Crowley, G., and R. R. Meier (2008), Disturbed O/N2 ratios and their transport to middle and low latitudes, in Midlatitude Ionospheric Dynamics and Disturbances, eds P. M. Kintner, A. J. Coster, T. Fuller-Rowell, A. J. Mannucci, M. Mendillo and R. Heelis, doi:10.1029/181GM20.

Crowley, G., B. A. Emery, R. G. Roble, H. C. Carlson Jr. J. E. Salah, V. B. Wickwar, K. L. Miller, W. L. Oliver, R. G. Burnside, and F. A. Marcos (1989), Thermospheric dynamics during September 18-19, 1984 2. Validation of the NCAR thermospheric general circulation model, J. Geophys. Res., 94(A12), 16945-16959, doi:10.1029/JA094iA12p16945.

Crowley, G., J. Schoendorf, R. G. Roble, and F. A. Marcos (1996), Neutral density cells in the lower thermosphere at high latitudes, Adv. Space Res., 18(3), 69–74, doi:10.1016/0273-1177(95)00841-2.

Crowley, G., A. J. Ridley, D. Deist, S. Wing, D. J. Knipp, B. A. Emery, J. Foster, R. Heelis, M. Hairston, and B. W. Reinisch (2000), Transformation of high-latitude ionospheric F region patches into blobs during the March 21, 1990, storm, J. Geophys. Res., 105(A3), 5215, doi.org/10.1029/1999JA900357.

Crowley, G., et al. (2006), Global thermosphere-ionosphere response to onset of 20 November 2003 magnetic storm, J. Geophys. Res., 111, A10S18, doi:10.1029/2005JA011518.

Coxon, J. C., S. E. Milan, and B. J. Anderson (2018), A review of Birkeland current research using AMPERE, in Electric Currents in Geospace and Beyond, Geophysical Monograph 235, eds. A. Keiling, O. Marghitu, and M. Wheatland, American Geophysical Union, John Wiley & Sons, Inc., ISBN: 978-1-119-32449-2. (http://www.wiley.com/WileyCDA/WileyTitle/productCd-1119324491.html)

David, M., J. J. Sojka, R. W. Schunk, and A. J. Coster (2016), Polar cap patches and the tongue of ionization: A survey of GPS TEC maps from 2009 to 2015, Geophys. Res. Lett., 43, 2422– 2428, doi:10.1002/2016GL068136.

DeMajistre, R, L. J. Paxton, D. Bilitza, "Comparison of ionospheric measurements made by digisondes with those inferred from ultraviolet airglow", Adv. Space Res., 39(5), doi:10.1016/j.asr.2006.09.037, 2007.

Deng, W., T. Killeen, A. Burns, and R. Roble (1991), The flywheel effect: Ionospheric currents after a geomagnetic storm, Geophys. Res. Lett., 18, 1845.

Deng, Y., and A. Ridley (2006), Dependence of neutral winds on interplanetary magnetic field, F10.7 and hemispheric power index at high latitude, J. Geophys. Res., 111, A09,306, doi:10.1029/2005JA011368.

Deng, Y., and A. Ridley (2007), Possible reasons for underestimating Joule heating in global models: E-field variability, spatial resolution and vertical velocity, J. Geophys. Res., 112, A09308, doi: 10.1029/2006JA012006.

Deng, Y., T. J. Fuller-Rowell, A. J. Ridley, D. Knipp, R. E. Lopez, (2013) Theoretical study: Influence of different energy sources on the cusp neutral density enhancement, J. Geophys. Res. Space Phys., 118(5), 2340-2349, doi:10.1002/jgra.50197.

Deng Y., et al. (2017), Comparisons of JOULE 1 rocket thermospheric wind observations in high latitudes with GITM simulations, Sci. China Tech. Sci., 60, 412–418, doi: 10.1007/s11431-016-0471-8.

Dhadly, M., J. Emmert, D. Drob, M. Conde, E. Doornbos, G. Shepherd, J. Makela, Q. Wu, R. Niciejewski, and A. Ridley (2017), Seasonal dependence of northern high-latitude upper thermospheric winds: A

quiet time climatological study based on ground-based and space-based measurements, J. Geophys. Res. Space Physics, 122, 2619–2644, doi:10.1002/2016JA023688.
Dhadly, M. S., et al. (2018), Seasonal dependence of geomagnetic active-time northern high-latitude upper thermospheric winds, J. Geophys. Res.: Space Physics, 123, 739–754, doi.org/10.1002/2017JA024715.

Drob, D. P., et al. (2015), An update to the Horizontal Wind Model (HWM): The quiet time thermosphere, Earth and Space Science, 2, 301– 319, doi:10.1002/2014EA000089.

England, S. L. (2012), A review of the effects of non-migrating atmospheric tides on the Earth's low-latitude ionosphere, Space Sci. Rev., 168(211), doi.org/10.1007/s11214-011-9842-4.

Fedrizzi, M., T. J. Fuller-Rowell, N. Maruyama, M. Codrescu, and H. Khalsa (2008), Sources of F-region height changes during geomagnetic storms at mid latitudes, in Midlatitude Ionospheric Dynamics and Disturbances, eds P. M. Kintner, A. J. Coster, T. Fuller-Rowell, A. J. Mannucci, M. Mendillo and R. Heelis, doi:10.1029/181GM22.

Fejer, B. G., J. T. Emmert, and D. P. Sipler (2002), Climatology and storm time dependence of nighttime thermospheric neutral winds over Millstone Hill, J. Geophys. Res., 107(A5), SIA 3–1–SIA 3-9, doi:10.1029/2001JA000300.

Forbes, J. (2007), Dynamics of the thermosphere, J. Meteorological Society of Japan, 85B, 193–213, doi.org/10.2151/jmsj.85B.193.

Forbes, J. M. S. E. Palo, and X. Zhang (2000), Variability of the ionosphere, J. Atmos. Solar Terr. Phys., 62, 685-693, doi.org/10.1016/S1364-6826(00)00029-8.

Forbes, J. M., S. L. Bruinsma, X. Zhang, and J. Oberheide (2009), Surface-exosphere coupling due to thermal tides, Geophys. Res. Lett., 36(15), L15,812, doi: 10.1029/2009GL038748.

Förster, M., and I. Cnossen (2013), Upper atmosphere differences between northern and southern high latitudes: The role of magnetic field asymmetry, J. Geophys. Res. Space Physics, 118, 5951– 5966, doi:10.1002/jgra.50554.

Förster, M., and S. Haaland (2015), Interhemispheric differences in ionospheric convection: Cluster EDI observations revisited, J. Geophys. Res. Space Physics, 120, 5805–5823, doi:10.1002/2014JA020774.

Förster, M., S. Rentz, W. Köhler, H. Liu, and S. E. Haaland, (2008), IMF dependence of high-latitude thermospheric wind pattern derived from CHAMP cross-track measurements, Ann. Geophys., 26, 1581-1595, doi.org/10.5194/angeo-26-1581-2008.

Förster, M., S. E. Haaland, and E. Doornbos (2011), Thermospheric vorticity at high geomagnetic latitudes from CHAMP data and its IMF dependence, Ann. Geophys., 29, 181–186, doi.org/10.5194/angeo-29-181-2011.

Foster, J. C., and W. J. Burke (2002), SAPS: A new categorization for sub-auroral electric fields, Eos Transactions, 83(36), 393, doi:10.1029/2002EO000289.

Foster, J. C., and H. B. Vo (2002), Average characteristics and activity dependence of the subauroral polarization stream, J. Geophys. Res. Space Phys., 107(A12), CiteID 1475, doi:10.1029/2002JA009409.

Foster, J. C., P. J. Erickson, A. J. Coster, J. Goldstein, and F. J. Rich (2002), Ionospheric signatures of plasmaspheric tails, Geophys. Res. Lett., 29(13), CiteID 1623, doi:10.1029/2002GL015067.

Frissell, N. A., J. B. H. Baker, J. M. Ruohoniemi, R. A. Greenwald, A. J. Gerrard, E. S. Miller, and M. L. West (2016), Sources and characteristics of medium-scale traveling ionospheric disturbances observed by high-frequency radars in the North American sector, J. Geophys. Res. Space Physics, 121, 3722–3739, doi:10.1002/2015JA022168.

Fritts, D. C., and T. S. Lund (2011), Gravity wave influences in the thermosphere and ionosphere: Observations and recent modeling, in Aeronomy of the Earth's Atmosphere and Ionosphere, Springer, Dordrecht, pp. 109-130.

Fuller-Rowell, T. J., M. V. Codrescu, R. J. Moffett, and S. Quegan (1994), Response of the thermosphere and ionosphere to geomagnetic storms, J. Geophys. Res., 99(A3), 3893– 3914, doi:10.1029/93JA02015.

Fuller-Rowell, T. J., M. V. Codrescu, H. Rishbeth, R. J. Moffett, and S. Quegan (1996), On the seasonal response of the thermosphere and ionosphere to geomagnetic storms, J. Geophys. Res., 101(A2), 2343–2353, doi:10.1029/95JA01614.

Fuller-Rowell, T. J., A. D. Richmond, and N. Maruyama (2008), Global modeling of storm-time thermospheric dynamics and electrodynamics, in Midlatitude Ionospheric Dynamics and Disturbances, eds. P. M. Kintner, A. J. Coster, T. Fuller-Rowell, A. J. Mannucci, M. Mendillo and R. Heelis, doi:10.1029/181GM18.

Garnder, L. C., and R. W. Schunk (2008), Pulsating of the generalized ion and neutral polar winds, J. Atmos. Solar Terr. Phys., 70(11-12), 1408-1418, doi:10.1016/j.

jastp.2008.03.019.

Guo, D., J. Lei, A. Ridley, and D. Ren (2019), Low-density cell of the thermosphere at high latitudes revisited, J. Geophys. Res. Space Phys., 124(1), 521-533, doi:10.1029/2018JA025770.

Hagan, M. E., and J. M. Forbes (2003), Migrating and nonmigrating semidiurnal tides in the upper atmosphere excited by tropospheric latent heat release, J. Geophys. Res. Space Phys.. 108(A2), CiteID 1062, doi:10.1029/2002JA009466.

Hanson, W. B., and R. J. Moffett (1966), Ionization transport effects in the equatorial F region, J. Geophys. Res., 71, 5559–5572, doi:10.1029/JZ071i023p05559.

Harding, B. J., J. J. Makela, J. Qin, D. J. Fisher, C. R. Martinis, J. Noto, and C. M. Wrasse (2017), Atmospheric scattering effects on ground-based measurements of thermospheric vertical wind, horizontal wind, and temperature, J. Geophys. Res. Space Physics, 122, 7654–7669, doi:10.1002/2017JA023942.

Harding, B. J., A. J. Ridley, and J. J. Makela (2019), Thermospheric weather as observed by ground-based FPIs and modeled by GITM, J. Geophys. Res. Space Physics, 124, 1307–1316, doi.org/10.1029/2018JA026032.

Häusler, K., and H. Lühr (2009), Nonmigrating tidal signals in the upper thermospheric zonal wind at equatorial latitudes as observed by CHAMP, Ann. Geophys., 27, 2643-2652, doi.org/10.5194/angeo-27-2643-2009.

Heelis, R. A., J. J. Sojka, M. David, and R. W. Schunk (2009), Storm time density enhancements in the middle-latitude dayside ionosphere, J. Geophys. Res., 114, 3315, doi:10.1029/2008JA013690.

Heppner, J. P., and M. L. Miller (1982), Thermospheric winds at high latitudes from chemical release observations, J. Geophys. Res., 87, 1633–1647.

Hosokawa, K., J. I. Moen, K. Shiokawa, and Y. Otsuka (2011), Decay of polar cap patch, J. Geophys. Res., 116, A05306, doi:10.1029/2010JA016297.

Huang, C., S. Sazykin, R. Spiro, J. Goldstein, G. Crowley, and J. M. Ruohoniemi (2006), Storm-time penetration electric fields and their effects, Eos Transactions, 87(13), 131–131, doi:10.1029/2006EO130005.

Huang, C. Y., Y. -J. Su, E. K. Sutton, D. R. Weimer, and R. L. Davidson (2014), Energy coupling during the August 2011 magnetic storm, J. Geophys. Res. Space Phys., 119(2), 1219–1232, doi:10.1002/2013JA019297.

Huang, C. Y., Y. Huang, Y.-J. Su, E. K. Sutton, M. R. Hairston, and W. R. Coley (2016), Ionosphere-thermosphere (IT) response to solar wind forcing during magnetic storms, J. Space Weather and Space Climate, 6(A4), 1, doi:10.1051/swsc/2015041.

Huang, C. Y., Y. Huang, Y.-J. Su, T. Huang, and E. K. Sutton (2017), High-latitude neutral mass density maxima, J. Geophys. Res. Space Physics, 122, 10,694–10711, doi.org/10.1002/2017JA024334.

Immel, T. J., E. Sagawa, S. L. England, S. B. Henderson, M. E. Hagan, S. B. Mende, H. U. Frey, C. M. Swenson, and L. J. Paxton (2006), Control of equatorial ionospheric morphology by atmospheric tides, Geophys. Res. Lett., 33, L15108, doi:10.1029/2006GL026161.

Jonah, O. F., A. Coster, S. Zhang, L. Goncharenko, P. J. Erickson, E. R. Paula, and E. A. Kherani, (2018), TID observations and source analysis during the 2017 Memorial Day weekend geomagnetic storm over North America, J. Geophys. Res. Space Physics, 123, 8749–8765.

Jones, M., J. M. Forbes, M. E. Hagan, and A. Maute (2014), Impacts of vertically propagating tides on the mean state of the ionosphere-thermosphere system, J. Geophys. Res. Space Physics, 119, 2197– 2213, doi:10.1002/2013JA019744.

Kelley, M. C. (1989), The Earth's Ionosphere: Plasma Physics and Electrodynamics, Academic Press, San Diego.

Kelley, M. C., D. J. Knudsen, and J. F. Vickrey (1991), Poynting flux measurements on a satellite - A diagnostic tool for space research, J. Geophys. Res., 96, 201.

Kiene, A., W. A. Bristow, M. G. Conde, and D. L. Hampton (2018), Measurements of ion-neutral coupling in the auroral F region in response to increases in particle precipitation, J. Geophys. Res. Space Physics, 123(5), 3900–3918, doi:10.1002/2017JA024999.

Killeen, T., and R. Roble (1984b), An analysis of the high-latitude thermospheric wind pattern calculated by a thermospheric general circulation model 1. Momentum forcing, J. Geophys. Res., 89, 7509.

Killeen, T. L., and R. G. Roble (1988), Thermosphere dynamics - Contributions from the first 5 years of the Dynamics Explorer program, Rev. Geophys., 26, 329–367, doi:10.1029/RG026i002p00329.

Killeen, T. L., P. B. Hays, G. R. Carignan, R. A. Heelis, W. B. Hanson, N. W. Spencer, and L. H. Brace (1984a), Ion-neutral coupling in the high-latitude F region: Evaluation of ion heating terms from Dynamics Explorer 2, J. Geophys. Res., 89(A9), 7495–7508, doi:10.1029/JA089iA09p07495.

Klimenko, M. V., and V.V. Klimenko (2012), Disturbance dynamo, prompt penetration electric field and overshielding in the Earth's ionosphere during geomagnetic storm, J. Atmos. Solar Terr. Phys., 90, 146–155, doi:10.1016/j.jastp.2012.02.018.

Knipp, D. J., B. A. Emery, A. D. Richmond, and M. R. Hairston (1994), Mapping ionospheric convection response to IMF By negative and Bzpositive conditions, J. Atmos. Terr. Phys., 56, 223–235, https://doi.org/10.1016/0021-9169(94)90032-9.

Knipp, D. J., W. K. Tobiska, and B. A. Emery (2004), Direct and indirect thermospheric heating sources for solar cycles 21–23, Sol. Phys., 224, 495, doi.org/10.1007/s11207-005-6393-4.

Knipp, D., S. Eriksson, L. Kilcommons, G. Crowley, J. Lei, M. Hairston, and K. Drake (2011), Extreme Poynting flux in the dayside thermosphere: Examples and statistics, Geophys. Res. Lett., 38, L16102, doi:10.1029/2011GL048302.

Knipp, D., L. Kilcommons, L. Hunt, M. Mlynczak, V. Pilipenko, B. Bowman, Y. Deng, and K. Drake (2013), Thermospheric damping response to sheath-enhanced geospace storms, Geophys. Res. Lett., 40, 1263–1267, doi:10.1002/grl.50197.

Knipp, D. J., D. V. Pette, L. M. Kilcommons, T. L. Isaacs, A. A. Cruz, M. G. Mlynczak, L. A. Hunt, and C. Y. Lin (2017), Thermospheric nitric oxide response to shock-led storms, Space Weather, 15, 325– 342, doi:10.1002/2016SW001567.

Larsen, M. F. (2002), Winds and shears in the mesosphere and lower thermosphere: Results from four decades of chemical release wind measurements, J. Geophys. Res. Space Phys., 107(A8), CiteID 1215, doi:10.1029/2001JA000218.

Laštovička, J. (2006), Forcing of the ionosphere by waves from below, J. Atmos. Solar-Terr. Phys., 68(3-5), 479-497.

Laundal, K. M., N. Østgaard, H. U. Frey, and J. M. Weygand (2010a), Seasonal and interplanetary magnetic field–dependent polar cap contraction during substorm expansion phase, J. Geophys. Res., 115, A11224, doi:10.1029/2010JA015910.

Laundal, K. M., N. Østgaard, K. Snekvik, and H. U. Frey (2010b), Interhemispheric observations of emerging polar cap asymmetries, J. Geophys. Res., 115, A07230, doi:10.1029/2009JA015160.

Laundal, K. M., et al. (2017), North–South asymmetries in Earth's magnetic field, Space Sci. Rev., 206, 225, doi.org/10.1007/s11214-016-0273-0.

Lei, J., J. P. Thayer, J. M. Forbes, Q. Wu, C. She, W. Wan, and W. Wang (2008), Ionosphere response to solar wind high-speed streams, Geophys. Res. Lett., 35, L19105, doi:10.1029/2008GL035208.

Lei, J., J. P. Thayer, A. G. Burns, G. Lu, and Y. Deng (2010a), Wind and temperature effects on thermosphere mass density response to the November 2004 geomagnetic storm, J. Geophys. Res., 115, A05303, doi:10.1029/2009JA014754.

Lei, J., J. P. Thayer, and J. M. Forbes, (2010b), Longitudinal and geomagnetic activity modulation of the equatorial thermosphere anomaly, J. Geophys. Res., 115, A08311, doi:10.1029/2009JA015177.

Lei, J., T. Dang, W. Wang, A. Burns, B. Zhang, and H. Le (2018), Long-lasting response of the global thermosphere and ionosphere to the 21 August 2017 solar eclipse, J. Geophys. Res. Space Physics, 123(5), 4309–4316, doi: 10.1029/2018JA025460.

Lin, C. H., C. C. Hsiao, J. Y. Liu, and C. H. Liu (2007), Longitudinal structure of the equatorial ionosphere: Time evolution of the four-peaked EIA structure, J. Geophys. Res., 112, A12305, doi:10.1029/2007JA012455.

Liu, A. Z., Y. Guo, F. Vargas, and G. R. Swenson (2016), First measurement of horizontal wind and temperature in the lower thermosphere (105-140 km) with a Na Lidar at Andes Lidar Observatory, Geophys. Res. Lett., 43(6), 2374–2380, doi:10.1002/2016GL068461.

Liu, H, H. Lühr, V. Henize, and W. Köhler (2005), Global distribution of the thermospheric total mass density derived from CHAMP, J. Geophys. Res. Space Phys., 110(A4), doi:10.1029/2004JA010741.

Liu, H.-L. (2016), Variability and predictability of the space environment as related to lower atmosphere forcing, Space Weather, 14, 634–658, doi:10.1002/2016SW001450.

Liu, H.-L. (2017), Large wind shears and their implications for diffusion in regions with enhanced static stability: The mesopause and the tropopause, J. Geophys. Res. Atmos., 122(18), 9579-9590, doi:10.1002/2017JD026748.

Liu, H.-L., C. G. Bardeen, B. T. Foster, P. Lauritzen, J. Liu, G. Lu, D. R. Marsh, A. Maute, J. M. McInerney, N. M. Pedatella, L. Qian, A. D. Richmond, R. G. Roble, S. C. Solomon, F. M. Vitt, and W. Wang (2018), Development and validation of the Whole Atmosphere Community Climate Model With Thermosphere and Ionosphere Extension (WACCM-X 2.0), J. Advances in Modeling Earth Systems, 10(2), 381–402, doi:10.1002/2017MS001232.

Liu, M., X.-X. Zhang, F. He, and W. Wang (2018), Hemispheric asymmetry of the vertical ion drifts at dawn observed by DMSP, J. Geophys. Res. Space Physics, 123, 10,213–10,223. doi.org/10.1029/2018JA025733.
Liu, R., H. Luhr, and S.-Y. Ma (2010a), Storm-time related mass density anomalies in the polar cap as observed by CHAMP, Annales Geophysicae, 28, 165.

Liu, R., H. Lühr, E. Doornbos, S. -Y. Ma (2010b), Thermospheric mass density variations during geomagnetic storms and a prediction model based on the merging electric field, Ann. Geophys., 28(9), 1633–1645, doi:10.5194/angeo-28-1633-2010.

Lu, G., A. D. Richmond, B. A. Emery, and R. G. Roble (1995), Magnetosphere-ionosphere-thermosphere coupling: Effect of neutral winds on energy transfer and field-aligned current, J. Geophys. Res., 100(A10), 19643–19659, doi:10.1029/95JA00766.

Lu, G., M. G. Mlynczak, L. A. Hunt, T. N. Woods, and R. G. Roble (2010), On the relationship of Joule heating and nitric oxide radiative cooling in the thermosphere, J. Geophys. Res., 115, A05306, doi:10.1029/2009JA014662.

Lu, G., M. E. Hagan, K. Häusler, E. Doornbos, S. Bruinsma, B. J. Anderson, and H. Korth (2014), Global ionospheric and thermospheric response to the 5 April 2010 geomagnetic storm: An integrated data-model investigation, J. Geophys. Res. Space Physics, 119, 10358, doi:10.1002/2014JA020555.

Lu, G., A. D. Richmond, H. Lühr, and L. Paxton, (2016) High-latitude energy input and its impact on the thermosphere, J. Geophys. Res. Space Phys., 121(7), 7108–7124, doi:10.1002/2015JA022294.

Lühr, H., M. Rother, W. Köhler, P. Ritter, L. Grunwaldt (2004), Thermospheric up-welling in the cusp region: Evidence from CHAMP observations, Geophys. Res. Lett., 31(6), CiteID L06805, doi:10.10229/2003GL019314.

Lyons, L. R., Y. Nishimura, S.-R. Zhang, A. J. Coster, A. Bhatt, E. Kendall, and Y. Deng (2019), Identification of auroral zone activity driving large-scale traveling ionospheric disturbances, J. Geophys. Res. Space Physics, 124, 700–714, doi.org/10.1029/2018JA025980.

Ma, G., and T. Maruyama (2006), A super bubble detected by dense GPS network at east Asian longitudes, Geophys. Res. Lett., 33(21), CiteID L21103, doi:10.1029/2006GL027512.

Maeda, S., T. J. Fuller-Rowell, and D. S. Evans (1989), Zonally averaged dynamical and compositional response of the thermosphere to auroral activity during September 18–24, 1984, J. Geophys. Res., 94(A12), 16869– 16883, doi:10.1029/JA094iA12p16869.

Maeda, S., T. J. Fuller-Rowell, and D. S. Evans (1992), Heat budget of the thermosphere and temperature variations during the recovery phase of a geomagnetic storm, J. Geophys. Res., 97(A10), 14947– 14957, doi:10.1029/92JA01368.

Mannucci, A. J., B. T. Tsurutani, B. A. Ligima, A. Komjathy, A. Saito, W. D. Gonzalez, F. L. Guarnieri, J. U. Kozyra, and R. Skoug (2005), Dayside global ionospheric response to the major interplanetary events of October 29-30, 2003 “Halloween Storms”, Geophys. Res. Lett., 32(12), CiteID L12S02, doi:10.1029/2004GL021467.

Maruyanm, N., et al. (2007), Modeling storm-time electrodynamics of the low-latitude ionosphere–thermosphere system: Can long lasting disturbance electric fields be accounted for?, J. Atmos. Solar Terr. Phys., 69, 1182-1199, doi.org/10.1016/j.jastp.2006.08.020.

Matsuo, T., A. D. Richmond, and D. W. Nychka (2002), Modes of high-latitude electric field variability derived from DE-2 measurements: Empirical Orthogonal Function (EOF) analysis, Geophys. Res. Lett., 29(7), 1107, doi:10.1029/2001GL014077.

Matsuo, T., and A. D. Richmond (2008), Effects of high-latitude ionospheric electric field variability on global thermospheric Joule heating and mechanical energy transfer rate, J. Geophys. Res., 113, A07309, doi:10.1029/2007JA012993.

McGranaghan, R., D. J. Knipp, S. C. Solomon, and X. Fang (2015), A fast, parameterized model of upper atmospheric ionization rates, chemistry, and conductivity, J. Geophys. Res. Space Physics, 120, 4936– 4949, doi: 10.1002/2015JA021146.

Meier, R., G. Crowley, D. J. Strickland, A. B. Christensen, L. J. Paxton, D. Morrison, and C. L. Hackert (2005), First look at the 20 November 2003 superstorm with TIMED/GUVI: Comparisons with a thermospheric global circulation model, J. Geophys. Res., 110, A09S41, doi:10.1029/2004JA010990.

Merkin, V. G., B. J. Anderson, J. G. Lyon, H. Korth, M. Wiltberger, and T. Motoba (2013), Global evolution of Birkeland currents on 10-min time scales: MHD simulations and observations, J. Geophys. Res., 118, 4977-4997, doi:10.1002/jgra.50466.

Mikkelsen, I. S., and M. F. Larsen (1991), A numerical modeling study of the interaction between the tides and the circulation forced by high-latitude plasma convection, J. Geophys. Res., 96, 1203–1213.

Miyoshi, Y., H. Jin, H. Fujiwara, and H. Shinagawa

(2018), Numerical study of traveling ionospheric disturbances generated by an upward propagating gravity wave, J. Geophys. Res. Space Physics, 123, 2141–2155, doi.org/10.1002/2017JA025110.

Mlynczak, M. G., et al. (2003), The natural thermostat of nitric oxide emission at 5.3 μm in the thermosphere observed during the solar storms of April 2002, Geophys. Res. Lett., 30(21), 2100, doi:10.1029/2003GL017693.

Mlynczak, M. G., et al. (2005), Energy transport in the thermosphere during the solar storms of April 2002, J. Geophys. Res., 110, A12S25, doi:10.1029/2005JA011141.

Mlynczak, M. G., F. J. Martin-Torres, C. J. Mertens, B. T. Marshall, R. E. Thompson, J. U. Kozyra, E. E. Remsberg, L. L. Gordley, J. M. Russell III, and T. Woods (2008), Solar-terrestrial coupling evidenced by periodic behavior in geomagnetic indexes and the infrared energy budget of the thermosphere, Geophys. Res. Lett., 35, L05808, doi:10.1029/2007GL032620.

Mlynczak, M. G., L. A. Hunt, B. T. Marshall, and J. M. Russell (2018a), Infrared radiation in the thermosphere near the end of solar cycle 24, Geophys. Res. Letts., 45, 11,581–11,587, doi.org/10.1029/2018GL080389.

Mlynczak, M. G. et al. (2018b), Space-based sentinels for measurement of infrared cooling in the thermosphere for space weather nowcasting and forecasting, Space Weather, 16, 363–375, doi.org/10.1002/2017SW001757.

National Academies of Sciences, Engineering, and Medicine 2016. Achieving Science with CubeSats: Thinking Inside the Box. Washington, DC: The National Academies Press. https://doi.org/10.17226/23503.

Newell, P., and C.-I. Meng (1992), Mapping the dayside ionosphere to the magnetosphere according to particle precipitation characteristics, Geophys. Res. Lett., 19, 609.

Newnham, D. A., et al. (2018), Observations and modeling of increased nitric oxide in the Antarctic polar middle atmosphere associated with geomagnetic storm-driven energetic electron precipitation, J. Geophys. Res. Space Physics, 123, 6009–6025, doi.org/10.1029/2018JA025507

Oberheide, J., J. M. Forbes, K. Häusler, Q. Wu, and S. L. Bruinsma (2009), Tropospheric tides from 80 to 400 km: Propagation, interannual variability, and solar cycle effects, J. Geophys. Res., 114, D00I05, doi:10.1029/2009JD012388.

Oberheide, J., J. M. Forbes, X. Zhang, and S. L. Bruinsma (2011), Climatology of upward propagating diurnal and semidiurnal tides in the thermosphere, J. Geophys. Res., 116, A11306, doi:10.1029/2011JA016784.

Oppenheim, M. M., G. Sugar, N. O. Slowey, E. Bass, J. L. Chau, S. Close (2009), Remote sensing lower thermosphere wind profiles using non-specular meteor echoes, Geophys. Res. Lett., 36(9), CiteID L09817, doi:10.1029/2009GL037353.

Otsuka, Y., K. Shiokawa, T. Ogawa, and P. Wilkinson (2004), Geomagnetic conjugate observations of medium-scale traveling ionospheric disturbances at midlatitude using all-sky airglow imagers, Geophys. Res. Lett., 31, L15803, doi:10.1029/2004GL020262.

Oppenheim, M. M., S. Arredondo, G. Sugar (2014) Intense winds and shears in the equatorial lower thermosphere measured by high-resolution nonspecular meteor radar, J. Geophys. Res. Space Phys., 119(3), 2178-2186, doi:10.1002/2013JA019272.

Pancheva, D., and P. Mukhtarov (2012), Global response of the ionosphere to atmospheric tides forced from below: Recent progress based on satellite measurements, Space Sci. Rev., 168, 175 doi.org/10.1007/s11214-011-9837-1.

Papitashvili, V. O., and F. J. Rich (2002), High-latitude ionospheric convection models derived from Defense Meteorological Satellite Program ion drift observations and parameterized by the interplanetary magnetic field strength and direction, J. Geophys. Res., 107(A8), doi:10.1029/2001JA000264.

Pedatella, N. M., K. Raeder, J. L. Anderson, and H.-L. Liu (2014), Ensemble data assimilation in the Whole Atmosphere Community Climate Model, J. Geophys. Res. Atmos., 119, 9793–9809, doi:10.1002/2014JD021776.

Pedatella, N. M., J. Oberheide, E. K. Sutton, H.-L. Liu, J. L. Anderson, and K. Raeder (2016), Short-term nonmigrating tide variability in the mesosphere, thermosphere, and ionosphere, J. Geophys. Res. Space Physics, 121, 3621–3633, doi:10.1002/2016JA022528.

Perlongo, N. J., and A. J. Ridley (2016), Universal time effect in the response of the thermosphere to electric field changes, J. Geophys. Res. Space Physics, 121, 3681–3698, doi:10.1002/2015JA021636.

Pettigrew, E. D., S. G. Shepherd, and J. M. Ruohoniemi (2010), Climatological patterns of high-latitude convection in the Northern and Southern hemispheres: Dipole tilt dependencies and interhemispheric comparisons, J. Geophys. Res., 115, A07305, doi:10.1029/2009JA014956.

Peymirat, C., A. D. Richmond, B. A. Emery, and R. G. Roble (1998), A magnetosphere-thermosphere-

ionosphere electrodynamics general circulation model, J. Geophys. Res., 103(A8), 17467-17478, doi:10.1029/98JA01235.

Picone, J.-M., A. E., Hedin, D. P. Drob, and A.C. Aikin (2002), NRLMSISE-00 empirical model of the atmosphere: Statistical comparisons and scientific issues, J. Geophy. Res., 107, 1468, doi: 10.1029/2002JA009430.

Price, G. D., R. W. Smith, G. Hernandez (1995), Simultaneous measurements of large vertical winds in the upper and lower thermosphere, J. Atmos. Terr. Phys., 57, 631–643, doi:10.1016/0021-9169(94)00103.

Prölss, G. W. (1982), Perturbation of the low-latitude upper atmosphere during magnetic substorm activity, J. Geophys. Res., 87(A7), 5260–5266, doi:10.1029/JA087iA07p05260.

Prölss, G. W. (1987), Storm-induced changes in the thermospheric composition at middle latitudes, Planet. Space. Sci., 35, 807-811, doi.org/10.1016/0032-0633(87)90041-9.

Prölss, G. W. (1997), Magnetic storm associated perturbations of the upper atmosphere, in Magnetic Storms, eds. B. T. Tsurutani, W. D. Gonzalez, Y. Kamide and J. K. Arballo, doi:10.1029/GM098p0227.

Prölss, G. W. (2011), Density perturbations in the upper atmosphere caused by the dissipation of solar wind energy, Surv. Geophys., 32, 101, doi.org/10.1007/s10712-010-9104-0.

Qian, L., S. C. Solomon, and T. J. Kane (2009), Seasonal variation of thermospheric density and composition, J. Geophys. Res., 114(A1), CiteID A01312, doi:10.1029/2008JA013643.

Randall, C. E., et al. (2005), Stratospheric effects of energetic particle precipitation in 2003–2004, Geophys. Res. Lett., 32, L05802, doi:10.1029/2004GL022003.

Randall, C. E., V. L. Harvey, L. A. Holt, D. R. Marsh, D. Kinnison, B. Funke, and P. F. Bernath (2015), Simulation of energetic particle precipitation effects during the 2003–2004 Arctic winter, J. Geophys. Res. Space Physics, 120, doi:10.1002/2015JA021196.

Rees, D., R. W. Smith, P. J. Charleton, F. G. McCormac, N. Lloyd, and Å. Steen (1984), The generation of vertical thermospheric winds and gravity waves at auroral latitudes - I. Observations of vertical winds, Plan. Space Sci., 32(6), 667–684, doi:10.1016/0032-0633(84)90092-8.

Richmond, A. D. (1995), The ionospheric wind dynamo: Effects of its coupling with different atmospheric regions, in The Upper Mesosphere and Lower Thermosphere: A Review of Experiment and Theory, eds. R. M. Johnson and T. L. Killeen, doi:10.1029/GM087p0049.

Richmond, A. D. (2016), Ionospheric electrodynamics, in Space Weather Fundamentals, ed., G.V. Khazanov, CRC Press, Boca Raton, p. 35

Richmond, A. D., E. C. Ridley, and R. G. Roble (1992), A thermosphere/ionosphere general circulation model with coupled electrodynamics, Geophys. Res. Lett., 19, doi.org/10.1029/92GL00401.

Richmond, A. D., C. Lathuillére, and S. Vennerstroem (2003), Winds in the high-latitude lower thermosphere: Dependence on the interplanetary magnetic field, J. Geophys. Res., 108(A2), 1066, doi:10.1029/2002JA009493.

Ridley, A., C. Clauer, G. Lu, and V. Papitashvili (1997), Ionospheric convection during nonsteady interplanetary magnetic field conditions, J. Geophys. Res., 102, 14,563.

Ridley, A. J., A. D. Richmond, T. I. Gombosi, D. L. de Zeeuw, and C. R. Clauer, (2003), Ionospheric control of the magnetospheric configuration: Thermospheric neutral winds, J. Geophys. Res., 108(A8), CiteID 1328, doi:10.1029/2002JA009464.

Ridley, A. J., T. I. Gombosi, and D. L. DeZeeuw (2004), Ionospheric control of the magnetosphere: conductance, Ann. Geophys., 22, 567–584, doi.org/10.5194/angeo-22-567-2004.

Ridley, A., Y. Deng, and G. Tòth (2006), The global ionosphere-thermosphere model, J. Atmos. Sol-Terr. Phys., 68, 839.

Rishbeth, H. (1997), Drifts and winds in the polar F region, J. Atmos. Sol. Terr. Phys., 39, 111–116.

Rishbeth,H., and M. Mendillo (2001), Patterns of F2-layer variability, J. Atmos. Solar Terr. Phys., 63, 1661–1680, doi.org/10.1016/S1364-6826(01)00036-0.

Rishbeth, H., R. A. Heelis, J. J. Makela, and S. Basu (2010), Storming the Bastille: The effect of electric fields on the ionospheric F-layer, Ann. Geophys., 28, 977–981, doi:10.5194/angeo-28-977-2010.

Ruohoniemi, J., and R. Greenwald (1998), The response of high latitude convection to a sudden southward IMF turning, Geophys. Res. Lett., 25, 2913.

Saito, A., et al. (2001), Traveling ionospheric disturbances detected in the FRONT Campaign, Geophys. Res. Lett., 28, doi.org/10.1029/2000GL011884.

Sangalli, L, D. J. Knudsen, M. F. Larsen, T. Zhan, R. F. Pfaff, and D. Rowland (2009), Rocket-based measurements of ion velocity, neutral wind, and electric field in the collisional transition region of the auroral ionosphere, J. Geophys. Res., 114(A4), CiteID A04306, doi:10.1029/2008JA013757.

Schlegel, K., H. Lühr, J.-P. -Maurice, G. Crowley, and C. Hackert (2005), Thermospheric density structures over the polar regions observed with CHAMP, Ann. Geophys., 23(5), 1659–1672, doi:10.5194/angeo-23-1659-2005.

Schoendorf, J., G. Crowley, R. G. Roble, and F. A. Marcos (1996a), Neutral density cells in the high latitude thermosphere--1. Solar maximum cell morphology and data analysis, J. Atmos. Terr. Phys., 58, 1751–1768, doi:10.1016/0021-9169(95)00165-4.

Schoendorf, J., G. Crowley, and R. G. Roble (1996b), Neutral density cells in the high latitude thermosphere--2. Mechanisms, J. Atmos. Terr. Phys., 58, 1769–1781, doi:10.1016/0021-9169(95)00166-2.

Siskind, D. E., C. A. Barth, and R. G. Roble (1989), The response of thermospheric nitric oxide to an auroral storm: 1. Low and middle latitudes, J. Geophys. Res., 94(A12), 16885–16898, doi:10.1029/JA094iA12p16885.

Siskind, D. E., S. D. Eckermann, J. P. McCormack, M. Joan Alexander, and J. T. Bacmeister (2003), Hemispheric differences in the temperature of the summertime stratosphere and mesosphere, J. Geophys. Res. Atmos., 108(D2), CiteID 4051, doi:10.1029/2002JD002095.

Siskind, D. E., A. W. Merkel, D. R. Marsh, C. E. Randall, M. E. Hervig, M. G. Mlynczak, and J. M. Russell III (2018), Understanding the effects of polar mesospheric clouds on the environment of the upper mesosphere and lower thermosphere, J. Geophys. Res. Atmos., 123(20), 11705–11719, doi:10.1029/2018JD028830.

Smith, A. K. (2012), Global dynamics of the MLT, Sur. Geophys., 33(6), 1177–1230, doi:10.1007/s10712-012-9196-9.

Spencer, N. W., L. E. Wharton, G. R. Carignan, and J. C. Maurer (1982), Thermosphere zonal winds, vertical motions and temperature as measured from Dynamics Explorer, Geophys. Res. Lett., 9(9), 953–956, doi:10.1029/GL009i009p00953.

Spicher, A., L. B. N. Clausen, W. J. Miloch, V. Lofstad, Y. Jin, and J. I. Moen (2017), Interhemispheric study of polar cap patch occurrence based on Swarm in situ data, J. Geophys. Res. Space Physics, 122, 3837–3851, doi:10.1002/2016JA023750.

Spiro, R. W., R. A. Wolf, and B. G. Fejer (1988), Penetration of high-latitude-electric-field effects to low latitudes during {SUNDIAL} 1984, Ann. Geophys., 6, 39.

Strangeway, R. J. (2012), The equivalence of Joule dissipation and frictional heating in the collisional ionosphere, J. Geophys. Res., 117(A2), CiteID AO2310, doi:10.1029/2011JA017302.

Strickland, D. J., R. E. Daniell, and J. D. Craven (2001), Negative ionospheric storm coincident with DE 1-observed thermospheric disturbance on October 14, 1981, J. Geophys. Res., 106(A10), 21049– 21062, doi:10.1029/2000JA000209.

Sutton, E. K., J. M. Forbes, and D. J. Knipp (2009), Rapid response of the thermosphere to variations in Joule heating, J. Geophys. Res., 114, A04319, doi:10.1029/2008JA013667.

Sutton, E. K., J. P. Thayer, W. Wang, S. C. Solomon, X. Liu, and B. T. Foster (2015), A self-consistent model of helium in the thermosphere, J. Geophys. Res. Space Physics, 120, 6884–6900, doi:10.1002/2015JA021223.

Tanaka, T. (2001), Interplanetary magnetic field By and auroral conductance effects on high-latitude ionospheric convection patterns, J. Geophys. Res., 106(A11), 24505–24516, doi:10.1029/2001JA900061.

Thayer, J. P. (1998), Height-resolved Joule heating rates in the high-latitude E region and the influence of neutral winds, J. Geophys. Res., 103(A1), 471–487, doi: 10.1029/97JA02536.

Thayer, J. P. (2000), High-latitude currents and their energy exchange with the ionosphere-thermosphere system, J. Geophys. Res., 105(A10), 23015-23024, doi:10.1029/1999JA000409.

Thayer, J. P., and J. Semeter (2004), The convergence of magnetospheric energy flux in the polar atmosphere, J. Atmos. Solar Terr. Phys., 66, 807–824. doi.org/10.1016/j.jastp.2004.01.035.

Thayer, J. P., J. F. Vickrey, R. A. Heelis, and J. B. Gary (1995), Interpretation and modeling of the high-latitude electromagnetic energy flux, J. Geophys. Res., 100(A10), 19715–19728, doi:10.1029/95JA01159.

Thayer, J. P., X. Liu, J. Lei, M. Pilinski, and A. G. Burns (2012), The impact of helium on thermosphere mass density response to geomagnetic activity during the recent solar minimum, J. Geophys. Res., 117, A07315, doi:10.1029/2012JA017832.

Tsurutani, B. T, O. P. Verkhoglyadova, A. J. Mannucci, A. Saito, T. Araki, K. Yumoto, T. Tsuda, M. A. Abdu,

J. H. A. Sobral, W. D. Gonzalez, H. McCreadi, G. S. Lakhina, and V. M. VasyliåœNas (2008), Prompt penetration electric fields (PPEFs) and their ionospheric effects during the great magnetic storm of 30-31 October 2003, J. Geophys. Res. Space Phys., 113(A5), CiteID A05311, doi:10.1029/2007JA012879.

Tu, J., P. Song, and V. M. Vasyliūnas (2014), Inductive-dynamic magnetosphere-ionosphere coupling via MHD waves, J. Geophys. Res. Space Physics, 119, 530–547, doi:10.1002/2013JA018982.

Vadas, S. L. and G. Crowley (2017), Neutral wind and density perturbations in the thermosphere created by gravity waves observed by the TIDDBIT sounder, J. Geophys. Res. Space Physics, 122, 6652–6678, doi:10.1002/2016JA023828.

Vlasov, A., K. Kauristie, M. van de Kamp, J.-P. Luntama, and A. Pogoreltsev (2011), A study of traveling ionospheric disturbances and atmospheric gravity waves using EISCAT Svalbard Radar IPY-data, Ann. Geophys., 29, 2101-2116, doi.org/10.5194/angeo-29-2101-2011.

Walker, I. K., J. Moen, L. Kersley, and D. A. Lorentzen (1999), On the possible role of cusp/cleft precipitation in the formation of polar-cap patches, Ann. Geophys., 17(10), 1298–1305, doi:10.1007/s00585-999-1298-4.

Walsh, B. M., J. C. Foster, P. J. Erickson, and D. G. Sibeck (2014), Simultaneous ground- and space-based observations of the plasmaspheric plume and reconnection, Science, 343, 1122–1125.

Waters, C. L., B. J. Anderson and K. Liou (2001), Estimation of global field aligned currents using Iridium magnetometer data, Geophys. Res. Lett., 28, 2165-2168.

Weimer, D. R. (2005), Improved ionospheric electrodynamic models and application to calculating joule heating rates, J. Geophys. Res., 110, 05,306, doi: 10.1029/2004JA010884.

Wilder, F. D., G. Crowley, B. J. Anderson, and A. D. Richmond (2012), Intense dayside Joule heating during the 5 April 2010 geomagnetic storm recovery phase observed by AMIE and AMPERE, J. Geophys. Res., 117, A05207, doi:10.1029/2011JA017262.

Wu, Q., D. A. Ortland, S. C. Solomon, W. R. Skinner, and R. J. Niciejewski (2011), Global distribution, seasonal, and inter-annual variations of mesospheric semidiurnal tide observed by TIMED TIDI, J. Atmos. Solar Terr. Phys., 73(17), 2482–2502, doi:10.1016/j.jastp.2011.08.007.

Wu, Q., W. Wang, R. G. Roble, Ingemar Häggström, and Anja Strømme (2012), First daytime thermospheric wind observation from a balloon-borne Fabry-Perot interferometer over Kiruna (68N), Geophys. Res. Lett., 39, L14104, doi:10.1029/2012GL052533.

Yakymenko, K. N., A. V. Koustov, and R. A. D. Fiori (2018), Interhemispheric asymmetry of the sunward plasma flows for strongly dominant IMF BZ > 0, J. Geophys. Res. Space Physics, 123, 315–325, doi.org/10.1002/2017JA024644.

Yigit, E. and A. Medvedev (2015), Internal wave coupling processes in Earth's atmosphere, Adv. Space Res., 55, 983–1003, doi.org/10.1016/j.asr.2014.11.020.

Yiğit, E., A. S. Medvedev, S. L. England, and T. J. Immel (2014), Simulated variability of the high-latitude thermosphere induced by small-scale gravity waves during a sudden stratospheric warming, J. Geophys. Res. Space Phys., 119(1), 357–365, doi:10.1002/2013JA019283.

Yu, Y., and A. J. Ridley (2009), Response of the magnetosphere-ionosphere system to a sudden southward turning of interplanetary magnetic field, J. Geophys. Res., 114, 03,216, doi:10.1029/2008JA013292.

Yue, J., C. -Y She, H. -L. Liu (2010), Large wind shears and stabilities in the mesopause region observed by Na wind-temperature lidar at midlatitude, J. Geophys. Res., 115(A10), CiteID A10307, doi:10.1029/2009JA014864.

Yue, J., Y. Jian, W. Wang, R. R. Meier, A. Burns, Q. Liying, M. Jones, D. L. Wu, and M. Mlynczak (2019), Annual and semiannual oscillations of thermospheric composition in TIMED/GUVI limb measurements, J. Geophys. Res. Space Phys., 124(4), 3067–3082, doi:10.1029/2019JA026544.

Xiong, C., H. Lühr, and B. G. Fejer (2015), Global features of the disturbance winds during storm time deduced from CHAMP observations, J. Geophys. Res. Space Physics, 120, 5137–5150, doi: 10.1002/2015JA021302.

Zesta, E., A. Boudouridis, J. M. Weygand, E. Yizengaw, M. B. Moldwin, and P. Chi (2016), Inter-hemispheric asymmetries in magnetospheric energy input, in Ionospheric Space Weather: Longitude Dependence and Lower Atmosphere Forcing, eds. T. Fuller-Rowell, E. Yizengaw, P. H. Doherty, and S. Basu, Geophysical Monograph Series, Vol. 220, Washington, DC: American Geophysical Union, p. 1–20, doi.org/10.1002/9781118929216.ch1.

Zhan, T. (2007), Mesosphere and lower thermosphere neutral winds observations using rocket-released chemical trails at Poker Flat, Alaska, Ph.D thesis, Clemson University, volume 68-07, Section B, pg. 4339, ISBN:9780549150268.

Zhang, Q.-H., Y.-Z. Ma, P. T. Jayachandran, J. Moen, M. Lockwood, Y.-L. Zhang, J. C. Foster, S.-R. Zhang, Y. Wang, D. R. Themens, B.-C. Zhang, and Z. Y. Xing (2017), Polar cap hot patches: Enchanced density structures different from the classical patches in the ionosphere, Geophys. Res. Lett., 44(16), 8159–8167, doi:10.1002/2017GL073439.

Zhang, X., L. Liu, and S. Liu (2017), Dependence of thermospheric zonal winds on solar flux, geomagnetic activity, and hemisphere as measured by CHAMP, J. Geophys. Res. Space Physics, 122, 8893–8914, doi:10.1002/2016JA023715.

Zhang, Y., L. J. Paxton, D. Morrison, B. Wolven, H. Kil, C.-I. Meng, S. B. Mende, and T. J. Immel (2004), O/N2 changes during 1–4 October 2002 storms: IMAGE SI-13 and TIMED/GUVI observations, J. Geophys. Res., 109, A10308, doi:10.1029/2004JA010441.

Zhu, J., A. J. Ridley, and Y. Deng (2016), Simulating electron and ion temperature in a global ionosphere thermosphere model: Validation and modeling an idealized substorm, J. Atmos. Solar Terr. Phys., 138, 243-260, doi:10.1016/j.jastp.2016.01.005.

Zou, S., M. B. Moldwin, A. J. Ridley, M. J. Nicolls, A. J. Coster, E. G. Thomas, and J. M. Ruohoniemi (2014), On the generation/decay of the storm-enhanced density plumes: Role of the convection flow and field-aligned ion flow, J. Geophys. Res. Space Phys., 119, 85438559, doi:10.1002/2014JA020408.

Zou, Y., Y. Nishimura, L. Lyons, M. Conde, R. Varney, V. Angelopoulos, and S. Mende (2018), Mesoscale F region neutral winds associated with quasi-steady and transient nightside auroral forms, J. Geophys. Res. Space Physics, 123(9), 7968–7984, doi:10.1029/2018JA025457.

Acronyms

AE	Atmospheric Explorer
AIM	Aeronomy of Ice in the Mesosphere
AMPERE	Active Magnetosphere and Planetary Electrodynamics Response Experiment
AWE	Atmospheric Waves Experiment
CDF	Common Data Format
CHAMP	Challenging Mini-satellite Payload
COSMIC	Constellation Observing System for Meteorology, Ionosphere, and Climate
CSSWE	Colorado Student Space Weather Experiment
CVV	Calibration, validation, and verification
CYGNSS	Cyclone Global Navigation Satellite System
DE-2	Dynamics Explorer-2
DMSP	Defense Meteorological Satellite Program
DoD	Department of Defense
ESA	European Space Agency
EUV	Extreme ultraviolet
EVE	EUV Variability Experiment
FP	Full Physics
FUV	Far Ultraviolet
GAIM	Global Assimilation of Ionospheric Measurements
GCM	Global Circulation Model
GDC	Geospace Dynamics Constellation
GOCE	Gravity field and steady-state Ocean Circulation Explorer
GOLD	Global-scale Observations of the Limb and Disk
GPS	Global Positioning Satellite
GRACE	Gravity Recovery and Climate Experiment
GUVI	Global Ultraviolet Imager
GW	Gravity Waves
HF	High Frequency
ICON	Ionospheric Connection Explorer
ISR	Intelligence, Surveillance, and Reconnaissance
ISS	International Space Station
IT	Ionosphere-thermosphere
ITM	Ionosphere-thermosphere-mesosphere
LBH	Lyman-Birge-Hopfield emission
LEO	Low Earth Orbit
LT	Local time
LWS	Living With a Star
MIGHTI	Michelson Interferometer for Global High-Resolution Thermospheric Imaging
MLTI	Mesosphere and Lower-Thermosphere/Ionosphere
NASA	National Aeronautics and Space Administration
NEXT	NASA Evolutionary Xenon Thruster
NLC	Noctilucent Clouds
NSF	National Science Foundation
NSWAP	National Space Weather Action Plan
OTHR	Over-the-horizon radar
PNT	Position/navigation/timing
R20	Research to Operations
RAAN	Right Ascension of the Ascending Node
RF	Radio Frequency
SABER	Sounding of the Atmosphere using Broadband Emission Radiometry
SDO	Solar Dynamics Observatory
SES	Communications satellite series
SPEDAS	Space Physics Environment Data Analysis Software
STDT	Science and Technology Definition Team
SWORM	Space Weather Operations, Research, and Mitigation
TAD	Traveling Atmospheric Disturbance
TEC	Total Electron Content
TID	Traveling Ionospheric Disturbance
TIMED	Thermosphere, Ionosphere, Mesosphere Energetics and Dynamics
UARS	Upper Atmosphere Research Satellite
UHF	Ultra High Frequency
UTC	Universal Coordinated Time
UV	Ultraviolet

APPENDIX A: THE GDC STDT PROCESS

Overview

The Geospace Dynamics Constellation (GDC) Science and Technology Definition Team (STDT) was established as a subcommittee of the Heliophysics Advisory Committee (HPAC), an advisory committee established under the Federal Advisory Committee Act. The Heliophysics Division Director appointed a Designated Federal Officer to serve as the subcommittee's Executive Secretary, who managed the membership, meetings, and other requirements.

The STDT's membership consisted of 17 experts from the Heliophysics community that covered relevant scientific and technical expertise.

NASA Science Mission Directorate, Heliophysics Division, charged the GDC STDT with conducting a mission concept study, including an assessment of the science rationale for the mission and the provision of science objectives, investigation requirements, key mission parameters, and any other scientific studies needed. The STDT was directed to provision the science objectives without considering the flow of technical requirements to a specific mission implementation.

Within the scope of its process, the STDT defined clear and focused Science Objectives for the GDC mission, examined a trade space for mission implementation, and made recommendations for supporting modeling and technology that would enable the GDC mission. The investigation requirements provisioned included the detailed Physical Parameters that flowed from the Science Objectives; those Physical Parameters included contextual measurements of the solar wind and geomagnetic activity (as guided by NASA).

Request for Information

Before the STDT was convened, NASA published a Request For Information for input on the GDC mission goals and implementation. 56 RFI responses were conveyed to the STDT by NASA. Those responses were redacted to remove information outside the scope of the STDT's process. The redacted material and those responses not conveyed were retained by NASA HQ for potential programmatic use. The documents were incorporated into STDT discussions and used for inspiration, direction, and specific input throughout the process.

STDT Structure

The STDT held 3 in-person meetings between the 2nd and 4th quarters of 2018. A writing group convened in April 2019 to do final assembly and formatting of the group text, and to fill the gaps in existing sections. In addition to these meetings, the STDT held organizational and preparatory teleconferences.

To organize key components of the final report before holding discussions with the entire membership, the STDT organized sub-groups consisting of 4-5 members and the Co-Chairs. These sub-groups addressed the Science Objectives, Implementation, Modeling, and Measurement Requirements. All final decisions were consensus-based with participation from the full STDT.

STDT Support

To provide technical support for the STDT's discussions, NASA contracted NASA Goddard Space Flight Center and Applied Physics Laboratory, The John Hopkins University.

The Community Coordinated Modeling Center (CCMC), NASA Goddard Space Flight Center, provided modeling support. This support included conducting analysis on global ionosphere-thermosphere models to inform the discussion of measurement requirements included in this report. Model outputs and analysis results from the CCMC have been made available on the latter's website (https://ccmc.gsfc.nasa.gov/) under the mission support section.

NASA Goddard Space Flight Center and Applied Physics Laboratory, The Johns Hopkins University, provided flight dynamics support. This support included providing technical information used in the analysis of orbit options and in the CCMC analysis.

This information is made available as tables in Appendix C of this report.

For both technical support groups, the STDT formulated requests that were vetted and, if necessary, adjusted by NASA to fit within the defined process. The final requests were then passed to the support groups, who delivered products to NASA.

Final remarks

The STDT wishes to thank all the individuals who submitted responses to the GDC RFI, the authors of the 2013 Heliophysics Decadal Survey, and all those who contributed to the GDC mission concept leading to the establishment of the STDT.

APPENDIX B: GDC CONTRIBUTION TO NATIONAL INTERESTS

As part of NASA's Heliophysics System Observatory, the GDC mission will provide a unique and vital dataset to execute a science investigation in order to advance our fundamental understanding of the ionosphere/thermosphere (IT) system. While these advances are scientifically compelling in their own right, they will also provide significant contributions to other national space interests.

In the NASA Office of Inspector General's 2019 report of NASA's heliophysics mission portfolio [IG-19-018], the national space interests were identified in two of the four recommendations to improve management of the portfolio. GDC will contribute to NASA's implementation of both recommendations.

> Recommendation 2: Complete implementation of 2015 NSWAP tasks in accordance with SWORM subcommittee deadlines
>
> Recommendation 4: Establish a formal mechanism to increase collaboration with DoD and the commercial space industry regarding heliophysics research and space weather modeling and forecasting efforts.

Recommendation 2: Complete implementation of NSWAP tasks

The 2015 National Space Weather Plan (NSWAP) outlined objectives related to improving understanding and forecasting of space weather phenomena and their effects in order to improve our nation's preparedness for space weather events. GDC's overall goals -- understanding the high-latitude IT during variable conditions, and understanding internal processes of the global IT system -- directly support establishing benchmarks for Space Weather Events and improving understanding/forecasting of space weather.

Currently, space weather forecasting is limited by the lack of full understanding of the internal processes of the IT system. By observing how the IT system responds and evolves during both quiet and disturbed conditions,

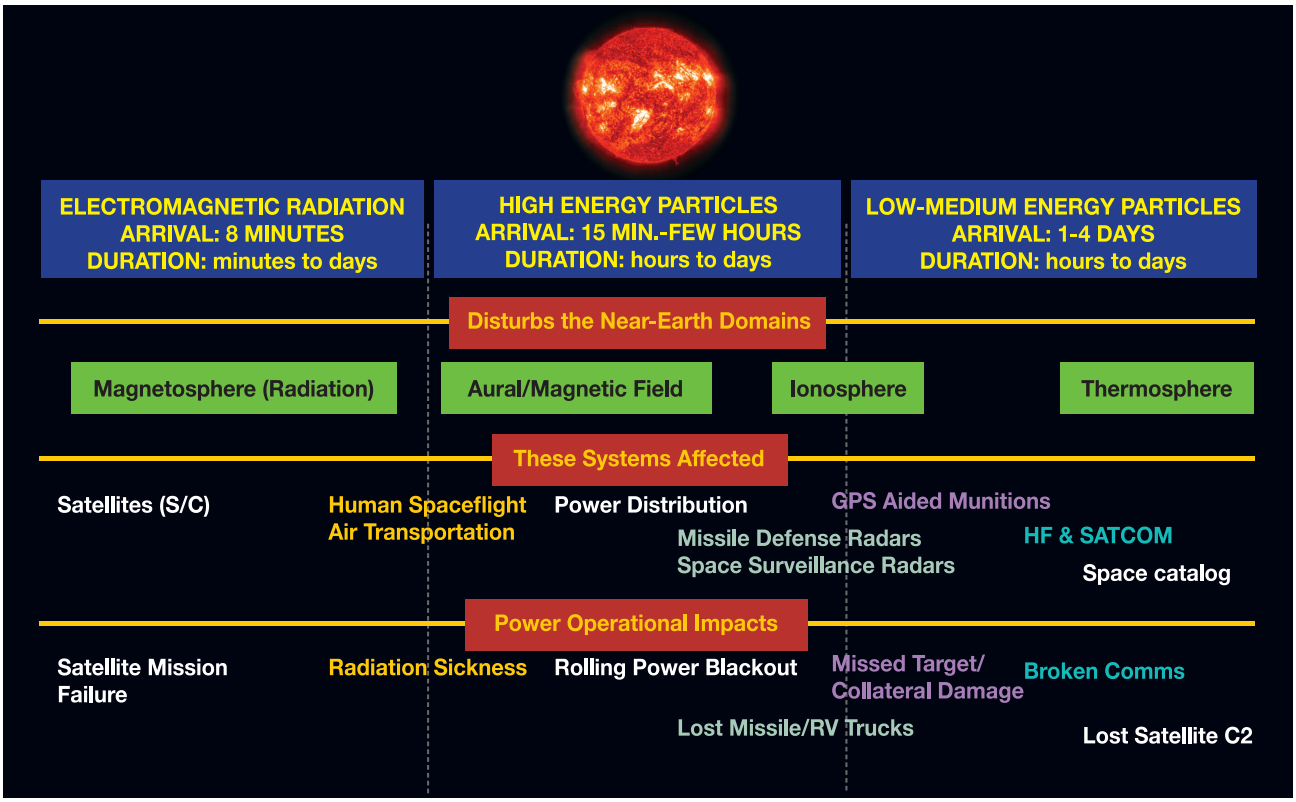

Figure B-1. Regions of the near-Earth environment that impacts various assets. After Handbook [2018].

GDC will provide the missing pieces needed to improve both fundamental physics models as well as current forecasting models.

In 2019, a National Space Weather Strategy and Action Plan was published. Within Objective II, Develop and Disseminate Accurate and Timely Space Weather Characterization, the strategy stated the need to "ensure baseline operational space weather observation capabilities, and networks." GDC, as a constellation, will provide global measurements of IT Physical Parameters, a unique observational capability that cannot be obtained by current or near-term IT satellite missions or disparate ground-based observations.

Recommendation 4: Increase collaboration with DoD

The four branches of the U.S. Armed Forces each have specific interests in the space environment and, in particular, the IT system. Even though each branch's applications of space weather information are different, they can be broken into three IT areas of interest along with the general application areas:

- Electron density gradients and instabilities
  - RF impacts: communication and positioning
- Thermospheric (neutral) density variability, from small to large scales
  - Orbital prediction: re-entry and collision avoidance
- Particle precipitation radiation (auroral electrons 100 eV-100 keV, ions 1 keV-1 MeV)
  - Satellite anomalies and human radiation exposure

The Army's interest in the IT system is limited to its ability to "…conducts space operations to deliver decisive combat power in support of the Army and joint warfighting communities" as described in the 1st Space Brigade's purpose statement [2018 Global Defender]. This primarily covers the impacts of the space environment on RF systems, specifically communications systems, navigation systems, battle-tracking devices, and intelligence, surveillance, and reconnaissance (ISR) assets [Handbook, 2018]. In the Army's handbook on operating in the space operational environment, space weather is specifically called out as a potential source for a denied, degraded, or disrupted environment. As illustrated in Figure C-1, the ionosphere and thermosphere have impacts on a wide variety of assets.

The Navy's interest in space weather and the IT system is associated with its ability to " …Conduct operations in and through cyberspace, the electromagnetic spectrum, and space to ensure Navy and Joint freedom of actions and decision superiority…" [2015-2020 Tenth Fleet Strategic Plan]. Similar to the Army's interest, Navy is primarily interested in the impact on RF signals including communication and positioning. Thus, understanding ionosphere dynamics and density structuring is critical in order to forecast their impact on RF systems. GDC objectives 1.2, 2.1, and 2.2 will directly support this application by determining processes giving rise to various ionospheric density features, thus enabling improved real-time specification and forecasting.

The Air Force not only has an interest in the space environment's impact on various assets, but it deploys operational space environment monitoring systems and actively supports forecasting of the space environment. The Air Force has a long history of on-orbit operational space sensors, including the DMSP satellite series and the recently launched COSMIC-2 satellite constellation. The GDC mission will complement, without unnecessary duplication, the equatorial COSMIC-2 satellite constellation. While this mission will provide real-time ionospheric observations, it will not provide the ionospheric and thermospheric measurements needed to improve our understanding of the formation of ionospheric density structures. Further, since the DMSP program has been discontinued, the Air Force's ability to monitor the high-latitude IT system in the future will be limited. GDC will not only provide measurements of fundamental physical parameters that will improve our understanding of the IT system and our ability to forecast it, but it will also be capable of providing the type of ionospheric observations needed to fill an observational gap until a future weather/space-weather follow-on mission is deployed.

The Air Force actively supports research to operations (R2O) activities. Similar to the other branches, it is interested in HF impacts, specifically over-the-horizon radar (OTHR), position/navigation/timing (PNT) errors/reliability, and satellite and ground communication reliability. OTHR especially requires

accurate specification of the ionosphere in all conditions. GDC will provide an invaluable dataset that the Air Force can utilize to continue their R2O activities.

The Air Force is also responsible for the tracking of space objects. With the proliferation of both commercial and foreign satellites, improved orbital prediction is critical in order to determine potential collision and perform avoidance maneuvers. That requires an understanding of the variations in the neutral density in LEO on scales less than an orbit. GDC is uniquely situated to make significant improvements to this operational area by reaching closure on Objectives 1.3, 1.4, 2.2, 2.3, 2.4, 2.5, and 2.6.

The final area of interest to the Air Force that overlaps with GDC is particle precipitation at high latitudes. As more assets are being deployed to LEO and high-altitude aircraft are developed and deployed, understanding auroral particle precipitation is becoming more important. While not the primary focus of GDC, many of the objectives outlined in this report will determine how auroral precipitation influence the upper atmospheric dynamics (e.g., 1.1, 1.2, 1.3, 2.2, 2.3, 2.5, 2.6). The data obtained in support of these objectives can be leveraged by the Air Force.

The Air Force provides operational forecasts to a variety of agencies. For ionospheric specification, the GAIM model is used with the eventual implementation of the Global Assimilation of Ionospheric Measurements Full-Physics (GAIM-FP) model. The advances in understanding internal IT processes (GDC Science Goal 2) will complement and can potentially be incorporated into GAIM-FP, further improving its forecasting capability.

In summary, GDC is not only a mission that will support our national space strategy by advancing scientific understanding of the IT system, but it is also a mission that has the potential for cross-agency utilization. The understanding gained through closure of GDC's Science Goals and Objectives, and the data provided by GDC to the entire scientific community, will be directly applicable to operational applications in many of our nation's branches.

APPENDIX C: ADDITIONAL ORBITAL DYNAMICS PRIMER

This section provides details of the dynamics of satellites in low Earth orbit (LEO) and provides definitions of orbital terms as they relate to the possible GDC mission architectures described in Chapter 3.

Orbital Velocity & Period: The orbital velocity or speed of a satellite in a circular orbit about the Earth as a function of satellite altitude is shown in Figure C.1. As the altitude of the satellite increases, the speed decreases. This is important when developing a mission concept for several reasons. First the orbital period, or time needed for the satellite to return to the same latitude and same side of the Earth, is dependent on the altitude. Second, given two satellites in the same orbital plane but at different altitudes, each will have a different orbital speed. This will result in the lower satellite eventually lapping the upper satellite with some frequency. In this document the term "conjunction" is used to indicate the time it takes the lower satellite to lap the higher one.

Inclination: A satellite's orbit inclination, *i*, is the angle between the orbit plane and the equator of the Earth. A slightly more precise definition is that the inclination is the angle between the satellite's orbital angular momentum and the Earth's rotational angular momentum. A 0° inclination orbit occurs when the equatorial and orbit planes are aligned and the satellite orbits in the same sense as the Earth's spin. A satellite with a 90° inclination, meaning the orbital plane is orthogonal to the equatorial plane, passes directly over the geographic northern and southern poles every orbit. For inclinations between -90° and 90°, the inclination indicates the maximum and minimum latitude that the satellite will pass over during each orbit. For example, a satellite that has an inclination of 38.9°, will pass over Washington DC, but no further north. It will also pass over -38.9°, but no further south. Orbits with $|i|<90°$ are referred to as prograde. Orbits with $|i|>90°$ are referred to as retrograde since the orbital angular rotation has a component that opposes that of the Earth's rotation. The maximum latitude that a satellite in a retrograde

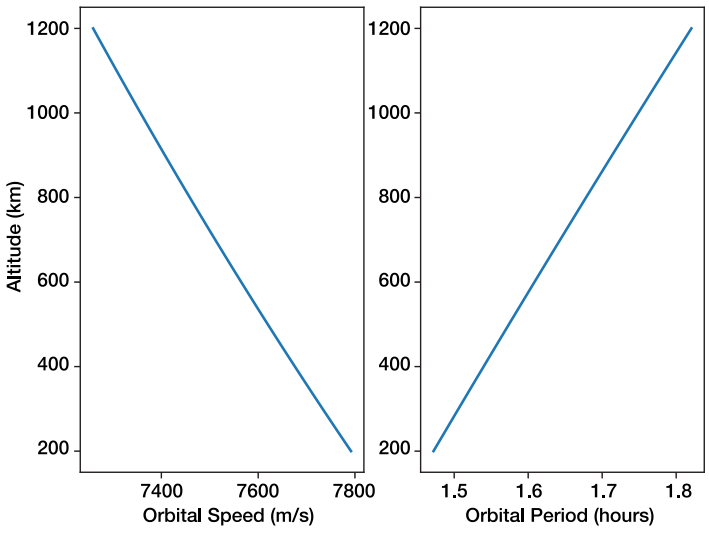

Figure C.1. The orbital speed (left) and orbit period (right) of a satellite as a function of circular orbit altitude above the Earth.

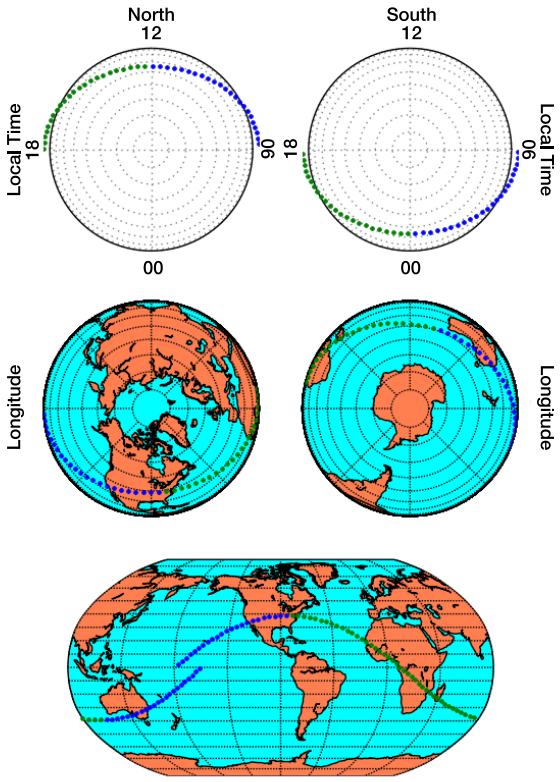

Figure C.2. A single 38.9° inclination orbit shown in three different ways. From top to bottom, these plots show the orbit from above the northern (left) and southern (right) poles in local time coordinates (with the sun at the top of the plot, dawn to the right, dusk to the left, and midnight at the bottom); above the northern (left) and southern (right) poles in geographic coordinates; and the orbit over the entire Earth. In each plot, the blue dots indicate when the satellite is moving from south to north, and red dots indicate when it is moving from north to south. In the bottom plot, the rotation of the Earth is apparent, since there is a clear discontinuity in the orbit at the equator, meaning that by the time the satellite reached the equator traveling northward at the end of the orbit, the Earth had rotated by approximately 22.5°.

orbit reaches is 180°-|i|. For example, a satellite with an inclination of 141.1° will just pass over Washington DC at 38.9°.

For studying global processes, including those at high-latitudes, higher inclination orbits are needed. In order to maximize the time in the auroral oval, where a significant amount of both particle heating and Joule heating occurs, an inclination of approximately 82° is required. Due to the offset between the geographic and geomagnetic coordinate systems, an inclination of 82° also provides significant opportunity to sample within the polar cap, all the way to the magnetic pole.

Ascending/Descending Nodes: When a satellite launches into Earth orbit, the coordinate system is best visualized by an observer at a far distance looking at the sun-Earth system. The Earth's equatorial plane is used as reference because the Earth's oblateness is symmetrical relative to the equator. When a satellite travels from south to north (north to south) passing through the equatorial plane, the point on the equatorial plane is referred as the ascending (descending) node. The right ascension of the ascending node (RAAN) specifies the angle of the orbit plane with respect to the Earth-Sun line at the vernal equinox. For a polar orbit, the orbit plane is being fixed in inertial space. For example, a polar orbit plane may have a local time of ascending node of dawn (0600 LT) and a descending node of dusk (1800 LT) at one time, but three months later the corresponding local times of the ascending and descending nodes will have shifted owing to Earth's orbit about the Sun to earlier local times, to 0300 LT and 1500 LT, respectively. The oblateness of the Earth exerts a torque on non-polar orbits that causes the orbit to precess in inertial space and hence changes this simple relationship between the ascending node's local time.

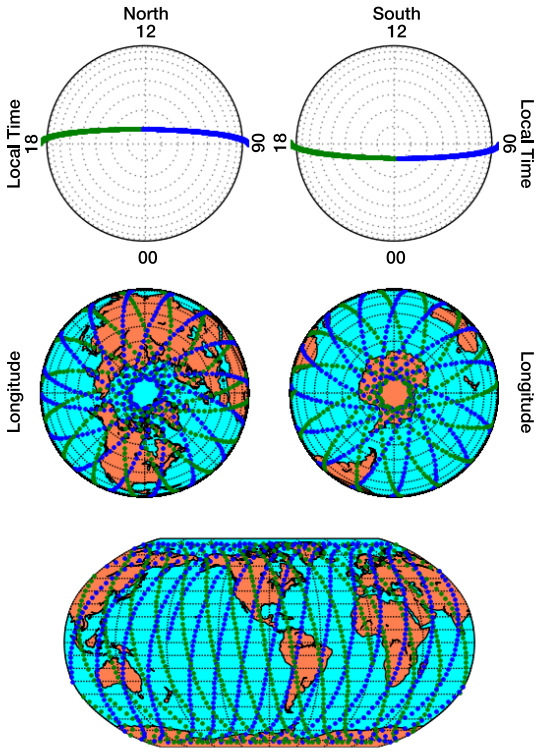

Figure C.3. 24 hours of satellite positions of an 82° inclination orbit in the same format as Figure C.2. The top figure shows single traces, since the orbits are approximately in a single local time plane, while the middle and bottom plots show that the satellites pass over many locations on Earth twice, once on the ascending node (blue dots) and once on the descending node (red dots).

Precession: Orbit plane precession refers to rotation of the orbit in inertial space, i.e. relative to the 'fixed' stars. The Earth's oblateness results in a gravitational torque on any satellite with an inclination not equal to 0° or 90° causing the orbital plane to rotate or precess about the Earth's rotation axis. This precession is westward for inclinations below 90° and eastward for inclinations

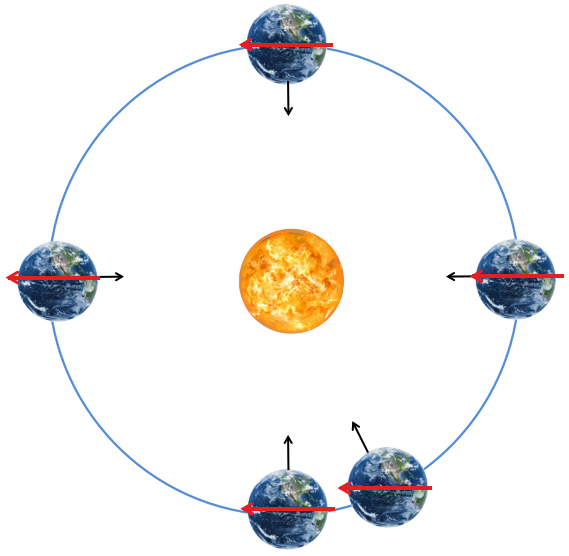

Figure C.4. The orbit plane of a 90° inclination satellite throughout a full year as seen from above the sun. In this coordinate system, the orbit plane, as illustrated by the black arrow, is fixed to being orthogonal to the sun-Earth line during the spring, but the definition of noon from Earth's point of view changes throughout the year. Therefore, the orbital plane appears to precess in Earth's coordinate system.

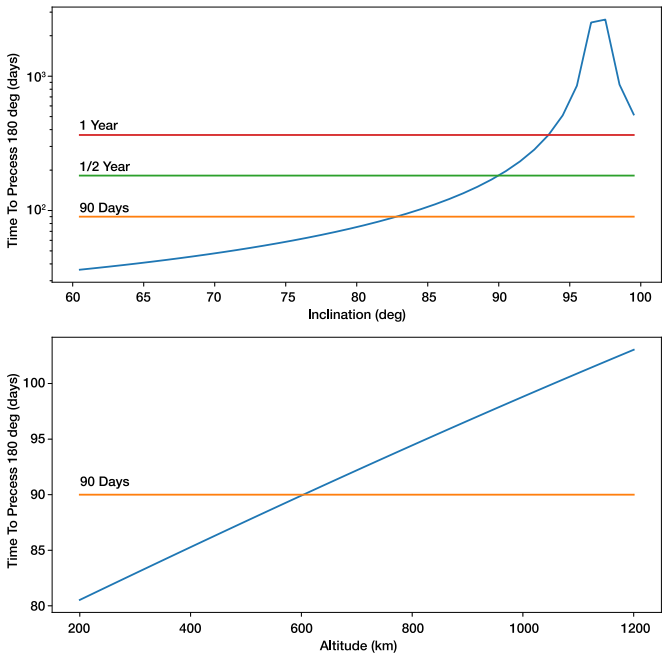

Figure C.5. The time to precess 180° in local time versus inclination (top) and altitude (bottom) relative to the baseline orbit (400 km altitude, 82° inclination). This includes both the precession in inertial space due to Earth's oblateness and the apparent local time precession due to the Earth orbiting the Sun.

greater than 90°. The rate of precession is a function of both inclination and altitude. At lower inclinations the satellite's orbit plane precesses faster than at higher inclinations. Further, with decreasing orbit altitude, the precession is faster due to the increasing gravitational torque (i.e. proximity to Earth's non-uniform mass distribution). Adding the inertial precession to the apparent rotation of the Sun relative to the orbit plane due to Earth's orbit about the Sun (just under 1° westward per day), yields the net local time precession rate. Orbits with inclinations somewhat greater than 90° have small eastward inertial precession rates, and depending on the altitude, an inclination exists for which the inertial precession matches the apparent solar rotation yielding a Sun-synchronous orbit. The local time precession rate versus orbit inclination and altitude relative to the baseline orbit, 400 km altitude and 82° inclination, are shown in the top and bottom panels of Figure C.5, respectively. For the baseline orbit, the inclination giving a Sun-synchronous orbit is near 97°.

Precession is important as it allows multiple vehicles to be dispersed into different orbital planes after being launched into a single plane aboard one launch vehicle. It also allows various mission configurations to be implemented throughout the lifetime of the mission. If there exists a desire to move one or more satellites to a different LTAN, then those satellites can either be moved to a different altitude or a different inclination. This will cause the satellites to have different precession rates, so that their orbit planes will slowly drift away from the original position. Once the planes are separated by the desired amount, the satellites can be moved back to the same altitude or inclination if desired, setting a separation in orbital planes between groups of satellites. Inclination change maneuvers are considered more expensive regarding delta-V than changing the apogee. However, inclination change has the benefit that all satellites stay at their initial altitudes throughout the precession maneuver, which may be important for measurement considerations. Overall, there are three considerations for determining the best method for separating the orbit planes: (1) how much fuel will it use to complete the maneuver (measured in terms of delta-V); (2) how long it will take to move the orbit plane; and (3) how much of the time will the satellite be able to conduct science while in the maneuver.

Drag: Drag was touched on in Chapter 4, but here we present a table which describes the amount of delta-V needed in order to raise a satellite from several altitudes to several other altitudes and the amount of time that it takes to decay from those altitudes for a given satellite with an typical mass-to-area ratio (150) and three different F10.7 values (80, 110, and 150). This is for illustration purposes only, since the drag is dependent on the mass-to-area ratio, which is not known for a mission such as GDC at this time, but was approximated as 150.0 kg/m^2. This table illustrates that with between 120 m/s and 416 m/s of Delta-V, a nominal satellite can be maintained between 400 and 350 km altitude for five years.

Spacing Within an Orbital Plane: Changes in along-track separations between two satellites, 'A' and 'B' can be accomplished by making small changes to the semi-major axis of the orbit to temporarily change their relative orbit periods until the desired along-track separation accumulates. Changes in the semi-major axis are efficiently done with an along track thrust. One way to do this and preserve circular orbits is to do a thrust that slows 'A' down at one point in the orbit. This reduces the orbital velocity and lowers the orbit altitude at the diametrically opposite point in the orbit – which is now the perigee for 'A'. Executing a similar along-track thrust half an orbit later (at the perigee point) can be used to

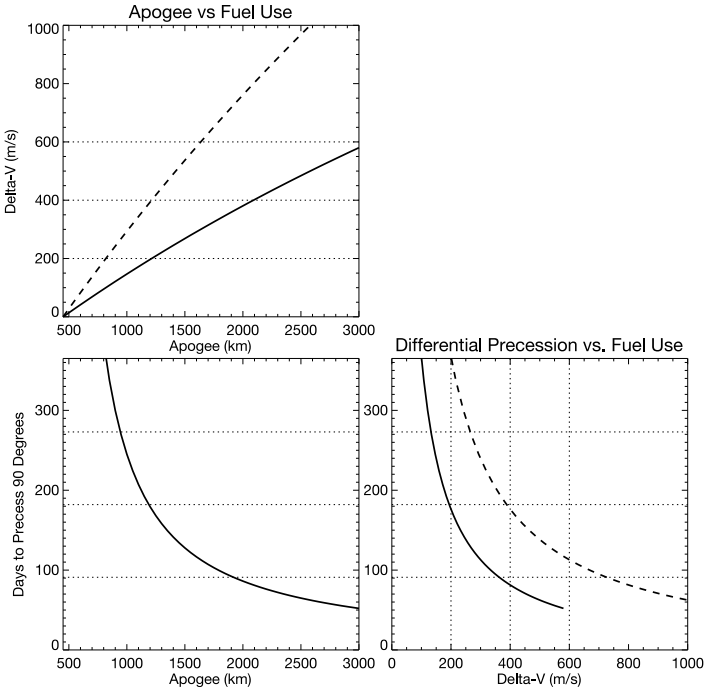

Figure C.6. Top Left: Apogee resulting from a maneuver versus delta-V needed to get to the new apogee from 500 km (horizontal lines indicate 200, 400, and 600 m/s); Bottom Left: Apogee during maneuver versus days to precess 90° in local time (horizontal lines represent 3, 6, and 9 months); and Bottom Right: Delta-V versus days to precess 90° in local time (horizontal lines represent 3, 6, and 9 months, vertical lines represent 200, 400, and 600 m/s). In each plot, the solid line shows the single maneuver to get to the higher apogee, while the dashed line shows the double maneuver needed to both raise the apogee and then lower it once the orbit plane has moved.

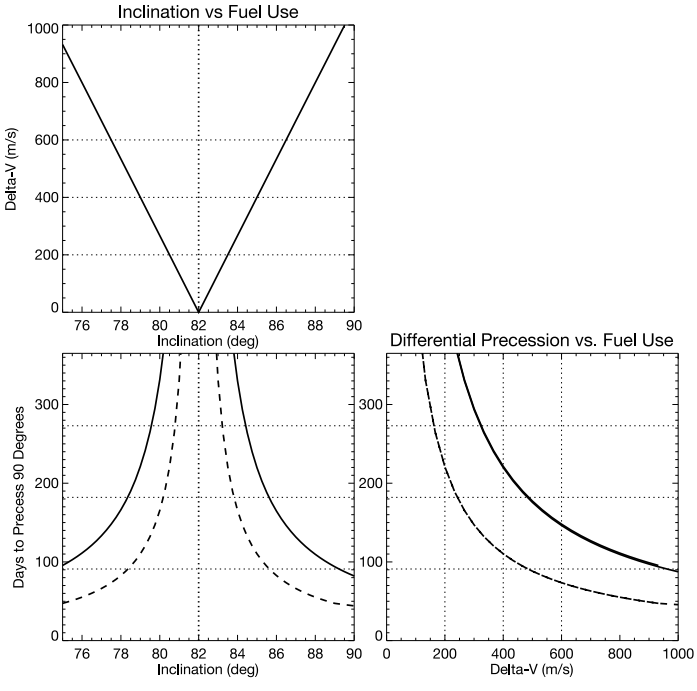

Figure C.7. Delta-V, days to precess 90°, and inclination in the same format as Figure C.6, except considering inclination change instead of apogee change. In this case, there is no reason to leave the control satellite at 82° inclination. Instead, it could be moved in the opposite direction as the other satellite. So, the dashed line shows the precession rate and the delta-V cost (for each satellite) if one satellite is moved up in inclination and the other satellite is moved down in inclination.

Table C.1. An illustration of how much Delta-V would be needed to maintain 4 hypothetical missions within a 50 km range using three different F10.7 levels (80, 110, and 150). This is calculated by determining how many days the satellites would take the orbit to decay from the upper altitude to the lower altitude, how much Delta-V is needed to raise the orbit from the lower altitude to the upper altitude, how many times this would be needed over a five year mission (maneuvers in 5 yrs), and then the total Delta-V needed during that five year mission for these maneuvers.

Upper Alt. (km)	Lower Alt. (km)	Days (80)	Days (110)	Days (150)	Delta -V	Man. in 5 yrs. (80)	Man. in 5 yrs. (110)	Man. in 5 yrs. (150)	Total Delta-V (80)	Total Delta-V (110)	Total Delta-V (150)
450	400	1184	598	297	28.13	1.54	3.05	6.15	43.4	85.9	173.1
425	375	720	382	188	28.28	2.54	4.78	9.75	71.7	135.1	275.4
400	350	434	229	125	28.44	4.21	8.00	14.62	119.7	228.6	415.9
375	325	247	138	82	28.60	7.40	13.24	22.18	211.7	378.8	634.5

reduce the altitude at apogee (where the first thrust was applied) down to the same as perigee to circularize the orbit. Satellite 'A' is then in a lower, shorter period circular orbit, and will moving ahead of 'B'. Once 'A' is as far ahead as desired, one can either do another pair of maneuvers on 'A' to raise its orbit to that of 'B' again, or do the same pair of orbit lowering maneuvers on 'B' to lower it to the same orbit as 'A'.

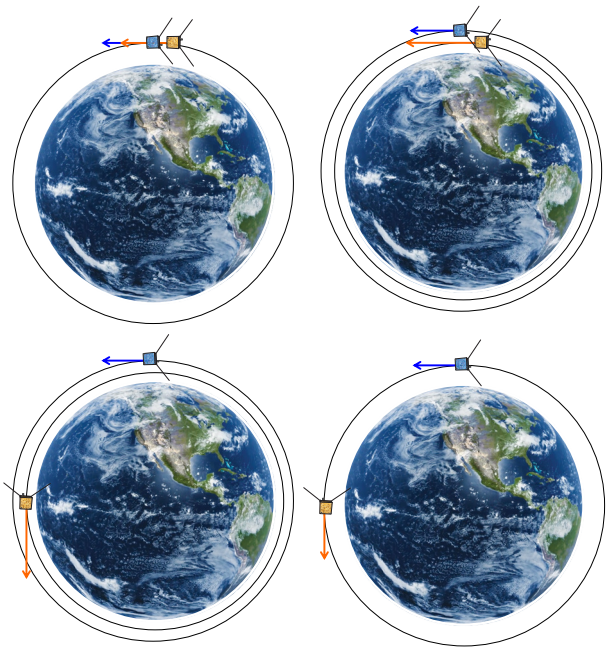

Figure C.8. An illustration of how the spacing of two satellites can be accomplished along an orbit plane. This figure is not to scale and represents days to weeks of orbit maneuvers or drag adjustments depending on the altitudes and changes in altitude. For differential drag, the orbit of the satellite 'A' (red) would not return to that of satellite 'B' (blue), but satellite 'B' would come down to the orbit altitude

The steps for spacing out two satellites as illustrated in Figure C.8. They are:

1. Satellite 'A' (red) would perform a pair of maneuvers maneuver to reduce its orbit altitude into a shorter period orbit.
2. Satellite 'A' (red) would then orbit faster than Satellite 'B' (blue).
3. When the proper spacing between Satellites 'B' (blue) and 'A' (red) is achieved, either Satellite 'A' (red) is raised back up to match the semi-major axis of Satellite 'B' (blue) or Satellite 'B' (blue) is lowered to the same semi-major axis as Satellite 'A' (red).

Rather than using active propulsion, one can instead use differential drag to do the same thing by creating different along-track drag forces first to satellite 'A' and then to satellite 'B'. Differential drag varies the ram-direction surface area of one satellite relative to another for example by changing the orientation of satellite 'A' or rotating its solar panels. Because the differential drag force is much smaller than an active thrust, it acts like a continuous very low level thrust and gradually lowers a satellite altitude preserving it as a circular orbit.

To achieve a stable separation using differential drag, the drag force of satellite 'A' would be increased relative that of a satellite 'B'. In this configuration the orbit altitude and orbit period of 'A' gradually decrease and it continuously moves ahead of satellite 'B'. Once the desired orbit difference is achieved, or when half of the desired separation distance is realized, the drag on 'A' would be reduced to its initial value, by rotating it back to the same orientation as it had initially. One could then wait while the separation between 'A' and 'B' continued to grow, or one could immediately rotate 'B' to increase its orbital drag and begin lowering its orbit to match 'A'. Satellite 'B' would then gradually move to lower orbit altitudes while 'A' continued to move ahead of 'B'. When 'B' reaches the same altitude as 'A' their along track separation would stop changing and the drag on 'B' could be reduced again to end the differential drag and hold the separation.

The major disadvantage of differential drag is the amount of time required to achieve the orbit period differences. In addition, the orbit period can only decrease so if one is dealing with more than two satellites, managing the relative drag and separations is somewhat more complex than when using propulsion. It offers the significant advantage however that it does not require propulsion.

Figure C.9 provides an example of how long it would take to space out two satellites at 400 km altitude by 180° along the orbit track as a function of the lower altitude that is moved to. It also provides the Delta-V that is needed to achieve the dispersion, including both the lowering and raising of the orbit of the satellite.

Revisit Time: Figure C.10 shows an example of the spacing between 4 satellites over the course of a year that are at altitudes of 360, 380, 410, and 450 km, and the resulting revisit times if the constellation were allowed to dynamically evolve over two years. With this altitude spacing, there are many periods with very rapid revisit times (e.g., day 550 has two sets of satellites that are very close to each other, resulting in rapid revisit times) as well as times with more equal spacing (e.g., near day 275, there are two sets of satellites that are roughly 15 minutes apart and two sets that are roughly 30 minutes apart). It should be noted that the constellation spacing can be "frozen" at any time by changing the altitudes of the satellites to be the same.

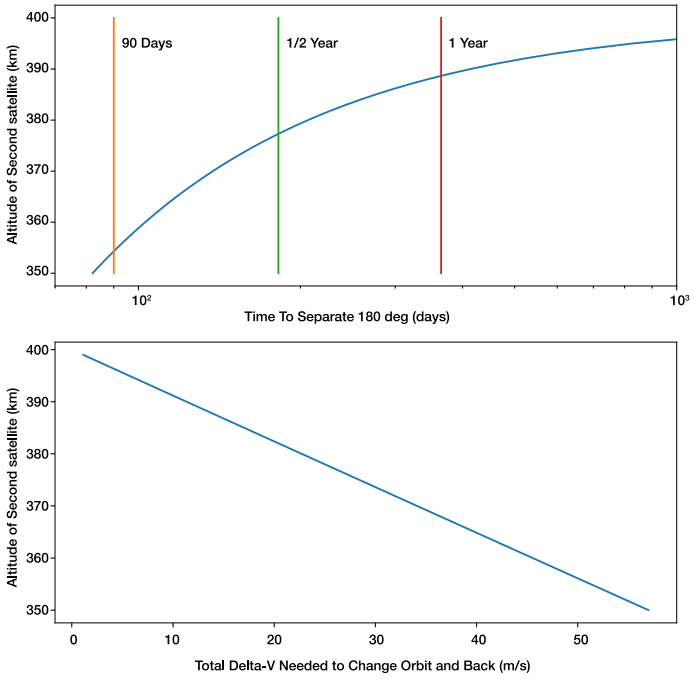

Figure C.9. The top plot shows the amount of time that it would take to separate 2 satellites by 180° with the top one at 400 km and the lower one at the altitude indicated, while the bottom plot indicates the amount of Delta-V that would be needed to accomplish both the lowering and raising of the orbits.

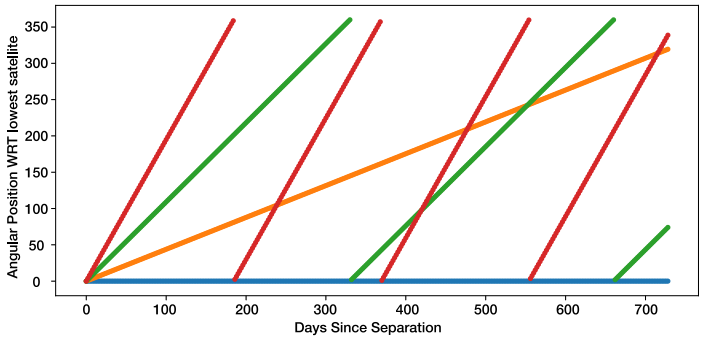

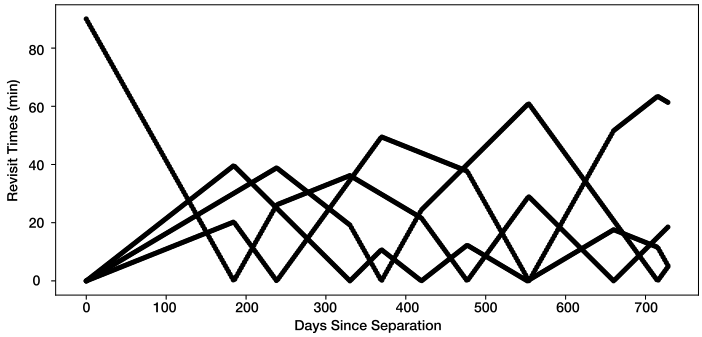

Figure C.10. Top: the angular separation between 4 satellites with respect to the lowest satellite over the course of two years. Bottom: the resulting revisit times with these angular separations.